A new approach to an old problem:

Investigating the molecular blueprints underlying the social defeat stress-induced resilient and susceptible phenotypes using engram-multiomics sequencing techniques.

Dissertation

Zur Erlangung des Grades

Doctor der Naturwissenschaften

Am Fachbereich Biologie

Der Johannes Gutenberg-Universität Mainz

Monika Chanu Chongtham des Doktorandin

Geb. am 1992 in Imphal

Mainz, 2023

Dean: Prof. Dr. Eckhard Thines

Supervisor 1:

Supervisor 2:

Date of oral examination: 20th February, 2024

Thesis advisory committee:

Other supervisors:

Declaration

I hereby, declare that I prepared the PhD thesis '**A new approach to an old problem: Investigating the molecular blueprints underlying the social defeat stress-induced resilient and susceptible phenotypes using engram-multiomics sequencing techniques'** on my own, apart from the resources mentioned in the acknowledgement section or within the thesis, where the contributions are properly credited and recognized.

Mainz, 2023

Monika Chanu Chongtham

Preface

You once said,

'Nothing looks beautiful

As they near death',

But Autumn looks the prettiest.

Winter is dreadful

But if you persist,

Spring follows,

Bearing gifts.

An eternal cycle

Of transience and change,

A shape-shifting entity,

Perceived by the mind,

Giving it

The highest mandate of a being,

For all battle is played out

In the mind first,

And victory or defeat

Is a manifestation of

What has already been decided

In the mind.

For all things must come to an end

In this eternal cycle of exchange.

Quote

'You can only bloom in the right environment. Choose it wisely.'

- Monika Chanu Chongtham

Acknowledgement

Abstract

Resilience and susceptibility are two plausible outcomes following stress exposure. Those individuals that can successfully cope with daily stressors and maintain normal daily functions are known to exhibit resilience, while those that succumb to the stressors are known to be susceptible to the stressor. Susceptibility to a stressor is a major precedent towards the development of mental health disorders. Unfortunately, mental health disorders not only compromise an individual's quality of life but also exert a huge burden on the global economy. Therefore, with the anticipated surge in mental health disorders following the recent COVID lockdowns, a more comprehensive understanding of resilience and susceptibility molecular mechanisms is crucial for facilitating early interventions.

As mechanistic studies on humans face certain limitations, we employ the chronic social defeat (CSD) paradigm for rodents - known for its high face validity, construct validity as well as predictive validity, mirroring the social stressors that humans experience. However, current molecular studies investigating the CSD stress impacts embody at least two limitations. First, most studies use bulk tissues rather than isolating engram cells/nuclei. As engrams play pivotal roles in the onset of diseased pathways, the use of bulk tissues limits the potential to identify rare but crucial signals. Second, the majority of the current literature investigates only one omics level at a stationary time point. Such an approach curtails the ability to delineate causative factors, which are potent therapeutic targets. Therefore, to circumvent these limitations, the thesis employs a study design centered around the implementation of transgenic mouse lines to facilitate the capture of specific engram nuclei. These nuclei will then be subjected to multiomics investigations to access different layers of molecular machineries at a single time point. This approach will facilitate the generation of a higher resolution picture of the ongoing alterations, thereby enhancing the potential to delineate plausible causal pathways.

Thus, within the framework of the study, I highlight the importance of employing optimal stressors for the transgenic mouse lines and engram nuclei isolation techniques to increase the confidence of the results from the engram-multiomics data. From such systematically curated multiomics data, I identified significant roles of the GTPase signaling and endocytic pathways behind the divergence and persistence of the susceptibility-resilience patterns post-stress. Further analysis of the results led to the identification of endocytosis-related *Arf6* GTPase as a potential therapeutic target, wherein I hypothesize that reducing *Arf6* expression in the ventral hippocampus within a defined window period, will enhance resilience outcomes.

Zussamenfassung

"Resilienz und Anfälligkeit sind zwei plausible Ergebnisse nach Stressbelastung. Diejenigen, die erfolgreich mit täglichen Belastungen umgehen können und normale tägliche Funktionen aufrechterhalten, gelten als resilient, während diejenigen, die den Belastungen erliegen, als anfällig für den Stressor gelten. Die Anfälligkeit für einen Stressor ist ein entscheidender Vorläufer für die Entwicklung von psychischen Störungen. Leider beeinträchtigen psychische Störungen nicht nur die Lebensqualität eines Einzelnen, sondern belasten auch die Weltwirtschaft erheblich. Daher ist mit dem erwarteten Anstieg psychischer Störungen nach den jüngsten COVID-Sperrungen ein umfassenderes Verständnis der molekularen Mechanismen von Resilienz und Anfälligkeit entscheidend, um frühzeitige Interventionen zu erleichtern.

Da mechanistische Studien am Menschen bestimmten Einschränkungen unterliegen, verwenden wir das Paradigma der chronischen sozialen Niederlage (CSD) für Nagetiere - bekannt für seine hohe Gesichts-, Konstrukt- und prädiktive Validität, die die sozialen Belastungen widerspiegelt, die Menschen erfahren. Allerdings haben aktuelle molekulare Studien zu den Auswirkungen von CSD-Stress zumindest zwei Einschränkungen. Erstens verwenden die meisten Studien Massengewebe anstelle der Isolierung von Engrammzellen/-kernen. Da Engramme eine entscheidende Rolle im Beginn von krankhaften Signalwegen spielen, beschränkt die Verwendung von Massengeweben das Potenzial, seltene, aber entscheidende Signale zu identifizieren. Zweitens untersucht die Mehrheit der aktuellen Literatur nur eine Omics-Ebene zu einem festen Zeitpunkt. Ein solcher Ansatz schränkt die Fähigkeit ein, kausale Faktoren zu ermitteln, die potenzielle therapeutische Ziele sind. Um diese Einschränkungen zu umgehen, verwendet die Dissertation einen Studiendesign-Ansatz, der auf der Implementierung von transgenen Mauslinien basiert, um die Erfassung spezifischer Engramm-Zellkerne zu erleichtern. Diese Zellkerne werden dann multiomischen Untersuchungen unterzogen, um auf unterschiedliche Schichten molekularer Mechanismen zu zugreifen. Dieser Ansatz erleichtert die Generierung eines Bildes mit höherer Auflösung der laufenden Veränderungen und verbessert so das Potenzial, plausible kausale Wege zu ermitteln.

Innerhalb des Rahmens der Studie betone ich die Bedeutung der Verwendung optimaler Stressoren für die transgenen Mauslinien und der Isolationstechniken für Engramm-Zellkerne, um das Vertrauen in die Ergebnisse aus den Engramm-Multiomics-Daten zu steigern. Aus solchen systematisch kuratierten Multiomics-Daten habe ich signifikante Rollen der GTPase-Signalwege und der endozytotischen Pfade bei der Divergenz und Persistenz der Anfälligkeits-Resilienz-Muster nach Stress identifiziert. Eine weitere Analyse der Ergebnisse führte zur Identifizierung der mit Endozytose verbundenen Arf6-GTPase als potenziellem therapeutischem Ziel, wobei ich die Hypothese aufstelle, dass die Reduzierung der Arf6-Expression im ventralen Hippocampus innerhalb

eines festgelegten Zeitfensters die Resilienz verbessern wird."NB: Translation by ChatGPT (chat.openai.com)

Table of Contents

Declaration iii

Preface iv

Acknowledgement v

Abstract vi

Zussamenfassung vii

I. Overview: Stress and the scope for resilience study 1

II. Introduction 3

1. Dissecting stress, its physiological mechanisms and impacts 3

1.1. Stress and stressors 3

1.2. Stress response and the Hypothalamic-Pituitary-Adrenal Axis (HPA) 3

1.3. Stress coping strategies – active (resilience) or passive (susceptible) 6

1.4. Physiological impacts of stress in the brain - regional and circuit levels 7

2. Models for stress research 10

2.1. Non-human model organisms in stress studies 10

2.2. Use of genetically modified model organisms for stress research – engram approach 12

2.3. Behavioral and physiological assays to determine the effects of the applied stress protocols 12

3. Epigenetic mechanisms and their relevance in stress 15

3.1. DNA methylation of the genome - methylome 16

3.1.1. Accessing the methylome 17

3.1.2 Relevance of DNA methylation in stress research 18

3.2. RNA (mRNAs and non-coding RNAs) – transcriptome 19

3.2.1. Accessing the transcriptome 20

3.2.2. Relevance of transcriptome alterations in stress 20

3.3. Crosstalks (multiomics) between different epigenetics levels 21

4. Scope of the thesis – aims and objectives 23

4.1. Summary background and identification of research gaps 23

4.2. Study design to bridge the gaps 25

4.3. Methodical steps to obtain engram-multiomics data 26

Chapter 1. Choice of TAM-inducible IEGCreER^{T2} mouse line and optimization of TAM injections for further experiments 30

1.1 Introduction 30

1.2 Methods 30

1.2.1 Animals and genotyping 30

1.2.2 Behavior experiment 31

1.2.3 Tamoxifen and 4-hydroxytamoxifen preparation 32

1.2.4 Brain tissue collection, immunohistochemistry, microscopy and nuclei sorting 32

1.3 Results 32

1.3.1. Determination of optimal window period for sfGFP accumulation 32

1.3.2. Choice of mouse line – cFos-GFP vs Arc-GFP 34

1.4 Discussion 34

Chapter 2. Optimization of the CSD paradigm for the TAM-inducible Arc-GFP mouse line to facilitate the segregation of resilient-susceptible phenotypes 36

2.1. Introduction 36

2.2. Methods 36

2.2.1. Animals 36

2.2.2. Chronic social defeat (CSD) stress 36

2.2.3. Behavioral tests 38

2.2.4. Tamoxifen and solvent preparations 41

2.2.5. Physiological assessments 41

2.2.5.1. Blood collection and CORT level assessment 41

2.2.5.2. Tissue collection, nuclei isolation and sorting 42

2.2.6 Statistical analyzes 42

2.3. Results 42

2.3.1. Determination of the necessary TAM dosage for tracing optimal amount of SI-engram specific nuclei 42

2.3.2. SI test of TAM-injected Arc-GFP mice did not show a stress effect, following subthreshold defeat 44

2.3.3. In the absence of TAM injections, the subthreshold stressor induces a deficit in the SI test after CSD 46

2.3.4. Usability of the TAM-inducible Arc-GFP mouse line for stress studies 46

2.3.4.1. TAM-injected Arc-GFP mice show stress effects after the implementation of a higher stressor CSD paradigm 49

2.3.4.2. Determining the divergence or convergence of the Arc-GFP mouse line and implications on its usability for cross-comparisons with other stress research 51

2.3.5. Impacts of TAM – comparisons in the C57BL/6J mouse line 56

2.4. Discussion 59

Chapter 3. Protocol generation – Nuclei isolation from low volumes of micro-dissected tissues 61

3.1. Introduction 61

3.2. Methods 62

3.2.1 Animals, behavioral experiments and TAM injection 62

3.2.2. Micro-region dissections 62

3.2.3. Nuclei isolation 63
3.2.3.1. Solutions 63
3.2.3.2. Protocol establishment and optimization 63
3.2.4. Flow cytometry and fluorescence-activated nuclei sorting (FANS) 65
3.2.5. Microscopy 66
3.2.5.1. Phase-contrast Microscopy 66
3.2.5.2. Wide field Fluorescence Microscopy 66
3.2.5.3. Confocal Microscopy 67
3.2.6. Image analysis 67
3.2.6. Statistics 67
3.3. Results 68
3.3.1. Choice of gradient solution 68
3.3.1.1 Validation of the isolation process efficiency 68
3.3.1.2. Adaptation of the homogenization setup to micro-dissected brain regions: Nuclei isolation and visualization 69
3.3.2. Modulating the ultracentrifugation protocol to increase yield and speed 71
3.3.2.1 Removal of the cushion layer during ultracentrifugation to increase yield 71
3.3.2.2 Decreasing the ultracentrifugation duration to increase speed 73
3.3.3 Techniques to improve sorting efficacy 75
3.3.3.1. Re-centrifugation and resuspension 75
3.3.3.2. Dilution with different buffers 75
3.4. Discussion 76
Chapter 4. Choice of technique for sfGFP+ nuclei separation - INTACT vs FANS 79
4.1. Introduction 79
4.2. Methods 80
4.2.1. Animals, behavior and TAM injection 80
4.2.2. Brain dissection, nuclei isolation and sfGFP+ nuclei separation 80
4.2.2.1. INTACT 80
4.2.2.2. FANS 81
4.2.2.3. Purity analysis of INTACT- and FANS-Nuclei 81
4.2.3. Parallel Processing of INTACT- and FANS-nuclei 81
4.2.4. Microscopy 82
4.2.4.1. Phase-contrast microscopy 82
4.2.4.2. Fluorescence microscopy 82
4.2.5. Image analyses and statistics 82
4.3. Results 82

4.3.1. Quantification of morphological attributes: FANS- and INTACT-nuclei in comparison to INPUT-nuclei 82

4.3.2. FANS vs INTACT: Speed and yield efficiency 87

4.4. Discussion 88

Chapter 5. Multiomics analysis of resilience-susceptibility engram nuclei in the vHipp 90

5.1. Introduction 90

5.2. Methods 91

5.2.1. Animals and behavior experiments 91

5.2.2.1. Basal character identification for test animals before CSD 91

5.2.2.2. Classification of animals to control and stress groups 91

5.2.2.3. Aggressive chronic social defeat experiments, TAM injection and SI test. 91

5.2.2.4. Animal weights 92

5.2.3. Tissue extraction, nuclei isolation and Fluorescence Activated Nuclei Sorting (FANS) 92

5.2.4. Molecular biology experiments and sequencing 92

5.2.4.1. Reduced Representation Bisulfite sequencing (RRBS-seq) 92

5.2.4.2. Small RNA sequencing (Small RNA-Seq) 94

5.2.5. Behavior data and omics data analyses 95

5.2.5.1. Behavior data statistical analyses 95

5.2.5.2. RRBS-seq data analyses 95

5.2.5.3. Small RNA-seq data analysis 95

5.2.5.4. Regulatory region overlap and motif enrichment analyses 96

5.2.5.5. STRING analysis and CYTOSCAPE 96

5.3. Results 96

5.3.1. CSD induces significant deficits in SI tests with CD1 mice 96

5.3.2. Accessing the DNA methylation landscapes in the divergent stress phenotypes as well as controls 99

5.2.2.1. Landscape and functional characterization of the differentially methylated cytosines (dmCs) and genes containing dmCs (dmGs) 99

5.2.2.2. Landscape and functional characterization of the differentially methylated regions (DMRs) and genes containing the DMRs (DMGs) 100

5.3.3. Regulatory functions of the DMRs point towards involvement of GTPase signaling in stress-related alterations 104

5.3.3.1. Motif enrichment analysis identifies E26 Transformation Specific (ETS) family of TFs to be strongly enriched in the DMRs 104

5.3.3.2. Relationship between differential methylation and gene expression at the sample collection point 105

5.3.4. Phenotype-specific differences in GTPase signaling and related processes transcending multiple omics levels 107

5.3.4.1 Multiomics network approach identifies phenotype specific divergence in other BPs. 109

5.3.4.2. Small RNA analysis supports findings from the methylome and transcriptome. 110

5.3.5. Identification of novel therapeutic targets 112

5.4. Discussion 115

5.4.1. Significance of the enrichment of GTPase signaling cascades and synaptic plasticity following stress exposure 115

5.4.2. Significance of the multiomics approach towards identification of novel therapeutic targets 117

Chapter 6. Tissue level differences in maintaining susceptibility and resilience 121

6.1. Introduction 121

6.2. Methods 121

6.3. Results 121

6.3.1. Comparison of stress affected biological processes in PFC (between phenotype comparison within the same tissue) with that of the vHipp. 122

6.3.2. Differential methylation patterns between the PFC and the vHipp (between tissue comparison within the same phenotype) 124

6.3.2.1. Baseline methylation differences between the tissues (control comparisons) 124

6.3.2.2. Different methylation patterns in the resilient group following stress exposure 125

6.3.2.3. Different methylation patterns in the susceptible group after stress exposure 127

6.4. Discussion 128

IV. General Discussion 130

1. Significance of investigating resilience and susceptibility mechanisms. 130

2. Strong points of our experimental approach 131

3. Merits and demerits of using TAM-inducible mouse lines 132

4. Loopholes to be addressed during nuclei isolation and sorting of engram nuclei 134

4.1. Use of nuclei for sequencing experiments 134

5. Benefits and complexities of applying a multiomics approach on the stress phenotype-specific engram-activated nuclei 136

5.1. Complex methylome and transcriptome relationship 136

5.1.1. Epigenome priming 137

5.2. Multiomics and network approach 137

6. Significance of tissue-specific stress response for drug applications. 140

7. Concluding remarks 141

7.1. Major findings of the thesis and their implications in stress research 141

V. Considerations and drawbacks 144

1. Limitations in the epigenetics study 144

2. Plausible limitations for cross-data comparisons 145
2.1. Use of Arc promoter and TAM-inducible mouse lines 145
2.2. Use of CSD models 145
VI. Perspectives and future scope 147
VII. Supplementary 149
1. Supplementary Figures 149
2. Supplementary Tables 158
3. Supplementary Data 165
VIII. Bibliography 166
IX. Appendices 199
1. List of Abbreviations 199
2. List of Figures 201
3. List of Supplementary Figures 202
4. List of Tables 202
5. List of Supplementary Tables 203
6. Contributions to other projects during the interim of the thesis 203
7. Other co-curricular work or achievements during the interim of the thesis 204
8. Declaration of online publications as co-authors for scientific work during the PhD, peer-reviewed and non-peer reviewed. 205
9. Breakdown of the timeline for the thesis 206
10. Curriculum vitae 208

I. Overview: Stress and the scope for resilience study

Any disturbance in the existing homeostatic equilibrium of an organism is termed as stress. Stress occurs as a physiological response to activate mechanisms to restore the perturbed homeostasis and promote adaptation[1,2]. However, excessive stress without proper coping mechanisms can be detrimental to the survival of the organism[2]. With the rapid changes in lifestyle over the past few decades in areas of nutrition, social bonding and competitive work culture, stress-associated mental disorders have been on the rise. From 1990-2019, an increase of 55.1% was noted[3,4]. Indeed, the World Health Organisation (WHO) report (2022)[5] estimated that 1 in every 8 people (approximately 12%) was living with a stress-related mental health problem in 2019. Unfortunately, mental disorders decrease the quality of life and reduce available human resources. In fact, by 2030, it is predicted that major depressive disorders (MDD) will be the leading cause of disability (WHO report cited by [6]). More alarmingly, the recent COVID lockdowns will, very likely, aggravate the steep increase in the rise of mental health disorders[7–11]. In other words, the impacts of the social isolation during the COVID pandemic along with the pending economic aftermath, foretell an increase in anxiety and depression cases in the next few years. Indeed, the WHO estimated a 26-28% increase in mental disorders within 1 year following the COVID-19 pandemic with anxiety and depressive disorders being the most common[5]. Notably, the result of a swiftly declining mental health is already evident in the civil unrest erupting in different countries. Apart from this, increasingly urbanised sedentary lifestyles paired with the growth of artificial intelligence and automation technology could, further, boost a bigger leap in the deterioration of global mental health.

Thus, studies for identifying the mechanisms behind stress and mental disorders have assumed a central role. It is noteworthy that there exists an interindividual variability in stress response, wherein some individuals demonstrate resilience, i.e., the ability to navigate environmental pressures without succumbing or becoming susceptible to stress- related disorders[12,13]. Consequently, investigating the molecular underpinnings behind resilience holds a significant promise for developing therapeutic targets to mitigate the potential surge in mental health disorders. Such identification of optimal targets would, in turn, facilitate effective interventions at an early stage.

To this end, the work for this thesis focusses on determining the mechanisms behind stress resilience, which holds a significant relevance in the current and nearby social scenario, by

employing state-of-the-art techniques. To facilitate a comprehensive understanding of the contemporary literature on stress and our research approach, the forthcoming sections will introduce concise overviews of key topics on 'the basics of stress and stress response', 'stress research models', and 'contemporary findings pertaining to mechanisms behind stress resilience'. Thereafter, the ensuing discussion of the contemporary literature will encompass diverse results from studies employing various psychosocial stressors in humans, primates, and rodents, with a predominant amount of research drawn from chronic social defeat stress, post-traumatic stress disorder and major depressive disorder studies. Following the exhaustive coverage of the foundational aspects, the subsequent sections will address the existing gaps in current stress research literature, followed by a detailed description of the study design to bridge the gaps. This will be followed by chapters describing the experiments and results in detail, supplemented by each chapter's discussion. Thereafter, to provide a cumulative overview, a general discussion section along with conclusions, drawbacks and future scope will unfold.

II. Introduction

1. Dissecting stress, its physiological mechanisms and impacts

1.1. Stress and stressors

As briefly introduced, stress is the body's natural response to any stimulus that challenges normal physiological functions and disturbs pre-existing homeostatic settings of an organismal system[1,2]. Meanwhile, the entity that evokes a stress response is termed as a 'stressor'[2] and can be real or perceived[14]. A stressor's pathogenic potential depends on the severity of the stress exposure as well as individual differences in stress response (see review by Wood and colleagues[15]). Based on the duration of exposure to the stressor, stress response can be broadly classified as acute (short time of exposure) and chronic (occur continuously over a period), emulated via environmental stressors – both psychological and non-psychological[16]. Non-psychological stressors include exposure to sunlight (UV), extreme coldness/hotness, hypoxia, malnutrition, internal metabolic triggers etc. Psychological stressors include early life stress/prenatal stress or stress that comes from social interactions in a social hierarchy in adults[16]. Prolonged psychological stress can increase an individual's risk to the development of mental disorders, other neuropsychiatric diseases or debilitating health conditions in the long run[16]. For example, experiencing stressful situations during young adulthood has been known to increase the likelihood of suffering from dementia, Alzheimer's dementia (AD), and Parkinson's disease (PD)[17–19]. On the other hand, individuals with underlying psychological disorders like autism or attention deficit hyperactivity disorder (ADHD) may exhibit a higher sensitivity to perceived stress[20,21]. Although stress carries a negative connotation, it is crucial to recognize that stress response is necessary for survival[22,23]. In fact, acute stress response evokes physiological pathways essential for the organism's adaptation of the organism to environmental demands[2,24,25]. For example, short-term stress, including high intensity trainings or exercises, promotes neurogenesis, critical for proper learning and adaptive outcomes[26–28].

1.2. Stress response and the Hypothalamic-Pituitary-Adrenal Axis (HPA)

Stress brings an organism's physiology to an arousal state, resulting in freezing, fleeing or aggressive behavior to meet the expected or unexpected environmental demands[14]. The immediate reactions of a stress response are governed by the autonomic nervous system,

specifically, the sympathetic (epinephrine) and parasympathetic (nor-epinephrine) nervous systems[14]. In contrast, the secondary phase of the stress response is regulated by the hypothalamic-pituitary-adrenal axis (HPA), along with the limbic system including the brain regions of amygdala, hippocampus, nucleus accumbens (Naccu) and pre-frontal cortex (PFC)[14,29], amongst others.

Within the HPA axis (**Figure 1a**), an active stress response prompts the release of corticotrophin releasing hormone (CRH) from the paraventricular nucleus (PVN) of the hypothalamus[30,31]. CRH, then, stimulates the anterior pituitary resulting in the release of adrenocorticotropic hormones (ACTH). ACTH signals the release of glucocorticoids (GCs) and mineralocorticoids from the adrenal cortices[31], with 'cortisol' as the primary glucocorticoid hormone in primates, and 'corticosterone' (CORT) in mice[32] (**Figure 1a**). These hormones bind to the GC receptors and mineralocorticoid receptors distributed over different regions of the body[32], thereby, relaying a **global stress response** via multiple signaling pathways.

Stress effects can be exerted within a few seconds or minutes through non transcriptional mechanisms via activation of glucocorticoid **membrane** receptors and downstream signaling machineries[33]. Alternatively, effects can manifest over longer periods (hours or days) through transcriptional mechanisms via the activation of **nuclear** glucocorticoid receptors or **glucocorticoid response elements** of specific genes[31,32,34]. Proper activation and curtailing of the signaling pathways from a stress response are critical for adaptive learning, while any deficit in the activation or deactivation of the stress response can lead to detrimental outcomes of stress exposure[32]. In fact, GC responses and activation of the HPA axis are necessary for an organisms' survival. Appropriate GC response to stress exposure is fundamental for mobilizing energy demands needed to mitigate the insults to the homeostatic balance[32]. However, timely dispensation of the activated HPA axis is equally important[32]. Prolonged activation of the HPA axis can drain resources from the individuals' normal physiological functions. For example, CRH, during stress, inhibits the secretion of gonadotropin releasing hormone, growth hormone, thyrotropin-releasing hormone, and thyroid-stimulating hormone[34], thereby, disrupting the reproductive, growth and thyroid functions[34]. Apart from this, prolonged circulation of GCs induces changes in neural functions and inflammatory responses, resulting in unfavourable long-term molecular and epigenetic modifications [32].

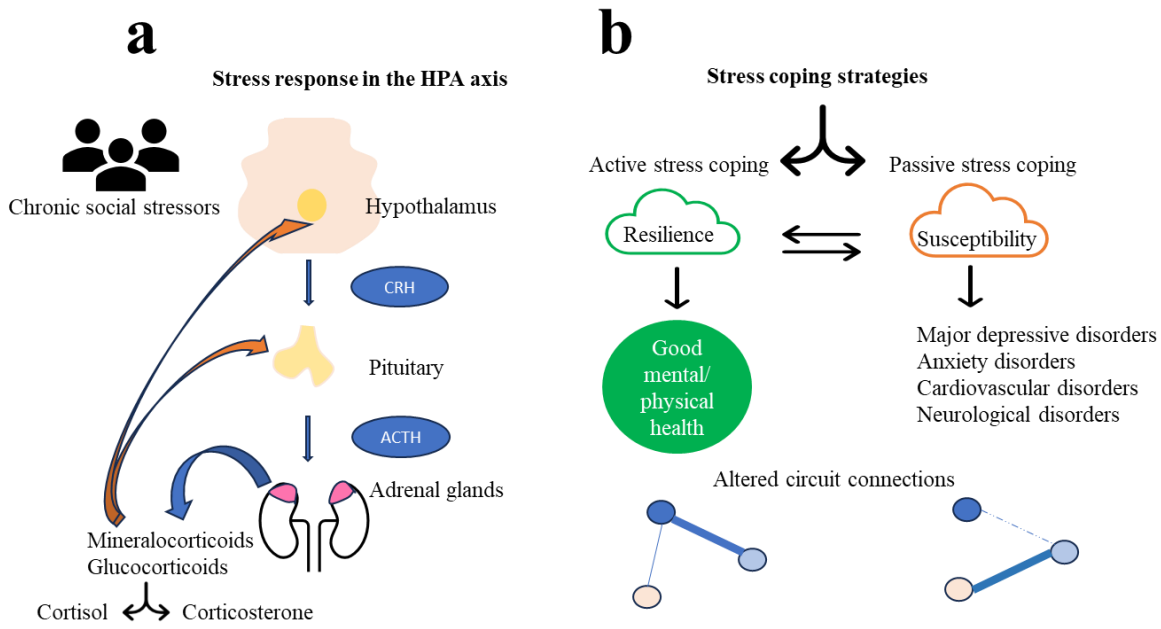

Figure 1: Stress response following stress exposure to chronic social stressors

a. Illustration of the hypothalamic-pituitary-adrenal (HPA) axis. During a stress response, the hypothalamus releases the corticotrophin releasing hormone (CRH), which stimulates the pituitary (in the brain) to release the adrenocorticotrophic hormone (ACTH). ACTH, then stimulates the adrenal glands (red) to release the glucocorticoids (GCs) and the mineralocorticoids (MCs). The GCs and the MCs, then, enact a negative feedback look to curtail the activity of the pituitary and the hypothalamus. Proper activation as well as timely dispensation of the HPA axis are required for the optimal functioning of the organism. Blue arrows represent activation while red arrows represent inhibitory feedback loops. **b.** Stress coping strategies depicting the path to resilience or susceptibility. Susceptibility to a stressor is a huge risk factor for the development of multiple disorders. On the other hand, resilience promotes a good mental and physical well-being, increasing the individual's chance of survival. Such visible symptoms are accompanied by altered structural as well as circuit connections. Altered circuit connections: Each node represents a different brain region, and the lines between the nodes indicate connections between the regions. Bolder the line, the stronger the connections. (HPA axis illustration adapted from Gjerstad and colleagues[35].)

From an evolutionary context, the release of GCs was associated with a flight or fight survival response requiring physical activity, limiting all non-essential activities of the organism[36,37]. However, in the modern context, where GCs are produced through psychosocial stressors without a demanding physical output, negative effects of stress (maladaptation) may ensue. Dysregulation of the stress response, whether in the sectors of activation or dispensation, results in the development of disorders such as anxiety, hypertension, obesity, fatigue, depression, and several systemic dysfunctions, including

cancer, that can be attributed to the continued inflammation and overactivation of the stress response system[34,38,39]. In addition to this, multiple longitudinal studies, involving non-human primates, have revealed that chronic exposure to GCs, activated by psychosocial stressors not only decrease the organism's longevity but also impacts the fitness of the next generations (see review by [40]). Thus, maladaptive stress response not only depletes human resources but also poses a significant challenge to the global economy. However, it is important to recognize that the outcomes of stress exposure are contingent on several factors, including genetics, prevalence or lack of favourable conditions and implementation of a particular 'stress coping strategy'[15].

1.3. Stress coping strategies – active (resilience) or passive (susceptible)

During a stress response, an organism can adopt an 'active' or 'passive' coping mechanism (**Figure 1b**) (see review by Wood and colleagues[15]). A coping mechanism is the manner in which the organism deals with the stressor. Active coping is associated with behavior responses such a social buffering, healthy diet, yoga etc., thereby, minimizing the physical or psychological burden following stress exposure[15,41–44]. This type of coping, generally, favours a 'resilient' outcome of the stress exposure[15]. In simple terms, resilience can be defined as the ability to continue with daily activities despite the presence of a stressor or the ability to regain mental health despite exposure to severe stressors[45]. Meanwhile, passive coping manifests as helplessness, withdrawal[15,16] etc. Passive coping mechanisms are usually associated with **susceptibility** to a stressor, where the stressor, negatively, impacts the usual behavioral and physiological functions of an individual[15]. Interestingly, both active and passive stress coping mechanisms exhibit divergent HPA axis response, with a lower reactivity in the former and a higher reactivity in the later[15].

Though the active coping strategies have been associated more with resilience, both strategies can be adaptive depending on the situation[15]. For example, passive coping, usually identified by a submissive behavior or immobile response to a stressor can be **maladaptive** under conditions, where an individual is exposed to brief durations of social stressors, repeatedly. However, it can be **adaptive** in situations, where a weaker organism faces a natural predator ([41] as cited by [15]), where passive coping could increase the chance of survival, and thus be considered more adaptive[46]. Hence, a specific coping strategy may be considered adaptive, in one context, and maladaptive, in another.

On the other hand, though resilience and susceptibility are usually associated with inter-individual variability, intra-individual variability in experiencing the perceived effects of a stressful exposure, can also occur[12]. An individual may become susceptible to a previous stressor, to which it exhibited resilience, depending on prevailing conditions like social buffer, healthy diet, additional stress etc. Overall, **resilience should be considered as a fluid response, and can be altered on prolonged stress exposure without suitable coping mechanisms**[12,13,15]**.** Thus, under conditions of chronic stress, when the coping response (passive or active) is not adequate, negative stress-induced psychological as well as physiological consequences may ensue.

1.4. Physiological impacts of stress in the brain - regional and circuit levels

Amongst the global impacts of stress at various physiological levels, the alterations in the brain are well-studied. Exposure to stress modifies brain structures as well as connectivities between different regions via the phenomenon of 'neuroplasticity'[47]. Briefly, neuroplasticity is the term given to the unique ability of the nervous system to adapt and alter over time in response to internal/external factors[48]. Neuroplasticity occurs in part by modulating the strength of 'synapses' – junctions between neurons and other neurons or other cell types - via increasing, decreasing or even deleting connections between synapses[49,50]. A synapse (term initially coined by Forster and Sherrington in 1897, as cited by [51,52]) is equipped with a pre-synaptic area and post-synaptic area, harbouring unique molecular machineries as well as their own local ribosomal machineries[53,54]. For example, in the pre-synaptic region, the precise orchestration of docking, priming and fusion of synaptic vesicles, that are crucial for neurotransmitter release or chemical synaptic communications, are tightly controlled by different gene families including the kinases, GTPases and Soluble N-ethylmaleimide-sensitive factor activating protein receptors (SNAREs)[55–57]. Such regulatory mechanisms facilitate efficient synaptic functions, aligning with the synaptic energy levels at the time point[58,59], thereby promoting optimal neuronal activity. Meanwhile, in the post-synaptic domain - the neurotransmitter receptors, post synaptic density proteins, the protocadherin family of cell adhesion molecules as well as GTPases and kinases, amongst other members – form the functional unit that relays the incoming signal to multiple regions of the cell[60], including the nucleus. Hence, synapses are critical functional units important for intercepting and relaying signals. Modifications of the synaptic strength, significantly, contributes to neuroplasticity and, thus, form the fundamental basis for higher level information integration

in dendrites, neurons and networks[61], thereby, modulating learning and memory as well as behavior.

As neuroplasticity occurs in response to environmental signals, stress also elicits multiple types of modifications in synapses, dendrites and spines[62,63], thereby, altering neural circuits in the brain. Such alterations lead to significant modifications in the reward pathway[64,65], emotion processing[66–69], decision making[70–72], learning and memory[73,74], etc. These behavior alterations are, indeed, symptomatic manifestations of underlying changes in neuroplastic connections between multiple brain regions including the PFC, dorsal and ventral hippocampus (vHipp), Naccu, hypothalamus, amygdala and the ventral tegmental area. For example, a study by Madur and colleagues[65] demonstrated that stress modified the basolateral amygdalar – Naccu pathway, along with dendritic hypertrophy and increased spine density of medium spiny neurons[75,76] in the Naccu. These types of modifications have been frequently associated with stress-induced anhedonia or shift in salience from reward to aversion[76]. Meanwhile, a decrease in the volume of the hippocampus (see review by Khan and colleagues[6]) that acts as a major hub for learning or memory formation and fear processing[77,78], is a consistently visible pattern in patients with major depressive disorders. The reduction in volume is associated with the loss of dendritic spinal density and neuronal death, that occur as a signaling cascade response to the influx of corticosteroids[6,79,80]. Indeed, these negative alterations can also be accompanied by a decrease in adult hippocampal neurogenesis[81] leading to cognitive decline as well as impairments of goal-oriented behavior[82]. Concurrently, the PFC region of the brain that is important for executive functions also shows a similar decrease in volume with reduction in neuronal density and dendritic atrophy of pyramidal neurons because of stress exposure[72,83]. In contrast, its connectivity with the amygdala, a part of the limbic system important for emotional reactivity, is increased[84]. In fact, a hyperactivated amygdala along with dendritic and synaptic hypertrophy in contrast to other brain regions, is, often, observed in depressed patients[67]. Apart from these critical brain regions, other regions that are important for sleep-wake cycle[85,86] as well as motor-related functions[87,88] are significantly altered following stress exposure.

As the neural circuit connections are intricately regulated by molecular machineries, the noted physical alterations in the synapses and brain structure suggest underlying modifications in the molecular signature. This aspect of molecular processes will be further explored in a later section. Though studies on humans, using non-invasive techniques offer

valuable insights into the brain volume or circuit alterations in mental-health disorders, in-depth mechanistic studies using human tissues for histological or molecular analyses can only be conducted using post-mortem samples. Unfortunately, use of post-mortem samples can only provide information on terminal changes and not the causative factors. Identification of the causative factors, or the early mechanisms underlying the development of debilitating stress effects, is critical for identification of potent therapeutics. Therefore, given the likely surge of stress-related disorders in the future, an early access to the ongoing alterations, soon after stress exposure, is imperative. As such, the judicious use of non-human models for advancing stress research and therapeutic discovery is fundamental[89]. The next section, thus, brings a brief overview of the existing models in contemporary stress research.

2. Models for stress research

To study the mechanisms behind stress response and resulting impacts, multiple models have been developed in Neuroscience. Though stress studies in humans remain the perfect tools for developing therapeutic applications, certain limitations ensue. This includes, first and foremost, the inability to study molecular mechanisms in the brain soon after exposure to stress. Therefore, for the purpose of the thesis, the following sections will discuss the current animal models, in brief.

2.1. Non-human model organisms in stress studies

Amongst many model organisms (*C. elegans*, *Drosophila*, rodents and non-human primates) used in neuroscience, rodents are the most commonly used stress models[90,91]. Although the research on rodents (mouse/rats) does not completely translate to human studies, such preclinical studies still provide important insights of molecular mechanisms behind behavioral modifications and therapeutic applications[92–94].

Different rodent models for stress induction – both acute and chronic stress – are prevalent in literature. Models for inducing acute stress [94,95] include forced swim test, tail suspension test, acute restraint stress etc., lasting for short durations. Meanwhile, models for chronic stress [29,91] include chronic restraint stress, chronic mild stress, chronic unpredictable stress, and **chronic social defeat (CSD) stress**. Amongst all the existing stress models, CSD is considered to possess **high construct validity, face validity and predictive validity**[96]. This is because CSD incorporates a form of social stressor, the most common type of stressors[15,97,98], responsible for depressive disorders in humans, wherein the defeated mice display individual differences in the stress response with a positive outcome following application of antidepressants[96].

CSD paradigm

Briefly, the CSD paradigm[64,98] is a modified form of the resident intruder stress exposure[99]. In this model, an intruder (male) is temporarily placed in the cage of a more aggressive male (see **Figure 2a**). Following the entry of the intruder, physical attacks from the resident ensue due to the territorial nature of rodents. Following brief periods of attacks, the resident and the intruder mice are then separated physically by a perforated mesh wall, while the sensory visual and odour stimulations are continued. The procedure is repeated for either a few days (acute) or for several days (chronic). The amplitude of stress delivered by this type of social

stressor is robust. For example, acute social defeat stress can elicit 30 times higher the number of arrhythmias as compared to non-social stressors such as foot shock, restraint stress or tail suspensions ([100] as cited by [101]) by activating the sympathetic autonomic nervous system. It also leads to an increase in blood pressure, higher amounts of plasma catecholamines and prolonged activation of the HPA axis[101–104]. This tunes in well with the robust activation of the HPA axis and the sympathetic nervous system in social stress experiments[15], thus implying a **high face** validity of this stress model.

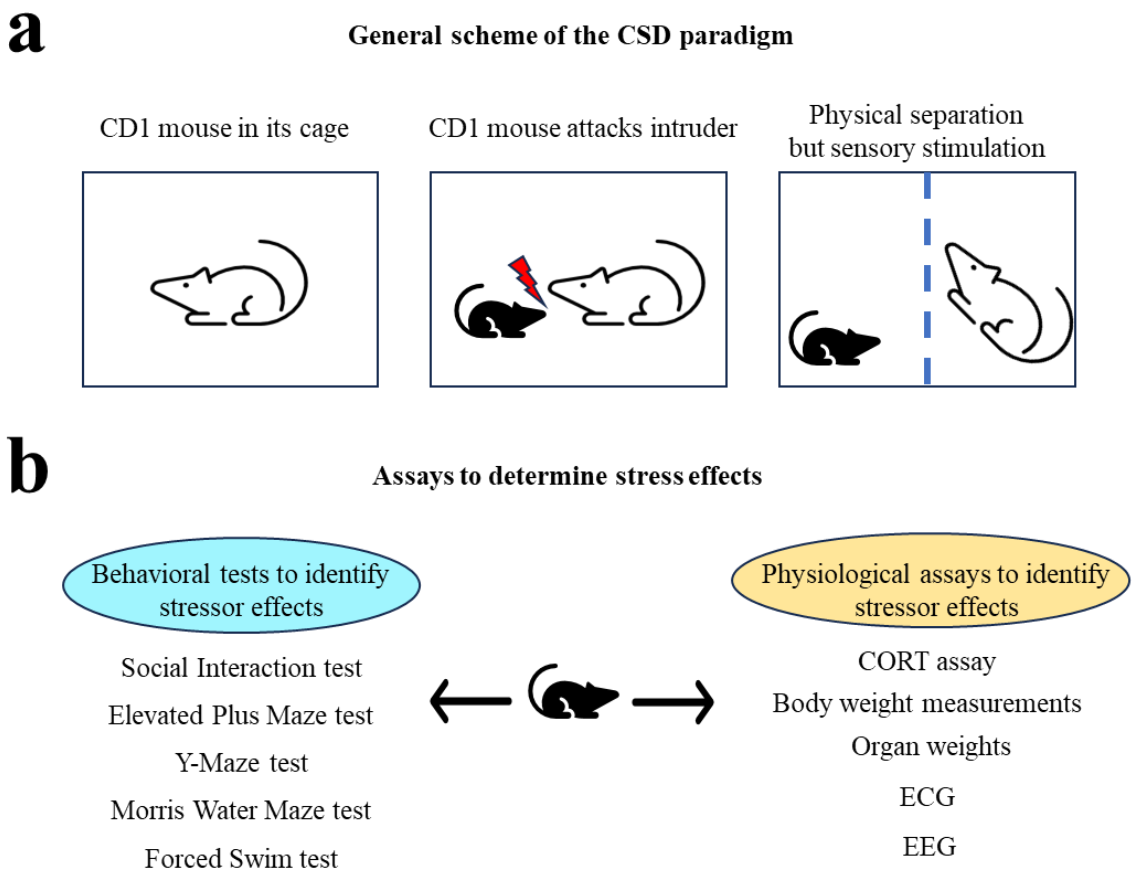

Figure 2: Chronic social defeat (CSD) stress paradigm and measures of stress effects.

a. General scheme of the CSD paradigm, where an intruder is placed in the cage of a resident male mouse (usually a CD1 mouse, white). Being territorial and owing to the larger size of the CD1 mouse, the black mouse suffers repeated physical attacks that could lead to the exhibition of social defeat and subordination behavior in the black mouse. The physical attacks last for a few seconds to minutes and is variable in different studies. Following the physical attacks, the mice are physically segregated by a perforated mesh wall, represented by the dotted blue line in **a**), usually for 24 hours. During this physical segregation, the black mouse is still subjected to both visual and olfactory stimulation from the dominant white mouse. **b.** Following the defeat procedure, the defeated mouse (black mouse) can be subjected to different assays (both behavioral and physiological) to determine the stress effect incurred by the applied stressors. Some of the tests are listed in **b**. **Abbreviations.** CORT – corticosterone, ECG – electrocardiography, EEG – electroencephalography

2.2. Use of genetically modified model organisms for stress research – engram approach

The use of genetically modified (GM) organisms in Neuroscience has been rapidly increasing. This is because GM models allow for the study of impacts of certain gene deletions or insertions either locally in a tissue region or globally[105,106], which would otherwise have not been possible in the wild-type model, devoid of gene manipulations. Recently, a genre of GM models that can be used for spatiotemporal tracing or control of cellular activities has gained popularity. This is because only a few cells termed as 'engram' cells[51,107] are activated during a particular stimulus to store certain patterns of information, related to the activity, in the brain. These cells are characterized by the expression of immediate early genes (IEGs) like *cFos* (Fos proto-oncogene, AP-1 transcription factor subunit) and *Arc* (activity-regulated cytoskeleton-associated) genes, rapidly, following the arrival of a stimulus/event[108,109]. Such engrams generated during a particular event persist for a long time[110] and upon recall of the memory or event, are more excitable than the non-engram cells[111]. The heightened excitability, in turn, allows for a faster expression of the IEGs. In stress research, this particular aspect of using only engram cells is very relevant as different engrams are known to be associated with susceptibility or resilience[112]. Since the brain consists of different types of cells with their own molecular signatures, it is indeed more desirable to increase resolution of a study by using only these engram cells. The GM systems that allow for the tracing of such spatiotemporally active cells focus on the Cre-LoxP with variations in activating the Cre recombinase, including Tetracycline-on/off systems, Tamoxifen_CreER^{T}/CreER^{T2} systems (see review by[113]) for rodents while GAL4/UAS systems[114,115] are popular in *Drosophila*. Amongst the available spatiotemporal control of gene expression for rodents, our study will focus on the Tamoxifen_CreER^{T2} system and will be described in more detail at a later section. Indeed, similar to the non-GM models (e.g., C57BL/6J), the GM models can also undergo stress. Effects of the induced stress can be examined by employing various assays, some of which are discussed in the next section.

2.3. Behavioral and physiological assays to determine the effects of the applied stress protocols

Stress-induced behavioral effects are determined by behavioral assays, which evaluate avoidance/interaction, exploration, memory, or hedonic/unmotivated behavior[94]. Some of

the common behavioral assays used to determine the impact of stress are enumerated below and depicted in **Figure 2b**.

Avoidance/Interaction - social interaction (SI) test– to assess deficits in social interaction after a stressful episode. In this test, the animals are assessed for their social interaction preference[96]. As mice are social animals, social bonding is known to be rewarding[116,117] and hence in a normal scenario, they would prefer interactions. However, in the case of depression/anxiety, the animals show avoidance behavior[118].

Exploration – elevated plus maze (EPM) test, light-dark preference (LDP) test – to determine anxiety. In these tests animals are assessed for their fear of open/ bright areas. A lower time spent in open areas is taken as a proxy for anxiety ([119,120] and review by Planchez and colleagues[94]).

Exploration/memory - Y maze test[121] – to determine memory deficits. In this test, animals are placed in a Y-maze box, where one of the arms of Y is initially closed. Then, the mouse is assessed on whether they could differentiate between the new arm and the old arm. (NB: There are other variations of the Y-maze experiment but will not be described further.)

Hedonic – sucrose preference (SP) test[122,123]– to investigate motivation, also used as measure for depression in animal models. In this test, the animals are tested for their preference of either water or sucrose, which they had access to *ad libitum.* Non-preference for sucrose is taken as a proxy for depressive behavior[94].

Motivation - Forced swim (FS) test[123]– to assess helplessness or depression. In this test, the animal is put in a half-filled cylinder to determine whether they would float (immobile) or swim. Immobility is considered a proxy for measuring hopelessness or depression[94]. Tail suspension test is also used as an assessment for helplessness[118].

Different behavior assays reveal underlying functions of distinct regions of the brain. As different stressors exert variable impacts on distinct brain regions[124,125], different behavior assays are employed for determining the spectrum of effects introduced by the stressors as in [126]. While each test has its own limitations, it falls beyond the scope of this thesis and hence will not be discussed further.

Physiological assays

Physiological assays aimed at determining the stress response, commonly, investigate the components directly or indirectly related to the HPA axis. For example, the most frequently

used tests to examine the physiological function of the HPA axis is the measurement of corticosterone (CORT) levels. In mouse experiments, an elevated basal CORT level predicts a resilient outcome, whereas a lower basal level is a predictor of susceptibility[127]. Indeed, low CORT levels following stress exposure are often associated with the development of post traumatic disorders[128]. In addition to the CORT tests, physiological assays such as measurements of heart rate (electrocardiography, ECG[129]) and brain activity (electroencephalography, EEG[130]) are also used to quantify the impacts of stress.

Of note, the physiological and behavioral manifestations of stress response indicate underlying molecular deviations from the norm, following stress exposure. These molecular machineries, especially 'epigenetics' will be comprehensively discussed in the next section.

3. Epigenetic mechanisms and their relevance in stress

Epigenetics, termed in 1942 by Conrad Waddington[131,132], refers to the heritable changes introduced in the (epi)genome of an organism, without altering the DNA sequence[133]. These alterations result from interactions with the environment, including exposure to stress[29], and can introduce far-reaching effects into the biology of the organism[132]. Epigenetic modifications encompass alterations in DNA methylation or hydroxymethylation, histone acetylation or methylation, chromatin accessibility as well as altered expression of mRNA transcripts, long non-coding RNAs and small non-coding RNAs[134,135].

Stressful life events dynamically alter epigenetic mechanisms by 'marking' the epigenome to generate cell-type specific epigenetic states and transcriptional profiles[136]. Thus, epigenetic mechanisms embed stressful life experiences within discrete neuronal populations, resulting in aberrant physiological and behavioral outputs in stress-related psychiatric disorders[137]. In this regard, DNA methylation, being a stable epigenetic marker, has garnered a significant interest as a plausible mechanism for encoding the long-term effects of stress in the epigenome, especially in post-traumatic disorder (PTSD) studies[138–140] .

Despite the prevalence of multiple epigenetic mechanisms, for the purpose of the thesis, the discussion of epigenetics is limited to the basics of DNA methylation and RNA (epitranscriptome), their crosstalks and contemporary relevance in stress studies, for the scope of this thesis. See **Figure 3** for a simplified representation of the molecular section to be discussed.

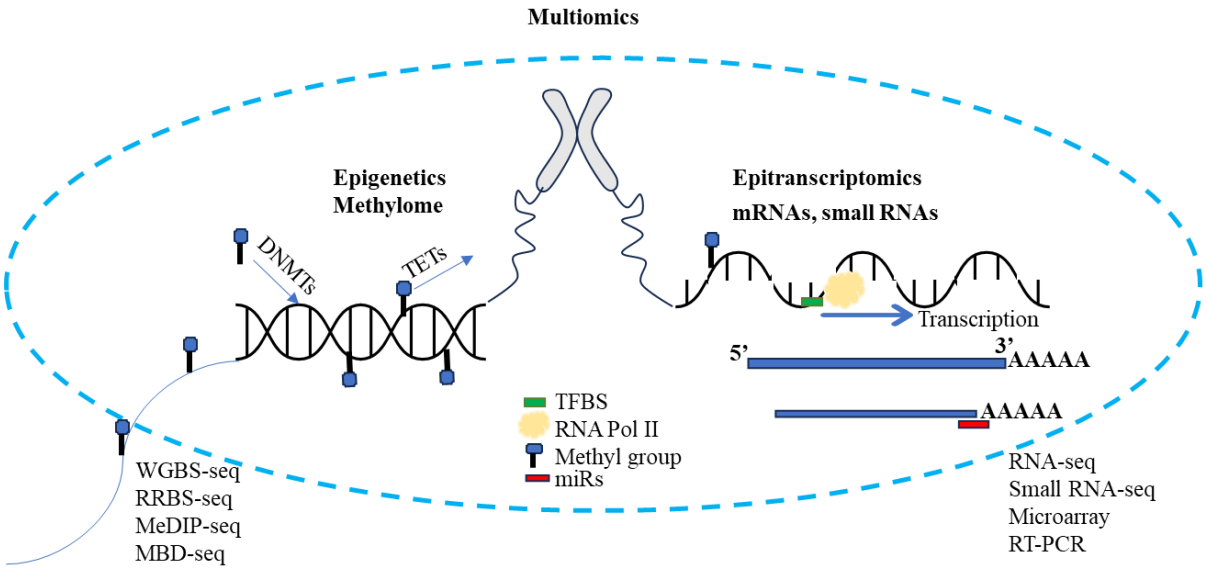

Figure 3: Simplified representation of the cellular omics machineries to be accessed within the framework of the thesis.

Methylome is modulated by the antagonistic activities of DNA methyltransferases (DNMTs) and ten-eleven translocation enzymes (TETs). DNMTs facilitate the addition of a methyl group to the cytosines and other bases of the DNA, while TETs oxidize the methyl groups, ultimately resulting in their removal. Methylome can be accessed by multiple omics sequencing techniques including, whole genome bisulfite sequencing (WGBS-seq), reduced representation bisulfite sequencing (RRBS-seq) methyl-DNA immunoprecipitation sequencing (MeDIP_seq) and methyl-CpG binding domain MBD2 sequencing (MBD_seq) On the other hand, transcription of mRNA is controlled by the presence of multiple components including transcription factors (TFs) in the transcription factor binding site (TFBS) and RNA Polymerase II (RNA Pol II) along with the favourable presence of other transcription initiation factors or in the rare case even a methyl group, upstream of the transcription start site. The resulting mRNAs usually possess a poly A tail at the 3' direction, which is targeted by the miRs. Very often, the binding of the miRs with the mRNAs lead to the degradation of the mRNAs, however in rare cases, miRs can upregulate the expression of its target mRNAs (see text). The ongoing epitranscriptomics dynamics can be assessed by different sequencing techniques including RNA-seq, small RNA-seq and RT-PCR. **Abbreviations:** DNMTs - DNA methyltransferases, TETs – ten-eleven translocation enzymes, WGBS-seq - whole genome bisulfite sequencing, RRBS-seq - reduced representation bisulfite sequencing, TF – transcription factor, RNA Pol II - RNA polymerase II, MeDIP-seq - methyl-DNA immunoprecipitation sequencing, MBD-seq - methyl-CpG binding domain MBD2 sequencing, RT-PCR – reverse transcription-PCR

3.1. DNA methylation of the genome - methylome

DNA methylation, commonly, refers to the addition of a methyl group on the cytosine base in the DNA, at CpG positions i.e., a cytosine base followed by a guanine base linked with a phosphate bond. More recently, other variations have been discovered. For example, methylation of cytosines in a non CpG context, i.e., CHH or CHG, H refers to adenosine or thymidine bases or methylation of non-cytosine bases at A and T positions of the DNA[141,142]. Apart from methylation, hydroxmethylation or formylation – oxidation by-products of methylation, have also been shown to possess biological importance[137]. As DNA methylation can be inherited over several cellular divisions, it is considered one of the most stable epigenetic

markers for cellular memory[143,144], making it a desirable candidate for studying long term maintenance of stress/fear memory.

DNA methylation was discovered in the early 1920's[145] much later than the transcriptome (1868). In the 1970s, methylation was thought to only suppress gene expression[145]. However, some of the recent findings show that the role of DNA methylation in gene expression may not be that of suppression only, but also activation[146]. DNA methylation is dynamic[147], i.e., it can be edited via the antagonistic functions of two enzyme families, DNA methyl transferases (DNMTs) and ten-eleven translocation enzymes (TETs). The interplay between the DNMTs and TETs forms the major basis for the dynamic control of activity dependent gene expression through DNA methylation. DNMTs (DNMT1, DNMT2, DNMT3A/B/C) catalyse the transfer of a methyl group from S-adenosylmethionine to a cytosine group or other groups, resulting in the formation of 5-methyl-cytosine or other methylated groups. DNMT3A and DNMT3B are responsible for the *de novo* DNA methylation (with DNMT3A being the most prevalent in the brain) while DNMT1 along with methyl-CpG-binding proteins maintain the methylated state during multiple rounds of cell division (see review [148]). On the other hand, the TETs (TET1, TET2 and TET3) convert the methyl group via iterative oxidization to hydroxymethyl, formyl and carboxyl groups (see review by [148]), subsequently, with each of the groups possessing unique biological importance[137]. Thereafter, the formyl and carboxyl groups are removed by thymine DNA glycosylase (see review by [148]).

Of note, DNA methylation modifications are confined not only to the genic regions but also extend to the intergenic positions[145]. Additionally, methylation, itself, is not restricted to DNA and can also occur in other biological molecules including RNA and histones with important functional roles. For more information, please refer to the reviews by [149,150].

3.1.1. Accessing the methylome

The methylome can be assessed by multiple techniques for either target-specific studies or genome-wide investigations[151]. For instance, gene-specific pyrosequencing technique is a popular technique for methylome analysis in target-specific studies[151,152]. Meanwhile, for genome-wide studies, protein-based techniques including methyl-DNA immunoprecipitation sequencing (MeDIP-seq[153]) or methyl-CpG binding domain MBD2 sequencing (MBD-seq[154]) and bisulfite-treatment based techniques including whole genome bisulfite sequencing (WGBS-seq[155]) or reduced representation bisulfite sequencing (RRBS-seq[156,157]) are prevalent[151].

An advantage of genome-wide studies over target-specific studies, is the ability to provide new insights in previously undermined/undetected regions. This is specifically important for our purpose as we aim to investigate previously undermined genes or networks behind stress resilience and susceptibility, globally. Of the mentioned genome-wide sequencing tools, WGBS-seq and RRBS-seq can report modifications at single bases, thereby increasing the resolution of a study. Between the WGBS-seq and RRBS-seq, we will employ the RRBS-seq due to its relative ease of access to regions of the methylated genome with a comparatively lower cost than WGBS-seq[151]. Briefly, in the RRBS-seq, bacterial MspI enzyme cleaves the genome at CCGG sites, thereby, retaining only fractions of the genomic DNA that contain these sites. Because of the smaller proportion of the genome to be sequenced, the cost is significantly reduced. Although a relatively smaller proportion of genomic DNA is retained, this proportion has been shown to cover 60% of the promoters[158].

3.1.2 Relevance of DNA methylation in stress research

Environmental stimuli, including neuronal activity, learning and memory or stress induction stimulate methylation/demethylation of certain regions in the genome[136]. This chain of effects is partially mediated by the binding of the GCs of the HPA axis to the nuclear glucocorticoid receptors (GRs)[159]. The GRs in turn stimulate active transcription-binding mediated DNA methylation/demethylation through glucocorticoid response elements[160], thereby altering the epigenomic landscape. Some well-known examples of stress-induced alterations in methylation including that for the systems involved in inflammation, neurotransmitters, neurotrophic factors and metabolism are discussed briefly.

Decreased methylation in the **inflammatory** cytokine *Interleukin-6 (IL-6)* gene was detected in elderly depressed individuals as compared to non-depressed healthy individuals[161]. This finding was corroborated by a decreased methylation of cytokine *IL-6* in African American men after childhood trauma[162]. Indeed, a decreased in intronic methylation (intron 7) of another immunoregulation gene, encoding FKBP Prolyl Isomerase 5 (*FKBP5*), was associated with a higher reactivity to psychological therapy in subjects with phobia[163]. Apart from the alterations in the inflammatory factors, DNA methylation modifications in **neurotransmitter** genes are also profound. For instance, methylation of '*oxytocin*' and '*serotonin*' neurotransmitter receptors are associated with susceptibility traits (see review by [164]). Meanwhile, an increase in the methylation of metabotropic glutamate receptors (mGluR) in the hippocampus, m*GluR1* and m*GluR5*, in prenatally stressed mice[165] is associated with depressive-like behaviors. On the other hand, childhood abuse has been associated with increased methylation of the 'happy

hormone' serotonin transporter gene, solute carrier family 6, member 4 (*SLC6A4* exon 1) (see review by [160]). Indeed, alterations in the methylation of genes linked to **neuroplasticity** are also consistent. For example, following early life stress, exon 4 of brain derived neurotrophic factor (*BDNF)* is hypermethylated in the hippocampus[166]. This could be the basis for synaptic atrophy and reduction of volume in the hippocampus[80] that accompanies maladaptive stress response. Remarkably, inhibition of DNMTs result in rapid changes in the expression of genes involved in neuronal plasticity[167]. Meanwhile methylation of **metabolic** genes in response to stress is also profound. For example, blood samples from adults with mothers exposed to the Dutch Hunger Winter showed less methylated cytosines (mCs) in the gene encoding insulin growth factor 2 (*IGF2, a* gene associated with glucose metabolism[168]). Apart from modulating these different systems, methylation can also modulate the HPA machineries themselves. For example, in a study by [169], the nuclear receptor subfamily 3 group C member 1, *NR3C1*, was hypermethylated at the genic region (exon 1F) in association with 'bullying' in adolescents. In fact, the hypermethylation at this genomic region is also known to be associated with internalising the psychopathological symptoms of atrocities faced during adolescence[170]. Thus, from these studies, we can clearly estimate the important role of methylation in association with stress and depression.

3.2. RNA (mRNAs and non-coding RNAs) – transcriptome

RNAs are functional single-stranded copies of the template strand of the DNA, broadly divided into coding RNAs and non-coding RNAs. Coding RNAs give rise to proteins, generally termed as messenger RNAs (mRNAs) and are transcribed by RNA polymerase II[171]. Based on the environmental influence (internal or external), different functional mRNA transcripts can be generated from the same primary transcript via alternative splicing of introns[172]. On the other hand, non-coding RNAs (ncRNAs) include transfer RNAs (t-RNAs) and ribosomal RNAs (rRNAs), which are transcribed by RNA polymerases I and III. They also undergo splicing of introns from the primary transcript. Apart from these, the other types of non-coding RNAs include long non-coding RNAs and small non-coding RNAs. Amongst the small non-coding RNAs, the most prominently studied are the miRs, first discovered in 1994[173]. miRs are macromolecules about 16 to 25 nucleotides in length, conventionally, transcribed from miR genes by RNA Polymerases II or III into a primary miR transcript (pri-miR)[173]. pri-miRs are further processed to obtain mature miRs, which are important for post transcriptional gene regulation by translational repression or direct mRNA degradation[174]. Interestingly, in a non-conventional role, miRs can also upregulate the expression of the target gene[175–178]. The other

relatively new non-coding RNAs include piRNAs (Piwi interacting RNAs), small nucleolar RNAs (snoRNAs) and snRNAs (small nuclear RNAs).

3.2.1. Accessing the transcriptome

RNA sequencing (RNA-seq, bulk sequencing or single cell sequencing) is the most widely used technique for accessing a wide range of gene expression pattern inside a cell. Apart from these, other commonly used assays include microarrays or reverse transcription (RT-PCR) for assessing the levels of expression of small portions of the transcriptome (domain-specific or gene-specific).

3.2.2. Relevance of transcriptome alterations in stress

Multiple modifications in the transcriptome have been identified in association with stress disorders or depression. In fact, the transcriptome is the most exploited area of stress research due to its ease of access. The next few paragraphs discuss some of the interesting findings from both coding and non-coding RNAs (miRs) in relation to stress studies.

As in the methylome, the association of stress response with **immunoregulation/inflammation** is also observed at the level of the coding transcriptome. Upregulation of cytokines is associated with susceptibility or the depressive state[179]. Meanwhile, a downregulation of the glutamatergic **neurotransmitter** system, *Camk2b/Glua1* pathway is observed in susceptible mice[180]. In addition to the impacts of stress on the immune and neurotransmitter systems, alterations in the **neurotrophic** factors are also reported. A decrease in *BDNF* expression is commonly associated with susceptibility and depression[181,182], although there are other reports showing contradictory results[183].

Apart from alterations in the coding RNA expression, miRs also play an important role in regulating stress and depression in individuals[184,185]. *miR-137,* that targets the cytokines like *IL-6*[186], is downregulated in depressed patients with suicidal behavior[187]. Meanwhile, *miR-124-3p,* that plays an important role in synaptic plasticity, was found to be upregulated in most brain regions in the post-mortem samples of patients diagnosed with major depressive disorder[188]. As *miR-124* targets the **glutamate** ionotropic receptors (*Gria3, Gria4*) and glucocorticoid nuclear receptors (*Nr3c1*)[188], an upregulation of *miR-124* would entail a depression of the glutamatergic system and GRs, which are commonly observed phenomena in stress-susceptibility and depressive-like behaviors[189]. Furthermore, *miR-135* and *miR-1202* that regulate **serotonergic neurotransmitter** systems have been found to be downregulated in major depressive disorder (MDD) patients[190,191]. Meanwhile *miR-9,* that is involved in the regulation of the dopaminergic system, showed a reduced expression in experimental subjects

that faced early life stress[192]. In contrast, elevated levels of other miRs, including *miR-221*, *miR-132*, *miR-182* and *miR-155* have been shown to be correlated with the decrease of **neurotrophic factors** like *Bdnf* and *Cntf* (see review by [184]). These highlight the critical roles of miRs in stress regulation. However, very little is known about the roles of the other small non-coding RNAs in stress-related disorders, though, they have been indicated to play important roles in cancer[193] and neurodegenerative diseases[194].

From the above sections, it is evident that multiple molecular machineries are affected by stress. Noteworthy is that most studies investigate only a part of the epigenetic machineries at a time point[183,195–198]. However, efficient cross-talks between the different levels regulate the execution of a particular phenotypic state, suitable for meeting an environmental demand/resilience. Therefore, studying only one omics level at a time point gives us only a snapshot and may not fully capture the cellular environment to understand 'causative' factors of a disorder[199]. To elaborate on this importance, the next section discusses the complicated cross-talks in brief.

3.3. Crosstalks (multiomics) between different epigenetics levels

DNA methylation can either increase or decrease the expression of a gene based on the prevailing factors. For example, methylation of cytosines at TFBS themselves could either inhibit the binding of transcription factors (TFs) via steric hindrance, thereby reducing gene expression or alternatively, the methylation itself can recruit transcription factors, thereby increasing gene expression[200–202]. On the other hand, methylation, itself, can occur as a consequence of gene repression[203,204]. Apart from this, changes in methylation may occur before or as a result of the alterations in the transcriptome at a given time point[205,206]. and thus, may not correlate at a given time point. Local synaptic alterations, from an incoming stimulus, can lead to prompt but transient transcriptomic changes, followed by slower epigenetic modifications[207], emulated by synapto-nuclear messengers[208], that can alter long-term cellular memory. Subsequently, in the complexity of biological cascades, the epigenetic modifications can generate a different molecular baseline via the generation of a permissive epigenome, thereby, modulating future transcriptional states[205] and cellular memory. This marking of the genome to embed experience (cellular or behavioral) primes the epigenome (epigenetic priming) to alter future transcriptional states. For instance, Provencal and colleagues[209], identified that the appearance of an epigenetic mark in response to glucocorticoid exposure, using mouse neural progenitor cells, may not necessarily lead to an alteration of basal level gene expression. On the other hand, gene expression does not depend only on DNA

methylation but can also be regulated by other small-RNAs, for example, the miRs. Though the miR-RNA relationship has been generally understood to be antagonistic in nature, it has been shown that miRs can also promote the translation of the target gene itself[210], or upregulate gene transcription by targeting promoter elements[211]. Additionally, miRs in the nuclei can interact with promoter DNA or enhancer regions, thereby leading to an upregulation of the RNAs instead of the conventional mechanism of downregulation via Dicer/RNA-induced silencing complex (RISC)[177].

Thus, the cross-talks between the different epigenetic mechanisms are complex and, specifically, after an environmental insult, alterations occurring at one level may not exhibit simultaneous manifestations at other levels, at a given time point. This is because a molecular module (wave) may propagate through the organismal system with varying speeds and temporal dynamics giving rise to the inevitable 'phase lag or time lag[212]' between different molecular levels as observed in [213] for transcription and chromatin accessibility. Apart from this, by the time the cellular machineries are investigated, the disease trajectory could already have deviated from the starting point[199]. As such, investigating the etiology of complex disorders such as stress and depression to determine the causative factors can be challenging by investigating only one level. Therefore, to capture a better picture, a more appropriate study design would be to assess as many epigenetic machineries as possible, within a single study, for cases, where longitudinal assessments are not feasible.

Genetic predisposition to susceptibility and resilience

Though the various levels of epigenetics and their cross-talks play an important role in stress response, it is imperative to note that the 'genetic predisposition', i.e., the influence of an individual's genetics, still exercises an equally substantial impact in determining stress outcomes[214–216]. In fact, genetic predisposition can influence the epigenome response itself[217], thereby, indirectly, influencing the reactivity to stress. For example, single nucleotide polymorphisms associated with either the presence of A/T or C/G in the intron 2 (containing a glucocorticoid response element) of *Fkbp5* can modulate the methylation levels[137,218]. Therefore, genetic predisposition is an important criterion in influencing the Waddington landscape[132] towards resilience or susceptibility.

4. Scope of the thesis – aims and objectives

4.1. Summary background and identification of research gaps

As discussed in the preceding sections, the incidence of stress-related disorders is increasing and will likely escalate in the next few decades as an indirect consequence of urbanisation. This escalation is potentiated by the recent COVID lockdowns, wherein the WHO estimates a substantial increase in mental health problems in the coming years[5]. Mental health problems alter not only an individual's personality but also decrease the overall quality of life. Most of the mental health problems arise out of the inability to cope with the varied types of stressors that individuals encounter. Of the myriad of stressors, psychosocial stressors are the most prominent in humans[15]. Susceptibility to such stressors results in mental handicap that can be transient or persist for a long term, for instance, in the case of PTSD. Apart from provoking psychological disorders, prolonged exposure to stressors, increases the risk of developing other debilitating disorders including neurodegenerative diseases[219], cardiovascular diseases[220] and even cancer[221]. Interestingly, an individual's experience with stress can even alter stress response dynamics of their progenies[134,137]. Therefore, unravelling the early causative mechanisms behind the divergent response towards resilience and susceptibility is imperative.

As surmised in the previous sections, it is noteworthy that different disciplines of stress-research have indeed contributed immensely to the field, with the identification of multiple structural as well as molecular alterations in different brain regions. However, majority of the molecular studies are derived from mouse models as human studies are limited to either non-invasive methods (e.g., magnetic resonance imaging, MRI[222]; electroencephalography, EEG[223]) or post-mortem samples[224]. The utility of inbred mouse models in epigenetic studies, is further accentuated by the diminished contributions from genetic predispositions within the obtained differential patterns between stress-resilient and stress-susceptible populations. The prevailing mouse model to study susceptibility-resilience patterns in response to social stressors is the CSD paradigm. Renowned for its high face validity, construct validity as well as predictive validity, the CSD model serves as an excellent social stress model[96,98]. However, despite the increasing number of publications using CSD stress models, **multiple factors impede the quest to identify the causative factors behind the two divergent behavioral patterns, thereby reducing the predictive potential of novel therapeutic targets.**

First, most of the molecular investigations for susceptibility-resilience mechanisms are derived from bulk tissues. Although studies using bulk tissues have provided interesting mechanistic

insights into the molecular alterations following stress exposure, they portray an average of the existing molecular profiles from heterogenous cell types. Recent studies[225,226] have demonstrated that the complexity of a disease phenotype could be overlooked when analysing bulk tissues, as different cell types within tissues express different or opposing signaling patterns and epigenetic signatures. In other words, not all cell types contribute equally to disease progression or disease spread[227–229]. Hence, data derived from bulk tissues can mask essential but subtle signals from specific cells (engram cells) that are involved in distinct behavioral activities. **As different stress phenotypes have been shown to be associated with different engram cells[112], use of bulk tissues diminishes the potential to identify elusive mechanisms from the relevant cells.** Therefore, specific engram studies have become increasingly relevant in contemporary literature for stress as well as non-stress related studies[107,111,230–233].

Second, a multitude of studies investigating the divergent stress phenotypes using the CSD paradigm analyze only one epigenetic machinery (single omics study) at a time. Indeed, **in section 3.3**, we noted the existence of a complicated dynamics between different epigenetic levels, highlighting that the analysis of only one molecular level, at a time point, will not be representative of the other levels. Additionally, the pathophysiology of stress disorders is complex and involves multiple modifications at the interconnected, yet different epigenomic modules. In such disorders with multiple etiological factors and no clear deterministic factors, a single layer of data, for example, transcriptome captures only a snapshot of the ongoing alterations. Therefore, such analysis will likely provide only associative results with less probability of identifying causative factors[199]. This is because, in biological disease cascades, the reactive paths triggered by the initial signaling cascades mask the few causative factors and the search for causative factors could be lost in associative result interpretations from just one sequencing data[199,234,235]. Thus, experimental approaches limited to analyzing a single molecular signature at a specific time point, such as only transcriptomics do not offer sufficient information to ascertain underlying causality of complex disorders or 'causative' factors of a phenotype. Therefore, endeavours to pinpoint critical junctures for susceptibility-resilience divergence and the subsequent identification of suitable drug targets are thwarted by study designs relying on single-omics investigations, covering only a particular timepoint.

Naturally, the best scientific approach would be to follow the molecular alterations with experiments to assess the alterations longitudinally as conducted by [183] and [213]. However, a longitudinal study is not always practical *in-vivo* or *in-vitro*. The other approach that

researchers follow to circumvent the analysis of only one omics level at a time point, is the comparison and integration of different studies, where complementary epigenetic mechanisms are investigated. Intuitively, such an approach is often complicated with the administration of different stress protocols and sample collection timelines in different studies, which are known to impact the molecular outcomes differentially[93]. Considering the limitations posed by longitudinal studies or literature comparisons, there is an urgent need for more comprehensive and integrative approaches that can capture the molecular changes occurring at different levels of the cellular machinery[199,234–239]. Thus, a multiomics approach applied within the same study would provide a more comprehensive insight into the complex molecular underpinnings behind stress disorders. Since multiomics provides access to the different levels of molecular machinery inside the cellular network, it creates an opportunity to integrate multiple layers of molecular information[240], that are not at the same state of transition. Such an approach would inevitably increase the resolution in following a disease pathway, thereby offering a better opportunity for a holistic understanding of the flow of information underlying complex neuropsychiatric diseases[238]. Subsequently, a better understanding of the causal pathways would allow for the development of potential therapeutic targets.

Conclusively, the two **research gaps** in studying resilience-susceptibility mechanisms include **use of bulk tissues and single omics approaches** (See **Figure 4a**). In the next section, we propose the experimental design to bridge the gaps.

4.2. Study design to bridge the gaps

In our study, we propose to bridge the current research gaps by investigating specific spatiotemporally activated **engram** populations using a **multiomics** approach (See, **Figure 4a,b**). For this purpose, we will employ a GM mouse line that will facilitate the tracing of engram populations. Thereafter, the engram populations will be analyzed with a combination of sequencing techniques to access multiple layers of molecular machineries.

The GM mouse line to trace spatiotemporally activated populations is obtained by coupling a Tamoxifen (TAM) – inducible IEGCreER^{T2} promoter mouse line[241,242] with the reporter mouse line *R26-CAG-LSL-Sun1-sfGFP-Myc*[243], that contains a loxp stop codon (**Figure 4b**). In the IEGCreER^{T2} mouse lines, *CreER^{T2}* mRNA is expressed within a few minutes of the stimulus interception, via the activation of the IEG promoters (spatial control). In the absence of TAM, CreER^{T2} (protein form) remains in the cytoplasm, while in the presence of TAM, the CreER^{T2} can enter the nucleus to cleave the loxP stop codon, upstream of the reporter superfolder GFP

(sfGFP). Once the stop codon is cleaved, the activated cell will continue expressing nuclear membrane sfGFP, which can be traced. Once the nuclei of the activated cells are marked, they can be segregated using contemporary methods. Though the marked cells, themselves, can be segregated, we argue that different cells have different sensitivity to a dissociation process, whereas nuclei are more robust. For example, in a single cell study by Vennin and colleagues[244], the majority of neurons was lost during the dissociation process, thereby skewing the representation of different cell types in the data.

The engram nuclei that are marked with sfGFP expression will, then, be processed with different sequencing techniques to facilitate the application of a multiomics approach. This is because a multiomics approach (RRBS-RNA-small RNA) would allow for a more exhaustive investigation of the convergence/critical diverging points of signaling cascades underlying the divergent phenotypes. Apart from this, network analyzes[245], which exploits the idea that genes do not function in an isolated manner but rather as components of intricate networks of protein-protein interactions, protein-DNA interactions, DNA-ncRNA interactions, mRNA-ncRNA interactions etc., that are tightly regulated by a complex orchestra of transcription factors, co-factors and several signaling cascades, will also be employed. We posit that such integrative approaches would facilitate a better understanding of the ongoing alterations, following stress exposure.

Therefore, the **uniqueness** of the work for this thesis lies not only in examining the cellular alterations **within the active populations that govern a stress-phenotype** but also in the adept integration of **DNA methylation, transcriptome and nuclei miR within the same experimental framework.** To our knowledge, this study presents the first case of adopting a multomics approach using engram nuclei for an in-depth investigation of the methylome and small RNA (from the nuclei) along with the transcriptome, for CSD studies. We hypothesize that such an integrative approach will help us formulate a high-resolution picture and thus, a more comprehensive understanding of the ongoing cellular modifications. Consequently, this would facilitate a proper delineation of the sequence of events to enable the identification of the causative factors. Such a holistic perspective could, perhaps, create new avenues for novel therapeutic targets.

4.3. Methodical steps to obtain engram-multiomics data

Attempts to determine the causal pathways underlying the divergent stress phenotypes poses a formidable challenge. To effectively address such challenges, an intricate study approach had

to be formulated. For practical implementation of the approach, systematic and meticulously curated experimental designs, incorporating appropriate controls, are fundamental (see **Figure 4c**). These measures are essential to guarantee a proper interpretation of thus obtained multiomics data. For a comprehensive overview, the systematic stages of the experiments to achieve our objectives are outlined below:

1. **Choice of Cre driver line:** Given that *cFos* and *Arc* show different expression patterns, implementation of a suitable experimental design was necessary to choose either the cFosCreER^{T2} system or ArcCreER^{T2} system to be coupled with the reporter line, for the subsequent studies.
2. **Establishment of an optimal CSD paradigm for the resulting GM mouse line (CreER^{T2}-GFP system):** Since GM mouse lines possess distinct behavior traits, an optimal stressor had to be developed for our study design.
3. **Development of a nuclei isolation protocol suitable for small tissue volumes:** As studies using dissociated cells can be biased, we opted for the use of nuclei. To gain access to the nuclei for small volumes of micro-dissected brain regions, an optimized nuclei isolation protocol to obtain nuclei of good quality and yield, had to be developed.
4. **Choice of a proper sorting technique to segregate the marked engram nuclei from the total nuclei:** To gain access to the engram nuclei, characterized by a marked appearance of the super folder GFP positive (sfGFP+) expression on the nuclear membrane of the stimulus-activated cell, a proper nuclei-sorting technique had to be optimized as required by the nature of the study.
5. **Curated multiomics data integration and interpretation:** Having systematically laid the groundwork in the preceding stages, resulting in the generation of the multiomics data, this stage deals with the main objective of the thesis to investigate the alterations in the epigenetic landscapes of stress-resilient and stress-susceptible engram nuclei by integrating data from different layers of molecular machineries. A better understanding of the flow of events would facilitate a better therapeutic approach.
6. **Tissue level differences in stress response and future implications:** Given the opportunity of the unique access to engram nuclei, we also looked at the differential patterns of tissues (PFC vs vHipp) towards stress response, with regards to DNA methylation. A sound understanding of the differences would be crucial for drug applications.

NB: The next pages present our findings in the form of chapters for the thesis.

Figure 4: Blueprint of the project design.

a. Flowchart representation of the identification of research gaps and postulations to fill the gaps. **b**. Mouse line: Use of double transgenic (TG) IEG-GFP mouse line obtained from cross breeding between IEGCreER^{T2} promoter line and R26*CAG-Sun1-sfGFP-Myc* reporter line. The IEG-GFP system allow for the tracing of nuclei that were spatiotemporally activated by a stimulus in the presence of tamoxifen (TAM). On the arrival of a stimulus, the promoter of the immediate early gene (*IEG – Arc/cFos*) becomes active and *CreER^{T2}* is transcribed. The *CreER^{T2}* is then translated into a protein and remains in the cytoplasm in the absence of TAM. In the presence of TAM, the Cre recombinase can enter the nucleus and cleave the STOP codon upstream of the Sun1-sfGFP-Myc reporter construct, allowing for the expression of nuclear membrane GFP, which accumulates over time and can be traced. Stress paradigm: Chronic social defeat paradigm, where the intruder mouse is subjected to repeated defeat sessions and the effect of stress on the test mice (black) will be assayed with a social interaction test (SI). During this test, mice that approach the CD1 mouse will be termed 'resilient' and mice that avoid the CD1 mouse will be termed 'susceptible'. Multiomics approach: Engram nuclei (marked in green) of selected mice will be analyzed using RRBS-seq, RNA-seq and small RNA-seq. **c**. Systematic approach towards the development of multiomics data for an exhaustive investigation of the differential landscapes of resilient and susceptible animals. With the choice of an appropriate promoter line, the resulting double TG mouse line will be characterized to develop a suitable stressor. Optimized protocols to facilitate extraction of GFP expressing engram nuclei will be developed. Thereafter, with refined protocols for library preparation, sequencing and analyses of RRBS-seq and miR-seq (small RNA-seq) along with RNA-seq[246], an exhaustive search for plausible causative factors underlying the divergence and persistence of the stress phenotypes will be performed, to determine potent therapeutic targets. **Abbreviations:** TG - transgenic, IEG - immediate early genes indicating either *cFos* or *Arc*, FANS - fluorescence-activated nuclei sorting, INTACT - isolation of nuclei tagged in specific cell types

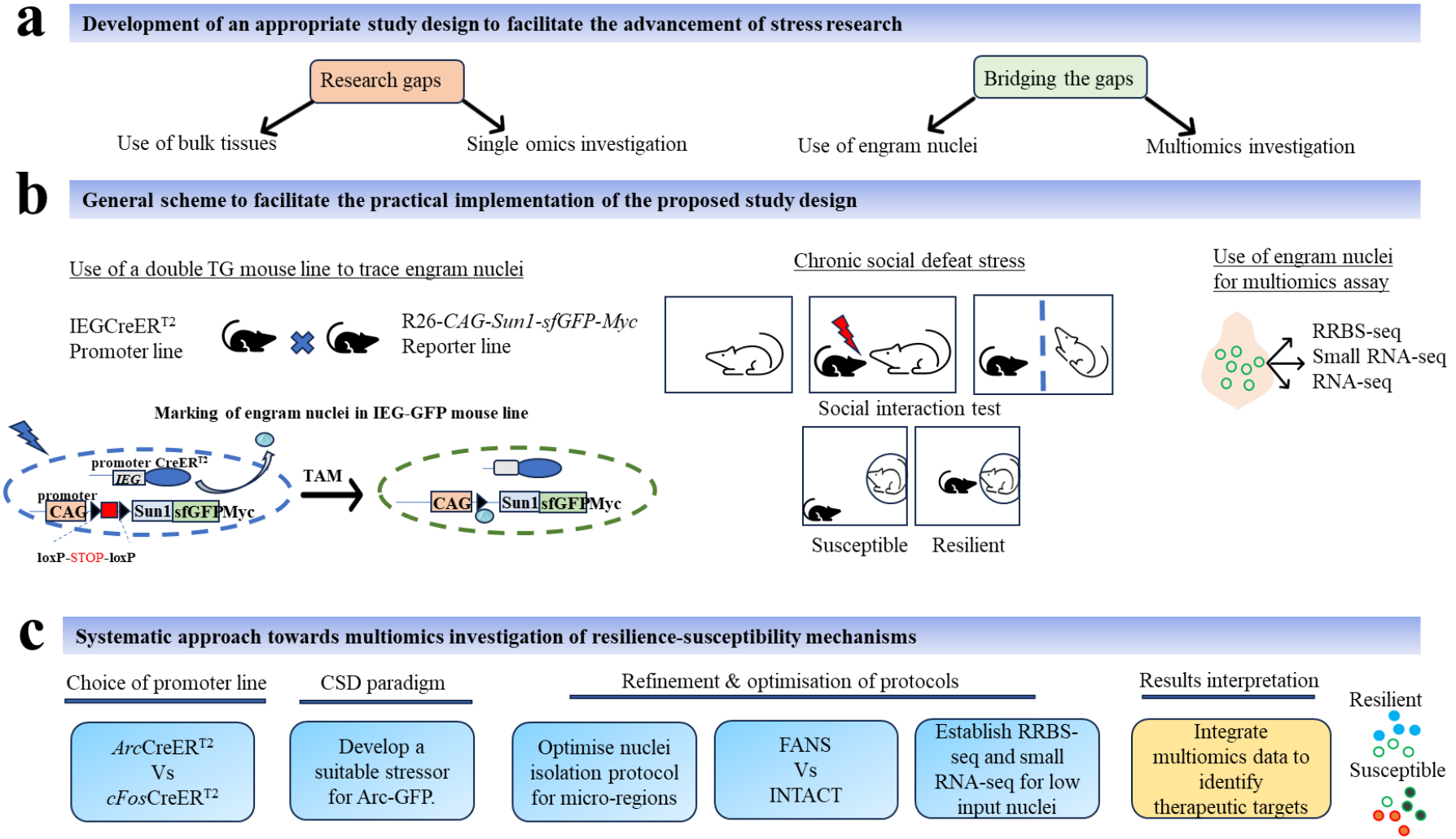
a
Development of an appropriate study design to facilitate the advancement of stress research
Research gaps
Use of bulk tissues
Single omics investigation
Bridging the gaps
Use of engram nuclei
Multiomics investigation
b
General scheme to facilitate the practical implementation of the proposed study design
Use of a double TG mouse line to trace engram nuclei
IEGCreER^{T2}
Promoter line
R26-*CAG-Sun1-sfGFP-Myc*
Reporter line
Marking of engram nuclei in IEG-GFP mouse line
promoter CreER^{T2}
IEG
promoter
CAG
Sun1sfGFPMyc
loxP-STOP-loxP
TAM
CAG
Sun1sfGFPMyc
Chronic social defeat stress
Social interaction test
Susceptible
Resilient
Use of engram nuclei for multiomics assay
RRBS-seq
Small RNA-seq
RNA-seq
c
Systematic approach towards multiomics investigation of resilience-susceptibility mechanisms
Choice of promoter line
*Arc*CreER^{T2} Vs *cFos*CreER^{T2}
CSD paradigm
Develop a suitable stressor for Arc-GFP.
Refinement & optimisation of protocols
Optimise nuclei isolation protocol for micro-regions
FANS Vs INTACT
Establish RRBS-seq and small RNA-seq for low input nuclei
Results interpretation
Integrate multiomics data to identify therapeutic targets
Resilient
Susceptible

Chapter 1. Choice of TAM-inducible IEGCreER^{T2} mouse line and optimization of TAM injections for further experiments

1.1 Introduction

Mammalian brain consists of distinct cell types, where only a subset of them actively participates during a specific behavioral activity or storage of memory, thereof. This subset of cells is termed 'engram cells' for that event[107,232,247,248]. Notably, studies have shown that resilience-susceptibility phenotypes are associated with different engrams[112]. Therefore, to enhance the precision of future omics experiments employing engrams, we sought to use a TAM-inducible IEGCreER^{T2} promoter mouse line[241,242], where IEG = *cFos* or *Arc,* coupled with a reporter mouse line R26-*CAG-Sun1-sfGFP-Myc*[243]. This reporter line contains a Cre target-loxP stop codon, upstream of the sfGFP insert (**Figure 5a**), facilitating spatiotemporal tracing of engram-activated nuclei. More elaborately, in the presence of TAM, CreER^{T2} enters the nucleus and cleaves the loxP stop codon upstream of the sfGFP insert, thereby allowing the stimulus-activated IEG-expressing cells to accumulate nuclear membrane sfGFP. Despite both the IEGS - *cFos* and *Arc* IEGs - being expressed within 15-20 minutes of a stimulus, they exhibit distinct expression patterns, spatially[242,249,250] as well as quantitatively, with *Arc* being expressed in higher amounts than *cFos*[251]. Additionally, *Arc* codes for a cytoskeletal protein while *cFos* is a transcription factor[252].

Our goal is to select the appropriate mouse line that can yield an optimal number of nuclei activated by a specific stimulus from an individual mouse for subsequent multiomics experiments. Therefore, the experimental strategy is centred on determining the Cre driver line that would provide a high signal- to-noise ratio within the window period of stimulus offset and GFP accumulation before sacrifice (trapping period).

1.2 Methods

1.2.1 Animals and genotyping

cFosCreER^{T2}(TG/WT) × R26-*CAG-Sun1-sfGFP-Myc* (M/WT) and ArcCreER^{T2}(TG/WT) × R26-*CAG-Sun1-sfGFP-Myc* (M/WT) mice were used for these experiments[241–243]. In the following, **the heterozygous mouse lines with the above genotypes (TG = transgenic, M = mutant, WT = wild-type allele) will be referred to as cFos-GFP and Arc-GFP for ease of use**. Genotyping for the TG mice were performed using PCR with genomic DNA isolated from ear punches and the following primers, under the following conditions.

NB: GFP and sfGFP will be used interchangeably in the remaining sections of the thesis, wherein they indicate the same entity.

Genotyping for ArcCreER^{T2}

Common forward primer – 5'-CAG CAT AAA TAG CCG CTG GT-3'; Wild-type reverse primer – 5'-CCG TCC AAG TTG TTC TCC AG-3'; Transgenic reverse primer – 5'-CGA CCG GTA ATG CAG GC-3'. Fragments for WT/WT allele and TG/WT allele are detected at 300 bp and 300 bp + 500 bp, respectively.

Genotyping for cFosCreER^{T2}

Common forward primer – 5'- CAC CAG TGT CTA CCC CTG GA-3'; Wild-type reverse primer – 5'-CGG CTA CAC AAA GCC AAA CT-3'; Transgenic reverse primer – 5'-CGC GCC TGA AGA TAT AGA AGA-3'. Fragments for WT/WT allele and TG/WT allele are detected at 215 bp and 215 bp + 293 bp, respectively.

Genotyping for *R26CAG-Sun1-sfGFP-Myc*

Common forward primer – 5'GCA CTT GCT CTC CCA AAG TC 3'; Wild-type reverse primer – 5'CAT AGT CTA ACT CGC GAC ACT G3'; Mutant reverse primer – 5'GTT ATG TAA CGC GGA ACT CC 3'. Fragments for WT/WT allele, M/WT allele and M/M allele are detected at 557 bp, 300 bp + 557 bp and 300 bp, respectively.

Only mice, which were heterozygous for both the promoter mouse line and reporter mouse line were selected for the experiments. Breedings were performed using mice heterozygous (TG/WT) for the promoter CreER^{T2} line (male or female) and homozygous mutant (M/M) for the reporter line (male or female). The mice were inbred to limit genetic variations, thereby, sensitising detection of the epigenetic modifications. All TG mice used were housed in the TARC facility in Mainz and transferred to the mouse behavioral unit, 3-4 days before experiments. Mice were fed *ad libitum* and allowed to follow the natural light on/off cycle. Only adult mice (above 6-8 weeks old) were used for the following experiments. All experiments were performed in accordance with the institutional animal welfare guidelines approved by the ethical committee of the state government of Rhineland-Palatinate, Germany (Ref. no. G-17-1-021).

1.2.2 Behavior experiment

For a quick assessment of the GFP accumulation following stimulus offset, the easily accessible tail suspension test was used. For the tail suspension test, the test mouse was lifted by its tail and left suspended in the air for 5 S, repeated thrice, after which they were left back

in their cages. This test is less stressful to the animals than the CSD, and hence was more suitable for the aim under this chapter, considering ethical reasons.

1.2.3 Tamoxifen and 4-hydroxytamoxifen preparation

TAM (Tamoxifen, Sigma–Aldrich, St. Louis, MI, USA, T5648-1G) was dissolved in a corn oil:100% ethanol mixture (9:1) ratio (Sigma Aldrich) at 42°C with constant shaking at 500 rotations per minute (rpm) in light protected Eppendorf tubes (Amber). 4-hydroxytamoxifen was also prepared in a similar way.

NB: TAM and 4-hydroxytamoxifen were prepared on the same day of injection to avoid product degradation during the storage of the TAM solution at -20˚C. Different syringes were used for administration of the drug to the stressed group and non-stressed controls.

1.2.4 Brain tissue collection, immunohistochemistry, microscopy and nuclei sorting

Brains were isolated at 4˚C or on ice and flash frozen in OCT. Tissues were stored at -20˚C until the time point of cryosection. Immunohistochemistry on 40 µm thick sagittal and coronal slices was performed using primary antibodies (anti-GFP, Takara Bio USA, Inc., Mountain View, CA, USA) and secondary antibodies (anti-mouse and anti-rabbit). Images were captured using Light Microscopy (40×) and Confocal Microscopy (20×) (More details of the microscopy techniques are in the methods section of **Chapters 3 and 4**). For details of nuclei isolation and sorting please refer to the methods section of **Chapters 3 and 4**.

1.3 Results

To be able to compare the two mouse lines (**Figure 5a**), Arc-GFP and cFos-GFP, our first step was to determine a suitable time point of mouse sacrifice, following stimulus offset, to enable optimal sfGFP accumulation and tracing. Therefore, we proceeded with the experiment to find an optimal sfGFP accumulation window period, following stimulus presentation.

1.3.1. Determination of optimal window period for sfGFP accumulation

Since sfGFP expression and accumulation are the only factors to be examined, we reasoned that use of either *cFos* or *Arc* promoter lines would suffice. As the Arc-GFP was available in-house during the timepoint of the experiment, it was used for this experiment. In this paradigm, TAM (80 mg/kg) was injected 5 hours before the tail suspension test. The 5-hour time point for TAM injection was chosen based on [241] and our initial experiments, where TAM injection 24 hours before the stimulus, showed a reduction in trapping, i.e., less than 2×the number of GFP nuclei compared to 5 hours (**Supplementary Figure 1 a,b)**. Indeed, pharmacokinetics

data from [253] indicate a peak concentration of the active form of TAM, 4-hydroxytamoxifen, 5 hours after injection. Thus, choosing this timepoint would allow for the maximal tracing of cells activated during this window period, where the peak concentration of TAM metabolites coincide with the stimulus. Following the injections and the tail suspension test (n = 6), 2 animals each were assessed at three different sacrificial time points of 24 hours, 48 hours and 72 hours after the TAM injection.

The qualitative assessments of trapping for 24-, 48- or 72-hours following injection, indicated a very low GFP accumulation within the trapping period for 24 hours (not shown), followed by 48 hours and 72 hours (**Figure 5b**, n = 2 mice each). Given the GFP accumulation quantity, a window period of trapping for 72 hours after the TAM injection was considered to be the optimal choice.

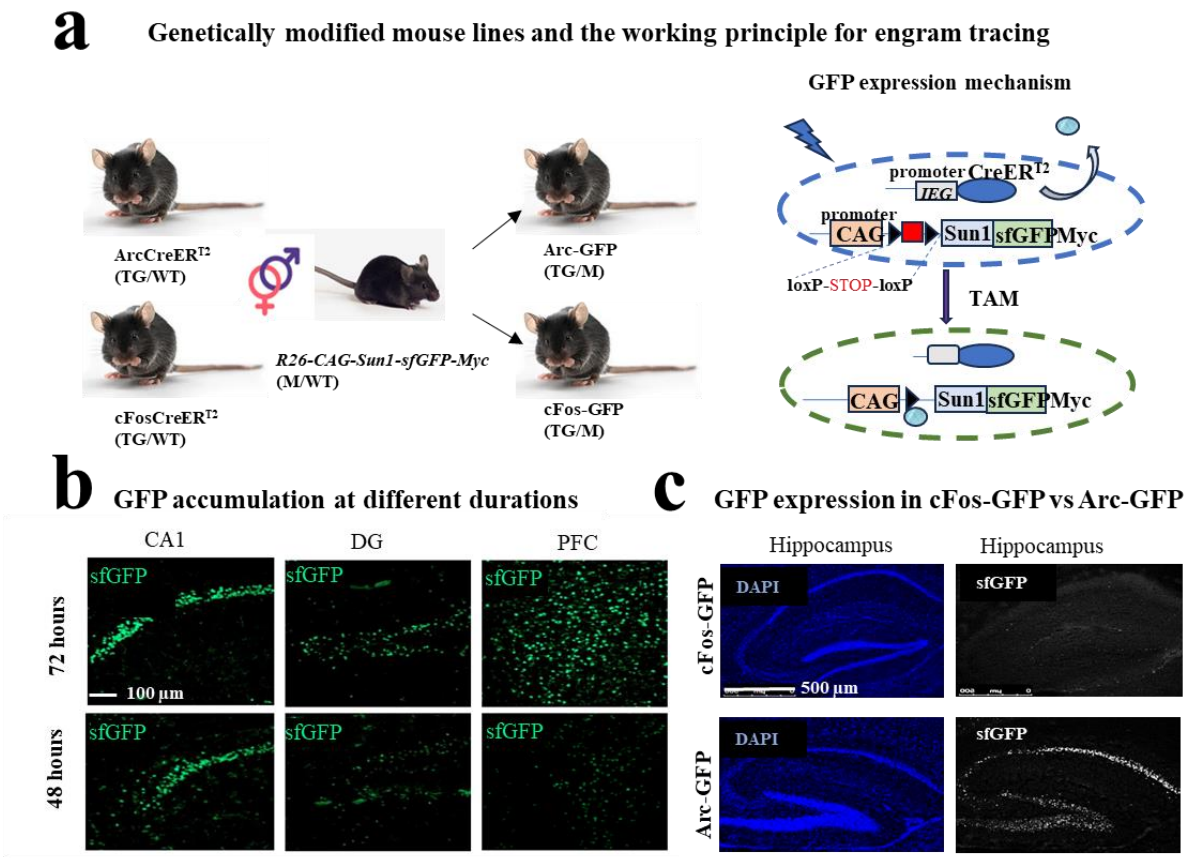

Figure 5: Optimization of experimental strategy for acquiring maximum stimulus-induced GFP accumulated engram using TG constructs.

a. Arc-GFP and cFos-GFP mice were obtained from cross breeding between Arc/cFosCreER^{T2} (TG/WT)[241,242] and *R26-CAG-Sun1-sfGFP-Myc* (M/WT)[243] mouse lines. The Arc-GFP and cFos-GFP systems allow for the tracing of nuclei that were spatiotemporally activated by a stimulus in the presence of TAM. On the arrival of a stimulus, the promoter of the immediate early gene (*IEG – Arc/cFos*) becomes active

and *CreER^{T2}* is transcribed. The *CreER^{T2}* system is then translated into the protein form and remains in the cytoplasm. In the presence of TAM, the Cre recombinase can enter the nucleus and cleave the STOP codon of the GFP reporter construct, allowing for the expression of nuclear membrane GFP, which accumulates over time and can be traced. **b**. Tail suspension-induced GFP expression (TAM dosage at 80 mg/kg, Arc-GFP, n = 2 each) at different time points of sacrifice indicates a higher prevalence of GFP accumulation following 72 hours of trapping compared to 48 hours in the brain regions of cornu ammonis 1 (CA1), dentate gyrus (DG) and prefrontal cortex (PFC) **c.** Representative images of Arc-GFP mice (n = 2) indicating a higher prevalence of GFP (TAM dosage at 80 mg/kg) compared to cFos-GFP (n =2, TAM dosage at 150 mg/kg) within 72 hours of tail suspension-induced GFP accumulation. Scale bars are as indicated, superimposed on the original. The logos for the mice are obtained from google images. **Abbreviations:** TG - transgenic, TG/WT - one allele with transgenic insertion and the other as wildtype allele, TAM - tamoxifen, CA1 - cornu ammonis 1, DG - dentate gyrus, PFC - prefrontal cortex.

1.3.2. Choice of mouse line – cFos-GFP vs Arc-GFP

Following the establishment of an optimal GFP accumulation window period of approximately 72 hours, we next aimed at comparing the quantity of traced cells in the two different mouse lines, using tail suspension test as the stimulus. Since preliminary in-house experiments showed a very low induction of cFos-GFP with 80 mg/kg TAM (data not shown), we increased the TAM dosage to 150 mg/kg for tracing spatiotemporally active populations in cFos-GFP (n = 2 mice). Next, injections of 50 mg/kg 4-hydroxytamoxifen (4-OHT) were delivered to another 2 mice of cFos-GFP, 0 hours before the stimulus onset to determine if the more active 4-OHT injections would allow for a better trapping for the less prevalent cFos expression. For Arc-GFP mice (n = 2), a TAM dosage of 80 mg/kg was retained. All mice were sacrificed 72 hours after the injections and equivalent sections were assessed for the stimulus-activated sfGFP expression. Interestingly, from the immunohistochemistry results, we concluded that the use of Arc-GFP mouse line allows for a higher trapping of the spatiotemporally activated nuclei (**Figure 5c).** On average, Arc-GFP mice showed detectable GFP expression in 1/3 of the total nuclei counted. Meanwhile, cFos-GFP mice showed detectable GFP expression only in 1/60 of the total nuclei counted. Therefore, using Arc-GFP would facilitate a higher yield of activated nuclei.

1.4 Discussion

Though SI (social interaction) test would have been a more fitting choice in light of the subsequent experiments, we opted for the tail suspension test due to its simplicity and accessibility, without the need for complicated tools. Since our focus was specifically on determining the optimal trapping duration for GFP, following TAM injection and stimulus presentation, we reasoned that any stress stimulus would be sufficient for this purpose. Using

this setup, we determined that a 72-hour window period for GFP accumulation (trapping) would be optimal for our experiments.

Indeed, the chosen time range of approximately 72 hours is distant from the time point of stimulus presentation, and hence could miss out some transient molecular changes related to the behavior activity. However, we reasoned that this approach still enables us to study persistent or subsequent alterations in the engram cells. In essence, it is a favourable compromise between the ability to trace activated cells for multiomics sequencing and the potential loss of some transient modifications. In fact, the 72-hour window period GFP accumulation was also the window period of choice in [243] and [254] for the same reporter line. Following the 72-hour trapping period, since the Arc-GFP mouse line showed a higher prevalence of sfGFP+ nuclei output compared to cFos-GFP mouse line, the Arc-GFP mouse line was selected for subsequent experiments within the framework of the thesis.

Chapter 2. Optimization of the CSD paradigm for the TAM-inducible Arc-GFP mouse line to facilitate the segregation of resilient-susceptible phenotypes

2.1. Introduction

The use of the Arc-GFP mouse line provides a certain advantage over the more frequently used C57BL/6J mouse strain, in allowing the tracing and selective investigation of spatiotemporally active engram populations. This is particularly relevant for our study, where we aim to dissect mechanisms of stress-resilient and stress-susceptible populations following CSD. This is because stress-resilient and stress-susceptible populations are known to activate different engram populations[112]. However, the Arc-GFP mouse line is a relatively new double transgenic mouse line, which has not been used for CSD experiments. Since different mouse lines possess distinct behavior patterns and exhibit a different stress tolerance threshold[255,256], an optimal stressor to elicit stress effects had to be determined for this novel line. Additionally, the use of TAM, an artificial estrogen for activating Cre in the Arc-GFP mouse line might bear unexpected effects. Therefore, in this results Chapter, we focus on establishing an appropriate stressor for this mouse line, considering both the plausible differences arising from the mouse line as well as the TAM injections.

2.2. Methods

2.2.1. Animals

7-8 weeks old Arc-GFP, WT-GFP (without the ArcCreER^{T2} transgene) and C57BL/6J adult male mice (Charles River) were used for the experiments in this section. Animals were bred, maintained, and genotyped as in **Chapter 1**. Acclimatization to the experimental environment was done at least 3-4 days before the start of any behavioral experiment. Experiments on the C57BL/6J and the behavioral battery tests were performed in accordance with the institutional animal welfare guidelines approved by the ethical committee of the state government of Rhineland-Palatinate for under the central project, Z02 of SFB 1193.

NB: The Arc-GFP mice used here are progenies of parental lines that were crossed with C57BL/6Rj (Janvier) and C57BL/6J. The former line possesses an inherent alpha-synuclein deletion.

2.2.2. Chronic social defeat (CSD) stress

For CSD experiments, CD1 mice were preselected for their aggressiveness, with the defining criteria for selection being an attack latency of less than 10 S towards an intruder mouse.

Two types of CSD stress paradigms with differing intensities of the stressors were used, as described below.

Subthreshold defeat stress

The subthreshold defeat CSD stress paradigm was developed for C57BL/6J and was pre-existing in the facility. **(**NB: the reason for the use of this term will be explained in the results section). This stress paradigm was aimed at introducing the least amount of stressor needed to elicit a significant stress response in accordance with the ethical guidelines. In this paradigm, the intruder mouse was placed in the cage of a novel CD1 mouse for 2 minutes, where the intruder mouse suffered sporadic attacks from the CD1 mouse. Following this brief episode, the resident CD1 mouse and the intruder mouse were separated by a mesh wire for 24 hours, allowing for the continuation of visual and olfactory stimulation, without physical attacks. This process was repeated for a span of 10 days, with the introduction of the intruder mouse to the cage of a new CD1 mouse every experimental day. The animals were allowed to rest for a period of 7 days. Social interaction test (SI, described in detail under the subsection **'Behavioral tests'**) was then performed on the 8th day after the last CSD. All cages were maintained in environmentally controlled cabinets (Uniprotect NG, Zoonlab GmbH).

Aggressive chronic social defeat stress (new CSD paradigm)

In this paradigm, the intruder mouse was subjected to 3 encounters, daily, with a new CD1 mouse in each encounter. In each encounter, a pure physical attack by the CD1 mouse, cumulating to 15 S each was counted, after which the CD1 mouse and intruder mouse were separated by a mesh wall for a 30 min interval time, allowing for visual, audio and olfactory stimulation but no physical attack. At the end of the third encounter session for the day, the intruder mouse was left undisturbed in the cage of the third CD1 mouse, physically separated by the mesh wall, for 24 hours till the next day of the CSD experiment. The whole procedure was repeated for a total of 10 days, similar to that of the subthreshold paradigm. After the last day of the CSD defeat session, stressed mice were placed into a new cage, where they remained undisturbed for 7 days. All cages were maintained in environmentally controlled cabinets (Uniprotect NG, Zoonlab GmbH). SI was performed on the 8th day after the last CSD similar to the subthreshold stress paradigm.

Handling of non-stressed controls

During the CSD paradigm, while the mice for the stressed group were subjected to repeated rounds of defeats, mice for the non-stressed control group were also handled daily, throughout

the 10 days, albeit without exposure to CD1 stressors. Each control mouse was housed with another conspecific, separated by a mesh wall. During the 10 days of experimental period, control mice were placed in environmentally controlled cabinets in a different room than the animals that were undergoing CSD and were handled before the stressed group to avoid transfer of stress. Following the 10-day period, control mice were also single-housed for 7 days, similar to the stressed group, before proceeding to the SI test.

2.2.3. Behavioral tests

2.2.3.1. Open field and eagle exploration test (OF/E)

Before the start of the CSD paradigm for some batches, to understand the basal behavior of the different genotypes, we used open field (OF) test combined with an eagle exploration (E) test, was used in some batches, as described in [127]. Briefly, spontaneous activity of the test mouse was assessed using an open field test in a grey plastic arena (40 × 40 × 40 length, width, and height). The animal was placed at a corner of the open field and was allowed to explore it for 10 minutes. The behavior was recorded by a PC-linked overhead video camera. "Ethovision XT 8" (Noldus Inc., Netherland) software was used to track the distance travelled and the time spent in the central zones of the open field. After the initial 10 minutes session, a toy eagle was placed in the centre of the arena and the mouse was reintroduced inside the arena. Exploration within 1 cm of the eagle position was recorded to assess innate fear/object exploration response of the test animals.

2.2.3.2. Social interaction (SI) test

The SI test was performed (on the 8th day after the last defeat session) similar to that described by Krishnan and colleagues[64] in two phases. Interaction zones of radii 1 cm, 3 cm or 8 cm, measured from an empty cylindrical mesh enclosure placed at the middle side of one edge of the arena (40 by 40 in cm), were predefined. Thereafter, test mice were placed in the corner opposite the cylindrical empty mesh enclosure and the movements were tracked for 2.5 minutes, using "Ethovision XT 8" (Noldus Inc., Netherland) software, to measure the total duration the mouse spends in the interaction zone. This is termed as the '**habituation phase'**. In the second phase, termed as the '**test phase**', the animals were re-placed in the arena, where a novel CD1 mouse now inhabits the previously empty cylinder. The movements were tracked for another 2.5 minutes to assess their presence in the interaction zone. The tip of the nose was used as a tracking point for interaction zones of 1 cm and 3 cm, while the body centre was used as the tracking point for the 8 cm interaction zone.

SI score was then calculated with the formula.

SI = (time spent exploring the interaction zone during the test phase)/(time spent exploring the interaction zone during the habituation phase) ×100

Mice that exhibited SI score > 100 was deemed resilient while those that showed SI score < 100 was deemed susceptible.

In addition to the SI calculated from the automatic tracking with the Ethovision software, manual scorings of the interactions from the recorded videos were also conducted as previously described in [127]. The additional scoring was performed to mitigate technical defects that could arise during tracking, especially when the mouse moves fast or remains in shadowy contrast areas, which are non-optimal for tracking[127]. Moreover, automatic SI scoring could lead to false positives, if the mice exhibited inactivity during the habituation phase or stays marginal to the interaction zone demarcation line. Thus, to address these concerns and ensure data accuracy for subsequent analyzes, manual scoring of the recorded Ethovision videos were performed. Interaction time was noted as the amount of time the test mouse showed any form of interaction (exploring the cylindrical enclosure/watching it/approaching it) within the maximal interaction zone of 8 cm, and SI was calculated using the same formula as above.

NB: Manual scoring was performed together with Marija Milic. All animals were injected with TAM (80 mg/kg or 150 mg/kg, 5 hours before the stimulus) or vehicle (corn oil:ethanol, 9:1) while animals for non-injected groups were only poked (without any fluid injection) before the SI test. The injections or no injections are appropriately mentioned in the respective results sections. All mice were habituated to the syringe needle with a single poke 1 day before the real injection/poking on the day of the SI.

2.2.3.3. Novel object recognition test

For this test, individual mice were acclimatized to a 40 × 40 × 40 cm grey chamber containing two identical objects for 20 minutes per day for 2 days. On the day of the test, the mouse was allowed to explore the two identical objects for 10 minutes each. Following this, the mouse was removed and one of the identical objects was replaced by a novel object. The mouse was then replaced in the arena to allow free exploration of either the novel one or the known object. NB: This test was performed only to compare the GFP induction of a different behavioral stimulus (NOR) to that of the SI test. Therefore, an assessment of the preference of the novel object or the familiar object was not calculated.

2.2.3.4. Elevated plus maze (EPM) test

EPM is a well-established behavior test to measure general anxiety[119]. In each experiment, the animal was placed on the central platform, facing an open arm of the plus-maze (made of grey Perspex with a central 5 × 5 cm central platform, 2 open arms, 30 × 5 cm, 2 enclosed arms, 30 × 5 × 15 cm; illumination 150 lux). Movements were tracked using "Ethovision XT 8" (Noldus Inc., Netherlands) software to measure the duration of time spent by a test mouse on either open or closed arms. The **percentage of time spent in open arms** compared to the total time of tracking was, then, calculated.

% time spent in open arms = (total time spent in open arms/total time spent in all arms) × 100

2.2.3.5. Light-dark test (LDP) test

Following the EPM test, the LDP was performed the next day. Similar to the EPM, the LDP assesses mouse anxiety and relies on the innate aversion of rodents to brightly illuminated areas[120]. The light-dark test apparatus consists of a 40 × 40 × 40 cm white plastic arena with one-third of the arena covered from the light (darkened). The darkened area is connected with the lit zone by a 4 × 4 cm hole, where the mice can enter/exit. The test mouse was placed in the dark compartment at the start of the experiment and were allowed to explore the arena within a 10 minutes test session. "Ethovision XT 8" (Noldus Inc., Netherland) video-tracking system was used to measure the **duration** that the mouse spent in the dark or lit zones of the arena, compared to the total duration of the test. In addition to this, the **latency** of the first entrance to the lit side was also recorded.

2.2.3.6. Spatial memory Y-maze test

The spatial memory Y-maze test was used to determine the hippocampal spatial reference memory[121]. In this test, the animals were introduced in a symmetrical elevated Y-maze, with one arm closed, under reduced light conditions (50 lux). Each arm was 30 cm long and 7 cm wide with black walls (15 cm high). Mice were allowed to roam the maze for 10 minutes, after which they were put back in their home cage for 30 minutes. They were then returned to the Y-maze with all arms open, to test their preference for the new arm (previously closed) or the familiar arm of the Y-maze. Their movements were then tracked for a total of 5 minutes, using "Ethovision XT 8" (Noldus Inc., Netherland) video-tracking system.

2.2.3.7. Sucrose preference (SP) test

In the SP test, the test animals had *ad libitum* access to both water and a 2% sucrose solution for 48 hours in the home cage. The fluids were delivered, separately, by two pre-weighed

bottles. Bottles were counterbalanced across the left and the right sides of the cage and positions were alternated in each cage twice a day. On the third day, the bottles were weighed again for calculating the sucrose preference.

% sucrose preference = (sucrose solution intake (mL)/total fluid intake (mL)) × 100.

The test is known to assess depression-like behavior of anhedonia in rodents[122].

2.2.3.8. Forced swim (FS) test

FS test is a well-known test to assess depression-like symptoms in animals, following behavioral despair in stressful and inescapable situations[123]. In this test, each experimental mouse was placed for 6 minutes in a glass cylinder of 18 cm width and 25 cm height, filled with water (21+/-1 °C) till 15 cm of height. Then, the duration during which the mice showed immobility, i.e., passive floating defined by the animal being motionless or exhibiting only slight movements with tail or a hind limb, or activity was measured against active mobility characterized by behaviors of struggling, climbing, or swimming using all four paws, for the last 4 minutes of the test.

NB: Majority of the technical parts of the behavioral tests were performed by the MBU while I planned, organized and coordinated the experiments along with the analysis of the results.

2.2.4. Tamoxifen and solvent preparations

Tamoxifen was prepared in 1:9 ethanol:cornoil mixture as in **Chapter 1** and injections were delivered at 80 mg/kg or 150 mg/kg of body weight of the animal. For vehicle solvent injections, bodyweight appropriate volumes of the solvent, 1:9 ethanol:cornoil, were delivered. All injections were administered intraperitoneally 5 hours before the SI or NOR test. Intraperitoneal single pokes were also delivered to the non-injected groups with acclimatization to the syringe needle in all cases, 1 day before the stimulus (injection/poke) application.

2.2.5. Physiological assessments

2.2.5.1. Blood collection and CORT level assessment

Blood samples were collected, by a tail cut, on two different days for CORT extraction. The first collection was performed 24 hours after the last CSD session, while the second collection was performed 20 minutes and 90 minutes after the FS test. Serum was extracted from fresh blood samples by centrifugation at 10,000 rpm for 10 minutes at 4 °C and stored at −80 °C until analysis as described in [127]. Corticosterone concentration from the serum was then measured using an enzyme-linked immunosorbent assay (ELISA) kit (Enzo Life Sciences, Inc.)

following the manufacturer's protocol. The absorbance was read at 450 nm using a microplate reader (Multiskan EX, Thermo Scientific, USA).

NB: The tail cut and blood collection were performed by Marija Milic while serum CORT collection was performed together with me.

2.2.5.2. Tissue collection, nuclei isolation and sorting

Following the last day of the experiments, body weights were measured, and mice were sacrificed by cervical dislocation. Hypothalamus and adrenal glands were collected in pre-weighed Eppendorfs containing RNA later. The collected tissues were then weighed using a sensitive balance. Gut was donated to Kristina Endres's group for their publication[257]. Hippocampus, vHipp, PFC and Naccu were dissected and processed for nuclei isolation (see more details in **Chapter 3**) while fluorescence-activated nuclei sorting (FANS, see more details in **Chapter 4**) was used to sort the activated GFP+ nuclei.

2.2.6 Statistical analyzes

All statistical calculations were performed using GraphPad Prism (8.4.2). Student's unpaired t-test was used for statistical comparisons of two groups with normal distributions, while ANOVA along with different *post-hoc* tests were used for comparison of three groups as specified in the text, unless otherwise mentioned. In all calculations, $p<0.05$ was considered statistically significant.

2.3. Results

2.3.1. Determination of the necessary TAM dosage for tracing optimal amount of SI-engram specific nuclei

In **Chapter 1**, we established that the Arc-GFP mouse line (TAM, 80 mg/kg) provided a higher quantity of trapped engram nuclei than cFos-GFP, following a tail suspension stimulus. Our next step was to ascertain that the intended TAM dosage of 80 mg/kg would be necessary and sufficient to elicit an optimal engram nuclei quantity for the subsequent multiomics experiments, following the SI test after the CSD paradigm. This was crucial to ensure that the stressor selection as well as other behavioral battery tests will be performed using the right TAM dosage.

To evaluate the yield of SI engram nuclei with the TAM dosage of 80 mg/kg after CSD experiments, we implemented the in-house available subthreshold defeat CSD paradigm. Briefly, in this paradigm, the resident CD1 mouse engaged in sporadic attacks on the intruder

Arc-GFP mouse for 2 min daily over a period of 10 days. After the 2 minutes exposure, the Arc-GFP mouse was separated from the CD1 mouse with a cage separator for the remainder of the day to allow for sensory stimulations without the physical attacks. Non-stressed controls were also handled during the entirety of the experiment (see **Methods**). 7 days after the conclusion of the last CSD attack, 80 mg/kg of TAM (as in **Chapter 1**) was injected 5 hours before the SI test to both the stressed group as well as non-stressed controls. Mice were then sacrificed 72 hours after the TAM injection, and hippocampus was collected to assess GFP induction. Quantitative evaluation was performed using fluorescence-activated nuclei sorting (FANS) while qualitative assessment was conducted with immunohistochemistry. Though immunohistochemistry revealed a clear GFP induction in the engrams **Figure 6a**, an estimate of the engram nuclei using FANS indicated that the total GFP positive (GFP+) nuclei that could be obtained with this dosage was substantially lower (approximately 15k nuclei) than that deemed necessary for the multiomics experiments. Therefore, we decided to increase the dosage to 150 mg/kg as used by Guenthner and colleagues[242], to enable the tracing of more engram nuclei for the intended multiomics experiments.

Since 150 mg/kg of TAM (administered 5 hours before the stimulus) is a relatively high dosage, it was necessary to assess whether the implementation of this dosage would still allow for the tracing of stimulus-specific engrams. To address this concern, we compared the %GFP accumulation that served as proxies for activated engrams for the SI stimulus against the NOR stimulus. Interestingly, we observed that there was a significant difference in the GFP% accumulation (tissue – vHipp), resulting from the two activity-dependent stimuli (**Figure 6b**), NOR test (n = 6) and SI test (n = 16). This indicates the retention of the sensitivity of stimulus-induced recombination despite the high TAM dosage. On the other hand, as *Arc* shows a basal level of expression in neurons, we performed an additional experiment to assess basal recombination by evaluating GFP induction in home cage controls against that of the SI test. We noted that the GFP induction (TAM, 150 mg/kg) by the SI test in different brain regions of PFC, vHipp and Naccu, were significantly higher than the GFP induction in the cage controls (**Figure 6b**). Thus, this precludes excessive impurities from Cre leakage and unwanted signal tracing, even with the high dosage of TAM. Additionally, we noted that single-housed home cage controls and group-housed home-cage controls showed non-significant differences in GFP expression (**Supplementary Figure 2a).** This demonstrates that the single housing period of 7 days after CSD, will exert relatively less impact on the engram tracing, i.e., single housing will probably not introduce significant divergent effects related to GFP accumulation in our

study. Altogether, we established that TAM administration at a dosage of 150 mg/kg to be the optimal choice for our next step of the experiments, i.e., establishing an appropriate stressor for the Arc-GFP mouse line.

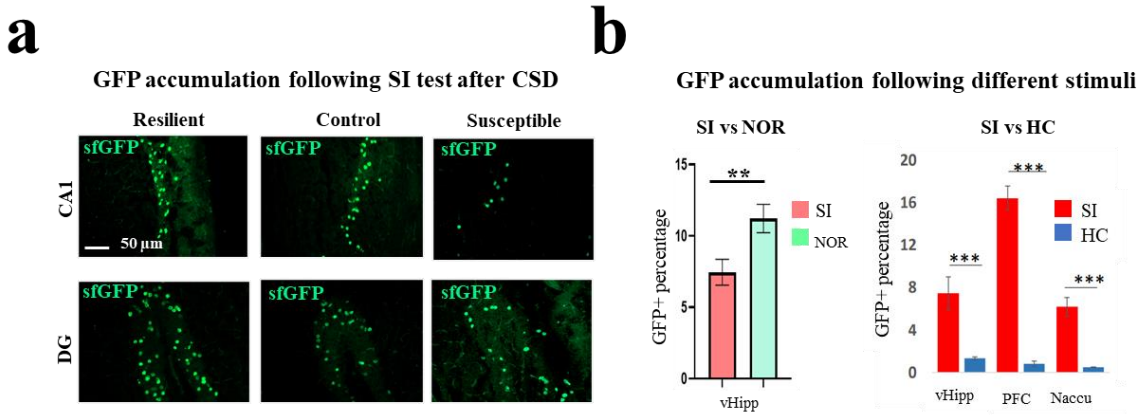

Figure 6. Stimulus-specific engram tracing with GFP accumulation.

a. Representative images showing SI test-induced GFP accumulation (72 hours) in Arc-GFP mice after CSD paradigm (n = 2 controls, 4 stressed: 1 resilient and 3 susceptible, TAM dosage at 80 mg/kg). **b.** Determination of the usability of 150 mg/kg (TAM) dosage in Arc-GFP mice to facilitate the tracing of more nuclei. The quantity of SI-induced GFP expression (approx. 8%) differs significantly (t-test, $p<0.01$, **) from the Novel Object Recognition test (NOR)-induced GFP expression (approx. 12%) (n = 16 for SI, n = 6 for NOR), indicating stimulus specificity, even with 150 mg/kg TAM dosage. Ventral hippocampus (Vhipp) tissue was used for the illustration. In the vHipp, PFC and nucleus accumbens (Naccu), the SI-induced GFP expression also shows a significantly higher level of GFP expression than that for home cage (HC) controls in the vHipp, PFC and Nucleus accumbens (t-test, $p<0.001$, ***) (n = 16, 16, 8 for SI, n = 6 ,6 , 3 for HC). HC controls were used as a proxy for basal *Arc* expression induced GFP accumulation. TAM was injected 5 hours before these experiments. Scale bars are as indicated. Error bars represent +/- S.E.M. Significance values are indicated as ** - p<0-01, *** - p<0.001. **Abbreviations**: SI - social interaction test, NOR - novel object recognition test, HC - home cage controls, CA1 - cornu ammonis 1, DG - dentate gyrus, PFC - prefrontal cortex, vHipp - ventral hippocampus, Naccu - nucleus accumbens, n - sample size.

2.3.2. SI test of TAM-injected Arc-GFP mice did not show a stress effect, following subthreshold defeat

Since TAM is an artificial estrogen with known effects in ameliorating psychiatric disorders, such as bipolar disorders[258], we hypothesized that the application of TAM (150 mg/kg) for activating Cre in the Arc-GFP mouse line could also potentially impact the stress readouts in a dose-dependent manner. Therefore, we, next, sought to determine an appropriate stressor for the TAM-inducible mouse line.

With ethical considerations of minimal damage to the test subjects, we started with the subthreshold defeat paradigm of daily attacks for 2 minutes (see scheme in **Figure 7a**) developed in-house for the C57BL/6J mouse line. However, using this paradigm, we could not discern a group stress effect on the TAM-injected Arc-GFP mouse line (**Figure 7b**) in the SI

test compared to the non-stressed controls. Subsequently, to enhance accuracy of the assessment as a control measure for the smaller size of the Arc-GFP mouse against the larger 8 cm interaction zone optimized for the larger C57BL/6J mouse line, we also implemented manual scoring methods (**Figure 7b**) for the SI test. In addition to the implementation of manual scoring methods, the interaction zones were reduced from 8 cm to 3 cm and 1 cm to accommodate the smaller size of the Arc-GFP mouse. However, in all cases, we still could not identify an effect of stress **(Supplementary Figure 2b)**. Therefore, we hypothesized that the lack of a discernible stress impact could be either due to the inherent characteristics of the mouse line or the potential improvement in interaction induced by the TAM application before the SI. For simplicity, since the stressor failed to evoke an observable stress response in our study, we classified it as a 'subthreshold defeat paradigm'.

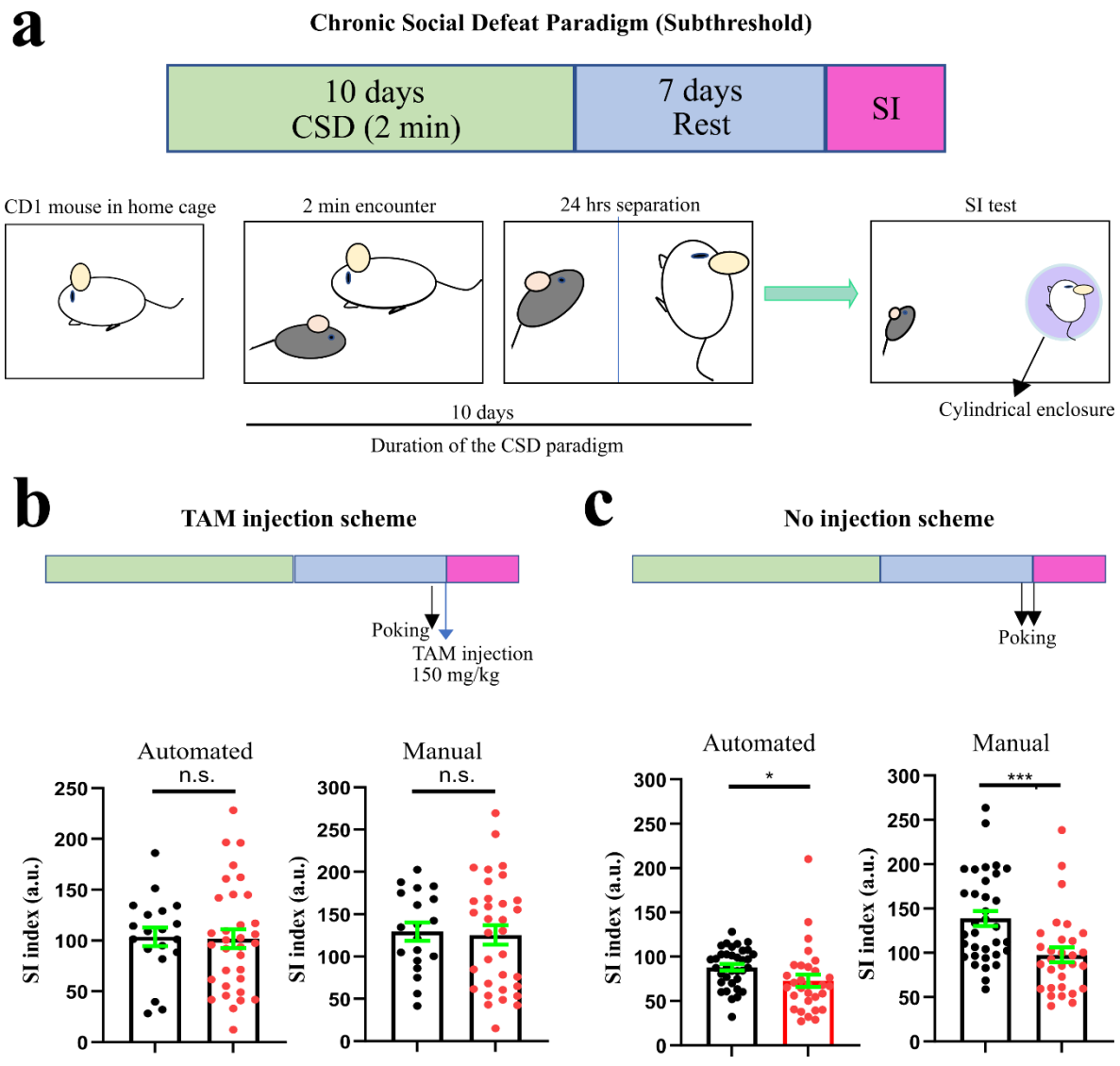

Figure 7: The differential impacts of the chronic social defeat paradigm on the Arc-GFP mice with and without TAM injection.

a. Scheme of the subthreshold CSD (chronic social defeat) paradigm. At the start of the paradigm, the Arc-GFP mouse is introduced into the home cage of the resident CD1 mouse for 2 minutes daily. During these 2 minutes, the Arc-GFP mouse suffers sporadic physical attacks from the CD1 mouse. After 2 minutes, a mesh wall is introduced between the two mice to curtail physical attacks for 24 hours. The mesh wall allows for the continuation of visual and olfactory stimuli devoid of physical attacks. The paradigm is repeated for a total of 10 days with a new CD1 mouse for each encounter. Upon the completion of the CSD paradigm, the mice were left undisturbed in single-housed cages for a rest period for 7 days, whereupon the SI test was performed on the 8th day after the last CSD**. b**. Scheme of the CSD paradigm with **TAM injection** (150 mg/kg 5 hours before the SI test). SI scores show a **non-stress effect** in both automated and manual scorings (t-tests, $p>0.05$, n.s.). **c**. Scheme of the CSD paradigm **without TAM injection** (150 mg/kg 5 hours before the SI test). SI scores show a **significant stress effect** in both automated and manual scorings (t-test, $p<0.05$, *; t-test, $p<0.001$, ***, respectively). Error bars indicate +/- S.E.M. * represents the significance value. Each dot in the bar graphs represents a single mouse with controls as black and stressed as red. Abbreviations: SI – social interaction test, TAM - tamoxifen.

2.3.3. In the absence of TAM injections, the subthreshold stressor induces a deficit in the SI test after CSD

To examine the inherent stress tolerance characteristic of the Arc-GFP mouse line in the absence of TAM, experiments were performed in another cohort under identical conditions as above, except for the TAM injection. Interestingly, we observed that the stress effect on SI was visible and significant without the injection (t-test, $p<0.05$, **Figure 7c, left**). The SI index from the manual scoring, also demonstrated a significant difference between the control and stressed group (t-test, $p<0.001$, **Figure 7c, right**), without TAM injection. This indicates that the SI test was influenced by the injections delivered 5 hours before the SI. It is important to highlight here that the observed effect of improved social interaction could be because of TAM (an artificial estrogen) or the solvent (ethanol:cornoil). However, as TAM is a synthetic form of estrogen, known to impact social behavior[259–261], I hypothesized that the SI improvement could be more likely associated with the use of TAM rather than the solvents. Thus, our next step was to develop a more robust stressor that could mitigate the SI improvement and discern the cause for the improvement. The steps were essential to determine the usability of the TAM-inducible system for the intended stress research to ensure segregation of resilient-susceptible phenotypes.

(NB: *Post-hoc* analyses of the TAM-injected stressed populations showed that some other behavior parameters were differentially affected in the bioinformatically computed tracks of the mice from the SI test (**Supplementary Figure 2c**, performed by Nicolas Ruffini). This indicated that the stressor exerted its effects but was not visible in the commonly accepted SI read out, following the injections).

2.3.4. Usability of the TAM-inducible Arc-GFP mouse line for stress studies

To determine an optimal stressor for the TAM-inducible system, we increased the intensity of the stressors from the 2 minutes encounters to 3 sets of 15 S daily attacks, keeping all other

conditions identical. In this new paradigm, pure physical attacks by a novel CD1 mouse were implemented for 15 S (**Figure 8**) repeated for 3 times, each with a new CD1 mouse (see more in **Methods**). Following the last day of the CSD, several assays, apart from the SI, were also introduced as depicted in the **scheme (Figure 8).** The introduction of other behavioral assays was to capture additional stress-affected parameters, should the TAM-improvement in SI persist despite the increased stressor intensity.

Next, since the patterns of the TAM-injected Arc-GFP mouse line for these assays following CSD had not been determined, parallel tests (with TAM injections) on the well-studied C57BL/6J mice were included. Additionally, to assess whether TAM injections selectively impact the Arc-GFP mice, WT-GFP mice were introduced as controls for potential environmental effects, given that the C57BL/6J mice were bred outside the facility. Lastly, to preclude the possibility that the solvent injections or syringe applications themselves contributed to the SI improvement, two cohorts of C57BL/6J mice were included - one subjected to solvent injections and the other with no injections.

Apart from the behavior stress readouts, we also included physiological assessments of the stress effects by measuring the weights of tissues involved in the HPA axis, namely the hypothalamus and adrenal glands along with the assessment of CORT levels (**Figure 8**).

Although all the experiments on the different groups were performed simultaneously, for clarity, we first describe the control vs stress comparisons for all tests conducted after CSD exclusively for the Arc-GFP mouse line, in the next section. This is followed by a comprehensive report of the comparisons between the different genotypes within the same treatment (TAM-injected) and then the same genotype (C57BL/6J) with different treatments to determine the origins of the abnormality noted in the initial behavior assay.

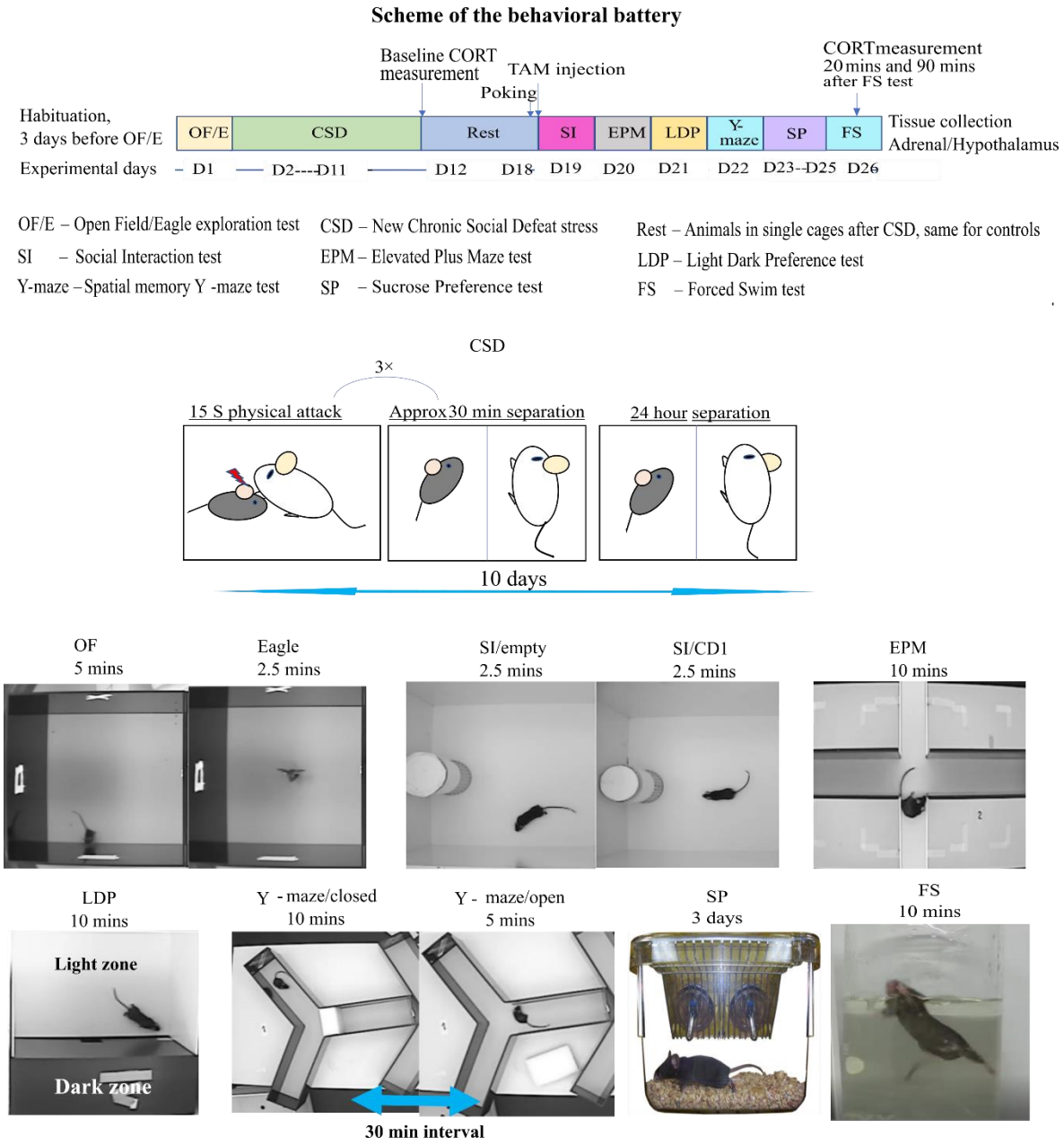

Figure 8:. Scheme of the behavioral battery tests and physiological assays along the longitudinal timeline.

Mice were habituated to the experimental environment 3 days before the open field eagle (OF/E) test and segregated into control and stress groups for the new CSD paradigm, based on the results from the OF/E test. In the new CSD paradigm, the intruder mouse was subjected to a 15 S pure physical attack by the CD1 mouse, repeated 3 times with a new CD1 mouse for each attack, daily. Each attack episode lasted with a 30 minutes' physical segregation between the CD1 mouse and the intruder mouse except for the last attack (See **Methods**). After the last attack episode, the intruder mouse was physically separated by the mesh wall from the last CD1 mouse and was left undisturbed for 24 hours till the next day of the stress experiment. The whole procedure was repeated for a total of 10 days as in the old paradigm and SI was performed on the 8th day. The following tests EPM, LDP, Y-maze, SP and FS, were performed on consecutive days as shown in the timeline. For physiological assessments, CORT was collected on the last day of CSD (baseline CORT), 20 minutes after FS test and 90 minutes after FS test. Approximately 24 hours after the FS test, mice were sacrificed and tissues – adrenal glands and hypothalamus were collected and weighed. For more details of the tests, see text.

Groups employed for this new scheme include control and stressed populations of mice injected with TAM, 5 hours before the SI test for Arc-GFP, WT-GFP and C57BL/6J along with vehicle-injected and non-injected groups (replacing the TAM injections) of C57BL/6J mice. (NB: The image for SP test was obtained from google images.) **Abbreviations**: CSD – chronic social defeat, SI – social interaction, EPM – elevated plus maze, LDP – light dark preference, FS – forced swim, SP – sucrose preference, CORT – corticosterone.

2.3.4.1. TAM-injected Arc-GFP mice show stress effects after the implementation of a higher stressor CSD paradigm

Remarkably, with the implementation of the more aggressive CSD paradigm, we observed a significant decrease in the SI index of the stressed Arc-GFP mice (**Figure 9a,** Welch's t-test, $p<0.05$). Interestingly, the other behavioral assays also indicated stress-induced alterations in behavioral tendencies, though non-significant (**Figure 9b-9g,** t-tests, ns). In the EPM, the stressed group spent a lower % time in the open arms (**Figure 9b**) compared to the control group. This was accompanied by a reduced duration of activity in the light zone (for the LDP test) (**Figure 9c**) for the stressed group. Interestingly, contradicting the expected behavior, we observed that the stressed populations showed tendencies toward a lower latency to enter the light zone (LDP test), a decreased immobility duration (FS test) and an increased % sucrose consumption (SP test) (**Figure 9d-9f**). Additionally, the stressed group of the Arc-GFP mouse line indicated a non-significant lower CORT level in the blood samples collected after the last day of CSD (**Figure 9g,** t-test, ns), compared to control group. However, in the Y-maze test (**Figure 9h**), the stressed group exhibited a similar behavior to the controls.

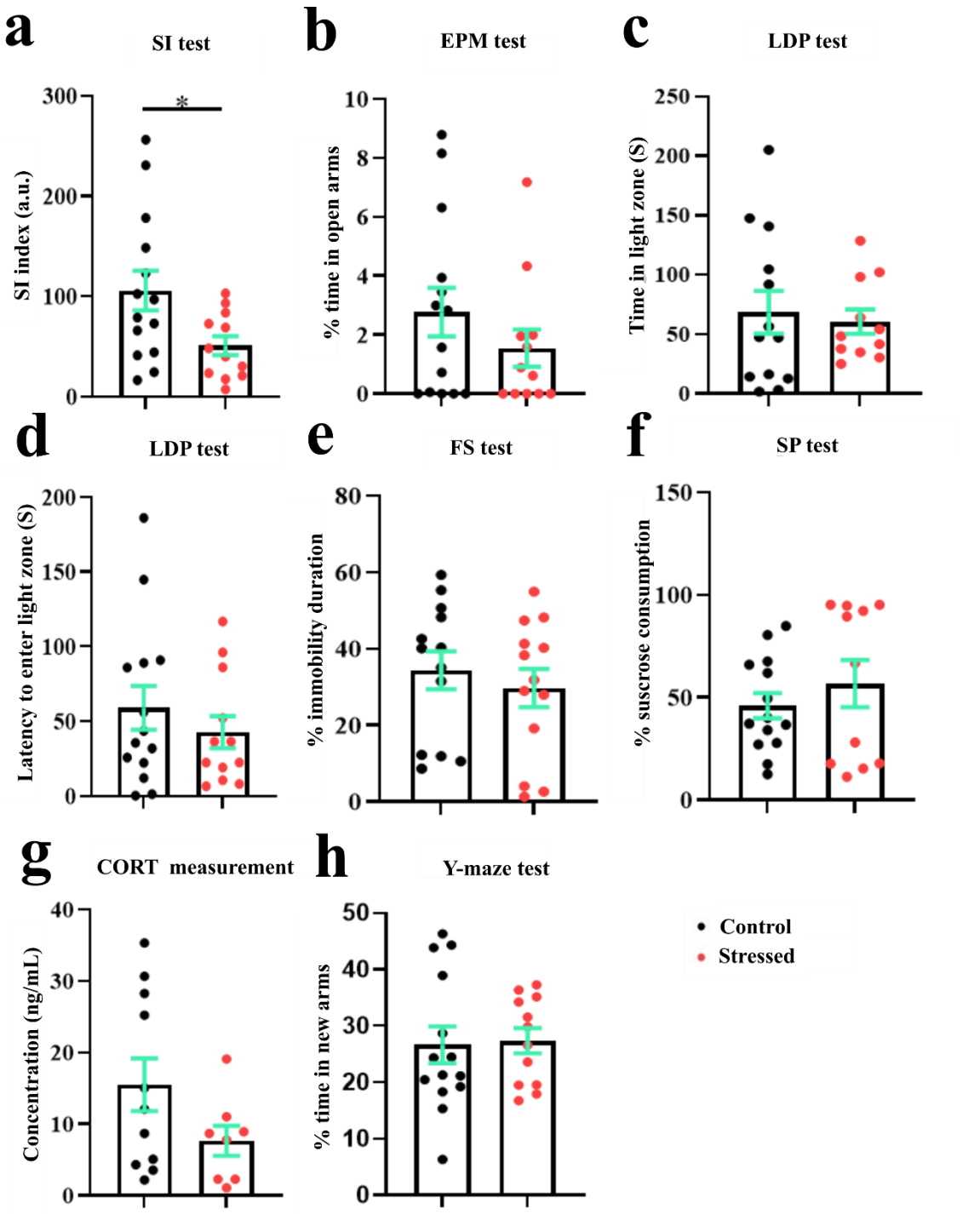

Figure 9: Arc-GFP mice exhibited stress effects in the new scheme with the use of a more aggressive stressor.

a. In the SI test, we identified a significant deficit (Welch's t-test, $p<0.05$, *) in the social interaction of the stressed group as compared to the control populations, following the use of the 3×15 S attacks. In the other tests **b-g**, including EPM, LDP, FS, SP and CORT measurements, non-significant effects of stress were observed (t-tests, $p>0.05$, n.s.) in the stressed group. Meanwhile, the Y-maze test (**h**) showed no visible difference. Error bars represent +/- S.E.M. * represents the significance value. Each dot in the graphs represents a single mouse (control - black and stressed - red). **Abbreviations**: SI – social interaction, EPM – elevated plus maze, LDP – light dark preference, FS – forced swim, SP – sucrose preference, CORT – corticosterone.

Having established that the Arc-GFP mouse line shows stress impacts with an aggressive stressor, the next step was to determine whether the results obtained from this mouse line will be comparable with stress-related findings from other mouse models. Therefore, we assessed if the Arc-GFP mouse line diverged or converged in the important behavioral and physiological aspects relevant for this study, compared to the most used mouse model, i.e., C57BL/6J.

2.3.4.2. Determining the divergence or convergence of the Arc-GFP mouse line and implications on its usability for cross-comparisons with other stress research

Divergence of the Arc-GFP mice from the C57BL/6J mice and WT-GFP mice (comparisons between the non-stressed controls)

In the above section, we noted unexpected trends in the stress-control comparisons of the Arc-GFP mice in some behavior assays (**Figure 9d-9f**). Therefore, to characterize the divergence of the Arc-GFP mice and determine its usability for stress research, we compared the behavior assays of the TAM-injected Arc-GFP animals to the other TAM-injected genotypes (C57BL/6J and WT-GFP), first, **using only the non-stressed controls**. Given the different facility origin of the C57BL/6J, WT-GFP was added as a genotype control for the Arc-insertion, should the injections interact exclusively with the transgenic insertion. Significant difference amongst the three genotypes was determined using analysis of variance (ANOVA) tests followed by *post-hoc* t-tests for pairwise comparisons of the genotypes.

In the **open field/eagle** (**OF/E) test**, performed before the CSD paradigm, ANOVA revealed a significant difference among the three groups in the duration of time spent in the central zone without the eagle ($F(2, 119) = 8.058$, $p = 0.0005$) and in presence of the eagle ($F(2, 118) = 7.675$, $p = 0.0007$). *Post-hoc* multiple comparisons test following ANOVA identified that in the open field test without the eagle, the Arc-GFP mice spent a significantly higher amount of time in the open area compared to both C57BL/6J and WT-GFP mice (**Figure 10a**, left, $p<0.001$, ###; $p<0.01$, ##, respectively). Meanwhile, in the presence of the toy eagle, the Arc-GFP mice spent a significantly lower amount of time interacting with the eagle, compared to the C57BL/6J mice (**Figure 10a**, right, $p<0.001$, ###), indicating either a higher innate fear or lower preference for inanimate objects. Similarly, we noted a significant difference amongst the three groups for the distance travelled without the eagle ($F(2, 119) = 19.04$, $p<0.0001$). The *post-hoc* multiple comparisons test following ANOVA test showed that the Arc-GFP mice travelled a significantly higher distance than the C57BL/6J mice (**Figure 10b**, $p<0.01$, ##), indicating hyperactivity. However, the distance travelled was significantly lower than WT-GFP mice (**Figure 10b**, $p<0.05$, #). On the other hand, there was no significant difference in distance

travelled amongst the three groups in the presence of the eagle ($F(2, 119) = 2.869$, $p = 0.06$). Altogether, the results from the OF/E test point towards a heightened sense of anxiety in the Arc-GFP mice. The implications towards a higher anxiety level were supported by the findings from the **SP test** ($F(2, 33) = 4.886$, $p = 0.0138$) and **FS test** ($F(2, 33) = 3.741$, $p = 0.0343$). In the SP test, Arc-GFP mice consumed significantly less sucrose than WT-GFP (**Figure 10c**, multiple comparisons test following ANOVA, $p<0.01$, #; t-test, $p<0.01$, *) and C57BL/6J (**Figure 10c**, t-test, $p<0.01$, *). Meanwhile, in the FS test, the % immobility duration of Arc-GFP mouse line was significantly higher than both the C57BL/6J (**Figure 10d,** multiple comparisons test following ANOVA, $p<0.05$, #; t-test, $p<0.05$, *) and WT-GFP (**Figure 10d,** t-test, $p<0.05$, *) mouse lines. Additionally, the physiological assessment of **CORT levels**, after the last day of CSD, revealed a significantly higher concentration of CORT in the collected plasma from the Arc-GFP compared to both the C57BL/6J (**Figure 10e**, multiple comparisons test following ANOVA, $p<0.05$, #; t-test, $p<0.05$, *) and WT-GFP (t-test, $p<0.05$, *). Cumulatively, these results point towards a more anxious nature of the Arc-GFP mice, distinct from that of the C57BL/6J and WT-GFP mice. Though a higher baseline CORT level could be interpreted as a higher resilience capacity in the Arc-GFP mouse line, the preceding results suggest a concurrent interpretation towards a more anxious nature.

Meanwhile, in the **EPM and LDP tests,** we observed divergence of both the Arc-GFP and WT-GFP mice from the C57BL/6J mice, with a significantly lower duration of time spent in the elevated open arms (**Figure 10f**, t-test, $p<0.05$, *; t-test, $p<0.05$, *) and a shorter duration of time spent in the light zone of the LDP arena (**Figure 10g**, t-test, $p<0.01$, *; t-test, $p<0.05$, *). The behavior tendencies observed in both these tests could reflect breeding facility-induced differences from the C57BL/6Rj breeds (as also observed in other in-house studies) or an impact of the presence of the mutant GFP reporter construct. Interestingly, in the **Y-maze** test, analyzing spatial memory, the different genotypes revealed no observable differences (data not shown).

Following these results, one can reinterpret the unexpected patterns (**Figure 9d-9g**) in control-stress comparisons of the Arc-GFP mice (in the previous section) to be partially derived from the divergence in the baseline behavior characteristics, themselves.

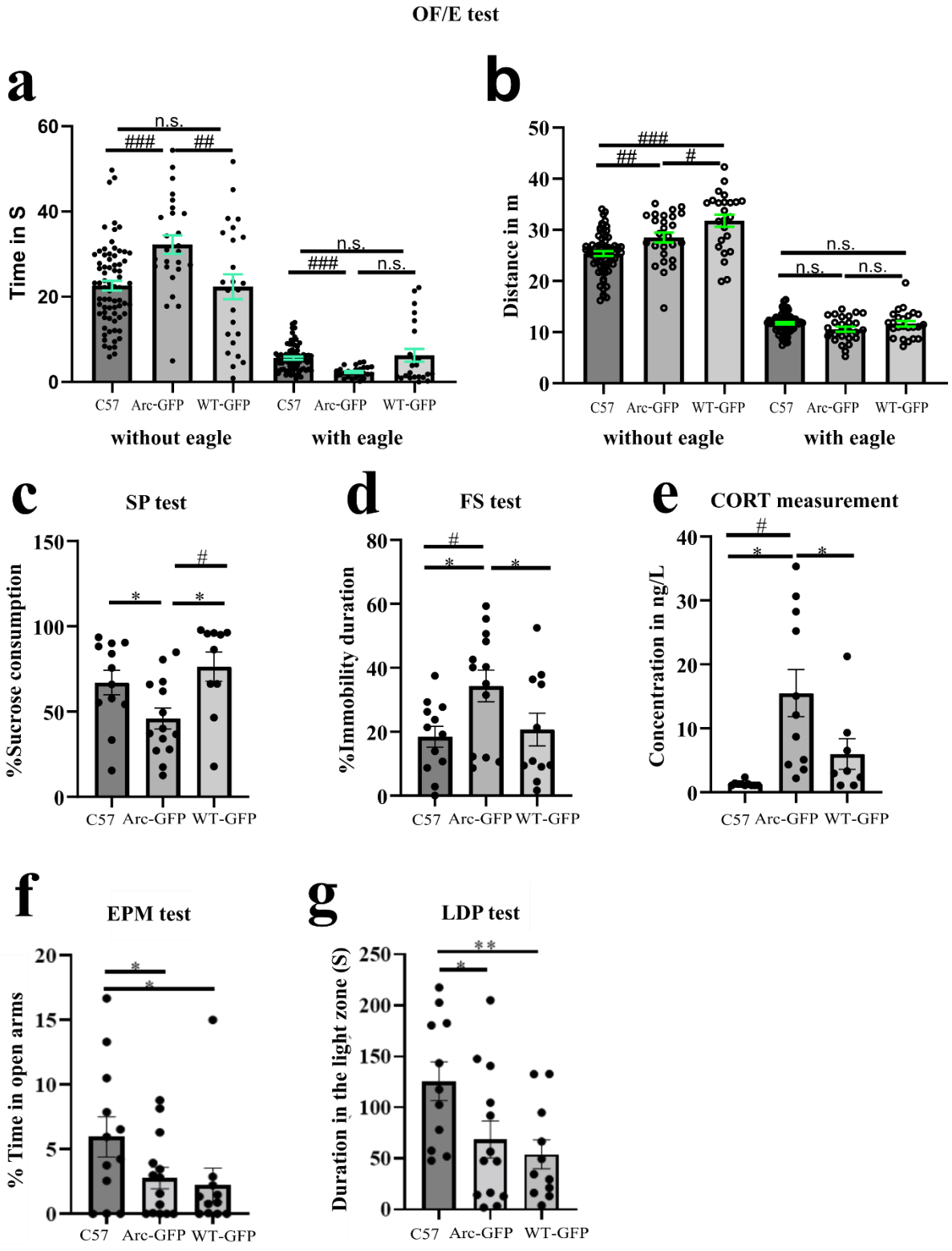

Figure 10: Genotype differences in behavior patterns of non-stressed controls as observed in multiple assays.

a,b OF/E tests showed a significant difference in both the duration of time spent at the centre zone of the open field as well as the corresponding distance parameter measured in both cases of 'without' and 'with' the eagle for the different mouse lines (ANOVA tests: $p<0.001$, ###; $p<0.01$, ##; $p<0.05$, #). **c-e** SP and FS tests along with CORT measurements (on the last day of the CSD paradigm) depicting significant

differences in the patterns exhibited by the Arc-GFP mice from both the C57 and WT-GFP mice (ANOVA test: $p<0.05$, #; t-test, $p<0.05$, *). **f.g** EPM and LDP tests revealed significant differences of the Arc-GFP and WT-GFP mice from the C57 (t-tests, $p<0.01$, **; $p<0.05$, *). Error bars represent +/- S.E.M. #, * represent the significance values from ANOVA tests and t-tests respectively, n.s. denotes non-significance. Each dot in the graphs represent a single mouse from the non-stressed populations. **Abbreviations**: OF/E – open field/eagle test, SP – sucrose preference, EPM – elevated plus maze, CORT – corticosterone, FS – forced swim, LDP – light dark preference, C57 – C57BL/6J, WT-GFP - single TG mouse line devoid of the ArcCreER^{T2} gene insertion.

Similarities in stress response of the Arc-GFP mice with the C57BL/6J and WT-GFP mice (comparisons including the stressed populations)

Though we noted a certain divergence in certain behavior traits as expected of GM animals, we also detected shared similarities in the stress response in the **SI, CORT** measured after the FS test and **organ weights** of the HPA axis (**Figure 11a-d**).

In the SI tests, all genotypes showed a significant effect of stress (**Figure 11a**, t-test, $p<0.05$, *) in the stressed group compared to non-stressed controls. In addition, we noted a similar increase in CORT at 20 minutes after FS test in all groups, **Figure 11b**, with a more elevated (non-significant) response in the respective stressed groups of each genotype. After 90 minutes of the FS test, the CORT levels decreased similarly in all genotypes, with a slightly lower (non-significant) level in the corresponding stressed groups (**Figure 11b**). On the other hand, a non-significant increase in the weight of the adrenal glands (**Figure 11c**) was observed in the stressed group compared to non-stressed controls of all genotypes, while a non-significant increase in the weight of the hypothalamus (**Figure 11d**) was observed only in the C57BL/6J and Arc-GFP mice. Last but not the least, we detected the persistence of stress effects in the Arc-GFP mice as the stressed group still displayed a similar avoidance of the CD1 mouse even after four weeks of the last CSD (See **Figure 11e**). Collectively, these results indicate that, despite some divergence, the Arc-GFP shares a similar HPA axis response to the C57BL/6J and WT-GFP mice. Apart from this, the persistence of stress effects suggests that the molecular results from this mouse line would be generalizable and comparable to other studies.

Having determined the comparability of the mouse line to the most commonly used mouse model, we, next, proceeded with the identification of impacts of TAM to ensure that the single injection would not sustain major impacts on the intended stress research.

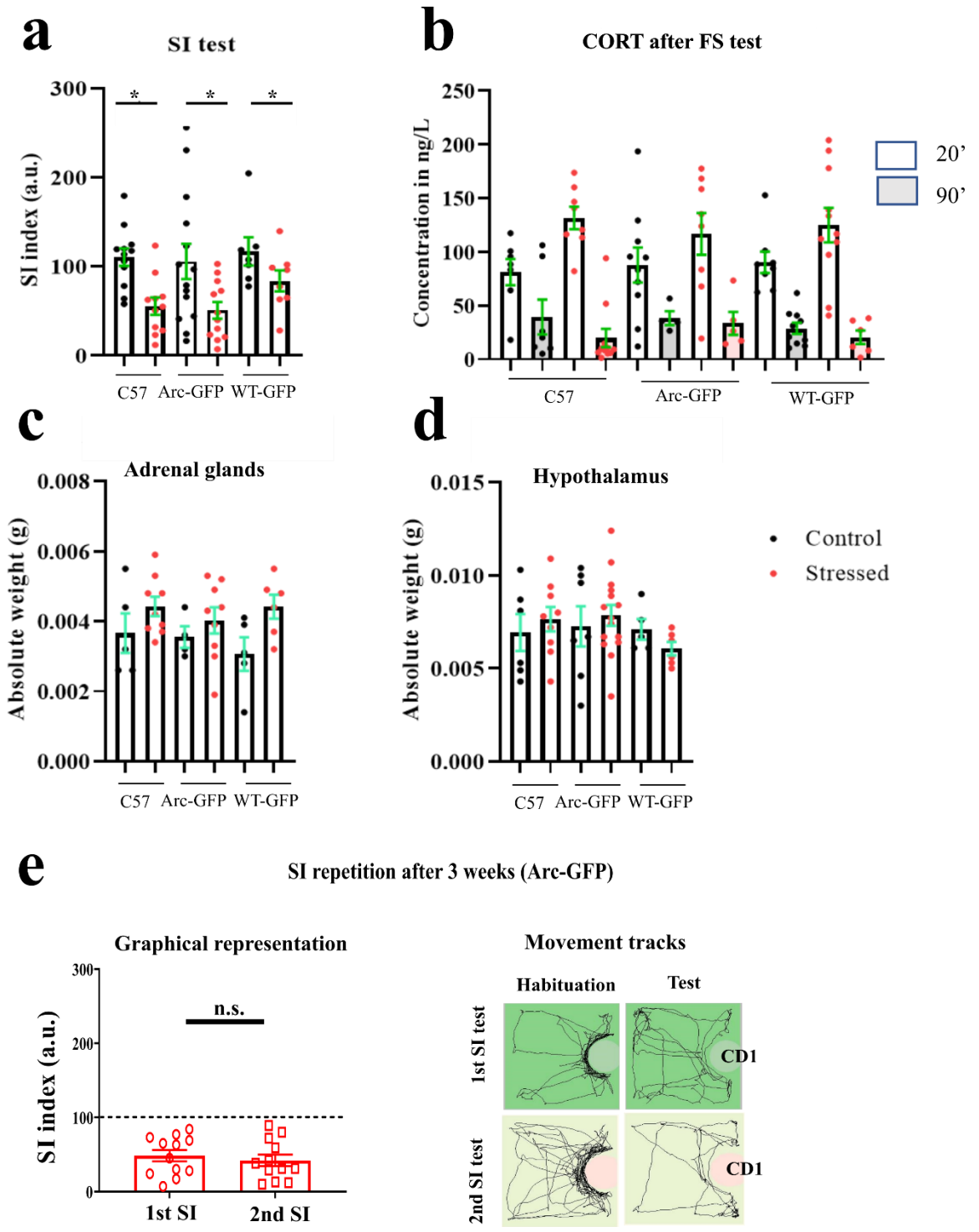

Figure 11: Similarities in the stress response despite genotypic differences in the TAM-injected groups.

a. All genotypes showed significant decreases in SI index (t-test, $p<0.05$, *) in the stressed groups, compared to the control groups. **b.** CORT measurements depicting a similar rise of CORT levels within 20 minutes of the FS test followed by a decrease in the CORT levels, 90 minutes after the FS test, indicating a functional HPA axis (activation and deactivation). **c,d.** Both adrenal and hypothalamus tissues showed a non-significant increase in weight in the stressed populations in all genotypes (except for WT-GFP, hypothalamus). **e.** Arc-GFP mice retained SI deficits in the stressed group (graphical representation, left panel) even after 4 weeks of the last CSD (i.e., 3 weeks after the first SI), indicating a long-term retention of the fear memory. The right panel shows the tracks of the animal movements during the 1st SI test and 2nd SI test of a representative mouse, showing similar avoidance of the CD1 mouse during the test phase of the SI test.

Error bars represent +/- S.E.M. * represents the significance value. Each dot in the graphs represents a single mouse (black = controls, red = stressed). Black lines in the right panel of **e**, represent the movement tracks of the mouse under observation. **Abbreviations**: SI – social interaction, CORT - corticosterone, FS – forced swim, HPA – hypothalamus-pituitary-adrenal.

2.3.5. Impacts of TAM – comparisons in the C57BL/6J mouse line

To assess the impacts of TAM injection, we conducted comparisons of the behavior assays following different modes of injection - TAM-injected (T), non-injected (N) and vehicle-injected (O) in C57BL/6J. Though the initial improvement of the SI test (**Figure 7b**) had been mitigated by the application of the more aggressive stressor (**Figure 9a**), we identified alterations in other follow-up assays. In the next following results, I present the findings from the comparisons of the **non-stressed controls** from each mode of injection.

In the FS test, ANOVA indicated a significant difference in the % immobility duration ($F(2,33) = 3.550$, $p = 0.0401$) as well as CORT levels ($F(2,20) = 7.563$, $p = 0.0036$) amongst the three C57BL/6J groups with different injection modes. *Post-hoc* multiple comparisons test revealed a significantly higher % immobility duration (**Figure 12a**, $p<0.05$, #) of the TAM-injected mice compared to the non-injected mice, while no significant difference was observed between the vehicle-injected and non-injected groups (**Figure 12a,** n.s.). Correspondingly, the rise in **CORT** level, 20 minutes after FS test for TAM-injected mice was significantly higher (**Figure 12b**, $p<0.01$, #) than for the non-injected mice, while no significant difference was observed between the vehicle-injected and non-injected group (**Figure 12b**, n.s.).

Next, from the ANOVA comparisons within the **stressed mice**, we identified significant differences amongst the three types of injections in the LDP test ($F(2,29) = 5.554$, $p = 0.0091$). *Post-hoc* multiple comparisons test showed that the TAM-injected mice exhibited a significantly lower latency to enter the light zone (**Figure 12c**, $p<0.01$, #) compared to non-injected mice. Additionally, the TAM-injected stressed mice also showed a significantly higher % of time in the open arms of the EPM test (**Figure 12d**, t-test, $p<0.01$, *) compared to the non-injected mice. The non-injected and vehicle-injected groups showed similar results in both cases. Altogether, these results indicate that a one-time injection of TAM can introduce significant effects on some aspects of behavior in both stressed and non-stressed mice.

On the other hand, assessing the effect of the injections on the direct **control-stress comparisons** of each injection type**, we observed divergent trends in the TAM-injected groups.** In the **EPM** test, the TAM-injected stressed mice spent more time in the open arms compared to the TAM-injected controls, while in the other two groups (non- and vehicle-injected), the stressed mice spent a lower % of time in the open arms (**Figure 12e,** t-tests, n.s.)

than the controls. Similarly, in the **LDP** test, the latency to enter the light zone was significantly lower for the stressed TAM-injected mice group (**Figure 12f**, t-test, $p<0.001$, ***) compared to TAM-injected non-stressed controls, unlike in the other groups (t-tests, n.s.). In the **SP** test, the TAM-injected stressed mice exhibited a decreased sucrose consumption compared to the TAM-injected non-stressed controls, a pattern different from the non-injected and oil-injected groups (**Figure 12g,** t-tests, n.s.). Thus, we can conclude that **TAM and not the vehicle injections impact behavior assays**.

The above findings raise the question of whether TAM injection would deviate the stress response. To answer this, we compared the components of the HPA axis. Interestingly, despite the unprecedented effects of TAM on some aspects of behavior, for example, a significant increase in the % immobility duration in the FS test (**Figure 10d**) in the controls of TAM-injected mice, we observed that physiological components of the HPA showed an appropriate response to stress. The rise and fall of **CORT** levels during FS test remained unaffected by the one-time injection of TAM (**Figure 12i**), indicating a still functional HPA axis. Additionally, weights of adrenal glands showed a tendency of weight gain in stressed mice compared to the controls (**Supplementary Figure 2d**). Correspondingly, weight of hypothalamus also displayed a non-significant increase in both TAM-injected and non-injected stressed mice (**Supplementary Figure 2d**).

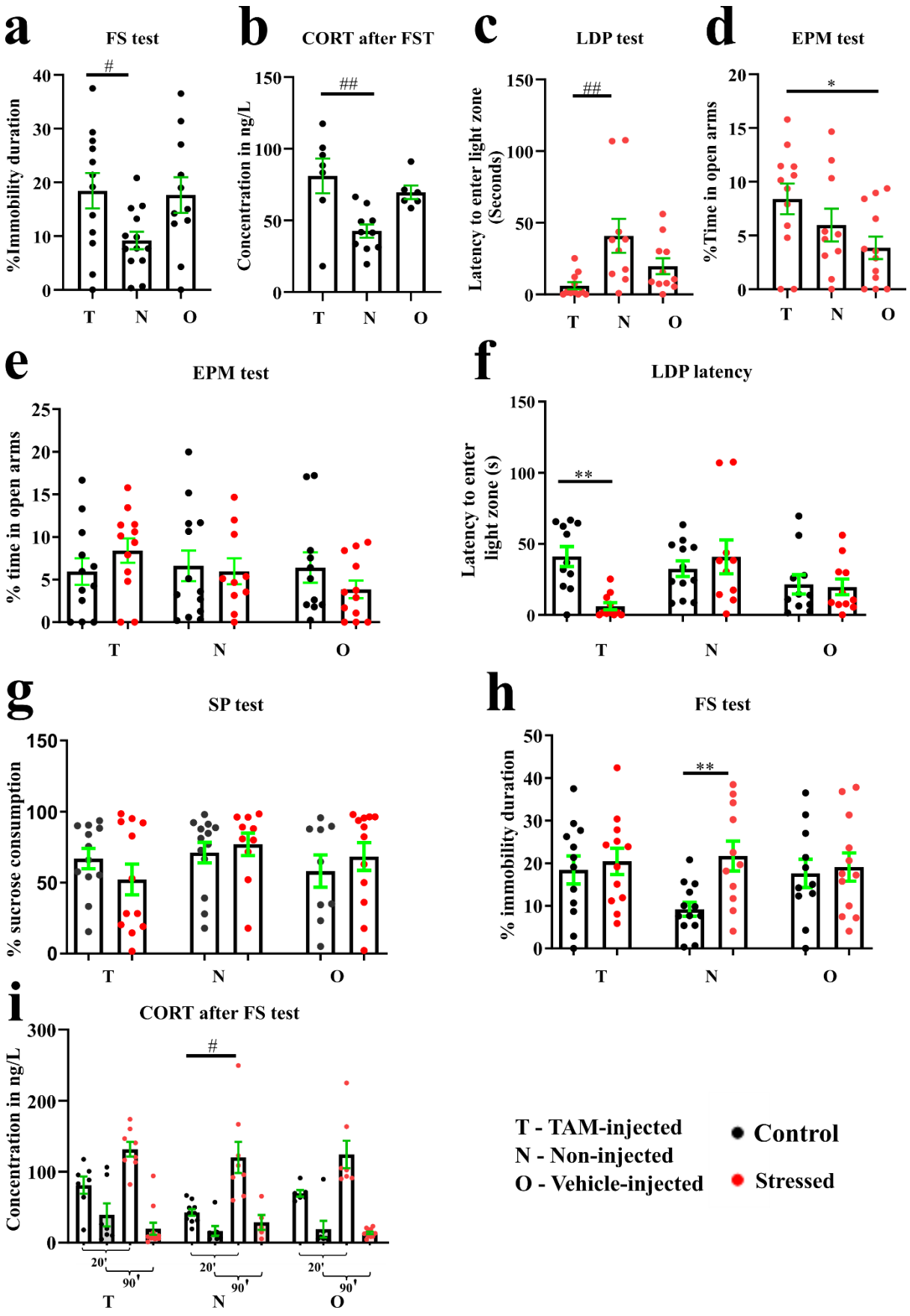

Figure 12: Implications of TAM injections.

a, b. Significant increase in %immobility duration in FS test accompanied by higher CORT concentration in TAM-injected controls compared to non-injected controls (ANOVA tests, $p<0.05$, #; $p<0.01$, ##), indicating plausible increase in anxiety. **c, d.** Significant decrease (ANOVA test, $p<0.05$, #) in latency to enter light zone in LDP and a significantly higher (t-test, $p<0.05$, *) % time spent in open arms in the EPM of the TAM-injected stressed populations compared to other groups, indicating plausible decrease in anxiety. **e-h**. Distinct patterns of control-stress relationship in the TAM-injected group (T) as compared to the non-injected and vehicle-injected groups. **i.** Similar rise and fall of CORT in all groups while only the non-injected group showed a significant increase in CORT (ANOVA test, $p<0.05$, #) in the stressed population as compared to the control population, 20' after the FS test. Empty bars indicate CORT levels at 20' after the FS test, while solid bars indicate CORT levels 90' after the FS test. Error bars represent +/- S.E.M, green for before CSD, black for after CSD. *, # denote the significance value from t-test and ANOVA test, respectively. Each dot in the graphs represent a single mouse. **Abbreviations**: T – TAM-injected, N – non-injected, O – vehicle-injected, SP – sucrose preference, EPM – elevated plus maze, CORT – corticosterone, FS – forced swim, LDP – light dark preference.

2.4. Discussion

Though the TAM-inducible Arc-GFP mice provides an ideal avenue for tracing and studying spatiotemporally active populations relevant in stress-susceptibility and -resilience research, it comes with its own baggage. First, appropriate TAM dosages for eliciting optimal stimulus-specific engrams had to be established. Following the curation of the appropriate dosage, we noted that TAM-injected Arc-GFP mice showed an improvement in SI after CSD (**Figure 7b,c**). Indeed, the impacts of TAM on SI was recently reported in an independent study by [262] (which was not known at the time we conducted the respective experiments). In our systematic approach, we identified that the improvements were partially due to the application of the artificial estrogen, that influences social behavior[259–261]. Indeed, an increase in the stressor, led to significant deficits of the stressed mice in the SI test, despite TAM injections (**Figure 9a**). However, it is interesting to note that a single exposure to TAM can still introduce long-term effects in behavioral assays performed days after the injection, for example, a higher tendency of TAM-injected mice to explore the open arms in the EPM test (**Figure 12d**) or decreased latency to enter the light zone (**Figure 12c**). All these alterations point towards an anxiolytic effect of TAM. However, not all the changes could be explained by the persistence of TAM in the body of the organism as the half-life of TAM is only about 12 hours (see citations in [263]) to 20 hours[253] and maximum 48 hours in some mouse lines (see citations in [263]). Therefore, we presume that the TAM injection during its effective phase could have intervened critical phases of epigenomic cascades or transcriptomic cascades originating from the exposure to the CSD stressor, thereby altering the resulting outcomes of the stress response. On the other hand, TAM seems to introduce an anxiety effect on the non-stressed controls. For example, in the FS test (**Figure 12a**), the TAM-injected non-stressed controls (C57BL/6J, T) exhibited a significantly higher immobility duration compared to the non-injected controls (C57BL/6J, N). This was

also reflected in the increased CORT level of the TAM-injected control mice as compared to the non-injected group (**Figure 12b**).

Thus, TAM injection itself can introduce side-effects to that of the activation of the Cre recombinase as also shown by other very recent studies[262,264–269]. However, it is a necessary component for TAM-inducible CreER^{T2} mouse lines. On the other hand, though Arc-GFP mouse line showed some divergence of behavior from the C57BL/6J mouse line, the stressed group (exposed to the aggressive stressor) showed SI deficits, which were visible even after a month. Apart from this, the mouse line exhibited a similar physiological stress response as the C57BL/6J. These findings suggest the usability of the TAM-inducible Arc-GFP mouse line for stress research. Despite the slight trade off due to the application of TAM, we believe that the use of this mouse line will provide a clearer insight into the ongoing molecular differences between the resilient and susceptible engram nuclei, following stress exposure. Thus, this part of the thesis contributes a CSD mouse model using TAM-inducible Arc-GFP mice for advancing stress research using engram-specific nuclei. Given our critical analysis, we posit that the multiomics results obtained from this mouse line will be generalizable and valuable for stress research.

Chapter 3. Protocol generation – Nuclei isolation from low volumes of micro-dissected tissues

Note: A semblance of this Chapter is also available as a non-peer reviewed article in bioRxiv (doi.org/10.1101/2020.11.18.374223) and will be submitted for review following the publication of the omics' manuscripts from this thesis.

3.1. Introduction

For optimal isolation of nuclei from micro-dissected brain regions of rare origin, suitable protocols to ensure optimal yield and quality are essential. Although a few nuclei isolation techniques with different extraction buffers were available, most of them were optimized for bulk tissues or large volumes of starting samples[243,270,271]. As our work restricted the number of mouse samples that can be obtained, a suitable protocol facilitating the extraction of nuclei from small volumes of micro-dissected tissues had to be established. Additionally, reducing the use of mice to a minimum possible is a promising ethical solution for studies using animals. Therefore, for the successful employment of the Arc-GFP mice in multiomics investigation, a suitable nuclei isolation protocol for optimal yield had to be developed. Though one can argue that instead of using the nuclei, the activated cells can be directly used, cells are sensitive to the tissue dissociation process, while nuclei are more robust to mechanical assaults[272]. Apart from this, some cell types are more sensitive to mechanical assaults than others, thereby reducing their representation during sequencing. An example can be stated for the work by Vennin and colleagues[244], where neuronal cell populations were underrepresented in their single cell studies. As such nuclei isolation is preferred over cellular dissociations. However, it is still a complex process from a biochemical point of view[273]. During nuclei isolations, chemical or mechanical disruption[271] is applied to rupture the cytoplasmic membrane of the cell while retaining the integrity of the nuclear membrane. Extensive chemical or mechanical stress during any step of the isolation process can stimulate nuclear leakage, releasing chromosomal DNA. This can induce clumping of nuclei and thereby result in a decreased yield. Besides this, the other pitfalls concerning proper choice of buffers, tissue dissociation methods, and reducing downstream processing duration that are critical for sensitive samples, have not been thoroughly investigated. Therefore, this Chapter deals with the establishment of a compact nuclei isolation protocol tailored for several important brain regions (microvolumes with minimum volume limit of 1 mm^3). Due considerations for multiple factors including buffers and speed of processing, have also been taken into account.

3.2. Methods

3.2.1 Animals, behavioral experiments and TAM injection

Both male and female Arc-GFP mice (n = 14) were used for these experiments. All mice were between 8 to 16 weeks old. Tamoxifen (TAM- 150 mg/Kg, Sigma Aldrich; solvent- 9:1 of corn oil:100%ethanol, Sigma Aldrich) was injected 5 hours before the SI test. SI tests were performed as described in **Chapter 2** (without the prior application of a stressor). Mice were euthanized by cervical dislocation, 72 hrs after the TAM injection.

3.2.2. Micro-region dissections

Following cervical dislocation, the brain was removed carefully to allow the pituitary to remain intact at the ventral portion of the skull. Pituitary was then collected into an Eppendorf containing homogenization buffer (HB). Coronal sections of 1 mm thickness were obtained using a brain matrix. Removing the initial frontal slice (less than 1mm), the PFC was dissected from the first, second and third tissue sections manually (**Figure 13**). The Allen Brain Atlas (https://atlas.brain-map.org/) was used for reference. From the second and third sections, the Naccu was dissected. Hypothalamus was then dissected from the remaining unsliced brain by scooping up the hypothalamic region. Finally, the hippocampus was then dissected from the left and right hemispheres of the brain.

Note: For all brain regions, both hemispheres were used.

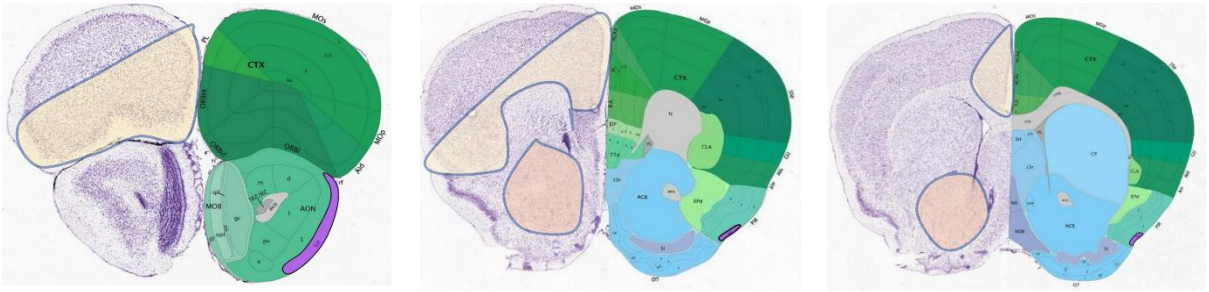

Figure 13: Regions for tissue dissections.

Locations of the dissected regions for PFC (prefrontal cortex) and Naccu (nucleus accumbens) shown in yellow, and orange shaded regions, respectively, superimposed on the mouse brain map representation from Allen Brain Atlas. The dissections were performed using 1 mm coronal slices.

3.2.3. Nuclei isolation

3.2.3.1. Solutions

Stock solutions

6× Tricine stock (pH-7.8, with KOH) - Tricine (120 mM, Sigma, #SLBR4300V), KCl (150 mM, Roth), $MgCl_2$ (30 mM, Sigma, #011M0118V) and ddH_2O and stored at 4˚C. Stock solutions of spermine (150 mM, Sigma, #BCBS6090V) spermidine (500mM, Sigma, #BCBW6017), cOmplete Mini EDTA-free protease inhibitor (PI) (1000× in ddH20, Roche, #29384100) were prepared in ddH_2O and stored at -20˚C for use within 2 months. 10% IGEPAL CA-630 (Sigma, 043K0654) stock solution was also prepared in ddH_2O and stored at room temperature. All other solutions were prepared on the day of the experiments and can be stored for at least one day at 4˚C.

Homogenization buffer (HB)

Sucrose (250mM, Sigma, #BCBT8436) was diluted in 1× Tricine stock solution (5 volumes of ddH_20 and 1 volume of 6× Tricine stock) and termed as HB. For dounce homogenization, HB was supplemented with a final concentration of 0.150 mM spermine, 0.500 mM spermidine, 1×cOmplete Mini EDTA-free PI, and 1 mM dithiothreitol (dTT, Applichem, #1P006802). The supplements were included to preserve nuclear membrane integrity and DNA along with reduction of protein degradation during the isolation process. This supplemented HB will be referred to as HB-supplemented in the following sections.

The rest of the HB (non-supplemented) was used for preparing the different gradients from the original 60% iodixanol stock solution (Sigma, #BCCB9914). 50% iodixanol solution was prepared using five volumes of 60% iodixanol and one volume of 6× Tricine stock. 40% and 30% iodixanol solutions were subsequently prepared from the 50% iodixanol solution as recommended in "OptiPrep, Application Sheet C01[274]" from "Alere Technologies" and stored on ice before use.

3.2.3.2. Protocol establishment and optimization

The nuclei isolation protocol for neocortices[243] was modified following the requirements of micro-dissected tissues to increase nuclei isolation efficiency. All steps were processed at 4˚C or on ice. The micro-dissected tissue samples were each transferred to 1.5 mL Eppendorf tubes containing 300 µL of supplemented HB. The micro-dissected tissues were dounced five times using the pestle (Z359971-1EA, Sigma Aldrich) in a soft twisting motion, initially. 9 µL of 10 % IGEPAL CA-630 was then added into each tube, achieving a final IGEPAL CA-

630 concentration of 0.3%. The addition of this non-ionic detergent is necessary to rupture the cytoplasmic membrane ([275,276]as cited in [277]) and the outer nuclear membrane. Following this, the douncing was repeated ten times with tight twisting rotations to obtain a good tissue homogenate. The identity of a good tissue homogenate was defined by the lack of visible tissue clumps with an orangish or whitish tinge, depending on the initial amount of tissue (and RBCs) in the Eppendorf tube. An equal volume (300 µL) of 50 % iodixanol was then added to this tissue homogenate, thereby bringing down iodixanol concentration to 25 %. For routine experiments for ultracentrifugation with the cushion layer, the prepared density gradients (40% iodixanol and 30% iodixanol) were layered as follows: 600 µL of 40% iodixanol followed by 600 µL of 30 % iodixanol transferred gently on top of the 40% layer along the wall of the 4 mL ultracentrifuge tube, with a pipette. The tissue homogenate in 25% iodixanol was then pipetted in a similar way to avoid disrupting the gradient formation. The tubes were then placed in the white polyvinyl chloride caste to fit the swinging bucket rotor (Sorvall HB-6) of the ultracentrifuge (Sorvall RC6+ Centrifuge) (refer to **Figure 14**). Ultracentrifugation was performed at 7820 rpm (10,000 ×g) at 4° C for 18 minutes for all experiments except for studying different centrifugation durations. Thereafter, nuclei were collected (300 µL) from the 30%-40% iodixanol layer interface in a slow swirling motion with a 1000 mL pipette and transferred into a 1.5 mL Eppendorf tube through a 20 µm strainer (Partec 04-0042-2315). This collected solution is termed as "nuclei solution". For flow cytometry, the nuclei solution was diluted with HB/0.4% IGEPAL) at a ratio of 3:1. This solution is referred to as the original buffer (OB). The modifications to determine the effects of various types of centrifugations are as follows.

Modifications to determine the effects of the various types of centrifugation

1. For validation of nuclei extraction efficiency, where the whole brain was used, the brain regions were micro-dissected into smaller pieces. 2-3 pieces of the micro-dissected tissues were independently homogenized in 1.5 mL Eppendorf tubes containing the homogenate. The homogenization was performed with the pestle (Z359971-1EA, Sigma Aldrich), which can be readily applied to the tiny micro-dissected brain regions instead of conventional tools for large tissues. The homogenates were then pooled to obtain a total of 5 mL. The pooling was performed as we were interested in determining the nuclei yield from the whole brain, and separate ultracentrifugation for each homogenate could contribute to nuclei loss. The pooled homogenate was then diluted with an equal volume of 50% iodixanol to give 10 mL of 25% iodixanol-homogenate mixture. The 50 mL centrifugation tube was then layered with equal

volumes of 40% and 30% iodixanol solutions. The 25% iodixanol-homogenate layer was then pipetted on top of the 30% iodixanol layer.

2. For Naccu (roughly one cubic mm), douncing was performed using a 0.1 mL tissue grinder (Art. No. 0296.1, Roth) with less than 100 µL homogenization buffer. After the initial douncing, volume was brought up to 150 µL by adding the homogenization buffer. The homogenate was then mixed with an equal volume of 50% iodixanol. Density gradient ultracentrifugation was then performed like for other brain regions with small reductions in volumes for the gradients - 40% (500 µL) and 30% (500 µL). Following this, 150 µL of nuclei solution was then collected from the 30-40% interface nuclei layer.

3. For the comparison experiments of "with and without" cushion layer, 800 µL was used for each of the 40% and 30% gradients instead of 600 µL. The volume change was, specifically, introduced to minimize damage to the nuclei during pelleting without the cushion layer. After ultracentrifugation, for the experiments without the 40% layer, the upper homogenate layer and 30% layer were removed entirely using a 1000 mL pipette, leaving only about 50 µL at the bottom of the tube. The remaining nuclei solution was resuspended with either 30% iodixanol: HB with 0.4% IGEPAL (3:1) or HB (with 0.4% IGEPAL) or phosphate-buffered saline (PBS) with 0.4% IGEPAL for various purposes.

4. For nuclei count comparisons from different ultracentrifugation times, ultracentrifugation was performed for different durations of 12 minutes, 8 minutes, and 5 minutes. The order of centrifugation with the set time was alternated between repeated replicate experiments to avoid unwanted errors introduced by the storage of isolated nuclei on ice for the length of the experiment per day. (NB: Parts of the experiments for this section were performed by J.E. Wettschereck, who is also recognized as a co-author in the manuscript[278] dedicated to this chapter.)

5. For re-centrifugation, equal volumes of PBS or HB were added to the nuclei solution and centrifuged at 5,000 ×g. The supernatant was removed, and the pellet was resuspended with PBS or HB.

3.2.4. Flow cytometry and fluorescence-activated nuclei sorting (FANS)

Flow cytometry analysis and FANS were performed using a BD FACSAria III SORP equipped with four lasers (405 nm, 488 nm, 561 nm, and 640 nm) and a 70 µm nozzle. GFP expression was detected using the blue laser and a 530/30 BP filter, whereas DAPI was detected using the violet laser and a 450/50 BP filter. 10,000 total events were recorded, before sorting and a

gating strategy was applied. First, nuclei were gated according to their forward- and side-scatter properties (FSC-A/SSC-A), followed by doublet exclusion using SSC-A and SSC-W. Nuclei were then gated according to their DAPI expression while GFP expression was used as the sorting gate. Sorted nuclei were collected in 1.5 mL Eppendorfs in PBS (with 0.4% IGEPAL), HB (with 0.4% IGEPAL), 30% iodixanol: HB with 0.4% IGEPAL (3:1) or 4% paraformaldehyde (PFA) to determine the effects of different buffers on nuclei integrity. The analysis was done using the BD FACSDiva 8.0.2 Software or FlowJo (v.10.6 or higher). Reanalysis of the sorted nuclei was performed by determining the percentage of sfGFP+ nuclei from at least 50 single DAPI positive nuclei. Dot plot axes fonts were enhanced in Inkscape v1.0.2.2 (https://inkscape.org/).

For analyzing nuclei degradation in different buffers, nuclei were sorted into PBS (0.4% IGEPAL), HB (0.4% IGEPAL) and original buffer.

NB: Flow cytometry analysis and FANS were performed by the IMB core facility. Part of the write-up for the flow cytometry and FANS section is contributed by the core facility.

3.2.5. Microscopy

3.2.5.1. Phase-contrast Microscopy

10 µL of the nuclei solution was pipetted on a hemocytometer (Neubauer) for visualization under the (Leica DM IL inverted) microscope. For experiments involving trypan blue staining, the nuclei solution was diluted with trypan blue at a 1:1 ratio. Images were captured using 20×/0.3, air objectives, or 40×/0.5, air objective. Nuclei counting was performed in the usual format for hemocytometers – an average of the nuclei counts in the four chambers of 1 mm by 1 mm, multiplied by 10,000/mL. For the nuclei count for comparing bright vs. total nuclei from experiments involving centrifugation with and without a 40% cushion layer, counts from each of the 1 mm by 1 mm chamber, were considered a technical replicate.

3.2.5.2. Wide field Fluorescence Microscopy

NB: No additional antibodies were used as the endogenous GFP was fluorescent enough to be captured in the microscopic techniques.

The wells in the µ-slide angiogenesis plate (IBIDI, # 81506) were incubated with a layer of polyethylenimine (PEI, 20 µL) for 20 minutes and then washed with 1× PBS and HB (with 0.4% IGEPAL) subsequently. 10 µL of the nuclei solution was then loaded into the inner well of the chamber gently and incubated for 5 to 10 minutes. Nuclei were then visualized using the Leica AF7000 Widefield microscope with 40x/1.1 water objective using bright field, DAPI

filter (A4), and GFP filter (L5). Tile scans were stitched using in-built software in the Leica LASX system.

For long-term imaging, nuclei embedded in the PEI were fixed using 1% PFA after removing supernatant solution from the IBIDI wells. For the fixation process, 1% PFA was applied for an incubation period of 5 minutes. Thereafter, the wells were washed with 15 µL of HB (with 0.4% IGEPAL) twice for 5 minutes each. A final volume of 10 µL of HB (with 0.4% IGEPAL) was pipetted into each well before the chamber was tightly sealed and stored at 4 ˚C for a month.

3.2.5.3. Confocal Microscopy

Leica TCS SP5 laser confocal microscope was used for all confocal microscopy images. 10 µL of nuclei solution was pipetted on "SuperFrost Plus" microscopic slides from ThermoFisher Scientific. The solution was then covered with a round coverslip with a thickness of 0.17 mm and diameter 1.5 cm for viewing the nuclei through the inverted objective lens. Images were captured using 20×/0.7, air objective, and 63×/1.4 (oil objective). For storing the samples for 1-2 days, the coverslips were sealed with commercially available nail polish.

3.2.6. Image analysis

All microscopic images were analyzed using Fiji[279]. A) For manual analysis of single nuclei, the steps are shown as hereunder:

1. Open "Image"
2. Click "Process" -> "Subtract background"
3. Click " " -> right-click and select "elliptical selections"
4. Draw "ellipse" around the nuclei of interest manually
5. Go to "Analyze"->" Set Measurements"-> select the required parameters from the menu and press "ok"
6. Go to "Analyze" -> "Measure"

3.2.6. Statistics

The statistical calculations were performed using GraphPad Prism (8.4.2). Student's unpaired t-test with the assumption that the standard deviation between populations is equal was used

for statistical comparisons of two groups, unless otherwise mentioned. In all calculations, $p<0.01$ was considered statistically significant, to decrease chances of false positives.

3.3. Results

3.3.1. Choice of gradient solution

Amongst several existing nuclei isolation protocols for large tissue regions, we chose the method described by [243] as the starting basis for modifications to suit micro-dissected brain regions. The choice was based on the use of the iso-osmotic iodixanol as a gradient solution. As mentioned previously, several steps during the isolation process can lead to reduced quality and yield. One of them is the choice of the gradient solution. Sucrose gradients have been the method of choice[280–282] for several organelles/cells for a long time. However, the use of sucrose gradients was gradually replaced by the less viscous, iso-osmotic iodixanol for the extraction of various cells/organelle/viral particles[95,270,283–290]. This shift in trend is due to the better resemblance of iodixanol solutions to the physiological fluids, thereby leading to a better preservation of cell organelles during the isolation step. Iodixanol-based density gradients have also been proven to be a better candidate than Ficoll-based density gradients[284,291]. For example, Quasem and colleagues[291] identified a loss of "quiescence" in yeast cells when centrifuged with Ficoll-based density gradients compared to the former. Therefore, iodixanol is the gradient solution of choice.

3.3.1.1 Validation of the isolation process efficiency

For all our experiments, we used the mouse model Arc-GFP (see **Methods**). Before the application of Mo and colleagues'[243] ultracentrifugation protocol for micro-dissected brain regions, we proceeded with the test for efficiency of our new tools. The tissue homogenization step is critical for nuclei yield, so, we employed a douncing system (grinding pestle), which can be readily applied to the tiny micro-dissected brain regions, instead of the douncers for large volumes of tissue, used by Mo and colleagues[243] (See **Figure 14**). As they did not report a total yield in their study using pooled neocortices, we reasoned that our first trial should be conducted using whole brains. This would allow for proper comparisons to nuclei yield from the available literature for C57BL/6J. To fit to our equipments, the whole brain was micro-dissected into several pieces of a maximum of 5 mm^3. For every sample, 2-3 pieces of the brain were homogenized using our Eppendorf- douncing setup. All the samples were then pooled for the ultracentrifugation step similar to Mo and colleagues (50 mL ultracentrifuge tube, see **Methods**). From our two independent nuclei isolation experiments, each from a biological

replicate, we obtained very similar amounts of nuclei yield (~ 33×10^6 nuclei – average of 32×10^6 and 34.6×10^6) from the whole brain (approx. 0.4 g each). This is on average 36% (1st quartile 30%, 3rd quartile 40%) of the total adult mouse brain cells as reported in literature[292–297]. In terms of nuclei/g weight of the brain, we obtained 82.5×10^6 nuclei/g. This number is in good agreement with the nuclei yield reported by Yu and colleagues[298] i.e., 80×10^6 nuclei/g of brain, where they used sucrose gradients. Interestingly, the percentage yield from our setup is higher than that reported by Sporn and colleagues[299] (11%) and Lovtrup-rein and colleagues[280] (20-25%), which used sucrose gradient solutions. Morphologically, the nuclei isolated with this set up possess a round/oval shape[300] and appear darker than the background in phase-contrast microscopy similar to that as described by [280,282] without a frizzled membrane or visible protrusion of nuclear content[301]. Thus, for our study, oval-shaped nuclei, which do not possess visible protrusion or appear excessively bright in phase-contrast microscopy will be termed as intact, good quality nuclei throughout the thesis.

3.3.1.2. Adaptation of the homogenization setup to micro-dissected brain regions: Nuclei isolation and visualization

Having established the efficiency of the douncing system, we, next, coupled it with the reduced volume ultracentrifugation protocol for the micro-dissected brain regions. Micro-dissected tissues (hippocampus, hypothalamus, pituitary, PFC, and Naccu) were dounce-homogenized in micro-volumes of supplemented homogenization buffer (see **Methods** and **Figure 14 a-c**). The homogenates were then loaded into 4 mL ultracentrifugation tubes containing microvolumes of iodixanol gradient solutions. Microvolumes were used to avoid nuclei dissipation, which could be increased with the use of larger volumes for such small amounts of nuclei. After 18 minutes of ultracentrifugation (as described by Mo and colleagues[243]), nuclei were collected from the 30-40% gradient layer (see **Figure 14 d-f**).

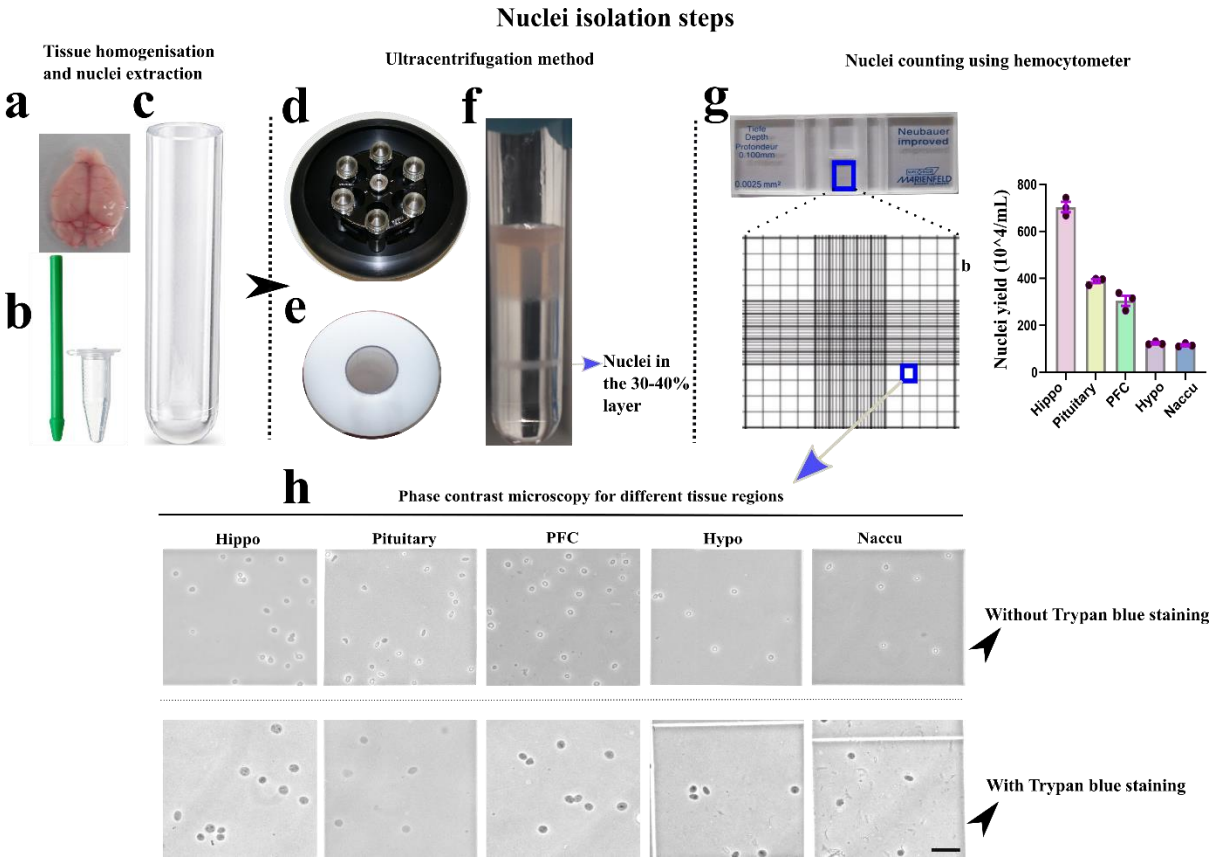

Figure 14: Nuclei isolation procedure and data quantification.

a. Mouse brain **b.** A pestle to homogenize micro-dissected tissues in a 1.5 mL reaction tube containing homogenization buffer **c.** 4 mL polypropylene ultracentrifugation tube to be used for layering the tissue homogenate over iodixanol gradients for ultracentrifugation. **d.** HB6 ultracentrifuge rotor **e.** Polyvinylchloride (PVC) caste used to fit the centrifuge tube into the rotor tubes holders **f.** Layer separation of the gradient iodixanol solution after ultracentrifugation of tissue homogenate. **g.** Nuclei, from the 30-40% layer, were counted using a hemocytometer for different brain regions (N = 3 biological replicates each). Nuclei yield was highest in hippo (hippocampus)> pituitary> PFC (prefrontal cortex)> hypo (hypothalamus)> Naccu (nucleus accumbens). **h.** Representative images of nuclei from the respective brain regions (square area of 0.25 mm × 0.25 mm). without trypan blue and with trypan blue staining in a ratio of 1:1. Scale bar corresponds to 30 µm. Error bars represent +/- SEM. Images were captured using a Leica DM IL inverted microscope, 40× air objective. **Abbreviations**: Hippo – hippocampus, Hypo – hypothalamus, Naccu – nucleus accumbens, PFC – prefrontal cortex.

The average nuclei yield (N = 3 biological replicates) estimated with a hemocytometer from the different brain regions with yield from the hippo (hippocampus)> pituitary> PFC (prefrontal cortex)> hypo (hypothalamus)> Naccu (nucleus accumbens) are shown in **Figure 14g.** The small deviations from the average between replicates could be due to individual variability in micro-dissections of biological samples, douncing or nuclei collection from the 30-40% iodixanol solution layer. The representative images (phase-contrast microscopy) of the nuclei without and with trypan blue staining are shown in **Figure 14h** (intact nuclei appear darker than background). Of note, trypan blue staining revealed some visible differences in the intensity patterns of nuclei coming from distinct areas. This could indicate differences in the nuclear membranes in different brain regions.

Having successfully adapted the iodixanol-gradient nuclei isolation protocol to microvolumes, we next proceeded with variations of the microvolume ultracentrifugation protocol with an aim to increase yield and speed.

3.3.2. Modulating the ultracentrifugation protocol to increase yield and speed

3.3.2.1 Removal of the cushion layer during ultracentrifugation to increase yield

Since most of the nuclei are lost during nuclei collection from the 30-40% interface layer, we, first, experimented with the removal of the 40% iodixanol layer. In this experimental design, experiments with the cushion layer **Figure 15a-d** and without **Figure 15e-h** were performed using the same neocortex homogenate. For the experimental design with the cushion layer (w), nuclei were collected as usual from the interface 30-40% layer. For the alternate design **without** the cushion layer (w/o), nuclei pelleted at the bottom of the tube during the ultracentrifugation process were resuspended in HB (0.4% IGEPAL). For a proper assessment, easily accessible and quantifiable parameters including nuclei yield, size, and optical density, were compared between the two types of nuclei (w/o **Figure 15h** and w **Figure 15d**) using FIJI.

Indeed, analyses of 100-200 individual nuclei per large square (1 mm^2) of the hemocytometer (n = 8 replicates) showed significant increase in nuclei yield for the paradigm without the cushion layer (w/o) (**Figure 15i,** $p<0.001$). However, this was accompanied by a significant increase in nuclei that appeared bright in phase-contrast microscopy compared to that extracted with the cushion layer. As these nuclei appeared bright in the phase-contrast microscopy, they were termed as "bright nuclei". The bright nuclei (indicated by blue arrows) and the normal dark nuclei (indicated by yellow arrows) are shown in **(Figure 15d, h**). For further characterization of the optical differences in the nuclei obtained from the two methods of centrifugation (resuspension with iodixanol buffers), we used a TCS SP5 laser confocal microscope (63×, oil objective). The screening revealed a more sporadic and spotted DAPI staining pattern in some of the nuclei extracted without the cushion layer (w/o) as opposed to the concentrated DAPI staining pattern in the nuclei extracted with a cushion layer (w) **(Figure 15j**). Further, sorting these nuclei (FANS) with the same homogenate origin, but different centrifugation methods revealed a significantly higher sfGFP+ nuclei % in the nuclei obtained from the w/o 40%-layer experiment (**Figure 15k**). Thus, we noted that there were trivial differences between the different types of centrifugation methods that affect downstream processing, even with the same homogenate origin. Although we obtained a larger quantity of nuclei and higher sfGFP% from the protocol w/o the cushion layer, we opted to adhere to the

use of the cushion layer, where we obtained dark/oval shaped nuclei, indicative of good quality nuclei, as we could not verify the origins of the bright nuclei.

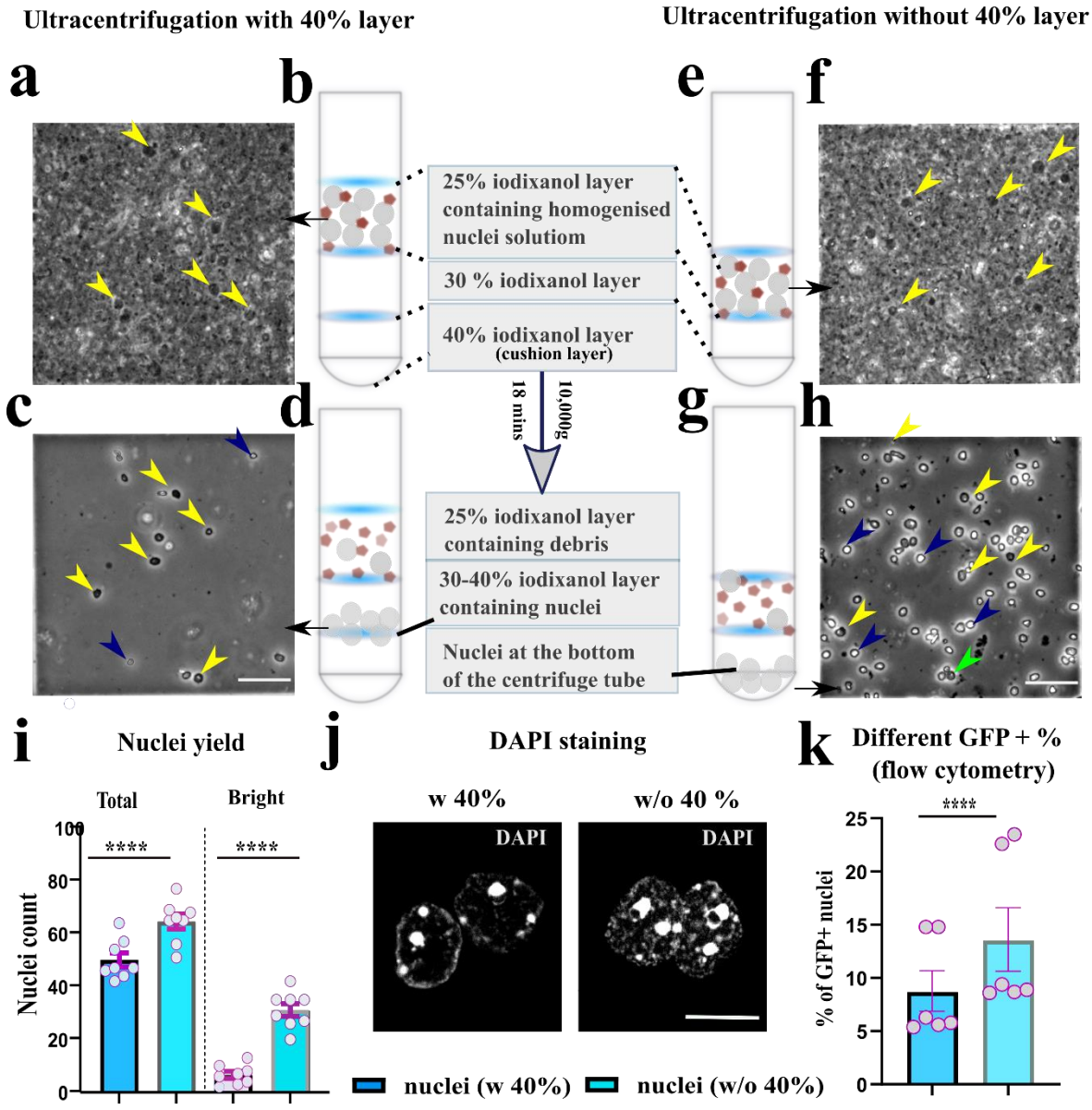

Figure 15: Comparison of ultracentrifugation with (w) and without (w/o) the 40% cushion layer.

Scheme and images for the w 40% and w/o 40% are shown in **a-d** and **e-h**, respectively. **a, f** shows the phase-contrast microscopy images of the neocortical tissue homogenate (nuclei and debris) in the 25% iodixanol layer before centrifugation in ultracentrifuge tubes (**b, e**). **c, h** Phase-contrast microscopy images of nuclei collected from the 30-40% layer (**c**) or the resuspended pellet (**h**) after centrifugation from tubes **d** and **g** as indicated in the figure. Yellow arrowheads indicate dark nuclei, blue arrows indicate the bright nuclei of smaller size and green indicates nuclei aggregation. Scale bar: 50 µm**. i** Quantification of total nuclei yield along with bright nuclei obtained from the ultracentrifugation with and without the 40% layer is shown. Total nuclei count increased significantly ($n = 8$, $p<0.0001$) in the centrifugation without the cushion layer. This was accompanied by a significantly higher number of smaller bright nuclei ($n = 8$, $p<0.0001$). **j** Qualitative differences in the DAPI staining pattern in the nuclei obtained from w 40% and w/o 40% layer (confocal microscope, 63× oil objective) Scale bars: 10 µm. **k** Percentage of sfGFP+ (GFP+) nuclei detected during sorting of neocortical nuclei obtained from w 40% or w/o 40% layer

show significant differences in the percentage of detected GFP+ nuclei ($p<0.0001$, paired t-test). All error bars represent +/- SEM. **Abbreviations**: w – with, w/o – without

3.3.2.2 Decreasing the ultracentrifugation duration to increase speed

As nuclei processing speed is essential for downstream analyzes of sensitive samples, we next sought to decrease the nuclei processing time.

Since we use micro-volumes of gradient solutions in our protocol, we hypothesized that less time would be taken by a nucleus to reach the 30-40% gradient layer from the homogenate layer. This hypothesis follows from $t \propto l$, where t = time of centrifugation and l = sedimentation distance/ radial length during maximum centrifugation minus radial length during minimum centrifugation with the same centrifugal force (Stokes' law[302]). Thus, we reduced the ultracentrifugation time from 18 minutes through 8 minutes to 5 minutes using tissue homogenates of neocortices. This was performed to determine the optimum duration for centrifugation for such small volumes without compromising nuclei yield. As can be observed from the nuclei counts in **Figure 16a,** reducing the ultracentrifugation duration from 18 minutes to 8 minutes led to a significant nuclei loss. The unexpected higher yield of the 5 minutes centrifugation time could be attributed to the profuse nuclei on the 25% layer that were not completely centrifuged, indicating an incomplete nuclei extraction from the tissue homogenate upon ultracentrifugation for 5 minutes. Therefore, we chose another time point between 18 to 8 minutes to test our hypothesis on efficient time reduction during ultracentrifugation. As shown in **Figure 16b**, we observed that 12 minutes of ultracentrifugation yielded similar nuclei to 18 minutes. Therefore, this duration was determined to be ideal for faster processing of multiple samples without significant nuclei loss and membrane integrity.

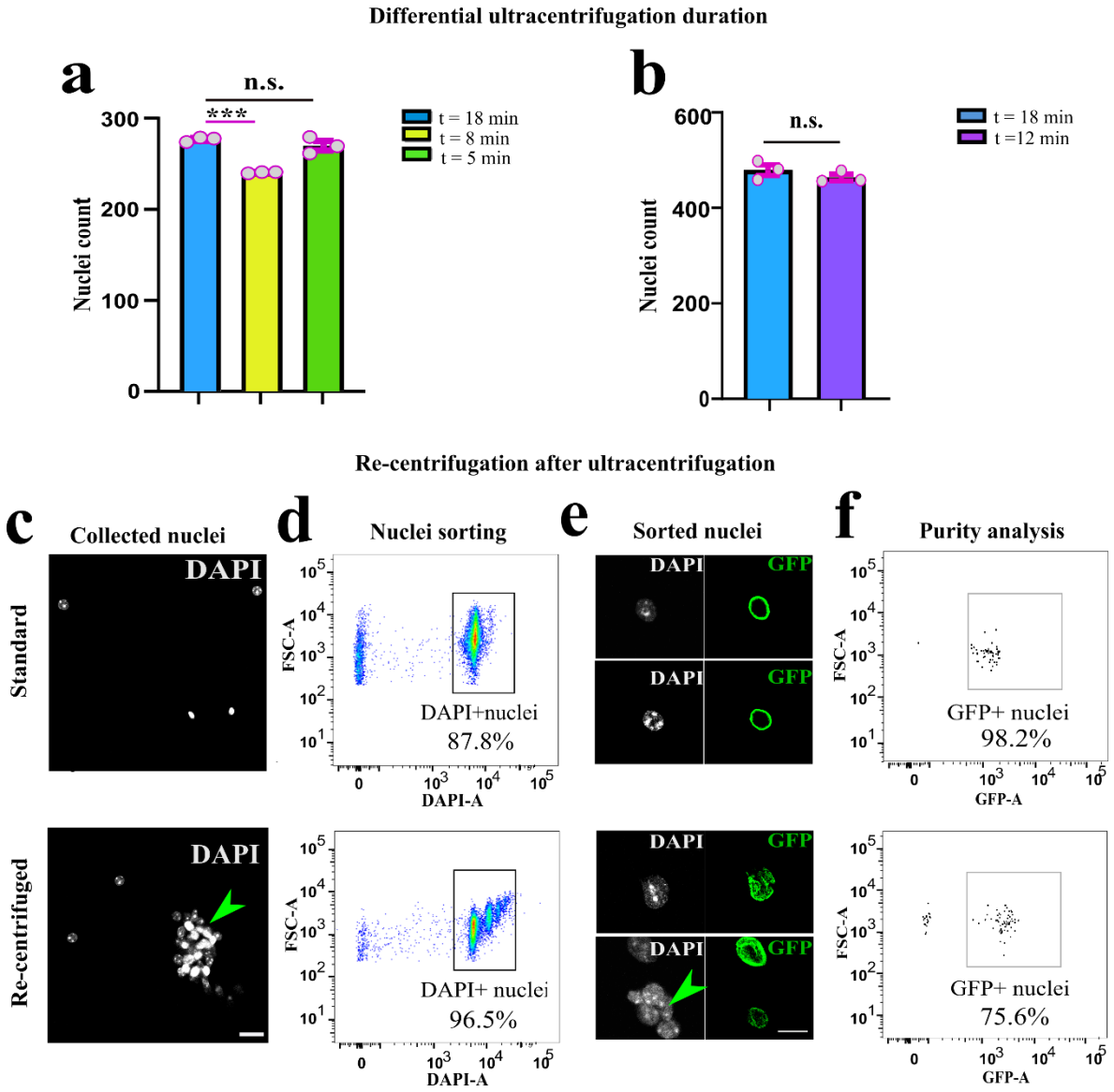

Figure 16: Strategies for optimizing nuclei processing duration.

a,b. Nuclei yield during different durations of centrifugation with the cushion layer. **a.** Graphical representation of differences in nuclei yield from the same homogenate when centrifuged for different durations -18 min, 8 minutes, and 5 minutes at 7820 rpm, n = 3 replicates each **b.** Similar nuclei count between centrifugation for 12 and 18 minutes. n = 3 replicates each. All statistical tests were performed using a student's t-test in GraphPad Prism. All error bars represent +/-SEM. (***, $p<0.0005$; n.s.- not significant) **c.** Comparison of microscopic images between standard and re-centrifuged nuclei revealing nuclei aggregation in re-centrifuged nuclei**.** Scale bar: 30 µm. **d.** Dot plot of single nuclei from the corresponding centrifugation methods with the detection of aggregates in re-centrifuged nuclei. **e**. Frizzled GFP membrane appearance and nuclei aggregation in the re-centrifuged nuclei but not in the standard nuclei. Scale bar: 10 µm. n = 3 replicates **f**. Reanalyses of the sorted nuclei revealing a lower purity of the nuclei from the re-centrifuged nuclei groups (representative image). **Abbreviation:** t – time.

3.3.3 Techniques to improve sorting efficacy

3.3.3.1. Re-centrifugation and resuspension

Since the extracted nuclei will, ultimately, be sorted for separating sfGFP+ from sfGFP negative (sfGFP-) nuclei, it was necessary to reduce the viscosity of the 30-40% interface layer nuclei solution. From our preliminary experiments, we noted that the duration for sfGFP+ nuclei sorting by FANS, directly using the collected nuclei in the viscous solution, was lengthy (approximately 10 minutes for collecting 10k nuclei). Therefore, viscosity reduction was an essential step to speed up nuclei processing. This could be achieved by dilution with another buffer (with low surface tension), though this method would still retain some viscosity. As an alternative, the collected nuclei solution could be re-centrifuged with low speed followed by resuspension of the pellet with low viscosity buffers including PBS (0.4% IGEPAL) or wash buffer (0.4% IGEPAL). For clarity, collected nuclei without re-centrifugation will be termed as "standard nuclei" in this section. During re-centrifugation, standard nuclei were pelleted at a low speed (5000 ×g at 4˚C) to reduce mechanical stress on the nuclei. The pellet was then resuspended using a buffer of choice: PBS (0.4% IGEPAL) or the wash buffer (0.4% IGEPAL). As hypothesized, the speed of processing by FANS increased by 10-fold compared to that of the original buffer (iodixanol, 1-2 minutes for 10k nuclei using the low viscosity buffers). However, despite proper gating, there were more nuclei clusters or aggregates, as detected in both the dot plot of the flow cytometer and fluorescence microscopy (**Figure 16c, d**). Additionally, sfGFP- nuclei were detected in the sorted populations of the recentrifuged samples as observed in the microscopy images **Figure 16e,** as well as purity analysis **(Figure 16f**). Thus, we concluded that although re-centrifugation would allow easier resuspension with any buffer, the associated time and nuclei loss during re-centrifugation as well as higher chances of false-positive nuclei sorting makes the modification undesirable.

3.3.3.2. Dilution with different buffers

Since re-centrifugation introduced unwanted results, our next attempt to reduce viscosity of the nuclei solution was to dilute the collected standard nuclei solution with a solution of low surface tension. It is expected that different buffers will have a distinct impact on nuclei integrity due to their different chemical composition. In fact, we observed an increase in sfGFP+ nuclei detection in flow cytometry (**Figure 17a,** $n = 7$, $p<0.0005$), when the standard nuclei solution is diluted with either PBS or HB (0.4% IGEPAL). However, sfGFP+ nuclei sorted into PBS (0.4% IGEPAL) showed a higher degradation than that in HB (0.4% IGEPAL)

or original buffer (**Figure 17b)**. Thus, for dilutions of standard nuclei solution for efficient sorting, HB (0.4% IGEPAL) was determined to be a better choice.

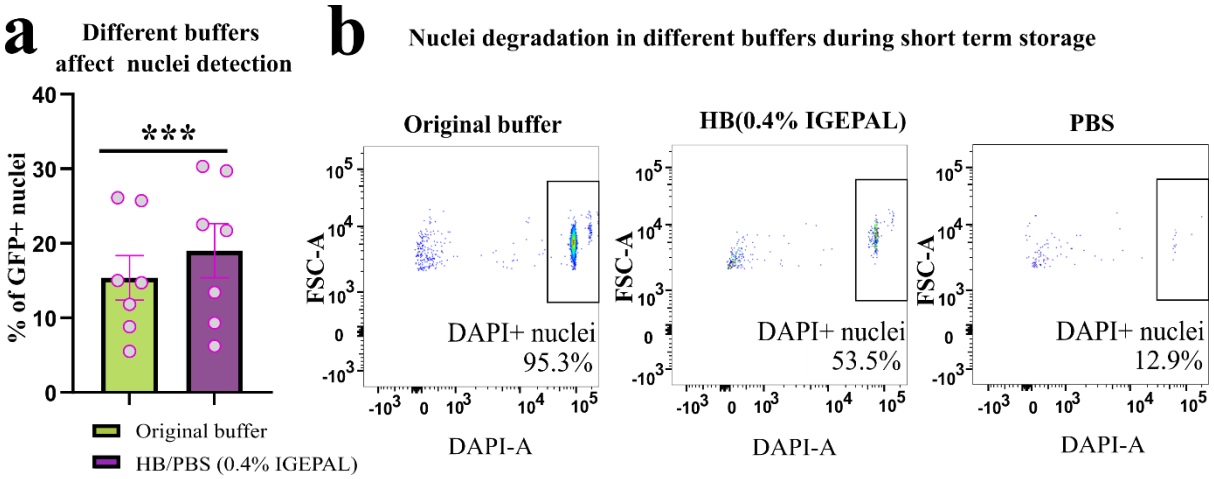

Figure 17: Effects of different buffers on nuclei detection and nuclei degradation.

a. Significant increase in the detection of sfGFP+ neocortical nuclei (FANS) when buffers of density lower than that of iodixanol, i.e., PBS or HB, were used (n = 7, p<0.0005) **b.** Flow cytometry of DAPI-positive nuclei depicting the disintegration of nuclei stored in iodixanol < HB < PBS over 24 hrs. All error bars represent +/- SEM. * indicates significance value. **Abbreviations**: HB – homogenisation buffer, PBS – phosphate-buffered saline

3.4. Discussion

Nuclei isolation is a critical step and utmost care must be taken to ensure that the sensitive molecular components to be assayed by downstream experiments suffer very little to no degradation during the duration of isolation. Thus, an optimal protocol for nuclei isolation should allow for not only the yield of a high number of nuclei but also of good quality, with the shortest possible time period involved in extraction. Apart from this, the extracted nuclei should be easily adaptable to different processing methods for end point experiments. Thus, in this chapter, we developed a novel iodixanol gradient based nuclei isolation protocol suitable for efficient extraction of nuclei from small tissue volumes of freshly micro-dissected brain regions. An idea of the expected nuclei quantity and nuclei appearance to be obtained using this protocol were also provided. Apart from the innovative technique, we revealed caveats that should be handled carefully during nuclei isolation.

In our attempt to increase nuclei yield, we opted for ultracentrifugation the homogenate without a cushion layer, as ultracentrifugation with the cushion layer often resulted in nuclei loss due to passive diffusion to the neighboring layers. Indeed, centrifugation without the cushion layer increased the nuclei yield. However, a subset of these nuclei lost the characteristic dark

appearance, indicative of good quality nuclei in phase-contrast microscopy and instead appeared 'bright'. Though we did not further investigate the origins of such nuclei, we hypothesize that the alteration in their refractive index[303] may be indicative of the shearing stress suffered by the nuclei during the pelleting. This stress could arise from collisions amongst the pelleted materials as well as walls of the centrifugation tube[304–308]. We presume that the bright appearance of these type of nuclei in phase-contrast microscopy has a similar basis as the bright appearance for apoptotic cells', indicative of damaged membrane integrity[309]. Although, we cannot exclude that the bright nuclei populations could also be from different cell types, which were absent from the interface layer of the cushion layer ultracentrifugation method, the likelihood is deemed low. This is because the interface with the 30% layer contains 90% of the total DNA[274]. Therefore, it is more plausible that the bright populations consist of nuclei with compromised nuclear integrity that settled at the bottom of the centrifugation tube. However, further investigations are necessary to trace the precise origin of the bright nuclei. The uncertainty of the origin of the bright nuclei from the ultracentrifugation without the cushion layer, steered our decision to use the cushion layer during ultracentrifugation, for all other experiments. Meanwhile, as we used lower volumes of solutions for micro-dissected tissues, duration of centrifugation could be shortened from 18 minutes to 12 minutes without compromising the yield and quality of nuclei.

Next, for efficient sorting of the good quality nuclei, a reduction in viscosity of the standard nuclei solution collected from the 30-40% interface layer of the viscous iodixanol-sucrose solution was required. Therefore, we experimented with pelleting the nuclei (from the collected standard nuclei solution) with a lower centrifugation speed. However, this method introduced aggregates as was shown for exosomes[305,310]. Aggregates not only reduce the yield of intact good-quality nuclei but also interfere with the purity while sorting. Therefore, the occurrence of clusters is detrimental when low cell numbers from rare tissues are considered or when pure populations are required, as is imperative for engram studies. As such, re-centrifugation is to be avoided. On the other hand, since viscosity reduction is important, dilution of nuclei collected from the 30-40% layer with a solution of low surface tension would be the best choice to speed up nuclei sorting. This was indeed the case as shown in [254], though at the time our experiments were performed, this study had not yet been published. We posit that the increase in sorting speed following viscosity reduction could be due to less viscosity contrast[311] between the adjacent microfluid lamina that is necessary to adequately detect particles during flow cytometry (as mentioned in EP1242804A2, Thermo Fisher), which uses a PBS sheath. For this

same reason, studies using sucrose gradient centrifugation methods also resuspend the nuclei in PBS[312].

Conclusively, we navigated through the treacherous terrains of the proper choice of density gradient buffer, ultracentrifugation steps and the drawbacks of resuspension, which are usually overlooked in studies using nuclei for downstream epigenetic experiments. A comprehensive analysis of the results leads us to the conclusion that for all nuclei isolation experiments related to the thesis, the newly generated iodixanol-gradient-based nuclei extraction protocol, complemented with a cushion layer, remains as the optimal procedure. For viscosity reduction, the nuclei obtained from the 30-40% interface layer are to be diluted with HB (0.4% IGEPAL) to expedite nuclei sorting. Notably, since the inception of this protocol, an increasing number of nuclei isolation protocols have surfaced[313–316]. Thus, one can deduce the high value and the rising demand for optimal nuclei isolation protocols in the era of omics sequencing, thereby marking our contribution as invaluable in meeting these evolving research requirements.

Chapter 4. Choice of technique for sfGFP+ nuclei separation - INTACT vs FANS

Note: This Chapter is similar to parts of the peer-reviewed manuscript published in International Journal of Molecular Sciences (doi: 10.3390/ijms22105335).

4.1. Introduction

Following the successful establishment of an efficient nuclei isolation protocol, the next step was to identify a better strategy for segregating the sfGFP+ engram nuclei from the nuclei pool that also contains the sfGFP- nuclei. The sorting step of sfGFP+ nuclei from the nuclei pool is an important step, where nuclei quality could still be compromised. Apart from this, the sorting step will be the deciding factor for the purity of the nuclei populations investigated by the multiomics sequencing. Therefore, in this Chapter we aim at selecting a proper sorting technique from the two plausible techniques of sfGFP+ sorting - FANS[312,317], and Isolation of Nuclei Tagged in specific Cell Types (INTACT[318–320]). FANS is a more established technique, based on fluorescence sorting while INTACT is a relatively newer technique, based on magnetic sorting coupled with antibody binding. Although flow cytometry (involved in FANS) is a widely used technique to separate specific cells/nuclei populations, certain disadvantages have been associated with it. For instance, FANS requires high-cost equipment and specially trained people. These requirements can be an unaffordable obstacle, particularly for smaller labs. Additionally, the high hydrodynamic stress in flow cytometry forms one of the major challenges[321,322], as this could trigger cellular stress responses leading to a subsequent modification of distinct molecular profiles[243,323–325]. Apart from this, FANS also comes with a high time–cost factor to isolate rare cell populations at a multiscale level[320,326,327]. On the other hand, INTACT has been shown to be suitable for conditions, where the quantity of cell types to be extracted is low[318,320], apart from it being a milder technique than FANS[243]. Though the two techniques have been used interchangeably, for our purpose, given the limited quantity of nuclei, it was necessary to identify which of the two techniques would yield a better quality, quantity, and purity of the sorted sfGFP+ nuclei with a lower time-cost.

4.2. Methods

4.2.1. Animals, behavior and TAM injection

13 to 16 weeks old male and female Arc-GFP mice were used for this study. Tamoxifen injections were performed as in the previous chapters, 5 hours before the SI test, for GFP induction.

4.2.2. Brain dissection, nuclei isolation and sfGFP+ nuclei separation

Mice were sacrificed by cervical dislocation. Brain regions - neocortex, PFC, hippocampus, hypothalamus, pituitary, and Naccu - were dissected according to region specifications in the Allen Brain Atlas (https://atlas.brain-map.org/) for mouse (as in **Chapter 3**). Nuclei were isolated using the iodixanol-based-gradient ultracentrifugation protocol for isolation of micro-dissected brain regions as in **Chapter 3**. The duration for high-speed ultracentrifugation (10000 ×g or 7820 rpm) for the neocortex was kept at 12 minutes, while for the other brain regions, it was kept at 18 minutes. After the ultracentrifugation process, nuclei were collected from the 30–40% iodixanol layer interface.

4.2.2.1. INTACT

For sfGFP+ nuclei separation, Dynabeads (Life Technologies, Carlsbad, CA, USA, 10003D) were incubated with an anti-GFP antibody (Life Technologies, Carlsbad, CA, USA, G10362) at 4 °C at a ratio of 5:2 (beads: anti-GFP) for downstream molecular biology experiments and at a ratio of 5:1 (beads: anti-GFP) for microscopy in order to decrease the number of beads bound to nuclei. The reduction of beads bound to a nucleus was to increase the visibility of bead-bound nuclei, which is important for microscopy analysis. The bead-antibody incubation was carried out in a cold room using an end-to-end rotator for 20 min to facilitate bead-antibody interaction in the solution.

In the meantime, the collected nuclei from the 30–40% iodixanol gradient layer was diluted with wash buffer (0.4% IGEPAL in HB) in the ratio 2:1. This was necessary to reduce the solution's viscosity and remove the outer nuclear membrane before affinity purification (as mentioned in [328]) to facilitate anti-GFP binding to sfGFP in the peri-nuclear membrane. The wash buffer-diluted nuclei solution was incubated with anti-GFP bead solution in the ratio of 40:1. Samples were then placed in an end-to end rotator in a cold room for 20 minutes. After the incubation period, samples were placed on a magnetic rack for 1 minute, and the supernatant was removed, retaining the bead-bound sfGFP+ nuclei clusters. These clusters were washed once with 500 µL wash buffer and twice with 250 µL wash buffer and

subsequently collected in 100 µL wash buffer. Thus collected nuclei was termed as **INTACT-nuclei**. For hemocytometer counting, proper dilutions were made so that not more than 200 bead-bound nuclei were present per large square.

4.2.2.2. FANS

For FANS, the nuclei collected from the 30–40% iodixanol layer were diluted with wash buffer (similar to INTACT), as in [254,278] in the ratio 2:1, to reduce viscosity during sorting. Flow cytometry analyses and FANS were performed as in **Chapter 3**. Sorted nuclei were collected in 1.5 mL Eppendorf tubes containing 100 µL of HB and termed as **FANS-nuclei.**

4.2.2.3. Purity analysis of INTACT- and FANS-Nuclei

For purity analysis of INTACT-nuclei, 4× of the wash buffer was added before flow cytometry to reduce the density of bead-bound nuclei. For FANS-nuclei, the sorted sfGFP+ nuclei were collected in wash buffer to keep the experimental conditions identical to that of INTACT. The nuclei purity analysis was performed using BD FACS Aria III (Becton Dickinson, Franklin Lakes, NJ, USA). Data were analyzed with FlowJo (v.10.6 or higher, Tree Star, Ashland, USA) from at least 50 single DAPI-positive nuclei.

4.2.3. Parallel Processing of INTACT- and FANS-nuclei

For comparing the processing speed, different brain regions (Naccu, hypothalamus, pituitary, PFC, neocortex) with different sfGFP+ nuclei percentages and nuclei yield per volume were used, to increase coverage and generalisability of results. The time taken of each processing was calculated to assess speed using the two different techniques.

For FANS, duration of sorting, to obtain 5k sfGFP+ nuclei, was determined for each sample type. INTACT was performed as usual for all sample types. Bead-bound nuclei were then counted using a hemocytometer and the volume that contained 5k bead-bound nuclei was calculated. The duration for sorting 50k nuclei using both techniques was then calculated using unitary method. For INTACT, the efficiency of sorting (yield) was estimated indirectly by subtracting the percentage of sfGFP+ nuclei that remained in the INTACT supernatant from the percentage of sfGFP+ nuclei in the original solution. NB: The supernatant and original solution sfGFP+ percentages were obtained from flow cytometry.

4.2.4. Microscopy

4.2.4.1. Phase-contrast microscopy

10 µL of the nuclei:Trypan mixed in a 1:1 ratio was loaded into the hemocytometer. Light intensity was maintained the same for all groups. Images were obtained using a Leica DM-IL inverted microscope with 40×/0.5, air objective. See more in **Chapter 3**.

4.2.4.2. Fluorescence microscopy

10 µL of the DAPI stained nuclei solution was loaded into the inner well of the µ-angiogenesis chamber. Images were obtained using a Leica AF7000 widefield microscope equipped with a Hamamatsu-Flash4-USB3-101292 camera, an LED lamp (Sola Light Engine, SE 5-LCR-VB, Lumencor, Beaverton, OR, USA) and LAS X software (Institute for Molecular Biology, Mainz, Germany). A HC PL FLUOTAR L 20/0.40 or a 40/1.1 objective lens were used to acquire each image (with the same settings). Images visualizing GFP fluorescence were acquired using an L5 filter (BP 480/40, FT505, BP 527/30), and DAPI was imaged using an A4 filter (BP 360/40, FT400, BP 470/40).

4.2.5. Image analyses and statistics

Images were analyzed using FIJI (v 1.51 h) as in [278]. Manual analysis was performed by drawing an ellipse in the image encompassing the nucleus under observation while automatic analysis was performed using a macroscript (see [278]). Statistical analyses were performed using Student's unpaired t-test (assumption: equal SD between populations) in GraphPad Prism (8.4.2).

4.3. Results

4.3.1. Quantification of morphological attributes: FANS- and INTACT-nuclei in comparison to INPUT-nuclei

To provide a comprehensive comparison between the two techniques, we used the Arc-GFP mice. Approximately 72 hours following TAM injection and SI test, mice were sacrificed. Nuclei were isolated from the neocortices of 13-16 weeks old Arc-GFP mice. For both FANS and INTACT, it was necessary for the nuclei solution to be less viscous for proper GFP detection in flow cytometry and antibody binding for the INTACT method. Therefore, the collected nuclei solution was diluted with wash buffer (HB with 0.4% IGEPAL), now termed as '**INPUT-nuclei'**. The INPUT-nuclei were then aliquoted into equal volumes to segregate

the sfGFP+ nuclei using either INTACT or FANS (**Figure 18a-c**). Depending on the technique used, the sorted sfGFP+ nuclei were termed as **'INTACT**-nuclei' or '**FANS-nuclei'**.

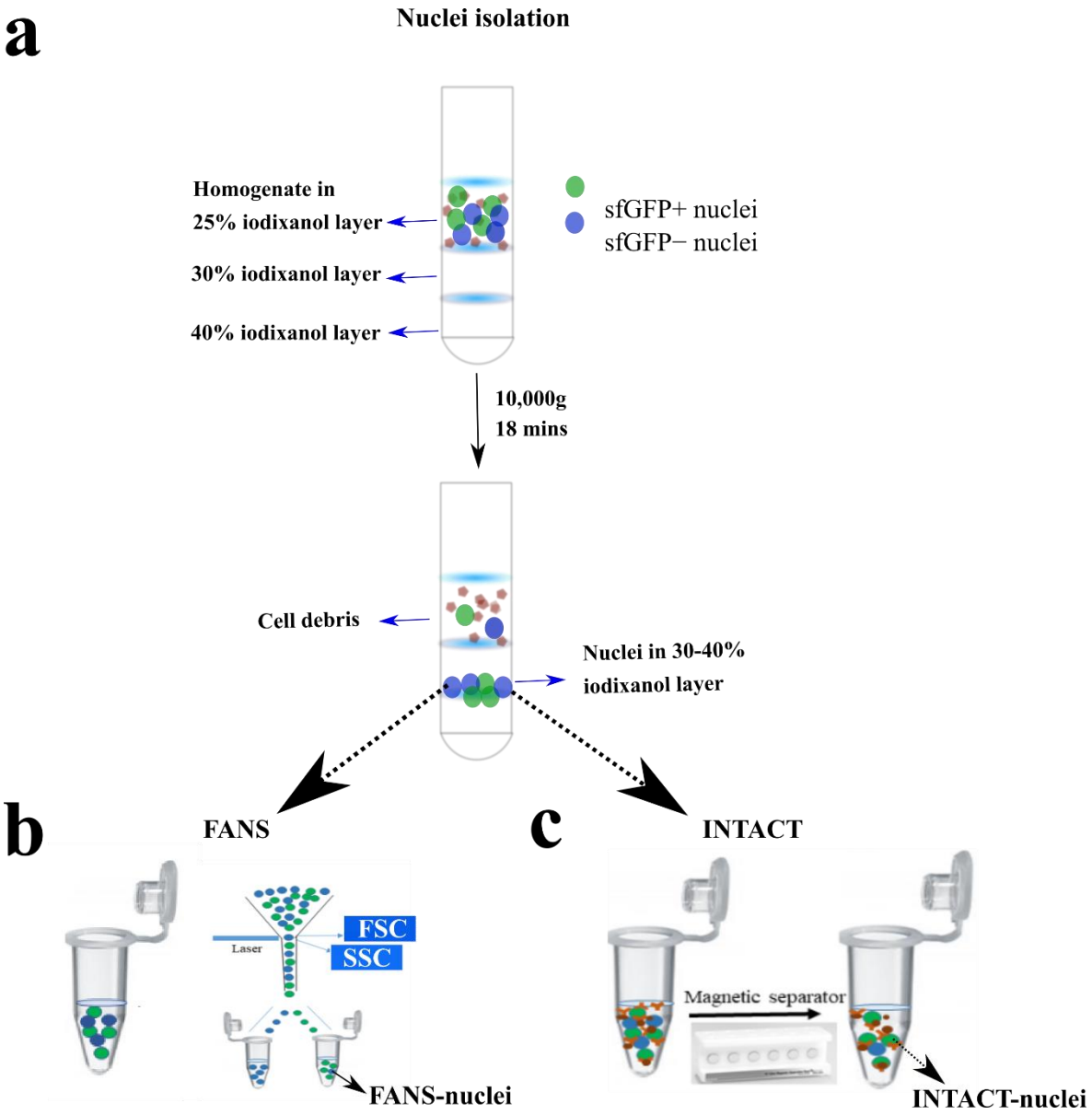

Figure 18: FANS vs INTACT: Procedural differences and purity estimation.

a. Nuclei extraction via ultracentrifugation **b.** GFP+ nuclei sorting using FANS is termed FANS-nuclei **c.** Magnetic separation of sfGFP+ bead-bound nuclei using INTACT. Thus sorted nuclei is termed INTACT-nuclei. **Abbreviations**: FANS – fluorescence -activated nuclei sorting, INTACT – isolation of nuclei tagged in specific cell types.

Upon verifying the purity of the separated sfGFP+ populations (see Supplementary Figure S2 of the IJMS publication[329], we proceeded with the investigation of structural differences. First, we used phase-contrast microscopy to compare the "area" and "perimeter" of FANS- and INTACT-nuclei to INPUT-nuclei (n = 100-200 nuclei for each replicate, **Figure 19a-b**) from

three different biological replicates. Within a few hours (<3 hours after sort), we detected a significant increase in both the area and perimeter of FANS-nuclei as compared to INPUT-nuclei ($p<0.05$, $p<0.0001$), while INTACT-nuclei did not show a detectable change (**Figure 19b**). Next, we quantified the "optical density" based on the staining intensity of the Trypan blue dye, as optical properties of a nucleus convey important information about the nucleus, including nuclear membrane integrity. Since the INTACT-nuclei beads affected the optical light transmission, we could only perform this analysis on FANS-nuclei compared to INPUT-nuclei. We observed no significant difference between FANS-nuclei and INPUT-nuclei <3 hrs after sorting ($p = 0.5397$, n.s., see more in Supplementary Figure S3C of [329]**).**

Using phase-contrast microscopy, we could only compare sfGFP+ FANS- and INTACT-nuclei to a pool of sfGFP- and sfGFP+ INPUT-nuclei. This was suboptimal because most sfGFP+ nuclei from the neocortices are likely to be nuclei from excitatory neurons where *Arc* expression is abundant, whereas sfGFP- nuclei contain a mixture of all different cell types of the neocortex. However, sfGFP- nuclei are derived from heterogenous cell types of the neocortex. Therefore, it was crucial to ensure that any observed differences in the results were solely attributable to the variations in techniques by comparing only sfGFP+ populations. As such, we used fluorescence microscopy for the next step to compare the sfGFP+ FANS- and INTACT-nuclei to sfGFP+ INPUT-nuclei. For these experiments, nuclei were embedded in the wells of a chambered PEI-coated coverglass (IBIDI) within 3 hours or 4-6 hours after sorting (More details in the **Methods**). Representative images of the INPUT-, FANS-, and INTACT-nuclei (<3 hours) are shown in **Fig. 19c**. Upon quantification, we observed a significant increase ($p<0.0001$, $p<0.0001$, n = 100-200 nuclei) in the size (area and perimeter) of sfGFP+ FANS-nuclei as compared to that of sfGFP+ INPUT-nuclei (**Fig. 19d**). The size of INTACT-nuclei did not change significantly when compared to sfGFP+ INPUT-nuclei. The observations remained similar to that in phase-contrast microscopy. Thereafter, the increase in the size of FANS-nuclei was validated over a larger sample size using a macroscript[278] for faster processing ($p<0.0001$, n = 300-400 nuclei, see Supplementary Figure S3D in [329], <3 hrs after sorting (A)). Interestingly, the increase in size was accompanied by a significant shift in the optical density of FANS-nuclei, which showed a brighter pattern in the brightfield image (see Supplementary Figure S3E of [329]. (NB: *These nuclei were without Trypan blue staining and hence exhibit the opposite pattern of Supplementary Figure S3C of [329]). This indicates a change in nuclei morphology as compared to the sfGFP+ INPUT-nuclei. Intriguingly, 4-6 hours after sorting, the size of FANS-nuclei decreased, as shown in Supplementary Figure S3D

of [329], $p<0.001$). This finding suggests a possible change in FANS-nuclei's osmotic pressure and membrane integrity within a few hours of sorting, followed by subsequent shrinkage.

Conclusively, the results indicate that FANS but not INTACT induces morphological changes in the sorted nuclei. The change in shape and optical density of FANS-nuclei, compared to INTACT-nuclei/INPUT-nuclei, could portray underlying alterations in chromatin dynamics and gene expression[330–334]. The epigenomic investigations of FANS-nuclei and INTACT-nuclei are discussed in detail in [329].

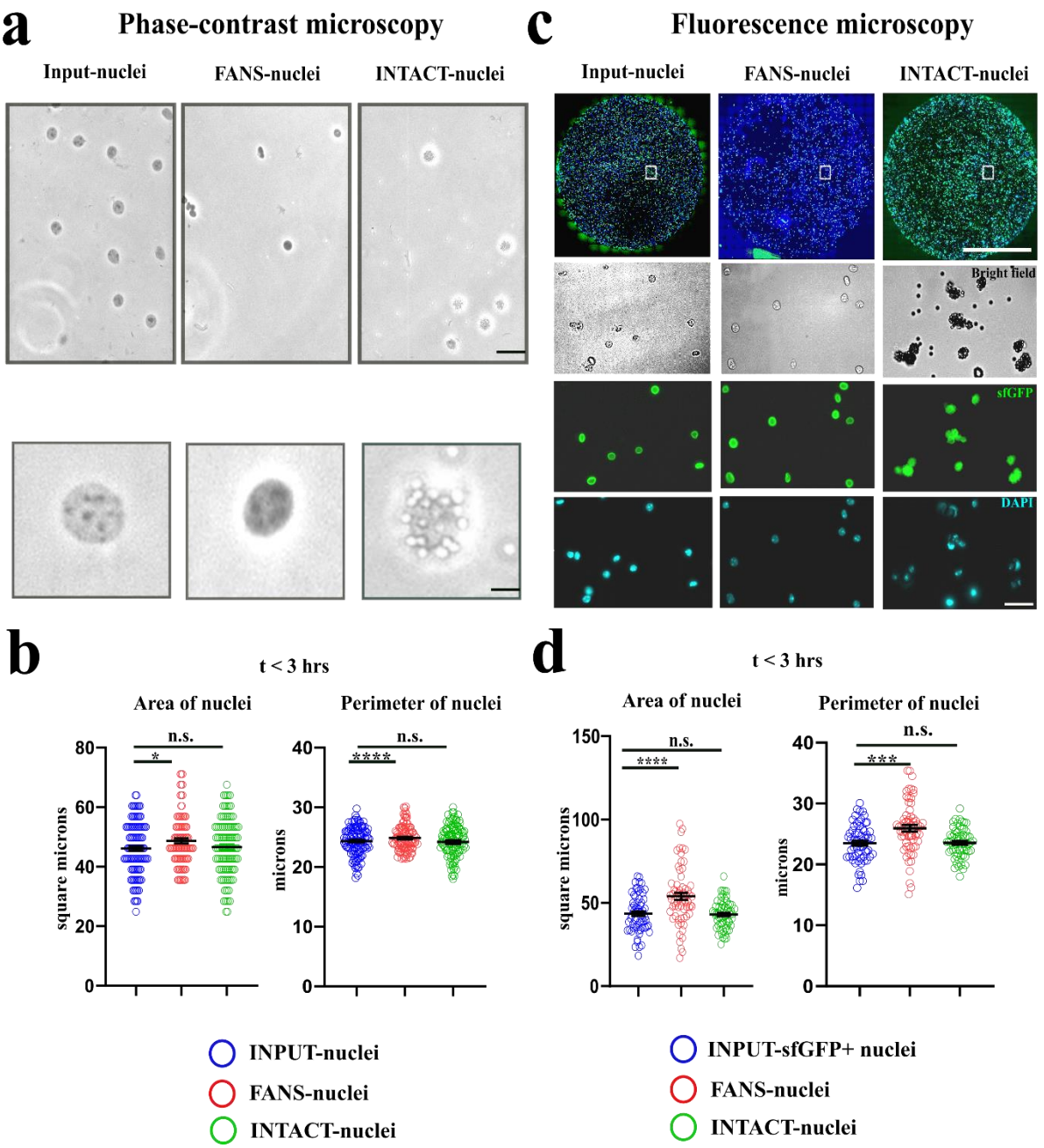

Figure 19: Morphological comparisons between FANS-and INTACT-nuclei.

Nuclei were isolated from the neocortices of 13-16 weeks old mice and sfGFP+ nuclei were sorted using FANS or INTACT. **a**. For phase-contrast microscopy, sorted nuclei were inspected within 2-3 hours of the sort. Representative images of INPUT-, FANS- and INTACT-nuclei. Scalebar: 25µm. **b**. Nuclei area and perimeter after sorting with FANS or INTACT (phase-contrast microscopy). Both parameters in FANS- but not INTACT nuclei increased significantly, as compared to the INPUT- nuclei ($p<0.05$, n = 100-200 nuclei, manual analysis) Scalebar: 5 µm, Air objective, 40×. **c**. For fluorescence microscopy, sorted nuclei were embedded in IBIDI chambers within 3 hours or within 4-6 hours of the sort. Representative images of INPUT-, FANS- and INTACT- nuclei (within 3 hours of the sort) in the wells of IBIDI chambers and the representative enlarged images showing brightfield, GFP and DAPI fluorescence, along with the magnetic beads (2.8 µm diameter) showing a green autofluorescence for the INTACT image are presented. Scale bar: 2 mm (inset), scale bar - 25 µm, Water objective, 20× and 40× **d**. Fluorescence microscopy image analysis of area and perimeter for only sfGFP+ nuclei embedded in the IBIDI chambers within 3 hours after sorting. Significant increase in the size of FANS- nuclei (area and perimeter) <3 hours of sorting as compared to the sfGFP+ INPUT-nuclei ($p<0.0001$, n = 100-200 nuclei, manual analysis) with no significant changes in INTACT-nuclei. Error bars represent +/- S.E.M. **Abbreviation**: t – time.

4.3.2. FANS vs INTACT: Speed and yield efficiency

Having determined the morphological differences, we then proceeded with analyzing the speed and yield between the two sorting techniques. INTACT has been considered more efficient at processing larger amounts of samples compared to FANS because it requires less processing time[327]. Therefore, we compared this aspect using both INTACT and FANS under different conditions. For this experimental design, we selected several micro-dissected brain regions, which provided variant nuclei yield and sfGFP+ nuclei percentages (**Table 1**, Yield:sfGFP%; 73×10^4/mL:18.95; 60×10^4/mL:12.8; 140×10^4/mL:47.45, 136×10^4/mL:23, 200×10^4/mL:29.3 for nucleus accumbens, hypothalamus, pituitary hippocampus and neocortex respectively). The regions were selected to represent diverse sample populations.

Table 1: INTACT vs FANS comparison of yield and purity

				Duration of sort						
Brain region\ Property tested	Nuclei yield (x 10^4/mL)	Total volume (µL)	Input nuclei sfGFP+%	Actual 5k nuclei/ sample (minutes)		Theoretical 50k nuclei/ 10 samples (minutes)		sfGFP+ nuclei yield from INTACT		
				FANS	INTACT	FANS	INTACT	sfGFP% Super-natant	Yield %	Purity
Small-medium brain regions										
Nucleus accumbens	73	300	18.95	2	35	200	60	16.5	15	98.5
Hypothalamus	60	400	12.8	3	35	300	60	7.6	44	98.2
Pituitary	140	400	47.45	1	35	100	60	28.9	40	99.1
Hippocampus	136	400	23	1.5	35	150	60	12.3	50	99.8
Large brain regions										
Neocortex 1	>200	900	29.3	-	-	-	-	3.6	87	98.5
Neocortex 2	>200	900	26.7	-	-	-	-	3.7	86	93.6

The experiments for all the brain regions were performed simultaneously. During these experiments, first, we noted the time required to obtain 5k sfGFP+ nuclei from a single sample using FANS or INTACT. Next, the theoretical time needed to obtain large numbers (for example, 50K) was calculated using the unitary method. Here, we observed that a single sample's processing speed was faster using FANS (**Table 1**, 1-3 minutes for FANS as compared

to INTACT – 35 minutes). However, when multiple samples were considered, and the theoretical time was calculated, the FANS technique was more time-consuming (100-200 minutes for FANS compared to INTACT: about 60 minutes). Interestingly, for INTACT, we observed that the sorting efficiency was dependent on nuclei yield and sfGFP+ percentages. For instance, using nucleus accumbens, where isolated nuclei count is low (yield), only 15% of sfGFP+ nuclei could be extracted from the total nuclei pool. In contrast, for pituitary with high nuclei yield as well as high sfGFP+ percentage, the extraction efficiency was about 40% (see **Table 1**, "yield"). As the nuclei concentration and sfGFP+ percentage increased, for example in the neocortex, the yield rose to approximately 86-90% (**Table 1**).

4.4. Discussion

The sorting step of engram nuclei, characterized by sfGFP+ expression in our study, is a crucial step before proceeding with any downstream omics investigation. Compromised nuclei quality at this step will affect downstream results even if the initial nuclei isolation step had been performed meticulously. Apart from this, the purity of the sorted sfGFP+ nuclei will determine the quality of the results obtained from the downstream sequencing processes. Therefore, we compared the more used but harsh technique of FANS, and the newer but milder technique, INTACT. Indeed, our results validated that the mechanical insult on the nuclei could be higher in FANS as indicated by the morphological alterations that accompanied FANS-nuclei. We hypothesize that the increase in FANS-nuclei size could be due to the high hydrodynamic pressure, shearing stress[243], or PBS-induced destabilization of membrane integrity during the sort[278,335]. Destabilized membrane integrity has been associated with flow cytometry as recognized in Binek and colleagues[324] resulting in adverse effects on the cells' viability and structure. We posit that the alterations in membrane integrity led to osmotic pressure changes, which dictated an initial increase in nuclei size followed by a subsequent reduction 4 h after the sorting for FANS-nuclei. All these structural and optical changes portray plausible molecular modifications occurring in the FANS-nuclei compared to INTACT-nuclei, as presented in [329]. This suggest that nuclei sorting using the two different techniques could lead to different molecular signatures of the same biological materials. Regarding processing speed, the INTACT method might be preferable in cases of large sample numbers, where fast processing of nuclei is required. In fact, one of the advantages of INTACT (compared to FANS) is the ease with which the sorted bead-bound nuclei can be concentrated into smaller buffer volumes[322]. However, when rather accurate nuclei numbers are required for downstream processing, FANS may be better suited, as counts from hemocytometer for INTACT are rough

estimates. Overall, we concluded that only one technique should be used for a particular study design. Opening the grounds for the possible inclusion of ATAC-seq at a future time point and for comparability of results with existing literature based on flow cytometry, we decided to use FANS for sorting sfGFP+ nuclei, within the framework of this thesis.

Chapter 5. Multiomics analysis of resilience-susceptibility engram nuclei in the vHipp

NB: Results presented in this chapter are parts of two different manuscripts, one submitted for peer review in Molecular Psychiatry and the other part will be submitted soon to a high impact journal.

5.1. Introduction

Chronic social stress forms one of the most prevalent stressors in humans. To closely model this type of stressor, the CSD paradigm on rodents was introduced. Since its initial popularization[64,96,98], multiple research studies have adopted the CSD paradigm to investigate the resulting effects following chronic social stress exposure at the circuit and structural levels[82,336–338] as well as molecular levels[183,244,339–341]. However, most of the molecular investigations are focussed on transcriptomic studies from bulk tissues[183,195,342,343]. First, bulk tissues possess different cell types with distinct molecular signatures, thereby averaging molecular information from specific cell types. Particularly, for our study, where different engrams are activated for stress-resilient and stress-susceptible phenotypes[112], the use of bulk tissues will decrease the resolution of identifying causative factors underlying the divergent phenotypes. Additionally, the transient nature of transcriptome alterations does not fully explain the mechanisms behind the persistence of stress effects[344,345]. In this regard, DNA methylation has emerged as a stable epigenetic marker, modulating long term effects of stress and is extensively studied in early life stress[346] and PTSD research[138–140]. Apart from this, miRs that are known to be active agents for transgenerational inheritance of stress[347], have not yet been investigated in relation to resilient- or susceptible- phenotypes, especially from the nuclei. Thus, the vast amount of literature often overlooks critical aspects by examining only one segment of the molecular machinery repeatedly. Therefore, to gain a comprehensive understanding of the complex etiology of the alterations following stress exposure, it is imperative to evaluate multiple molecular machineries, simultaneously, through a multiomics approach[199,238,348]. Such a thorough investigation would generate a clearer picture of the underlying alterations, thereby the probability of determining causal factors [234,235,349], or critical diverging points between resilience and susceptibility.

Thus, to gain more insights into the cellular dynamics behind stress-resilience and stress-susceptibility, we employed a multiomics approach to investigate the methylome with the coding and non-coding transcriptome simultaneously. The methylome will be accessed by

reduced representation bisulfite sequencing (RRBS-seq) while the small non-coding transcriptome will be accessed by small RNA-seq. The transcriptome is accessed by RNA-seq (data published in [246]). We hypothesize that the multiomics approach coupled with the use of specific engram nuclei from stress-susceptible and stress-resilient populations would reveal a higher resolution picture of the intricate flow of information between interconnected signaling pathways.

5.2. Methods

5.2.1. Animals and behavior experiments

7-8 weeks old Arc-GFP and WT-GFP adult male mice were used for all our experiments as approved by the Ethics Committee (See **Chapter1**). Animals for these experiments were progenies of parental lines backcrossed only with C57BL/6J. Multiomics experiments were performed only on samples from WT-GFP.

5.2.2.1. Basal character identification for test animals before CSD

For a controlled non-biased separation of test animals into the stressed and non-stressed groups, we used the open field/eagle exploration (OF/E) test as described in **Chapter 2**. In addition to the OF/E test, we also included the SI test with conspecifics in this section. The SI with conspecifics was to assess the basal social interaction capacity of individual mice. SI test was performed in a similar way as in the previous chapters, except for the use of a conspecific instead of a CD1 mouse in the test phase. The SI index was also calculated using the same formula.

5.2.2.2. Classification of animals to control and stress groups

For a non-biased experimental approach, the results from the OF/E and SI/CO test were used for the segregation of the test mice into control and stress groups. SI/CO scores of the test mice were listed in an increasing order and mice with consecutive scores were placed in stressed and control groups. Apart from this, littermate controls were also introduced by assigning the animals from the same parents to the opposite groups. Thereafter, OF/E scores were taken into consideration, ensuring that the newly segregated list shows a similar mean score between the stressed and control group.

5.2.2.3. Aggressive chronic social defeat experiments, TAM injection and SI test.

Chronic social defeat experiments (CSD aggressive, with the increased stressor intensity of 3×15 S), TAM preparations, injections and SI tests (with CD1 mice) were performed as in **Chapter 2**. The representatives from resilient, susceptible and control populations to be

processed for nuclei isolation and molecular analyzes, were also assessed via proper screening of the videos, for stringency.

5.2.2.4. Animal weights

As stress can result in weight gain[350], weights of the test animals were also noted on three different experimental days - first day of CSD, last day of CSD and on the day of the SI test before the TAM injections (see **Figure 20**). These weight measurements were aimed at monitoring the animals' health and any potential changes in the body weight of the animals during the experiment.

5.2.3. Tissue extraction, nuclei isolation and Fluorescence Activated Nuclei Sorting (FANS)

Mice were sacrificed by cervical dislocation, roughly 72 hours after TAM injection. vHipp was dissected and pooled from two mice before proceeding for nuclei isolation. Nuclei isolation was performed as in **Chapter 3** and the extracted nuclei were subjected to FANS, using the same set up as previously described (see **Chapter 4**). Nuclei were then sorted into 1.5 mL Eppendorfs containing 100 µL of Trizol for miRNA extraction (13,000 nuclei), 100 µL of buffer ATL (Qiagen) for DNA extraction (30,000 nuclei), and 100 µL of RLT buffer for RNA extraction (10,000 nuclei). After collection, all Eppendorfs were rapidly frozen in a mixture of dry ice and 100% ethanol and stored at -80˚C to maintain the integrity of the samples until the extraction procedures could be performed.

NB: For experiments and primary data related to RNA-seq, please see [246].

5.2.4. Molecular biology experiments and sequencing

5.2.4.1. Reduced Representation Bisulfite sequencing (RRBS-seq)

DNA extraction

DNA was extracted using QiAamp DNA Micro Kit (#56304, Qiagen, protocol for small volumes of blood). Additional changes to the protocol included warming the AE buffer at 37˚C before pipetting to the MinElute column in Step 13 of the protocol. DNA quantity was measured using the Qubit 2.0 Fluorometer and intact genomic DNA quality was assessed with the Agilent 2100 Bioanalyzer system.

Library preparation

Library for RRBS-seq[158] was prepared using the Diagenode protocol with slight modifications. As our DNA quantity was low, we used 50 ng (instead of 100 ng) as input for bisulfite treatment. Bisulfite treatment allows for the conversion of non-methylated cytidine into

thymidine, which can then be assessed bioinformatically to identify differential methylation patterns. Preliminary RRBS-seq experiments were conducted to ensure that the use of 50 ng DNA as input for the library preparation would provide similar results to the use of 100 ng DNA (**Supplementary Figure 3**). These results were also validated using gene-specific pyrosequencing for some selected candidates (not shown). Additional modifications were introduced in the following steps of the premium RRBS kit protocol http://www.diagenode.com/

Step 3.2, 3.3 and 3.5 – Volumes reduced by half.

Step 3.7 – 40 µL of Ampure beads (instead of 60 µL).

Step 4.9 – Sample pooling was performed for 5 libraries instead of 6 libraries in the original protocol.

Step 5.6 - 97.5 µL instead of 116 µL of BS conversion reagent.

Step 5.9 – Inversions were done for a total of 30 times.

Steps 5.14 and 5.15 – 5 minutes of standing time for elution buffer containing column and 2min for the next step.

NB: The modifications were necessary as we used 50 ng of DNA instead of the 100 ng input specified in the original protocol. The volume of the BS conversion agent was reduced due to the specific conditions of the experiment, where the FANS-nuclei had been stored for over 6 months in Buffer ATL. While using the recommended volume of the BS reagent with DNA derived from such nuclei, we could not retrieve any DNA in the PCR step. Thus, this modification was necessary to ensure successful DNA retrieval from the stored nuclei, as the original protocol was optimal for the fresh nuclei but required adaptations for the frozen nuclei.

Sequencing

Following the library preparation, the DNA concentration was measured by both Qubit dsDNA High sensitivity kit on a Qubit 2.0 Fluorometer and the Agilent High Sensitivity 2100 Bioanalyzer. Single end sequencing was performed using a NextSeq 500/550 High Output Cartridge (150 cycles). 2 DNA pools (each containing 5 different sample libraries) were used for each sequencing run. Using Illumina recommendations, a final concentration of 1.2 pM of the DNA library was loaded per sequencing run (78 µL of 20 pM DNA library, 520 µL of 1.5 pM - 20% PhiX-freshly prepared and 702 µL of HTT). As the library for RRBS-seq is a low-

diversity library containing a high fraction of CG rich oligonucleotide fragments, due to the selective cleavage of the MspI enzyme, a higher amount of PhiX was added to increase oligonucleotide fragments rich in A/T to prevent clustering, during sequencing.

(NB: Matthias Linke, Eva Weiss and Diagenode company provided the technical and intellectual support for establishing the RRBS-seq.)

5.2.4.2. Small RNA sequencing (Small RNA-Seq)

Total RNA extraction

Total RNA was extracted using the miRNeasy Micro Kit (#216084). The following step modifications were made:

Step 1: 600 µL of Trizol was used instead of QIAzol as 100 µL of Trizol was previously used to collect nuclei.

Step 14: 10 µL instead of 14 µL of elution buffer

Library preparation

Next generation sequencing (NGS) library prep was performed with NEXTFLEX Small RNA-Seq Kit V3 following Step A to Step G of Bio Scientific`s standard protocol (V19.01) using the NEXTFLEX 3' SR Adaptor and 5' SR Adaptor (5'rApp/NNNNTGGAATTCTCGGGTGCCAAGG/3ddC/and5' GUUCAGAGUUCUACAGUCCGACGAUCNNNN, respectively) in a 1/4 dilution. Step A (NEXTFLEX 3` 4N Adenylated Adapter Ligation) was performed overnight at 20°C. Libraries were prepared with a starting amount of 6,25 ng and amplified in 20 PCR cycles.

Amplified libraries were purified by running an 8% TBE gel and size-selected for 15 – 40 nt insert size.

Sequencing

Libraries were profiled in a High Sensitivity DNA Chip on a 2100 Bioanalyzer (Agilent technologies) and quantified using the Qubit dsDNA HS Assay Kit, in a Qubit 2.0 Fluorometer (Life technologies). All 24 samples were pooled in equimolar ratio and sequenced on 2 High Output NextSeq 500/550 Flowcell, SR for 1×75 cycles plus 7 cycles for the index read.

NB: Library preparation and sequencing for miR was performed by the IMB genomics core facility, with support from Perkin Elmer company. The core facility contributed to the text for the methods.

5.2.5. Behavior data and omics data analyses

5.2.5.1. Behavior data statistical analyses

All statistical calculations were performed using GraphPad Prism (8.4.2). For behavioral data with normal distribution. student's unpaired t-test with the assumption that the SD between populations is equal was used for statistical comparisons of two groups. For data with non-normal distribution, other tests were used as specified in the results section. In all calculations, $p<0.05$ was considered statistically significant.

5.2.5.2. RRBS-seq data analyses

After the sequencing bcl2fastq v2.20 conversion software (Illumina, San Diego, CA, USA) was used to demultiplex sequence data and covert base call (BCL) files into Fastq files. Quality check and adapter trimming were performed using Trim Galore! v0.5.0 (http://www.bioinformatics.babraham.ac.uk/projects/trim_galore/) and –rrbs as option for RRBS sequence reads. The mapping of the trimmed data to the mouse (mm10) reference genome and the methylation calling were conducted using Bismark v0.20.1[351]. The obtained methylation calls for the CpG context were further analyzed using the R package methylKit v1.10[352]. For differentially methylated cytosines (DMC) and differentially methylated regions (DMR) bases with less than 10× coverage and more than 99.9% percentile of coverage in each sample, were filtered out. A window of 1kb length and 1kb step-size was applied for the DMR analysis with a q-value cutoff < 0.01 for both DMC and DMR analysis. The genomic annotation of the DMC/DMR were performed using the R package annotatr v1.14[353]. Genes were assigned to the longest transcript. Assignment of the genes to protein coding or non-coding were derived from https://www.informatics.jax.org/. Enrichment analysis and UMAPs derived from Enrichr[354–356] are stated as such in the text.

NB: Raw data RRBS-seq bioinformatic analysis (sequence alignment, detection of differential methylation and initial GO analysis) was performed by Dewi Hartwich with inputs from me. We received substantial support from Diagenode during this analysis. Manhattan plots, LogOdds ratio and gene distribution Venn and pie charts were plotted by Hristo Todorov. Text for the methods was contributed by Dewi Hartwich Results interpretation was performed by me.

5.2.5.3. Small RNA-seq data analysis

Raw miRNA sequencing data were processed using exceRpt pipeline v5.0[357]. Briefly, the raw reads were pre-processed by removing the adapter and low-quality reads. Afterwards,

alignment of the filtered reads to the endogenous mouse genome (mm10) and transcriptome including miRNA, tRNA, piRNA, longRNA and circRNA was performed. The differential expression analysis for small RNAs was conducted using the combination of the DESeq2 v1.32[358] and edgeR v3.34[359] R packages. Pairwise comparison analysis was carried out using CPM (counts per million) > 1 and adjusted p-value < 0.05 as cutoff. The network enrichment analysis of differentially expressed small RNAs was carried out using the clusterProfiler v4.0 R package[360].

NB: Bioinformatic analysis (sequence alignment, detection of differential expression, GO term analysis) of raw data small RNA-seq was performed by Dewi Hartwich, with inputs from me. Text for the methods was contributed by Dewi Hartwich. We received a substantial help from PerkinElmer during the interim of the analysis. Interpretation of the results was performed by me.

5.2.5.4. Regulatory region overlap and motif enrichment analyses

Enhancer annotation for mouse brain and neuron regions were downloaded from EnhancerAtlas 2.0[361], other regulatory regions were from cENCODE (as published in[362]) and CATlas[363]. Motif enrichment analysis was performed using HOMER[364].

5.2.5.5. STRING analysis and CYTOSCAPE

STRING platform[365–367] (https://string-db.org/) was used for network analyses using the following settings: Network type – full string network, active interaction sources from experiments, co-expression, gene fusion and co-occurrence with a confidence of 0.400 or 0.700 as specified in the results section. Hubs were generated using CytoHubba[368] App in Cytoscape[369] based on 'Degree', with the 'top 10 and expanded network' feature.

5.3. Results

5.3.1. CSD induces significant deficits in SI tests with CD1 mice

To obtain stress-relevant phenotypes for tracing engrams in the Arc-GFP mice (**Figure 20a**), the first step was to expose the test subjects to an appropriate stressor to elicit a group stress effect as compared to the non-stressed controls (scheme in **Figure 20b**). Before subjecting the test mice to the stress paradigm, basal character of each individual mouse was determined using the open field/eagle test (OF/E) and the SI test with conspecifics (SI/CO) (as in[127]. The assessment was necessary for an unbiased segregation of the mice into control and stressed group (**Supplementary Figure 4a**, **left** for OF/E and **Figure 20c, left** for SI/CO). Following the segregation, mice assigned to the stressed group were subjected to the CSD paradigm. In

this paradigm, the Arc-GFP intruder mice experienced 15 S of physical attack from the resident CD1 mouse, repeated thrice daily with each attack session by a novel CD1 mouse. After the daily defeat sessions, the intruder mouse was separated from the CD1 mouse for 24 hours with a cage separator to allow sensory stimulation (odour and visual) in the absence of physical attacks. The procedure was repeated over a span of 10 days. Following the induction of stress, each mouse that underwent the stress paradigm was single-housed for 7 days and left undisturbed. Controls were also handled regularly (see **Methods**) in the interim of the 10 days experiment and were single-housed for the subsequent rest period of 7 days. On the 8^{th} day after the CSD, both the stressed group and non-stressed control group were subjected to the SI test with TAM (150 mg/kg), injected 5 hours before the SI for engram tracing. Remarkably, the results revealed a significant deficit in the SI index of the stressed group (**Figure 20c, right**) compared to the controls (Kolmogorov-Smirnov test, $p<0.05$, n = 43 controls, 73 stressed). Additionally, weights measured at regular intervals (**Supplementary Figure 4a, right)** depicted a gradual increase in weight in the stressed group, reaching a significant weight gain (t-test, $p<0.05$) on the 19^{th} day of the experiments. These results are conclusive of the successful application of an optimal stressor. Further, from within the stressed group, mice that showed a strong interaction with the CD1 mice in the SI test, similar to the control populations, were segregated as **resilient** populations (**SI index>100**), while those with a very low social interaction were labelled as **susceptible** (**SI index<100**). From these segregated stress phenotypes of resilience and susceptibility, some representatives (n = 22 for each of controls, resilient and susceptible phenotypes) were selected for the multiomics approach, encompassing RRBS-seq (n = 3 controls, 4 susceptible and 3 resilient from a pool of 2 mice each), RNA-seq (n = 6 controls, 6 susceptible and 6 resilient from a pool of 2 mice each) and small RNA-seq (n = 3 controls, 3 susceptible and 3 resilient, each from a pool of 4 mice). Mice selected for different levels of molecular analysis were sacrificed by cervical dislocation 72 hours after the TAM injection. Nuclei from the ventral hippocampus (vHipp) were isolated and activated nuclei (sfGFP+) were sorted with fluorescence-activated nuclei sorting (FANS) for multiomics experiments (methylome, mRNAs and small RNAs). The following sections will describe the results from the methylome, followed by an integration of the other omics datasets.

NB: Behavior results from the WT-GFP as genotype control for the *Arc*-insertion are depicted in **Supplementary Figure 4b**.

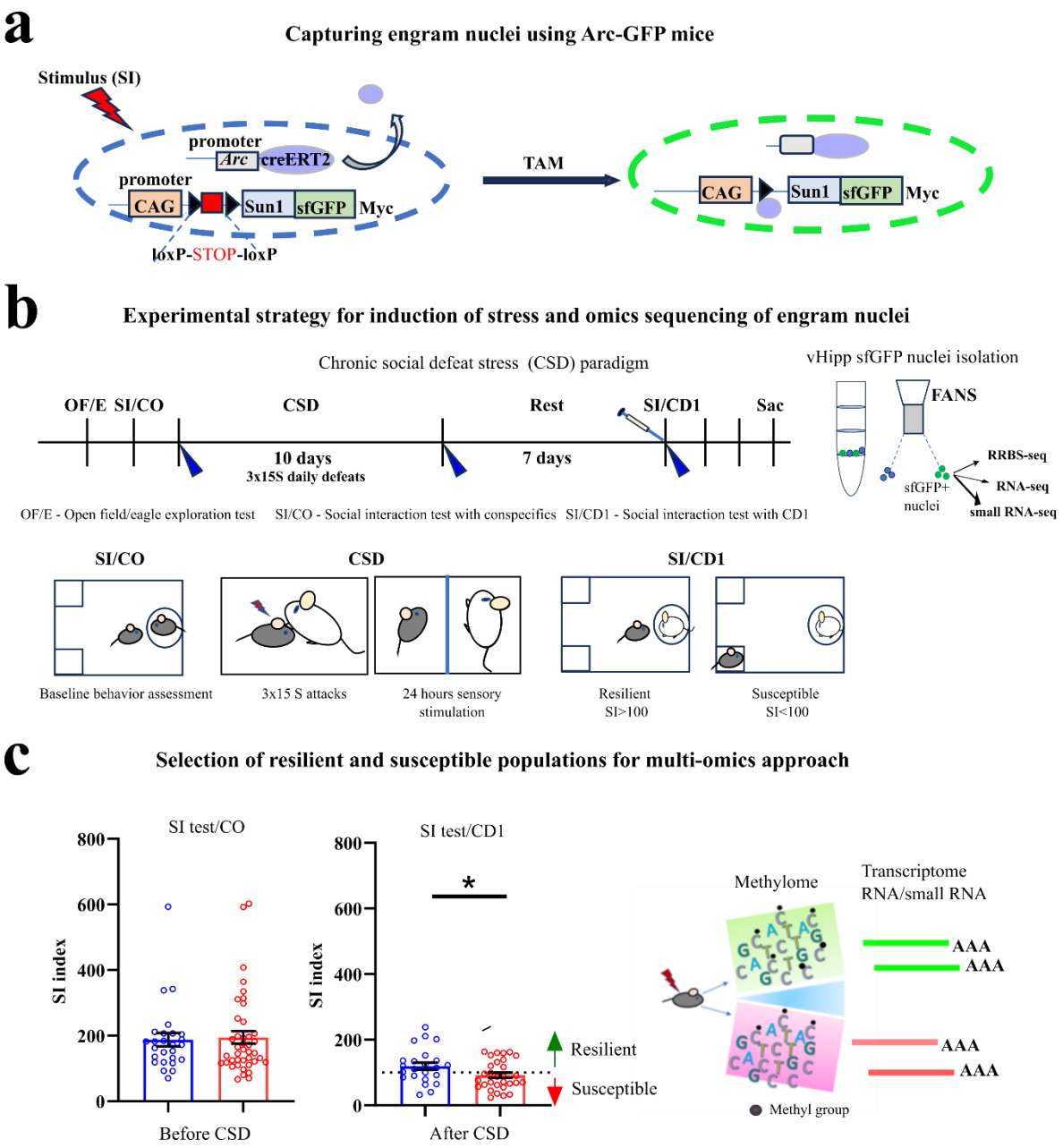

Figure 20: Experimental design for the engram-multiomics approach.

a. Working principle for tracing the engram nuclei in Arc-GFP mouse line with temporal control by TAM injection. **b.** Experimental scheme depicting the behavior paradigm and TAM injection 5 hours before the SI test to trace the engram nuclei. Weights are measured at regular intervals, thrice as indicated by the blue arrows. Roughly 72 hours after the TAM injection, mice were sacrificed, and engram nuclei were extracted by sorting of the sfGFP+ nuclei using FANS **c.** Results from the SI test with conspecific (SI test/CO) showing unbiased segregation of the test animals to the groups for control and stress populations. Meanwhile, following the application of the CSD paradigm, a significant decrease ($p<0.05$) in the SI index was observed in the SI test with CD1 mice (SI test (CD1). Representatives of the resilient (SI>100) and susceptible (SI<100) populations were then selected for multiomics sequencing (RRBS-seq, small RNA-seq and RNA-seq) to determine differential patterns between the divergent stress phenotypes. Error bars represent ± S.E.M. values. * represents significance value. RNA-seq data is in [246]. **Abbreviations:** RRBS-seq – reduced representation bisulfite sequencing, SI test/CO – SI test with conspecifics, SI test/CD1 – SI test with CD1 mice

5.3.2. Accessing the DNA methylation landscapes in the divergent stress phenotypes as well as controls

For investigation of the methylome landscape using RRBS-seq (input 50 ng of genomic DNA for library preparations, Diagenode kit), sfGFP+ nuclei were collected from a pool of 2 mice each from the selected control, resilient and susceptible populations to yield 3, 3 and 4 biological replicates respectively. We obtained, approximately, 30 million reads per sample, detecting 3.4×10^7 cytosines in resilient, 3.8×10^7 cytosines in susceptible, 3.0×10^7 cytosines in control populations with >10×coverage (average per sample – 3.5×10^7). All groups of resilient, susceptible and control populations showed similar global methylation (**Supplementary Figure 5a)** levels indicating genomic stability even after CSD treatment. Following this verification, we focussed on the CpGs (>10× coverage) as we detected a low percentage of CHHs and CHGs in our methylation data (less than 5%), though cytosines in the CHGs and CHHs have also been reported to play important roles in disease progression/synaptic function[205,362,370].

5.2.2.1. Landscape and functional characterization of the differentially methylated cytosines (dmCs) and genes containing dmCs (dmGs)

For an exhaustive investigation of the methylation landscape, we initiated our analyses with investigating the DNA methylation differences at single cytosine sites. This approach is essential because single cytosine methylation modification at genomic locations of importance can alter gene expression drastically[202]. Using a 25% difference in methylation levels as a threshold in all dual comparisons, we identified 1421 unique dmCs in **resilient compared to control** (**Res_c),** 911 unique dmCs in **susceptible compared to control** (**Sus_c**), and 1316 dmCs in the direct comparison between the stressed phenotypes, i.e., **susceptible compared to resilient** (**Sus_r**). Heatmap plot visualization of the absolute methylation values of the common cytosine sites in **Supplementary Figure 5b** depicted the prevalence of active modifications in both the susceptible (Sus) and resilient (Res) populations in genic as well as intergenic regions. Tracing the genomic locations of these modifications using log odds ratio, we noted significant enrichments of CpG shelves, introns and 3'untranslated regions (UTRs) in all comparisons (**Supplementary Figure 5c**) as also reported previously[205,362,371,372]. The significant enrichment of methylation in intronic regions indicate active neuronal modifications[205], following stress exposure. Focussing only on the genic regions, we traced the alterations to 884 genes in Res_c, 598 genes in Sus_c and 920 genes in Sus_r (see **Supplementary Figure 5d**), with most of the genes (>70% dmGs) harbouring only one dmC

(**Supplementary Figure 5e**). Interestingly, certain alterations detected in Sus_r were specific to either of the two stress phenotypes with 124 genes specific to Res_c, while 72 genes specific to Sus_c (**Supplementary Figure 5f**). However, we could not detect any specific risk-loci using a Manhattan plot, as we observed an equivalent spread over the different chromosomes **(Supplementary Figure 5g**). Gene ontology (GO) analyses on the combination of all genes obtained from all dual comparisons, we noted an enrichment of biological processes (BP) including 'pattern specification', 'neuron cell fate commitment' and 'axonogenesis', while enrichment in molecular functions (MF) include 'transcription-related genes' and 'ion channels'. On the other hand, GO cellular compartments (CC) revealed an enrichment of 'synaptic membrane', 'actin-based cell projection' etc., (**Supplementary Figure 6a**). Remarkably, reflecting the GO terms, volcano plots of the dmGs depicted a higher representation of transcription factor (TFs, orange dots) compared to synaptic genes (SGs[61], blue dots, **Supplementary Figure 6b)**.

5.2.2.2. Landscape and functional characterization of the differentially methylated regions (DMRs) and genes containing the DMRs (DMGs)

As the next step, we sought to determine regional methylation modifications (DMRs) as these have been considered better indicators of gene expression alterations and more robust to statistical power[139,373]. For this purpose, we determined the differential methylation averaged over blocks of genomic DNA (1000bps). The DMRs were equivalently distributed in the genic and intergenic regions and showed active alterations in both the susceptible- and resilient-phenotypes (**Supplementary Figure 7a**). The DMRs were enriched in the genomic locations (**Figure 21a)** of CpG shelves, 3' UTRs and intronic regions (mostly first introns, **Supplementary Figure 7b**). While Manhattan plots indicated a more or less similar distribution of DMRs along the genome in all stress group comparisons (**Supplementary Figure 7c**), it is interesting to note that chromosome 2 possessed the highest number of DMRs in both Res_c (152) and Sus_c (116). Focussing on the genic regions, the DMRs were assigned to 790 DMGs in Res_c (**Figure 21b**), 578 DMGs in Sus_c (**Figure 21b**) and 728 DMGs in Sus_r (**Figure 21b**). Amongst the DMGs in Sus_r, 130 were specific to Res_c, 69 to Sus_c, 41 in both Res_c and Sus_c (**Supplementary Figure 7d**), while 488 genes were not detected in either comparison with the controls. Nevertheless, majority (74%) of the DMGs belonged to the protein coding genes (**Supplementary Figure 7d**) with most genes harbouring only one DMR (**Supplementary Figure 7d**), as in the dmGs.

To estimate the probable functional roles of these genes, we performed GO enrichment analyses of the DMGs. Across all pairwise comparisons, we observed a significant enrichment of GO BP 'synapse organization' in all pairwise comparisons, (**Figure 21c**) indicating extensive neuronal remodelling after stress exposure. This observation was supported by a higher prevalence of synaptic-associated genes (Syngo genes [61], blue) in the volcano plots as opposed to the dmCs (**Supplementary Figure 7e**). Indeed, we noted a low overlap between the dmGs and DMGs (**Supplementary Figure 7f**). Other top GO terms include 'small-GTPase mediated signal transduction' in Res_c with 'regulation of Wnt signaling pathway' and 'regulation of endocytosis' in Sus_c. On the other hand, 'regulation of neurogenesis' and 'regulation of neuron differentiation' were significantly enriched in Sus_r (**Figure 21c).** A deeper analysis of the remaining BPs revealed that the GO terms of 'neuronal differentiation', 'gliogenesis' and 'axonogenesis' were **specific to Res_c** while 'endocytosis', 'cell-matrix adhesion' and 'Wnt signaling' were **specific to Sus_c** (**Supplementary Figure 7g)**. Next, UMAP dimensional reduction (**Figure 21d**, Enrichr[354–356,374] was employed to visualise major alterations in MFs following stress (combining the DMGs from all dual comparisons). With this approach, we identified significant enrichment ($p<0.05$) of major gene set clusters for guanine nucleotide exchange factors (GEF)/GTPase activator activity (cluster 6), Wnt signaling (cluster 9), tyrosine kinase activity (clusters 2,5,6,9), ion channel/receptor binding activity (cluster 3) and actin/tropomyosin binding (cluster 12). Thereafter, clustering the common methylated regions based on absolute methylation values (**Figure 21e**), we identified that MF tyrosine kinase activity was the most representative for gene sets that lost methylation in both the stressed phenotypes ($p<0.05$, Enrichr[354–356] while MF guanine nucleotide exchange factors (GEFs) and cell-cell adhesion activities were most representative for gene sets that gained methylation in the resilient. Interestingly, GO MFs of actin binding and microtubule binding are most representative of gene sets that gained methylation in the susceptible. On the other hand, for the GO CCs, both stressed phenotypes lost methylation for genes associated with GO terms of synaptic membrane and extracellular matrix (ECM). Meanwhile, the genes that gained methylation in resilient were enriched for CC including cell-cell contact, glutamate receptor complex etc., (**Figure 21e**) whereas that for susceptible were enriched in CC cytoskeletal fibre, actin filament and membrane rafts (**Figure 21e**).

Collectively, the findings in this section reveal that despite some common stress-invoked pathways in the stressed phenotypes, there were clear divergent molecular attributes active in the resilient and susceptible phenotypes.

Figure 21: Divergent regional methylation landscape of the differentially activated engram nuclei from the resilient and susceptible phenotypes post CSD stress.

a. Odds ratio depicting genomic distribution of the DMRs, enriched at the CpG shelves, introns and 3'UTRs (Log_e (odds ratio) >0) and depleted at the other regions (Log_e (odds ratio) <0). **b**. Venn diagrams indicating the genes containing only hypo/hypermethylated regions or both for resilient compared to control (Res_c), susceptible compared to control (Sus_c) and susceptible compared to resilient (Sus_r) groups **c.** Top 5 enriched biological processes (q<0.05) that correspond to the differentially methylated genes in the respective pairwise comparisons **d.** Overview of the collective alterations in MF following stress exposure, plotted on the first two UMAPs using Leiden algorithm from the Enrichr platform[354–356]. Each point represents a term with more similar gene sets positioned closer together. The larger and darker the point, the more significantly enriched the term (p<0.05, Enrichr). The description is as presented on the Enrichr platform. Top molecular functional attributes enriched within the clusters are listed **e.** Heatmaps depicting the absolute methylation percentages in the individual groups at regions identified as differentially methylated in any one of the comparisons and detected in all three groups. Regions were sequestered based on the highest methylation level detected in either control, resilient or susceptible individual groups. GO terms (molecular function -black and cellular component -purple, p-values < 0.05, Enrichr) most representative of the hypermethylated genes within a group are shown in the right panel.
Abbreviations: Res_c –resilient compared to control, Sus_c – susceptible compared to control, Sus_r – susceptible compared to resilient, hypo – hypomethylated, hyper – hypermethylated, DMGs – differentially methylated genes, Con – control populations, Res – resilient populations, Sus – susceptible populations, GO – gene ontology, BP – biological process, MF – molecular function, CC – cellular compartment, meth – methylation.

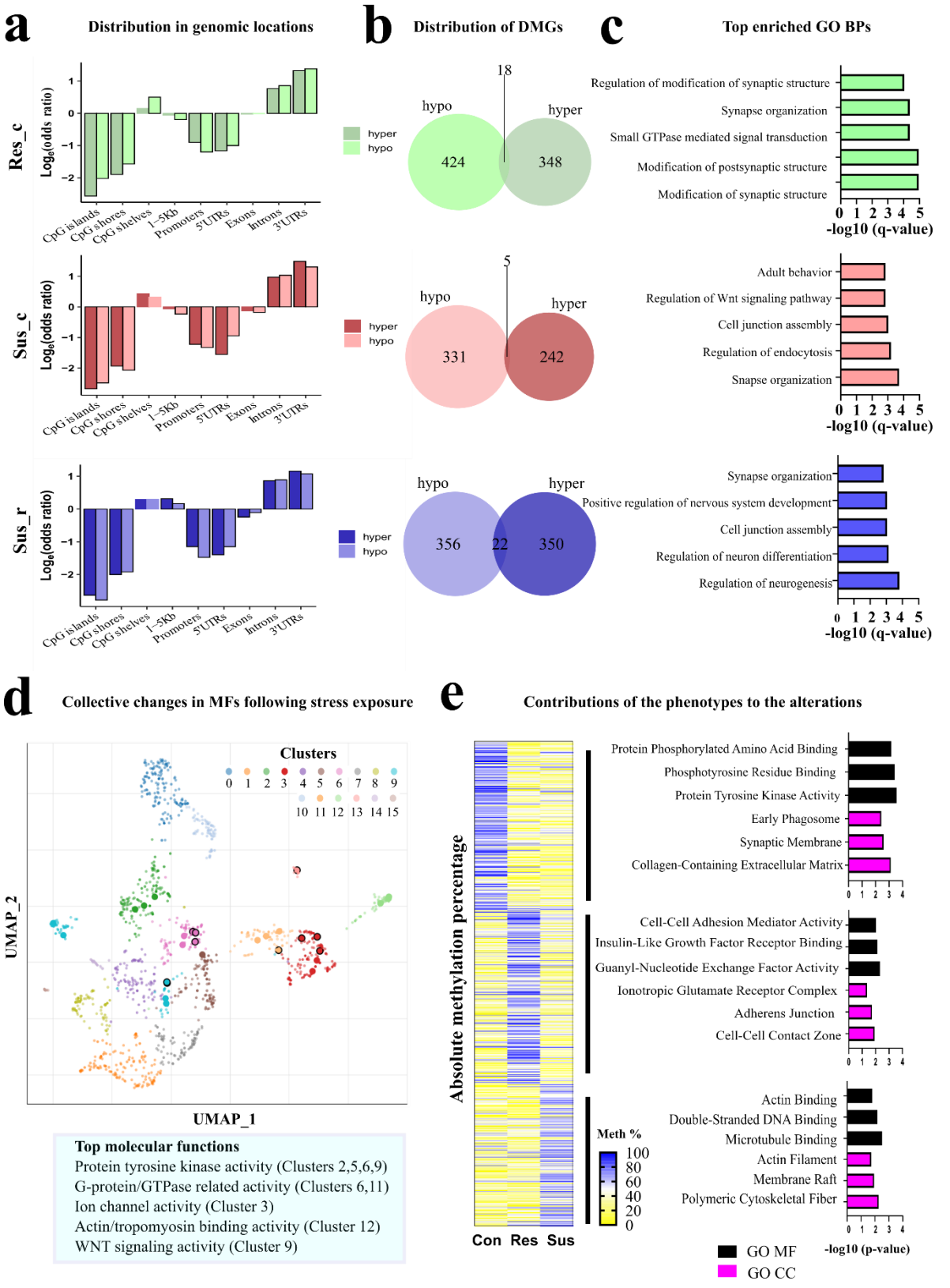
a
Distribution in genomic locations
Res_c
Sus_c
Sus_r
Log$_e$(odds ratio)
CpG islands
CpG shores
CpG shelves
1–5Kb
Promoters
5'UTRs
Exons
Introns
3'UTRs
b
Distribution of DMGs
hyper
hypo
18
424
348
5
331
242
356
22
350
c
Top enriched GO BPs
Regulation of modification of synaptic structure
Synapse organization
Small GTPase mediated signal transduction
Modification of postsynaptic structure
Modification of synaptic structure
Adult behavior
Regulation of Wnt signaling pathway
Cell junction assembly
Regulation of endocytosis
Snapse organization
Positive regulation of nervous system development
Regulation of neuron differentiation
Regulation of neurogenesis
-log10 (q-value)
d
Collective changes in MFs following stress exposure
Clusters
UMAP_1
UMAP_2
Top molecular functions
Protein tyrosine kinase activity (Clusters 2,5,6,9)
G-protein/GTPase related activity (Clusters 6,11)
Ion channel activity (Cluster 3)
Actin/tropomyosin binding activity (Cluster 12)
WNT signaling activity (Cluster 9)
e
Contributions of the phenotypes to the alterations
Absolute methylation percentage
Con Res Sus
Meth %
Protein Phosphorylated Amino Acid Binding
Phosphotyrosine Residue Binding
Protein Tyrosine Kinase Activity
Early Phagosome
Synaptic Membrane
Collagen-Containing Extracellular Matrix
Cell-Cell Adhesion Mediator Activity
Insulin-Like Growth Factor Receptor Binding
Guanyl-Nucleotide Exchange Factor Activity
Ionotropic Glutamate Receptor Complex
Adherens Junction
Cell-Cell Contact Zone
Actin Binding
Double-Stranded DNA Binding
Microtubule Binding
Actin Filament
Membrane Raft
Polymeric Cytoskeletal Fiber
GO MF
GO CC
-log10 (p-value)

5.3.3. Regulatory functions of the DMRs point towards involvement of GTPase signaling in stress-related alterations

Having determined the probable functional roles (GO terms) of the genes that harbour DMRs, we next investigated if these DMRs could possess potential regulatory roles. For this purpose, we matched the genomic co-ordinates of the DMRs with publicly available data of cis regulatory elements such as enhancers, insulators and inhibitors using brain specific data from CATlas[363] as well as non-brain-specific data from cENCODE[362]. Interestingly, we noted a substantial overlap of the DMRs (68.59%, CATlas and 50.69%, cENCODE) with the regulatory regions (hence termed **'rrDMRs'**, **Figure 22a**). This substantial overlap of the DMRs with the regulatory regions indicates a potentially crucial regulatory role of the methylation modifications (rrDMRs) following stress exposure. Indeed, enrichment analyses revealed that the genes that harboured the rrDMRs were top enriched (p-adjusted<0.05, Enrichr) for the GO BPs of 'regulation of intracellular/small GTPase mediated signal transduction', 'enzyme linked receptor protein signaling pathway' and 'petidyl-tyrosine modification/phosphorylation' (**Figure 22a**). These findings suggest that the alterations in the methylome landscape could potentially influence key signaling pathways. To increase stringency, we overlapped our data with age-matched brain enhancers available from EnhancerAtlas2.0[361] (*Mus musculus,* brain). Supporting the previous findings, the majority of the genes, containing DMRs overlapping with enhancer regions (now termed '**eDMGs**') were associated with GTPase signaling (*Arhgap9, Cdk14, Rasgef1a, Gabbr2, Arhgap35, Gnas, Tbc19db*), tyrosine kinase signaling (*Tex14, Aatk)*, synaptic vesicle functions (*Ap1m1*, *Sorl1*, *Coro1c*) and synaptic plasticity (*Map7, Camk2b, Fmnl1, Npas4*, *Arpc3*, *Prph, Cdh22*) (**Figure 22b)**.

5.3.3.1. Motif enrichment analysis identifies E26 Transformation Specific (ETS) family of TFs to be strongly enriched in the DMRs

Following the substantial overlap of the DMRs with the regulatory regions **(**refer to previous **Figure 22a, b**), we hypothesized that there could be several transcription factor binding sites (TFBSs) within the DMRs. Methylation of TFBSs plays important roles in TF binding and chromatin accessibility[202], thereby affecting gene expression[204]. Therefore, we performed TF binding DNA sequence motif enrichment analyses using hypergeometric optimization of Motif EnRichment (HOMER)[364] similar to Zhang and colleagues[206]. Interestingly, we identified that members of the ETS family of TFs[375], including ETS-like 4 (Elk4), $p = 10^{-126}$ (**Figure 22c**) and

ETS-like 1 (Elk1), $p = 10^{-65}$ were significantly enriched in the DMR regions. Of note, both Elk4 and Elk1 possess very similar motif seeds (TTCCGG)[375,376]. Further HOMER analyses of dual biological comparisons of Res_c, Sus_c and Sus_r identified a similar top enrichment of the ETS family of TFs, with slight differences in the TFs of lower ranked p-values. (see **Figure 22d**). This is an interesting observation as the ETS family of TFs are nuclear targets of the Ras (GTPase)-extracellular signal-regulated kinase (ERK) signaling[377,378], crucial for activity-dependent transcription[378], synaptic plasticity, learning and memory, among other important neuronal functions[379–381]. Though one could argue that the observed enrichment of the ETS TF could be because of the enrichment of the CG rich genomic regions in the RRBS-seq. However, this is unlikely because RRBS-seq data for non-stress research in hippocampus showed enrichment of other TFs, for example NeuroD1 in [362].

Overall, it is important to note here that modifications related to the GTPase signaling appeared in different layers of our analyses. Taken together, these findings implicate an important role for the ETS family of TFs and GTPase signaling in regulating the effects of stress via the methylome.

5.3.3.2. Relationship between differential methylation and gene expression at the sample collection point

Having determined a huge potential regulatory role of the DMRs, we next aimed at identifying the impacts in gene expression following stress exposure. For this, we overlapped the DMGs with the differentially expressed genes (DEGs, from [246], obtained using the same samples). Interestingly, we identified only about 10% (190) of the total DEGs overlapping with DMGs (**Figure 22e**). This is consistent with the existing literature[213], where epigenetic modifications do not alter transcript levels, shortly after an environmental insult but instead act as a priming module for future alterations. Surprisingly, despite the low overlap, the genes common between the two omics data sets showed GO MF enrichment of GTPase signaling activities (**Figure 22e, GO terms**) and GEFs (highlighted in rectangle in **Figure 22e**). However, these genes revealed a complicated, non-conventional relationship between DNA methylation and gene expression (**Supplementary Figure 8a**). Surprisingly, even the eDMGs (black arrows **Figure 22b**) showed a complex relationship with the RNA transcripts (**Figure 22e, left panel**) following stress exposure. Notably, these findings are similar to the existing reports of low convergence between the methylome and transcriptome[28] after an environmental insult.

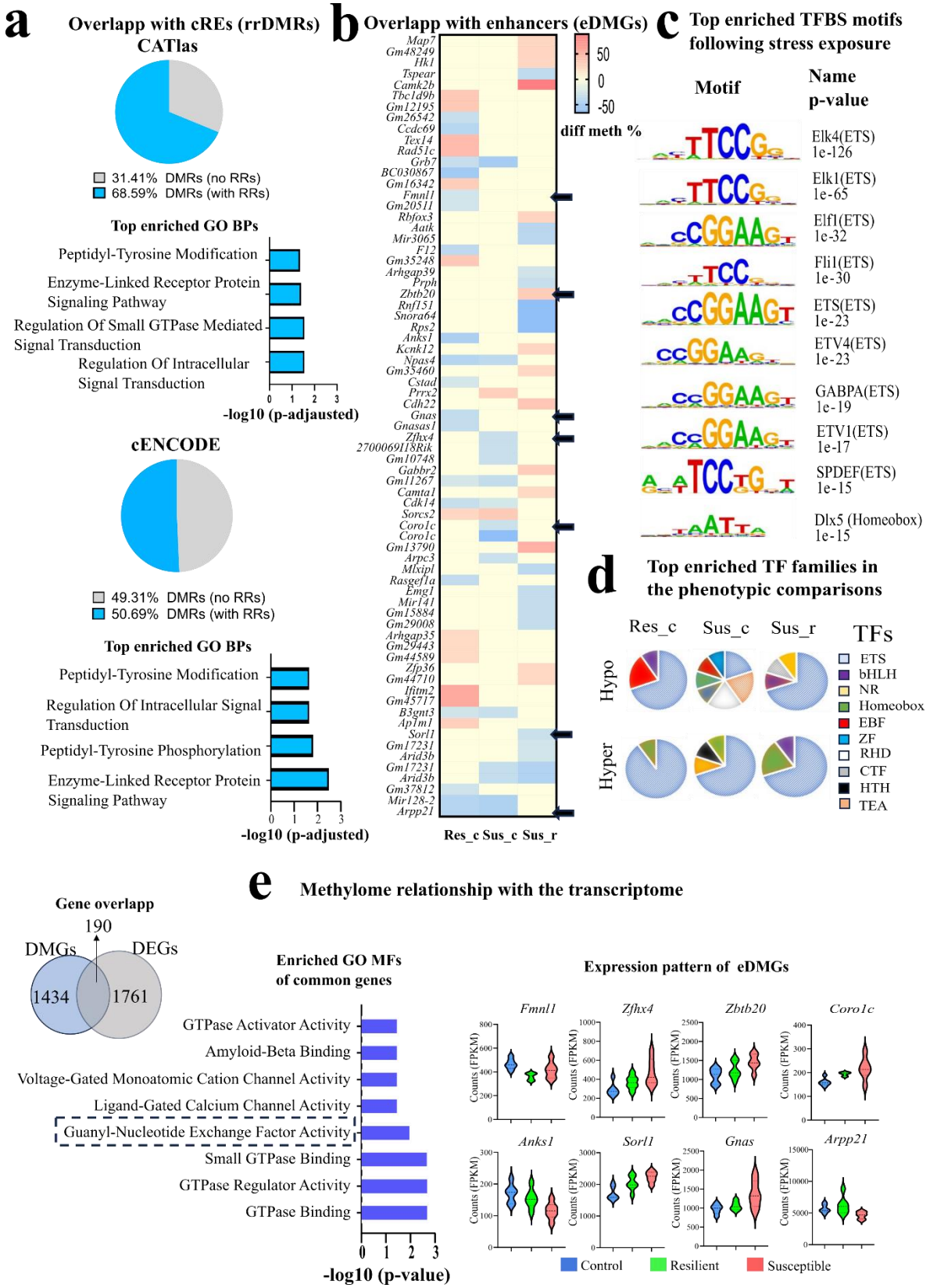

Figure 22: Assessing plausible regulatory functions of the DMRs.

a. Overlap with regulatory regions. Pie charts depicting the % of DMRs that harbour regulatory regions from CATlas and cENCODE along with the significantly enriched GO BPs (p-adjusted < 0.05, Enrichr) of the respective DMGs. **b**. Heatmap of % methylation differences of the DMRs overlapping with enhancer regions (eDMGs) **c**. Top enriched TF motifs of the DMRs (combined for all phenotypic comparison) determined using HOMER analysis, depicting prevalence of ETS binding sites **d**. Pie chart of enriched TF motifs of the DMRs segregated for each dual comparison, showing ETS TF family to be the top enriched. **e**. Methylome regulation of gene expression. Venn diagram identifying common genes between methylome and transcriptome changes after stress exposure along with the significantly enriched top molecular functions (p<0.05, Enrichr) of the common genes. Expression levels (read counts) of eDMGs (black arrows in **b**) indicating non-traditional relationship between methylation and expression even with the overlap with enhancer regions. **Abbreviations**: BP – biological process, MF – molecular function, TFBS – transcription factor binding site, TFs – transcription factors, DMRs – differentially methylated regions, DMGs – differentially methylated genes, DEGs – differentially expressed genes, RRs – regulatory regions, rrDMRs – DMRs that overlap with regulatory regions, eDMGs – DMGs that harbour DMRs overlapping with enhancer regions, hyper – hypermethylated, hypo – hypomethylated, Res_c – resilient compared to control, Sus_c – susceptible compared to control, Sus_r – susceptible compared to resilient.

5.3.4. Phenotype-specific differences in GTPase signaling and related processes transcending multiple omics levels

Since GTPase signaling appeared at different layers of analyses, we picked up this pathway for an in-depth analysis. For this purpose, we employed the multiomics profile to examine plausible phenotype-specific divergence in components of this signaling pathway, directly or indirectly related to the GTPases. To this end, we adopted a networks approach by integrating the genes that exhibited altered methylation or expression patterns into plausible protein-protein interactions in the STRING platform (See **Methods**). Such integrated analyses recognize the concept that genes do not function in isolation. Genetic/epigenetic modifications exert their effects in the physiology of an organism through their interactions with other genes, Therefore, employing a network approach facilitates potential identification of alternative therapeutic targets for downstream or upstream modulation of undruggable causative factors in the directly linked networks[382,383].

Interestingly, a preliminary screen identified an enrichment of the domains of the GEFs (GTPase regulators) in our methylome (combined DMGs) and transcriptome (combined differentially expressed genes, DEGs) datasets (Pfam[384] and SMART[385], see **Supplementary Figure 8b).** Therefore, this family was investigated in-depth. Intriguingly, we identified a divergent pattern in the RhoGEFs between the two stressed phenotypes with a higher fraction of **hypermethylated** GEF (intronic) prevalent in the resilient animals (**Figure 23a,** Res_c_s, resilient compared to either control or susceptible) as opposed to a higher fraction of **hypomethylation** in the susceptible (Sus_c_r, susceptible compared to either control or resilient). Interestingly, this trend was accompanied by a higher fraction of upregulated GEFs in the resilient (**Figure 23a,** Res_c_r) as opposed to downregulated genes in the susceptible (Sus_c_r). This phenotype-specific divergence in the RhoGEF family, surpassing different

omics layers, suggests a central and novel role of this GTPase regulator in directing the stress phenotypes.

Analyzing hub genes within the networks, we ascertained that GTPases functioned as hub genes (CytoHubba[368]) albeit with a unique and distinct pattern in the Res_c compared to Sus_c in both omics' levels. Specifically, in the methylome Res_c, GTPases (eg., *Rhoa*, *Gnas*, *Fras1*) and GTPase regulators (*Kalrn*, *Syngap1*) formed the majority of top 10 hubs (**Figure 23b**), while the hubs in Sus_c showed a low representation of the GTPase genes (*Gnas*). In contrast, for the transcriptome, the GTPases formed the top 3 hubs in Sus_c (eg., *Rhoa*, *Rac1*) while the spliceosome family of heterogenous nuclear ribonucleoprotein particles (*hnrnps*) and serine/arginine rich splicing factors (*srsfs*) dominated the top hub ranks in Res_c (**Figure 23b**). The hubs for Sus_r for the two omics levels are illustrated in **Supplementary Figure 8c**.

Though the detection of GTPases as hubs reversed when transitioning from the methylome to the transcriptome, the phenotype-specific differences in GTPase regulation at each omics level was evident. While the role of GTPase signaling is clear at this stage, given the observation of genes involved in other diverse BPs as hubs, our next step was to identify if we could observe phenotype-specific differences, directly or indirectly related to GTPase function, in the other BPs with the network approach.

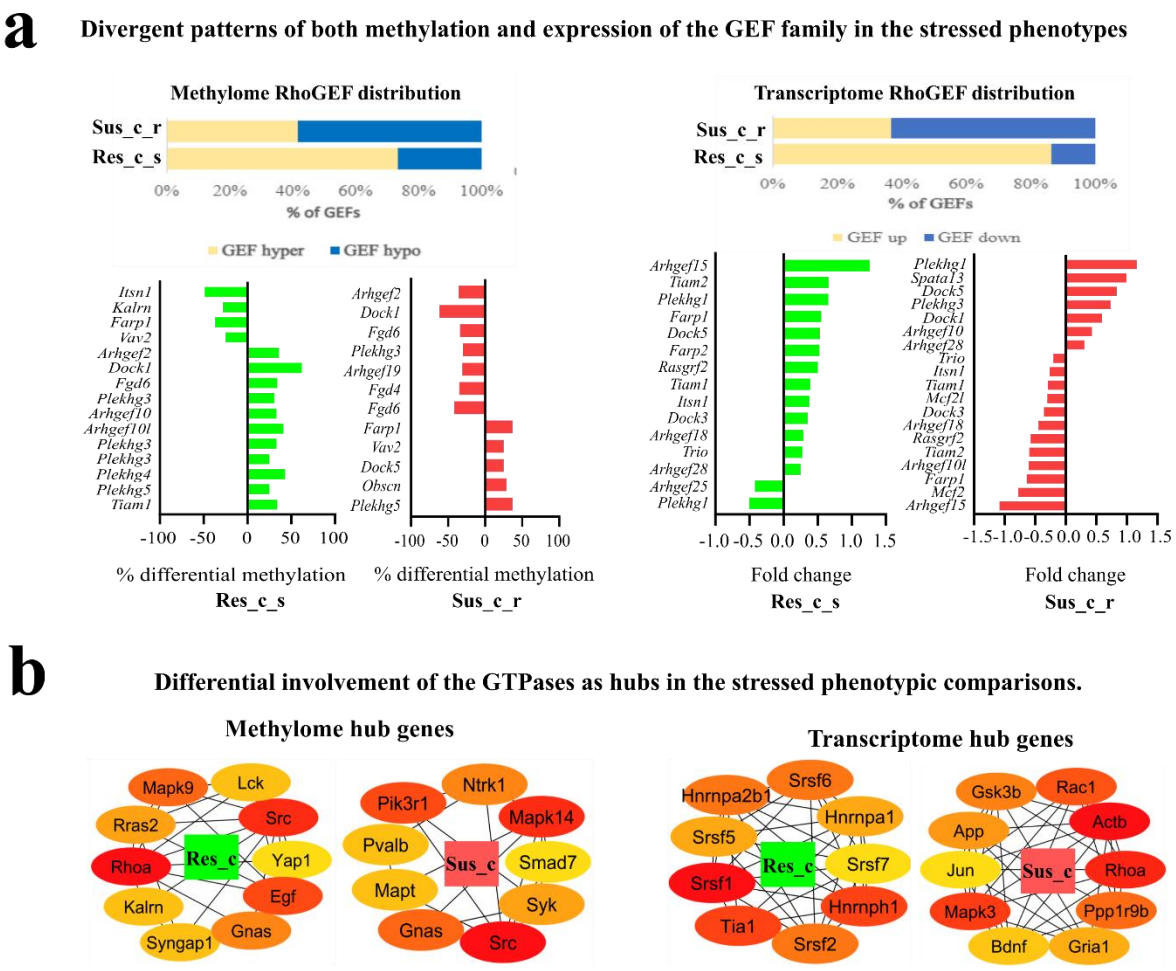

Figure 23: Multiomics network approach identifies phenotype-specific divergence in important biological processes.

a. Phenotype-specific divergence in methylation and expression patterns of RhoGEFs. Bar graphs depict an interesting trend of hypermethylation and upregulation of multiple genes from the RhoGEF family in the resilient (compared to control and susceptible) **b.** Phenotype-related divergence of GTPases at hub networks. Top 10 hubs (degree, CytoHubba) in Res_c and Sus_c in methylome and transcriptome network analyses indicating divergent molecular signatures in the stress phenotypes at different omics levels. Colour code red to yellow denotes rank in the ascending order, where a higher rank indicates lower connections. **Abbreviations**: GEF – guanine nucleotide exchange factor, Res_c – resilient compared to control, Sus_c – susceptible compared to control, Sus_r – susceptible compared to resilient, hypo – hypomethylated, hyper – hypermethylated, up – upregulated, down - downregulated, Res_c_r – resilient compared to control or susceptible populations, Sus_c_r – susceptible compared to control or resilient populations.

5.3.4.1 Multiomics network approach identifies phenotype specific divergence in other BPs.

To determine other BPs specific to a phenotype, we reasoned that combining the DMGs and DEGs for each phenotypic comparison could provide a better representation of the ongoing interconnected molecular changes in the phenotypes. The resulting integrated multiomics data of **multiomics resilient compared to control (RES_C)**, **multiomics susceptible compared to control (SUS_C)** and **multiomics susceptible compared to resilient (SUS_R)** were used to generate three separate networks in the STRING platform. From this multiomics integrated

network of each phenotype, we noted distinct BPs (**Supplementary Table 1**) activated in the RES_C and SUS_C. For instance, BPs related to 'synaptic vesicles recycling', '**exocytosis/endocytosis'**, 'actin nucleation', 'Wnt signaling', and 'myelination' were specific to SUS_C network, whereas amongst the limited terms specific to RES_C, we noted 'mRNA processing', and 'Rho protein signal transduction' to be of significance. Further, we identified distinct local network clusters: cadherin (CL:38951, CL38948, **Supplementary Table 2**) and spliceosome assembly (CL:16161, **Supplementary Table 2**) in RES_C with clusters of cell adhesion (CL:8461), oligodendrocyte development (CL:8865) and actin nucleation (CL:5993) in SUS_C. Noteworthy is that changes in myelination and oligodendrocyte differentiation have been observed before in the susceptible populations of the medial PFC[341]. On the other hand, GTPase families still remained as hubs (**Supplementary Figure 8d**) in the integrated data.

Though the STRING output revealed valuable insights, we noticed that many genes were excluded from the generated networks. Therefore, to gain a comprehensive overview of the multiomics dataset, we also employed the Enrichr platform. Apart from validating the results from STRING for SUS_C, specifically the enrichment of BPs related to 'synaptic vesicles', we noted specificity in 'cell-cell adhesion' (**Supplementary Table 3**) for SUS_C, while 'cell-matrix adhesion' and 'ERK1-ERK2 signaling cascade' were specific to RES_C. These phenotype-specific differences were substantiated by the enrichment analyses of the direct stress-phenotype comparisons for SUS_R. In particular, we highlight the enrichment of BP '**endocytosis**' (**Supplementary Table 3**) in the SUS_R comparison as this term's specificity to Sus_c persisted across different omics levels (**Supplementary Figure 8e)**.

Summarily, as the **GTPase signaling terms and synaptic vesicle-related** terms were overrepresented in the methylome and transcriptome data, we next aimed at identifying whether the miRs revealed a similar pattern.

5.3.4.2. Small RNA analysis supports findings from the methylome and transcriptome.

From amongst the small RNAs detected in our data (**Supplementary Table 6**), we focussed mainly on the miRs as their roles in stress regulation[386] and local synaptic modulation of protein synthesis[387] are well known. From our low-input sequencing of small RNAs (NEXTFLEX, see **Methods**), we identified 23 miRs upregulated in Res_c, 19 miRs downregulated in Sus_c and 137 downregulated in Sus_r. Noteworthy is that the Res_c and Sus_c showed distinct patterns of expression of the miRs.

GO enrichment analyses revealed significant alterations in '**GTPase signaling**' as well as '**synaptic vesicle** recycling' (**Figure 24a**) in both Res_c and Sus_c, lending a substantial

support to the results from the methylome and transcriptome. In fact, since the miRs are all downregulated in Sus_c (miR analysis), the substantial enrichment of vesicle-related processes (**Figure 24a**) correlates well with the specific enrichment of vesicle-related processes in multiomics SUS_C (**Supplementary Table 1**). Further, we noted that the miRs, predicted to target GEFs, showed a lower level of expression (read counts) in the resilient samples as opposed to susceptible (**Figure 24b**). This correlates well with the increase of GEF expression in the DEGs (**Figure 23a**).

Thus, from the **multi-level analyses** of different molecular machineries, the stark alterations in the synaptic, **GTPase-related functionalities and vesicle-related processes** are visible. Given the exhaustive analysis, our next step was to identify whether we could secure plausible causative factors, that could partially act as a therapeutic target.

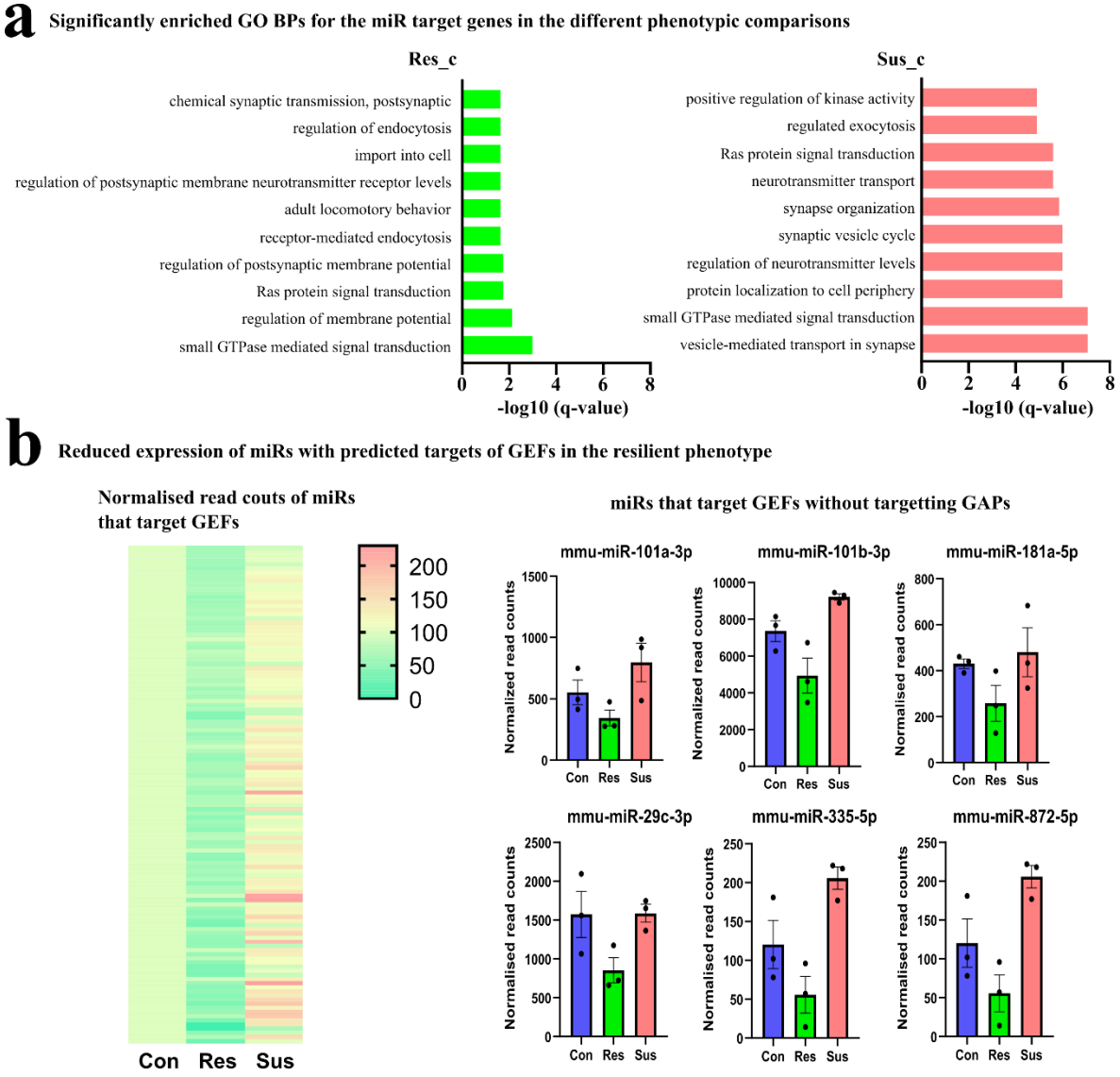

Figure 24: miRs show convergence with the results from the methylome and the RNA transcriptome.

a. GO BPs show significant enrichment of synaptic and GTPase related processes in Res_c (q<0.05) and Sus_c (q<0.05) **b.** miRs that are predicted to target RhoGEFs are downregulated in the resilient (Res) compared to controls (Con), while susceptible (Sus) showed an upregulated expression. Error bars represent ± S.E.M. values. **Abbreviations**: BPs – biological processes, GEFs – guanine nucleotide exchange factors, GAPs – GTPase-activating proteins, Res_c – resilient compared to control, Sus_c – susceptible compared to control, Sus_r – susceptible compared to resilient, Res – resilient populations, Sus – susceptible populations, Con – control populations.

5.3.5. Identification of novel therapeutic targets

For identification of a proper therapeutic target, we reasoned that the target should possess the following characteristics. First, the target should belong to a family/a part of a network that shows alterations at the multiomics levels. Such a family would possess the potential to alter the flow of information between the interconnected cellular machineries, albeit in different omics layers. Second, the target should either be a hub or possess direct relevance to a hub for exerting maximal influence on signaling mechanisms via this target. Third, the target should be relevant to a phenotype-specific alteration as this increases the likelihood of it being a causative factor underlying the phenotypic divergence.

To achieve our first aim of demarcating the common pathways prevalent at the multiomics levels, we gathered the collective stress-related alterations in molecular functions for each omics level and generated integrated enrichment maps (**Figure 25a**, Cytoscape Version 3.8.2). We excluded miRs from this collection as the target genes giving rise to the MFs are mostly predicted targets). From the collected enrichment map, we identified a large overlap of alterations in targetable molecular functions of ion channels and receptors (Cluster 3) at all omics levels. Additionally, the alterations in the DMGs and DEGs overlap at the targetable MFs of GTPase activities (Cluster 5) and actin/cytoskeletal binding (Cluster 6). Thus, we reason that these sectors can be exploited to identify novel therapeutic targets, especially since, they are relevant to synaptic functions, and stress disorders.

Given that synaptic functions play a crucial role in the development of stress disorders, we focussed our target search within the synaptic genes. For this purpose, first, we generated a network of the synaptic genes detected as significantly different in any dual group comparisons for any omics level. Next, to identify novel targets, we followed a systematic approach to screen out any gene that has been reported as prominently relevant to depression or stress research. Our screening list was generated by pooling data from the 'major depression' gene list in Harmonizome 3.0[388] Bagot and colleagues[183] (vHipp only), Fan and colleagues[389] Scarpa and colleagues[390], Gammie and colleagues[391] (Top 1000 gene list); and Kuehner and colleagues (only from data relevant to Figure 3 of [390]**).** First, we noted that multiple genes in our data, including GTPases, Rho GTPase activating proteins (GAPs) and RhoGEFs, have been

identified as stress-relevant (**Figure 25b**). Remarkably, we determined novel genes (**Figure 25b**, **Supplementary Table 4),** that has not yet been implicated to stress pathways with major relevance in previous studies. From these genes, we focussed on 5 novel genes (black, **Figure 25b**) relevant to the GTPase family and regulators, as our data highlights a critical role of GTPase signaling in the long-term effects of stress. To ascertain the novelty, we then screened for any new publications that contained any of these 5 genes as protagonists for stress-associated effects. Indeed, a regulatory role of *Ophn1* (Oligophrenin 1, encoding a RhoGAP) in depressive-like behaviors following stress was reported in a very recent publication[392]. From amongst the remaining genes, we identified the **GTPase**, ***Arf6*** (ADP-ribosylation factor 6), as the most prominent novel target due to its importance in **synaptic vesicle functions including endocytic** pathway and actin polymerisation[393]. The significant enrichment of 'endocytosis process' specific to the susceptible phenotype in both the methylome and transcriptome (**Supplementary Figure 8e**) accompanied by a stark difference in BPs of vesicle dynamics and endocytosis (**Figure 24a**) for miRs, substantiates the hypothesis. Coincidentally, Arf6 protein upregulates integrins and downregulates E-cadherin[394], which goes well with our data where integrin signaling pertains to Sus_c and cadherin signaling to Res_c. Additionally, Arf6 functions upstream of the Wnt signaling[395], which is specifically enriched in the susceptible phenotypes. Apart from this, *Arf6* also shows physical connections to the major hubs of GTPases *Hras*, *Rac1* as well as the RhoGEFs, which depicted distinct patterns in the divergent stressed phenotypes. This crucial positioning of Arf6 increases its probability of being a 'causative factor' and hence a suitable therapeutic target. Remarkably, *Arf6* expression is upregulated in the susceptible (log2 fold change ~ 0.4) compared to resilient group while its miRs are downregulated. Decreasing the activity of Arf6 has been shown to be important for the regenerative capacity of the axons in the central nervous system (CNS)[396]. Noteworthy is that downregulation of *Arf6* in the synapses lead to an increase in the readily releasable pools[397] to facilitate efficient synaptic communication. Intriguingly, *gm9887*, long non-coding RNA that partially overlaps with *Arf6*[398], displays 3 CpGs (dmCs) differentially methylated in Res_c at the 1-5kb upstream of the gene start site, which are also in the positions for *Arf6*. This could, hypothetically, entail a decrease in *Arf6* expression in the resilient group. It is noteworthy to highlight that *Arf6* has not been indicated as a prominent gene in any stress-related study. However, its crucial role in synaptic depression as well as neuronal differentiation[380] is well known**.** In fact, Arf6 has been identified as a highly potent therapeutic target for cancer research, very recently[399]. As noted above, Arf6 already possess a plethora of drugs from cancer

and cardiovascular studies. Therefore, it will be easy to transition to stress research, without the need for developing new drugs from scratch.

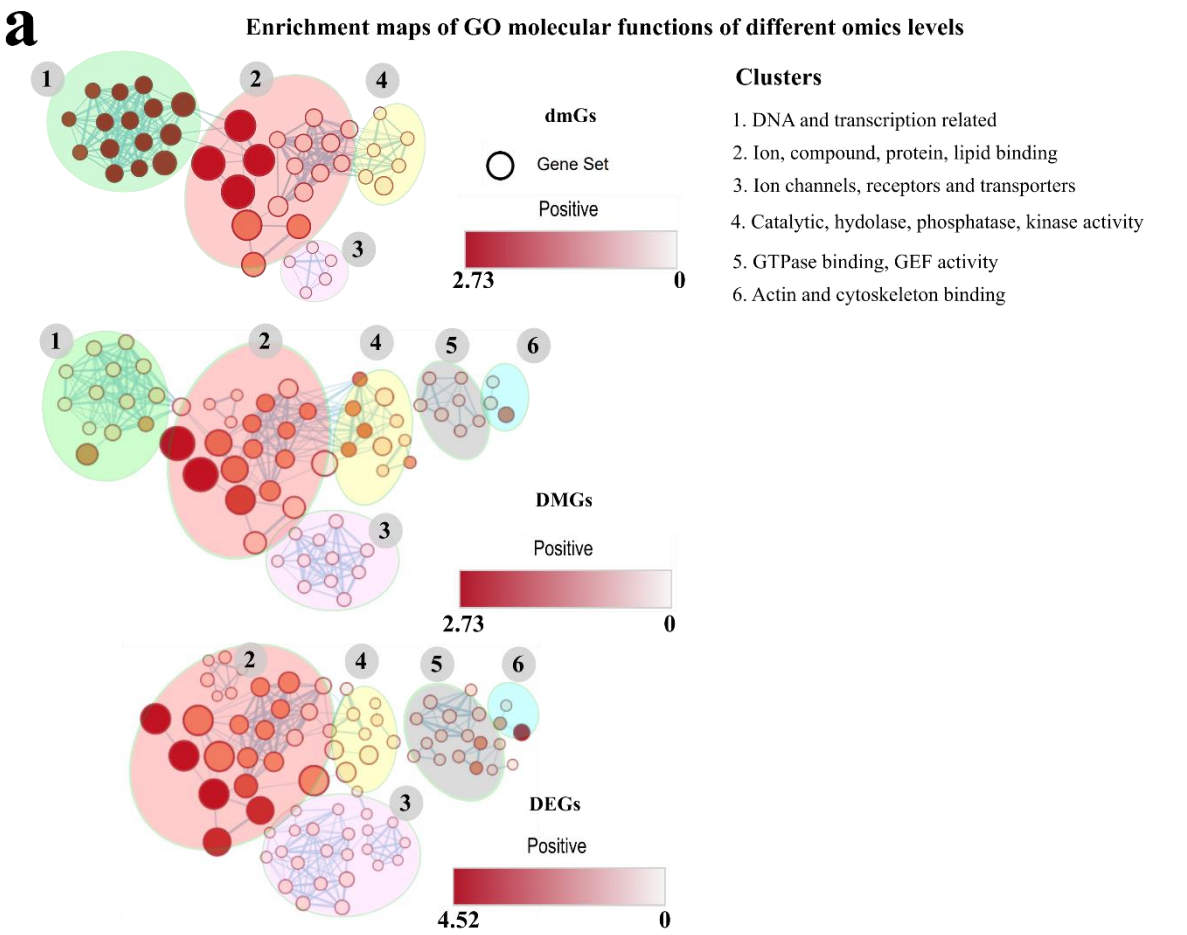

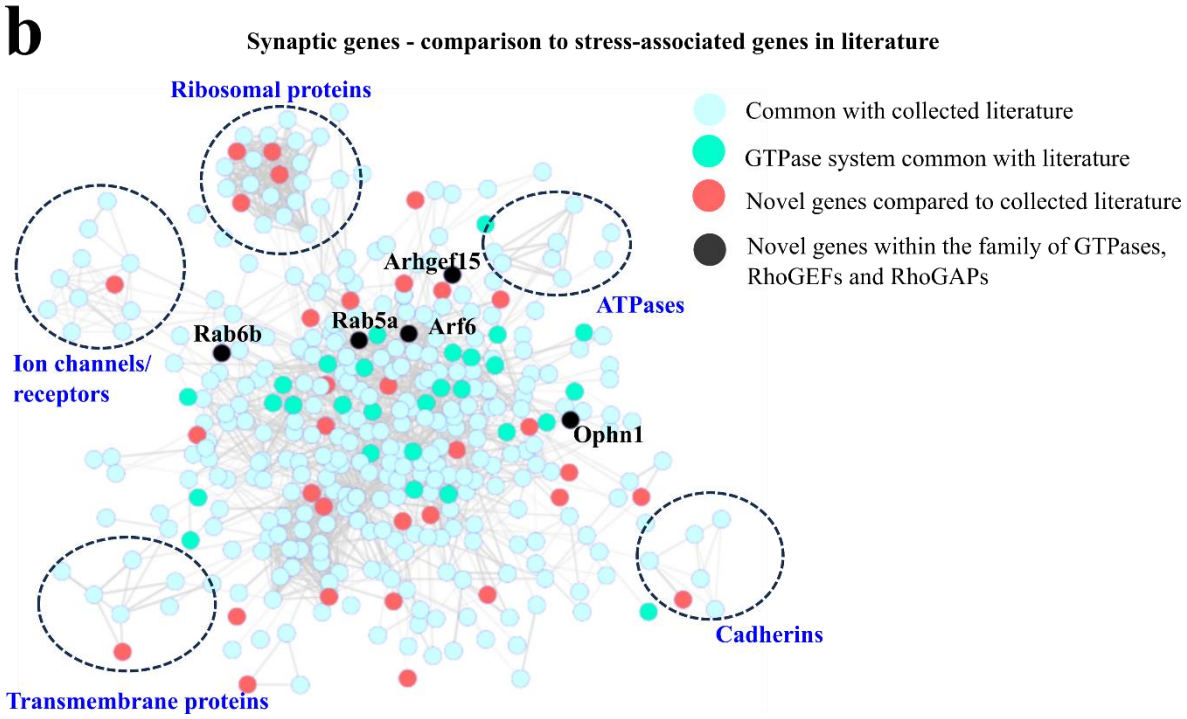

Figure 25: Overview of the multiomics modifications and determination of novel therapeutic targets.

a. Integrated maps of the significantly enriched GO molecular functions (q<0.05, STRING) of the combination of genes that were detected as differentially methylated (dmGs, DMGs) or expressed (DEGs). The major clusters of the enriched terms are enclosed within circles of different colours, wherein the nomenclature is shown on the right panel of the figure. Each node in the figure indicates gene sets with the node size determined by the number of genes in the gene set, while the colour of the node indicates the enrichment value (NES score). **b**. STRING network of the synaptic genes that were found to be altered at any of the omics levels, following stress exposure, where each node represents a gene. Genes already reported in literature as majorly associated with stress disorders or depression are marked in cyan or green, while those genes that are newly identified as relevant to the CSD stress response, via our integrated engram nuclei-multiomics approach, are highlighted in red or black. **Abbreviations**: dmGs – genes containing differentially methylated cytosines, DMGs – genes containing differentially methylated regions, DEGs – differentially expressed genes, GEF – guanine nucleotide exchange factor.

5.4. Discussion

Using the CSD model on TAM-inducible Arc-GFP mice, our data traced the shifting molecular landscape in specific engrams of control, susceptible and resilient mice, employing both methylome, transcriptome (data from [246]) and miRome. It is interesting to note that both stressed phenotypes of susceptible and resilience, showed a higher amount of hypomethylation compared to controls, indicating a possible difference in the levels of DNA methyl transferase (DNMTs) or ten-11 translocation (TETs) enzymes. Indeed, Wei and colleagues [371] reported decreased DNMT3A after stress. Consistently, reinvestigation of our transcriptome data (from [246]) showed that DNMT3A and DNMT1 levels were downregulated in the susceptible groups. Apart from this, we uncovered a complicated relationship between the methylome and transcriptome in the divergent phenotypes. Additionally, our multiomics approach using only engram specific nuclei, at an important phase post-stress exposure, provided us with the unique opportunity to uncover intriguing biological phenomenon revolving around GTPase signaling.

5.4.1. Significance of the enrichment of GTPase signaling cascades and synaptic plasticity following stress exposure

The methylome data identified a significant enrichment of functionalities directly related to GTPase signaling in all dual phenotypic comparisons, supported by a similar overrepresentation in the transcriptomics data[246]. This highlights a critical role of this signaling cascade following stress exposure. Interestingly, the members of the GTPase family form major hubs (**Figure 23b**) in both the methylome (DMGs) and transcriptome (DEGs). Indeed, the Ras superfamily of GTPases and its regulators have been widely known to be involved in learning and memory[400]. Calcium dependent GTPases are important for preventing depolymerisation of the actin cytoskeleton, which is important for spine reorganisation[401],

following a learning-induced activity[107]. Meanwhile, malfunctions in the GTPase system (rasopathies) are known to cause cognitive dysfunctions like autism spectrum disorder[402,403], apart from being associated with depression and early life environmental/social stress[404]. In fact, in a recent study by Lutz and colleagues[370] integrating multiple epigenetic levels of histone marks, methylation and transcriptomics, small GTPases were determined to be critical factors for developing a risk for depression following childhood abuse. Consistently, involvement of GTPases has been constantly highlighted in multiple neurodevelopmental and psychiatric disorders as mentioned in [405]. However, research regarding the role of the GTPase regulators in resilience/susceptibility is extremely limited. Though, Lutz and colleagues[370] mentioned the involvement of GTPase regulators in early life stress, they did not investigate further. Therefore, the novel findings in our study of the differential pattern of the GEF families gaining intronic methylation in the resilient group (**Figure 23b)**, accompanied by an upregulated expression in the transcriptome (**Figure 23b**), provides a further mechanistic insight into the stress affected mechanisms involving GTPase signaling. Remarkably. the differential trend visible in the **upstream signals**, for example, adhesion mechanisms (**Supplementary Table 1 and 3**), coupled with prominent alterations in the **downstream processes** of a. endocytosis and b. actin/microtubule processes in the susceptible, could enhance the synaptic GTPase-nuclei divergent signaling in the stressed phenotypes. In fact, this divergence could be encoded into the epigenome via their nuclear targets, namely the ETS family of activity dependent TFBSs[406–408] (**Figure 22c**), which were significantly enriched within the DMRs.

The GTPase-ETS coupling provides one mechanism by which effects of stressors can be sustained long-term in the epigenomic landscape[409], despite the eventual removal of the stressor. More elaborately, the ETS family of TFs integrates synaptic GTPase signaling in the nuclear epigenome[410] via the ETS-SRF (serum response factor) ternary complex factor at TFBSs[406,411] to regulate activity-dependent IEGs, actin cytoskeletal or synaptic plasticity genes[401,412]. Such repeated waves of signal integration of neuronal activities, i.e., differential synaptic-nuclei encoding and nuclei-synapse decoding via the Ras-SRF-ETS signaling could, over time, prime the epigenome[401], differentially for future responses. Such a differential priming entails altered cytoskeletal dynamics[411] and synaptic architecture, manifesting as differential behavioral patterns[207] between resilience and susceptibility. Interestingly, apart from its critical role in synaptic nuclei-signaling via the ETS family of TFs, RhoGTPase signaling can directly modulate epigenome/chromatin plasticity and gene transcription[413–415], via actin remodelling in the nucleus itself[416]. Thus, our findings suggest a crucial link in intercepting and integrating alterations in the extracellular/synaptic environment into the long-

term epigenome of an organism, via the GTPase signaling. Such differential signaling could potentially generate distinct homeostatic equilibrium in the divergent stress phenotypes for future responses. In fact, the Ras-ERK-ETS (Elk) could be one path by which post traumatic disorder (PTSD) states emerge[198] in stress-susceptible groups apart from the ETS family's involvement in immediate reactions to acute stress[237]. Indeed, recent studies demonstrated that modulation of *Elk1* is important for antidepressant functions[407,417,418] and that of Ras-ERK-ETS signaling for longevity[408]. Interestingly, apart from synaptic-nuclei signal encoding, alterations in the GTPase signaling pathways could also contribute to the differences in neurogenesis[419] via ERK signaling[420] or RhoGEFs (DOCK1)[421]. *Artemin,* a neuroprotective factor inhibited by Rac GTPase[422] was found to be upregulated in a study of resilient mice[423] in females, which is interesting as *Rac1* expression was decreased in the resilient populations in our data[246].

Given the critical role of GTPases in regulating stress outcomes, it is surprising that GTPase pathways were not significantly enriched in terminal neurological disorders though cell adhesion pathways were found to be modified[424]. This could suggest that GTPases play critical roles during crucial window periods of signal integration for long term epigenetic modifications, following an environmental insult. Thus, modulation of the GTPase signaling or related mechanisms in synaptic functions could be important for rescuing susceptibility phenotypes.

5.4.2. Significance of the multiomics approach towards identification of novel therapeutic targets

Besides the revelation of interesting alterations in the GTPase signaling, our engram-specific multiomics approach facilitated an integrative view of the ongoing molecular changes in the divergent stress phenotypes, that would, otherwise, have not been possible with contemporary techniques. Indeed, the low overlap of epigenetic mechanisms with transcriptome is consistent with literature[213,371], where the sample collection point is close to the period of environmental insult. This can be due to the temporal difference in the activation of the interconnected but different omics layers, i.e., DNA methylation could occur before or follow transcriptional alterations[425,426]. Though only 10% of the DMGs showed alterations in expression, the high overlap of the DMRs with putative cis regulatory regions and enrichment of ETS TFBSs strengthen the likelihood of the generation of a primed epigenome[372,427]. A primed epigenome could potentially influence future transcriptional states by facilitating a faster or stronger transcription of certain genes, thereby modulating behavior upon reintroduction of a similar stimuli[427]. For instance, Chastain and colleagues[428], demonstrated that the epigenetic

remodelling following alcohol exposure resulted in transcriptome changes only at a later stage in life. Following the norm of these differential waves between transcriptome and epigenome, we noted a few biological processes reversed phenotype specificity at the different omics layers (DMGs vs DEGs) (**Supplementary Figure 7e**). Given the temporal dissonance between the transcriptome and methylome[205] after an environmental insult, such observations allow for the speculation that molecular modifications in the resilient and susceptible groups could themselves possess a different sequence/speed of recruiting a particular molecular pathway. In fact, Bagot and colleagues[183] highlighted the possibility that resilient compared to susceptible phenotypes exhibit a faster rate of adaptive modifications compared to susceptible in their bulk transcriptomic studies.

Though accessing and interpreting the different omics layers is a challenge, the integrated use of multiomics and network analyses approach, facilitated the determination of **susceptible-specific** alterations in '**endocytic processes'** across both the methylome and transcriptome levels. Supporting this specificity, the miR analyses revealed an enrichment of synaptic vesicle processes to be largely affected in the Sus_c, where the detected miRs were all downregulated. Though the Res_c miRs showed enrichment of BP of 'endocytosis', the miRs are upregulated and could entail a downregulation of genes for endocytosis. Conclusively, our findings put emphasis on the stark differences in the regulation of 'vesicle dynamics or endocytotic processes' between the susceptible- and resilient- phenotypes across all omics levels. Thus, the identification of ***Arf6*, a GTPase that plays a central role in endocytosis**[393,429–431] in the screening analysis presents itself as an intriguing result. Remarkably, *Arf6*'s potential of being a therapeutic target in other non-stress studies (cancer) has recently been recognized[399]. Apart from its critical role in regulating readily releasable pools of vesicles and synaptic depression[380], its strong molecular interactions with hub GTPases like RhoA and Rac1[430] and susceptible-specific pathways like Wnt and integrin signaling[429], highlights its central role as a potentially effective target to rescue susceptible phenotypes. As *Arf6* is upregulated in the susceptible phenotype, we posit that decreasing the expression of *Arf6* could increase resilience outcomes. Given the recent finding of *Ophn1*, which is a RhoGAP and an intellectual disability gene as a potent therapeutic target for depressive-like behavior[432], the therapeutic potential of *Arf6,* which is a specific target of the guanine nucleotide exchange factor (GEF) encoded by the intellectual disability gene *IQSEC2*[433], in rescuing susceptible phenotypes, is substantial. Apart from this, its strategic association with the mTOR pathway[434], an important therapeutic target for stress research[244,435], adds weight on its effective potential. However, it is crucial to

note here that the relevance of *Arf6* as a therapeutic target may be only for the window period along the timeline of our experiments.

Overall, it is important to highlight the importance of employing a multiomics integrative approach in identifying crucial modules/pathways underlying phenotypic divergence of complex disorders. For example, with the conventional approach of investigating just transcriptomics while screening only genes with high fold changes as therapeutic targets, I would not have been able to determine either the relevance of endocytosis or that of the GTPase *Arf6* (fold change ˜0.4). Apart from these, the modifications of the piRs that have recently been found to be important for regulating synaptic plasticity[436–438] and transgenerational epigenetic inheritance[437], as well as other small RNAs (**Supplementary Table 6**) add weight to the prevalence of stark differences, between the divergent populations. Thus, the study underscores the relevance of a multiomics and network analyses approach to increase the resolution of investigating differential molecular landscapes following stress exposure to identify previously overlooked therapeutic targets.

Chapter 6. Tissue level differences in maintaining susceptibility and resilience

6.1. Introduction

Different brain regions exhibit different molecular signatures owing to the heterogeneity of the cell types as well as functional importance[439]. In fact, expression levels differ between tissue regions of the same animal following stress exposure[237]. For example, in a chronic mild stress model, miR-16 was shown to be upregulated in the ventral tegmental area but downregulated in the medial PFC[440,441] in male wistar han rats. Meanwhile, mRNA expression in the PFC for resilient and susceptible mice were reversed in the dorsal hippocampus[442]. In the context of DNA methylation, chronic social-predator stress did not affect *Bdnf* promoter methylation in either PFC or amygdala but influenced methylation levels in the different sub-tissue regions of the hippocampus (CA3 vs. CA1 and DG) ([443] as cited by [29]). Thus, previous studies revealed differential responses of tissues in different sectors of the epigenome including methylation, following stress exposure. However, a systematic investigation of the alterations in the methylation landscapes of stress-phenotypes between vHipp and PFC is still missing. Thus, given the unique opportunity in our study to compare between PFC and vHipp, we performed an in-depth analysis between the two tissue regions, within the same phenotype. The main aim of this analysis was to identify trends of either similarities or opposing molecular alterations in the two regions post-stress. Since a tight spatiotemporal control of gene methylation or expression is crucial for a healthy physiological state, we posit that the findings will be relevant for studies aiming for global inhibition or induction of methylation for rescuing phenotypes.

6.2. Methods

Samples were collected from the same animals that were used for the experiments in **Chapter 5**. PFC was dissected as described in **Chapter 3**. For the rest of the experiments, the same methods used in **Chapter 5**, were followed.

6.3. Results

Following CSD, as in **Chapter 5**, PFC samples were pooled from two each of 12 controls, 14 susceptible and 12 resilient populations. The pooling allowed for 6, 7 and 6 biological replicates to be processed with RRBS-seq. Upon data analysis, we identified a similar coverage of reads as in the case for vHipp.

6.3.1. Comparison of stress affected biological processes in PFC (between phenotype comparison within the same tissue) with that of the vHipp.

For an exhaustive comparison of the difference in stress response between the PFC and the vHipp, we first proceeded with an initial analysis to compare the gene sets affected in the different stress phenotypes in the PFC with that of the vHipp. For this purpose, we first performed DMR analysis of the PFC data and assigned the genes corresponding to the DMRs. From this analysis, we identified a total of 307 DMGs altered in the resilient compared to the control (Res_c), 160 DMGs in the susceptible compared to the control (Sus_c) and 221 DMGs in the susceptible compared to the resilient (Sus_r) in the PFC. Thereafter, gene ontology (GO) analysis was performed on the distinct sets of genes. Interestingly, GO analyses revealed a significant enrichment of BPs of 'cell-substrate adhesion' and 'protein serine/threonine kinase' to be prominent in the Res_c (**Figure 26**) while the 'bone morphogenetic protein' (BMP) pathway was specifically enriched in the Sus_c (**Figure 26**). It is interesting to note that the other morphogenetic pathway 'Wnt signaling' was enriched in BPs for the dual comparison of Sus_r (**not shown**).

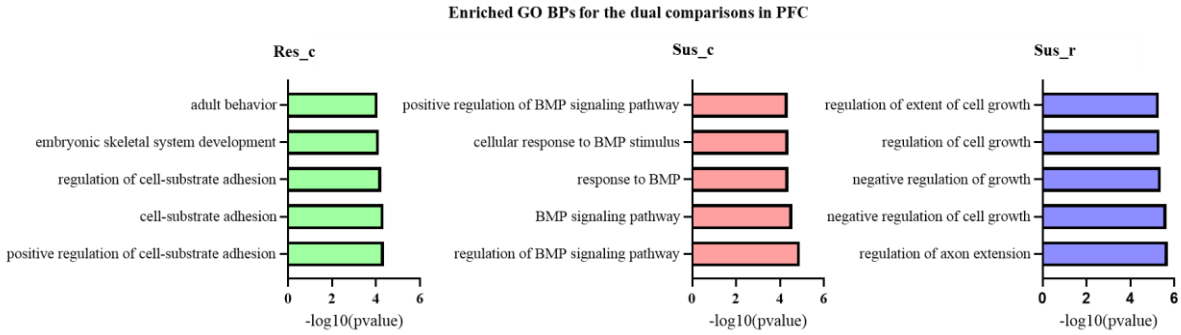

Figure 26: Enriched GO BPs in the phenotypic comparisons of PFC following stress exposure.

Bar plots of top enriched GO BPs for each of the dual comparisons of resilient compared to control (Res_c), susceptible compared to control (Sus_c) and susceptible compared to resilient (Sus_r). Res_c BPs are more inclined towards 'adhesion' process, while Sus_c BPs showed an inclination towards BMP pathway. **Abbreviations**: PFC – prefrontal cortex, Res_c – resilient compared to control, Sus_c – susceptible compared to control, Sus_r – susceptible compared to resilient.

Next, to determine the collective stress-affected pathways, we performed GO analyses on the DMGs combined for all dual phenotypic comparisons. The GO analyses for the cumulative DMGs revealed that some GO terms were similarly enriched in the PFC as that observed in the vHipp. These include that of the GTPase signaling, axonogenesis, and neuron differentiation (see **Table 2**). In contrast, we also noted BPs that were enriched only in the PFC. These GO BPs pertained more towards morphogenesis, BMP pathways and endothelial cell activation

(see **Table 2**)**.** Thus, we noted similarities as well as variances in the stress response pathways between the two regions.

Table 2: Top 20 significantly enriched (q<0.05) BPs of combined DMGs, ranked according to the detected number of genes involved in the process.

ID	Description	qvalue	Count
GO:0007409	Axonogenesis	0.001281	25
GO:0001654	eye development	0.001192	24
GO:0150063	visual system development	0.001192	24
GO:0048880	sensory system development	0.001192	24
GO:0001558	regulation of cell growth	0.001192	24
GO:0001667	ameboidal-type cell migration	0.002039	23
GO:0050767	regulation of neurogenesis	0.004476	22
GO:0007389	pattern specification process	0.008008	22
GO:0031589	cell-substrate adhesion	0.00127	21
GO:0043010	camera-type eye development	0.002039	21
GO:0048638	regulation of developmental growth	0.004077	21
GO:0032535	regulation of cellular component size	0.004751	21
GO:0031346	positive regulation of cell projection organization	0.006307	21
GO:0045664	regulation of neuron differentiation	4.94E-05	20
GO:0048562	embryonic organ morphogenesis	0.00127	20
GO:0007168	transmembrane receptor protein serine/threonine kinase signaling pathway	0.004476	20
GO:0007264	small GTPase mediated signal transduction	0.013464	20
GO:0045785	positive regulation of cell adhesion	0.01397	20
GO:0050673	epithelial cell proliferation	0.026555	19
GO:0060560	developmental growth involved in morphogenesis	0.001281	18

Having identified tissue-specific peculiarities in the stress-affected BPs, we next sought to determine the differences directly at the level of the methylation patterns between the two different tissues within the same phenotype. We posit that a thorough understanding of these differences would be crucial in determining the impact of drug delivery modes - application of global epigenetic drugs or local epigenetic modifiers.

6.3.2. Differential methylation patterns between the PFC and the vHipp (between tissue comparison within the same phenotype)

6.3.2.1. Baseline methylation differences between the tissues (control comparisons)

To understand the existing tissue-specific baseline methylation patterns, we first assessed the methylation pattern differences within the control populations. Interestingly, we identified 583 unique DMGs **(Figure 27a**) that harboured differential methylation patterns between the two tissue regions. Amongst these DMGs, the top hypermethylated genes in the vHipp compared to PFC include TF *Zfp503* (+83%), *Phf24* (+81%) and *B530045E10Rik* (+80%). Meanwhile, top hypomethylated include *Gm3554* (-88%), *Dnah14* (-76%) and *Adck5* (-74%). It is noteworthy that the top differentially methylated regions possess the potential of functioning as biomarkers for the different tissue regions.

Interestingly, the GO term analysis of the DMGs between the two tissues indicate existing differences ($p<0.05$, Enrichr) in molecular functions for protein tyrosine kinase and glutamate receptor activities as well as cell-adhesion amongst other functions (**Figure 27a,** Enrichr**).**

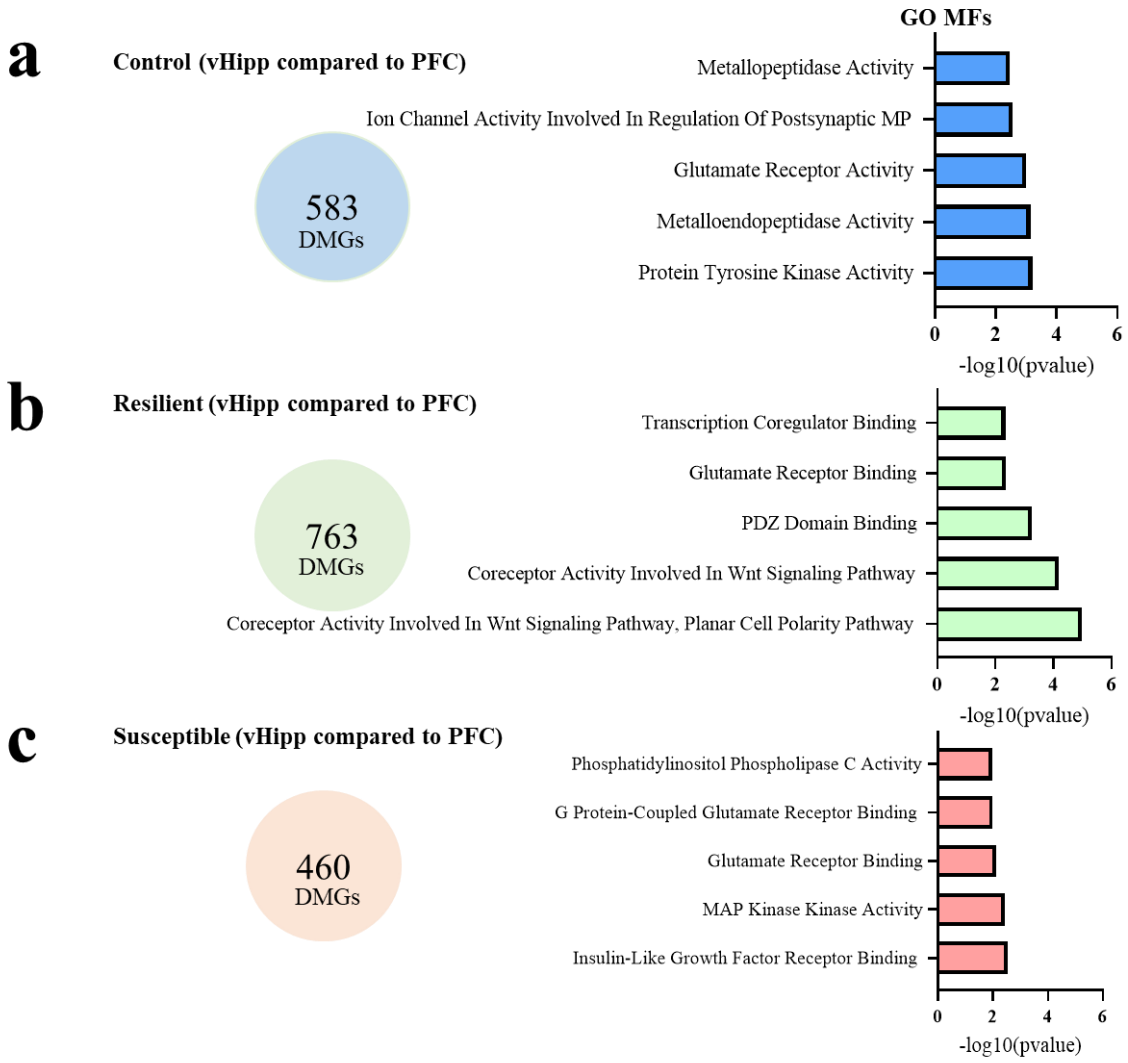

Figure 27: Between tissue comparisons of vHipp and PFC for each phenotype.

a. Control (vHipp compared to PFC). Total DMGs detected along with the top enriched MFs showing basal differences including protein tyrosine kinase and glutamate receptor activities. **b**. Resilient (vHipp compared to resilient PFC). Total DMGs detected along with the top enriched MFs including Wnt signaling and neurotransmitter binding. **c.** Susceptible (vHipp compared to PFC). Total DMGs detected along with the top enriched MFs including neurotransmitter receptor binding and kinase activities. **Abbreviations**: vHipp – ventral hippocampus, PFC – prefrontal cortex, DMGs – differentially methylated genes, MFs – molecular functions.

6.3.2.2. Different methylation patterns in the resilient group following stress exposure

Having demarcated the baseline differences at the methylation levels between the tissues, we next aimed at screening the differences relevant to the resilient populations. This analysis revealed two interesting patterns.

First, following the removal of the genes that differed at their baseline levels, i.e., those that different within the control comparisons, we identified 763 unique genes (**Figure 27b)**, which were differentially methylated in between the PFC and the vHipp. Top hypermethylated genes in the vHipp compared to that of the PFC include *8430426J06Rik* (+83%), *Ptk7* (+73%), *Ns1*

(+70%), *Shh* (+69%) while top hypomethylated genes include - *Serpina1b (-87%), Katnal1 (-89%), Fam155a (-88%)*. Interestingly, GO term analyses revealed that the differences ($p<0.05$, Enrichr) pertained to MFs related to Wnt signaling, and neurotransmitter receptor binding or regulator activity (see **Figure 27b and Table 3,** Enrichr).

Second, including the genes that showed baseline differences, we identified 57 genes that were previously detected in the control comparisons, that also showed differential methylation for the resilient. From these 57 genes, it is interesting to note that 8 genes completely reversed their methylation patterns at the specified DMR positions, i.e., hypomethylated in control comparisons but hypermethylated in resilient comparisons or vice versa. These include *Ap1m1* (clathrin-associated adaptor protein complex1), *Med13l* (transcriptional co activator for RNA pol IIa gene), *Slc1a5* (solute carrier), *Tenm4* (gene contributing to schizophrenia[444] via neurogenesis- and ATPase- related activity), *Anks1* (important for neuron projection and tyrosine kinase transport), *Axin2* (important for adult neurogenesis[445] and *Tmem132b*. Its related member *Tmem132d* is associated with a number of anxiety attacks and depressive disorder[446]. The complete reversal in methylation pattern of these 8 genes suggest a crucial involvement of these genes in mediating tissue-specific response to stress.

Apart from the identification of these genes, which reversed methylation patterns between the two tissues from control to resilient, we also noted other genes, which exacerbated their existing methylation differences in the resilience, albeit in the same direction. For example, *Cux2* (Cut-like homeobox2) and *Mdga1* (MAM Domain Containing Glycosylphosphatidylinositol Anchor 1), which showed hypomethylation patterns in the vHipp compared to the PFC. Since *Cux2* is an important hippocampal neurogenesis gene[447], its baseline hypomethylation in the vHipp of the control populations compared to that of the PFC, is expected. Therefore, it is even more interesting that the hypomethylation in *Cux2* increased in the resilient (-76% as compared to baseline controls with hypomethylation value of -26%). Meanwhile, *Mdga1*, a new schizophrenia susceptibility gene, essential for neuronal migration[448], exhibited a reduced hypomethylation in the resilient group (-36% in resilient comparisons in contrast with -73% in control comparisons). Though the exact functional attributes of these alterations are unknown, the tissue-specific response to stress existing at the level of methylation is clear. Alternately, we noted that some top differentially methylated genes in the control comparisons were no longer detectable in the resilient comparisons, indicating that they have also been altered. However, this is not covered within the scope of this thesis.

Table 3: Top enriched GO MFs from Enrichr of PFC and vHipp comparisons for the resilient phenotype.

Index	Name	P-value	Adjusted p-value	Odds Ratio	Combined score
1	Coreceptor Activity Involved In Wnt Signaling Pathway, Planar Cell Polarity Pathway (GO:1904929)	0.00001019	0.004678	101.38	1165.21
2	Coreceptor Activity Involved In Wnt Signaling Pathway (GO:0071936)	0.00006708	0.0154	33.79	324.69
3	PDZ Domain Binding (GO:0030165)	0.000541	0.08277	4.32	32.5
4	Glutamate Receptor Binding (GO:0035254)	0.004193	0.4139	7.24	39.61
5	Transcription Coregulator Binding (GO:0001221)	0.004508	0.4139	2.86	15.43
6	Ionotropic Glutamate Receptor Binding (GO:0035255)	0.007253	0.5549	9.49	46.74
7	Transcription Coactivator Binding (GO:0001223)	0.008863	0.5812	4.37	20.65
8	Adenylate Cyclase Regulator Activity (GO:0010854)	0.01346	0.6745	16.85	72.59
9	Cyclase Activator Activity (GO:0010853)	0.01346	0.6745	16.85	72.59
10	Acetylcholine Receptor Regulator Activity (GO:0030548)	0.01469	0.6745	6.9	29.12

6.3.2.3. Different methylation patterns in the susceptible group after stress exposure

Following a similar approach as in the resilient comparisons by removing the genes that show baseline differences in the control comparisons, first, we identified 460 unique genes (**Figure 27c),** that exhibited a differential methylation pattern between the two tissue regions within the susceptible populations. Amongst these, top hypomethylated genes include *Gm30551 (-74%)*, *Pbx3 (-76%)*, Gm12387 (-75%) and *Cbl (-69%)*, while top hypermethylated genes include *Hivep2 (+64%)*, *Tbkbp1 (+64%)*, *Atxn1 (+64%)*, *Zc3hc1 (+72%)*, *Wipf3 (+65%)*. Interestingly, the 460 DMGs pertained to MFs of receptor binding, neuropeptide activity, phospholipase activity etc., (See **Figure 27c** and **Table 4,** Enrichr). It is interesting to note that the CCs for the susceptible tissue comparisons were enriched for cytoskeleton and actin-based cell projection compartments (**Supplementary Table 5**). In the second case, we included the genes that showed alterations in control comparisons. In this analysis, we identified 63 unique genes with reversed or exacerbated methylation patterns as compared to the patterns observed in the control comparisons. Interestingly, only *Gm36431* showed complete reversal of methylation with hypomethylation in vHipp (from +60% to -36%).

Table 4: Top enriched GO MFs from Enrichr for between tissue susceptible group comparisons.

Index	Name	P-value	Adjusted p-value	Odds Ratio	Combined score
1	Insulin-Like Growth Factor Receptor Binding (GO:0005159)	0.002911	0.6137	12.82	74.86
2	MAP Kinase Kinase Activity (GO:0004708)	0.003642	0.6137	11.65	65.44
3	Glutamate Receptor Binding (GO:0035254)	0.007627	0.6636	8.54	41.66
4	G Protein-Coupled Glutamate Receptor Binding (GO:0035256)	0.01027	0.6636	17.06	78.12
5	Phosphatidylinositol Phospholipase C Activity (GO:0004435)	0.0103	0.6636	7.54	34.49
6	Ephrin Receptor Binding (GO:0046875)	0.01182	0.6636	7.12	31.6
7	Phospholipase C Activity (GO:0004629)	0.01521	0.7154	6.41	26.82
8	Neuropeptide Activity (GO:0160041)	0.02123	0.7154	5.57	21.46
9	Neuropeptide Hormone Activity (GO:0005184)	0.02123	0.7154	5.57	21.46
10	Protein Serine/Threonine/Tyrosine Kinase Activity (GO:0004712)	0.02123	0.7154	5.57	21.46

6.4. Discussion

Distinct tissue-specific methylation patterns have been described by several contemporary literature[449–451]. Reflecting this, in the tissue level comparisons (between PFC and vHipp) within the non-stressed control populations, we also identified existing basal level differences in the methylome. For example, *Cux2,* an important gene for neurogenesis, showed hypomethylation in the vHipp control compared to the PFC control. Notably, one can posit that the resulting data from the control comparisons can be used for demarcating biomarkers for the two different tissue regions. However, since we use only engram nuclei, this has to be validated using whole tissues.

Given the existing baseline differences, it becomes particularly interesting to note that the different tissue regions also show distinct stress responses at the epigenetic level of methylation (**Figure 27a-c**). Despite their collaborative role in regulating stress response, the observed differential patterns of methylation between the two tissue regions, sometimes even exhibiting opposing trends, caution against cross-data comparisons of studies using different tissues and the indiscriminate application of drugs, inhibitors or enhancers with a global impact. For example, induction or inhibition of methylation globally could result in ineffective results as different tissue regions require distinct levels of methylation to maintain resilience. Consequently, our findings advocate for such practices to be reviewed and replaced with local

or targeted drug applications[452,453] for rescuing phenotypes, to deliver more precise and effective interventions.

IV. General Discussion

1. Significance of investigating resilience and susceptibility mechanisms.

Stress is a normal part of life and stress response can contribute to the survival mechanisms necessary for adaptation to a changing environment[454]. However, excessive stress without proper coping mechanisms[15], for example, passive coping characterized by a combination of a sedentary lifestyle, existence of other stressors, bad nutrition etc., can lead to susceptibility to the stressor. Susceptibility leads to inability to cope with environmental demands or perform daily activities that are necessary for the organism's well-being. In fact, susceptibility is a route towards the development of anxiety, depression (see more in [216]) as well as other psychiatric disorders, neurological disorders, and cardiovascular disorders etc[219,220,455]. Thus, susceptibility to stress is not only detrimental to an organism's survival but also drains human resource potential.

Although certain individuals exhibit resilience to specific stressors, the contemporary sedentary lifestyle characterized by low social bonding has led to a rapid decline in mental health. Additionally, the recent COVID 19 impacts on mental health are predicted to hasten the stark increase in stress-related disorders[456–458] accompanied by a general decrease in resilience. Therefore, there is a growing demand for research to understand the molecular mechanisms behind resilience and susceptibility. As such, the work on the **PhD thesis is centred around the aim to dissect the molecular divergence in resilience and susceptibility outcomes at the epigenetics level using an engram-multiomics approach.**

2. Strong points of our experimental approach

To answer some of the critical questions regarding molecular divergence in resilient and susceptible populations, we employed the CSD stress mouse model. CSD possesses a high face validity as well as predictive validity[96,98] compared to that of the human social stressors. Additionally, in comparison to human and non-human primate models, inbred mouse models provide more homogeneity in terms of the genomic background, thereby allowing better access in understanding the epigenomic variances within a shorter duration. Next, compared to the invertebrate models, mouse models provide a social construct that is of higher resemblance to the humans and are required to comprehend the resilience-susceptibility impacts by social stressors. Additionally, mouse models can be genetically modified to satisfy certain aims of a particular study. For example, in our case, to increase resolution of the important alterations in stress-susceptible and resilient engrams, we worked with the genetically modified TAM-inducible Arc-GFP mice[241,243]. In the presence of TAM, the Arc-GFP mouse allows for the expression of nuclear membrane sfGFP in stimulus-activated cells. Thus, the use of Arc-GFP mice enabled the tracing of cells that were activated during the social fear recall in the SI test, namely, the engram nuclei. This facilitated assessments of the various omics levels in the specific resilience-susceptible engrams[82] via RRBS-seq, RNA-seq and small RNA-seq. This multiomics approach provided a better overview of the ongoing cellular modifications from multiple levels, thereby increasing the resolution to facilitate identification of causative factors as compared to single omics studies. Apart from this, given a good access to the less accessible methylome, we could gather possible mechanisms behind the persistence of stress effects, long after the stressor is removed. The next sections provide an in-depth discussion of the pros and cons of using TG mouse lines, nuclei and, the multiomics approach along with the importance of considering tissue level molecular differences in therapeutic designs.

3. Merits and demerits of using TAM-inducible mouse lines

The employment of TAM- inducible mouse models such as the Arc-GFP in our study allowed for the tracing of cellular populations that were spatiotemporally active during a behavioral activity in the presence of TAM and its metabolites. The access to specific cell types with a higher resolution, certainly, increases its desirability, as this would increase the precision of the data obtained from such studies. However, there are certain caveats associated with using such TG mouse lines.

First, the promoter line (e.g., *cFos* or *Arc* promoters) will determine which cells are captured, as *cFos* and *Arc* exhibit differential expression patterns[250]. This also reduces comparability over studies using different promoters.

Second, the transgenic mouse lines could be behaviorally distinct from the C57BL/6J line on which they were built. For example, in our study in **Chapter 2,** we demontrated the existence of baseline behavior differences between the Arc-GFP mouse line and C57BL/6J as well as WT-GFP mice. This indicates that the expected results of a behavior test, determined from studies on C57BL/6J, could bear different results while using the TG mice. Thus, it is necessary to characterize the baseline behavior patterns of a TG mouse line of interest to determine its usability for a particular study. Apart from this, different mouse lines can exhibit different molecular responses[239] and therefore, data comparisons across mouse lines should be conducted with cautionary measures.

Third, the use of TAM-inducible mouse lines necessitates the application of TAM, for the activation of the Cre recombinase. However, since TAM is an artificial estrogen, it can potentially interact with the estrogen receptors[459], thereby introducing unexpected effects in the physiological system, apart from the intended facilitation of DNA recombination using the CreER^{T2} system. Indeed, TAM was initially used for treating breast cancer[460] before its application on the CreER^{T2} system was exploited. Apart from this, TAM has been shown to alleviate neuropsychiatric symptoms[267] via its action on estrogen receptors. Indeed, a few studies have indicated the relevance of TAM in improving symptoms in bipolar disorders[258] and schizophrenia[267]. Additionally, there are reports for positive impacts on contextual memory as well as spatial memory in an amyloidosis mouse model[268] with contradicting negative impacts on cognition[267]. The literature findings on the side-effects of TAM are relevant for our study, where stress effects are assessed in terms of social fear memory recall

as well as social interaction. Supporting the contemporary literature, we also identified that a single application of a high dosage of TAM (150 mg/kg) can alter behavior including SI and other assays, for example, immobility duration in the FS test, an important test for assessing depressive-like behavior. The effects of improved social interaction and reduced social anxiety in behavior are consistent with the regulatory roles of estrogen. Indeed, in an independent study, reported by Li and colleagues[262], the effects of TAM on improving social interaction after chronic social defeat experiments on mice were observed, amongst other long-term impacts on behavioral assays long term. In lieu of this, it is interesting to note that **TAM could be the next ketamine-like antidepressant for mild stress.** Given the profound impacts on some behavioral parameters, it was intriguing that the HPA response seemed normal in the physiological assays used for the study. Perhaps, other assays could bear different results.

Interestingly, apart from the impacts on behavioral assays, recent studies have demonstrated multiple physiological and molecular effects of the use of TAM. For example, the application of TAM, used for Cre recombination, has been shown to impact neurogenesis[269] and bone homeostasis[459] as well as induce alterations in transcriptomic studies[461]. However, there is no record of alterations in DNA methylation (with 100 mg/kg of TAM[462]) yet. However, given the effects of TAM unfolding in several behavioral and molecular studies and the increasing use of CreER^{T2} lines in stress research, the unexplored effects of TAM should be thoroughly investigated. This is because TAM can result in off-target effects apart from its normal role of facilitating DNA recombination. Thus, our findings throw caution on the liberal use of TAM and urge researchers to **thoroughly examine the behavioral and physiological outputs of TAM manipulation before implementation of a particular experimental approach.**

4. Loopholes to be addressed during nuclei isolation and sorting of engram nuclei

4.1. Use of nuclei for sequencing experiments

The use of nuclei for sequencing has increased over the past few years, thereby increasing the demand for the development of optimal nuclei isolation protocols[463,464]. Use of nuclei provides a better methodology for accessing the nuclear contents especially from frozen tissues or tissues where cell dissociation to obtain specific cells are difficult[465]. Specifically in our experimental approach, where we seek engram nuclei, the optimal extraction of nuclei followed by a proper sorting strategy to incur minimal damage on the nuclei, is essential. As most literature studies use bulk tissues or macrovolumes of starting material coupled with different centrifugation techniques or buffers for nuclei extraction, the protocols needed to be curated for our study design. Thus, the work for the thesis resulted in the development of an optimal nuclei isolation protocol required for our specific purpose (more details in **Chapter 3**). During the steps required to access SI-activated nuclei from microvolumes of tissues, we experimented with different nuclei isolation techniques to optimize the quantity and quality of the extracted nuclei. Our experiments revealed that the optimal approach of ultracentrifugation, to segregate the nuclei from the cellular contents, should be with the inclusion of a buffer layer to reduce damage to the nuclei. Indeed, ultracentrifugation without cushion layer yielded more nuclei albeit with different patterns of optical density than the expected dark appearance in phase-contrast microscopy. Importantly, our findings align with that of Yamashita and colleagues[305], who reported in their study on exosomes that different types of centrifugation methods led to the yield of exosomes with distinct physicochemical properties. Meanwhile, the liberal use of different buffers for diluting or resuspending nuclei should be practiced with caution, as different buffers exert diverse effects on nuclei quality. For example, use of PBS as suspension buffer under our experimental conditions led to aggregation of nuclei as well as shrunken appearance compared to the HB. In fact, Lima and colleagues[335] also reported the adverse effects of PBS in their study using iPSCs. Thus, the use of the original HB for any dilution or resuspension is recommended.

Following the development of a well-optimized nuclei isolation protocol, we next worked with the available methods of FANS and INTACT for sorting the sfGFP+ engram nuclei from the pool of nuclei. FANS is rather popular and has been commonly used to isolate fluorescently labelled nuclei. However, it is known to be a harsh technique that can induce molecular alterations[324,325]. Meanwhile, the alternative method of INTACT is based on magnetic-based isolation principle. Though recent, it has gained popularity due to its milder

approach and ability to condense to smaller volumes[318,320,329]. Interestingly, these two techniques have been interchangeably used[466] without scrutinising plausible impacts on the isolated nuclei. Having identified this gap in literature, our experiments, detailed in **Chapter 4**, systematically investigated the qualitative and quantitative differences between the two techniques, INTACT and FANS, using sfGFP+ nuclei. Indeed, FANS-derived sfGFP+ nuclei were different from the original nuclei as well as the INTACT-nuclei, strengthening the claims of FANS being a harsher procedure. Thus, for experimental studies where a gentler method is needed, INTACT could be a better procedure. Despite this caveat, our study identified that both techniques have individual merits and demerits (see more details in **Chapter 4**). Briefly, in terms of processing speed and costs for multiple samples, INTACT has an advantage over FANS. However, for the INTACT protocol to be applied efficiently, the protocol must be adjusted for different input material. In contrast, while employing the FANS technique, regardless of the starting concentration of nuclei, the protocol need not be changed. Therefore, in this aspect, FANS is more advantageous over INTACT.

Overall, since FANS-nuclei and INTACT-nuclei are distinct at both the morphological and molecular levels[329], this study underscores the importance of the employment of only **one type of sorting method for an experimental setup.** We advocate that the choice of either INTACT or FANS for a particular study should be based on the volume of the starting tissue material and the intended purpose of study.

5. Benefits and complexities of applying a multiomics approach on the stress phenotype-specific engram-activated nuclei

Investigating the etiology of complex disorders such as stress and depression to determine the causative factors can be challenging with one omics level. This is because a single omics level only provides a snapshot of the cellular changes and by the time the cellular machineries are investigated, the disease trajectory could already have deviated from the starting point[199]. Therefore, multiomics can partially exploit the phase lag between different molecular levels to identify plausible causative alterations in the converging biological mechanisms. Such an approach increases the reliability of the data outputs and increases the statistical confidence on claiming the pathogenicity of a particular molecular pathway[236].

Of all the omics levels, transcriptome is the most accessible and hence more prevalent in stress literature. However, methylome studies as well as small RNA studies, especially with low-input amounts are rare due to its difficulty in both technical as well as bioinformatics processing. Thus, this thesis stands out with the **specific establishment of the RRBS-seq and miR_seq for low input nuclei**, **and its integrated use thereafter**. The employment and integration of a multiomics network approach facilitated the generation of a higher resolution picture of the molecular landscape post-stress exposure using engram-specific nuclei. In addition to this, the employment of this novel approach facilitated the exploration of the complicated yet interconnected relationships between the different layers of omics.

5.1. Complex methylome and transcriptome relationship

During our systematic investigation, we noted that the methylome modifications, pertaining to the stress response, were not restricted to the promoters. Apart from this, the relationship between the methylome and gene expression was more complicated as also suggested in other recent findings[449]. For instance, 3' UTR methylation has been shown to increase expression instead of suppression of expression, that is usually associated with promoter methylation[467,468]. Additionally, DNA methylation modifications at the intronic sites could create permissive environments for alternative splicing mechanisms[469,470], which are known to be relevant in altered physiological states (see reviews by [471,472]). Intriguingly, DNA methylation could occur before or as a result of the transcriptional changes[426] and thus the overlap between the two could be low, as also observed in our findings. Apart from this, methylome showed higher alterations in the transcription-related activities compared to the transcriptome, where the synaptic activities were dominant. This shows a clear phase lag

between the activation of different omics levels. Indeed, since the cellular machineries after the stress insults are at a dynamic phase to reestablish homeostasis, it is possible that following the stress defeats, remodelling of the synaptic genes represents the acute demand on the cellular machinery followed by long term modifications in the transcription-related genes. Though it is still not clear how a cell directs methylation and demethylation at specific sites or over a region, it is generally accepted that DNA methylation forms an important mechanism of biological embedding of experience and can prime the epigenome to modulate future transcriptional states[209,428]

5.1.1. Epigenome priming

Indeed, the high overlap of our differential methylated regions with regulatory regions of the genome, indicate a huge potential for the existence of a primed epigenome, thereby, setting a different 'genomic action potential' in the diverse phenotypic outcomes[473]. A primed epigenome could facilitate a faster or more robust transcription of certain genes by providing substrates for further epigenetic marks or TF binding[213,474]. Whether all the alterations in the differential methylation have a functional output is an ongoing debate. However, it is assumed that the changes accumulated over time will result in a different functional response[475], even if no corresponding mRNA changes are observed at that time. We believe that the sequencing insights from our study will prove to be extremely relevant for the researchers in the field of stress research.

5.2. Multiomics and network approach

The existence of phase lags between the different omics levels made it challenging to identify genes that have been altered or will be altered at the different omics levels, following stress exposure. However, it is intriguing that our multiomics data revealed a common modulation of the synaptic processes across all omics levels. Indeed, since synapses play an important role in modulating brain and behavior functions, stress-induced alterations in synaptic processes are expected. Interestingly, from amongst the multiple signaling systems involved in synaptic functions, we noted an overrepresentation of GTPase signaling. GTPase signaling involves the family of G proteins including GTPases, its family of regulators (GAPs, GEFs and GDIs), downstream effectors and upstream modulators. Notably, the GTPase system exercises a substantial influence over collapse or expansion of the actin networks[476], thereby influencing the synaptic structure, i.e., increase or decrease in synaptic density or dendrites and spines. Interestingly, aberrant signaling of the GTPase family is responsible for diverse neuropsychiatric disorders[477–479]. For example, G proteins and their regulators[480] play critical

roles in regulation of depression mechanisms, through G-protein coupled receptors (GPCRs) including beta-adrenergic receptors, metabotropic glutamatergic receptors, 5-HT receptors, GABA-B receptors, D1/2/3/4 receptors.

From the previous paragraph, one might infer that there is abundant literature, indicating aberrations in the GTPase pathway following stress exposure. Thus, one might question the novelty of the finding on GTPases in our interpretation of the multiomics data. At this point, we would like to draw the attention of the readers to our crucial employment of the phenotype-specific engram nuclei. The results from the disease-relevant cellular networks increase the confidence of the claims from the bulk studies. Moreover, our in-depth analysis identified for the first time the existence of an opposite pattern of alteration in one facet of the GTPase signaling, namely the GTPase family regulators (GEFs), between the resilient and susceptible phenotypes across all omics levels. Noteworthy is that GEFs' roles have been implicated in amyotrophic lateral sclerosis and other neurodegenerative diseases[481], however it has not been properly investigated in relation to stress studies. Though, Bondar and colleagues[482] slightly indicated the involvement of GEFs in their CSD study as two RhoGEFs were downregulated in the stressed population, they did not specify a pattern between resilience and susceptibility. Apart from this, they used only one omics level (transcriptomics). Thus, our finding that the resilient compared to the susceptible group exhibited a higher fraction of intronic hypermethylation at RhoGEF genes, accompanied by an upregulation in the transcriptome and downregulation of the miRs (targeting RhoGEF genes) is a unique discovery pertaining to this study. Though we focussed only on the RhoGEFs due to the higher relevance of the Rho family in synaptic functions, we argue that a similar skewed alteration would be prevalent in the GEFs of the other Ras GTPase superfamily. Cumulatively, the novelty of our findings pertains not only **to the determination of GTPase signaling defects at multiple omics levels using specific engram nuclei but also to the reporting, for the first time, of the stark divergence in the GEF family of regulators between resilient- and susceptible- phenotypes.**

Additionally, the access to the less prevalent methylome data revealed plausible mechanisms of sustaining stress effects through the ETS family of TFs that are nuclear targets of GTPases[377,483]. Apart from the link to the epigenome via the ETS family, Sheu and colleagues[484] showed that serotonin receptor-triggered activation of Trio (RhoGEF)- RhoA pathway in the axon-cilium synapse can modulate histone acetylation and chromatin

accessibility of the epigenome. This **adds to our hypothesis of the relevance of synaptic-nuclei GTPase signaling in priming the epigenome.**

On the other hand, our study design provided the opportunity of employing an integrative networks approach. The use of a networks approach in investigating the molecular signature of diseased states as compared to normal healthy states[382,485], has garnered a huge interest. This is because genes function in a network and thus, network analyses allow for the determination of critical genes (hubs), that interact with multiple other molecules (genes in the RNA/protein form) within the network[486]. Modifying these hubs, such as by altering their expression levels or pharmacological interventions can introduce a significant effect on multiple other molecules, based on the central lethality rule[383]. Consequently, this can lead to the modification of the diseased state. Therefore, a network approach is of crucial relevance in identifying disease trajectories and molecular convergence[236] as they can provide more mechanistic insights into determining causal factors, important for therapeutic interventions. Indeed, in our study, the employment of such a multiomics networks approach paved the way for the identification of a novel potential therapeutic target, the *Arf6* GTPase, that functionally interacts with hub genes, is regulated by the GEFs, and regulates endocytosis. Of note, this identification would not have been possible with a traditional approach of using only one omics level.

From our findings, **I posit that the altered GTPase functionalities could be largely involved in a volatile period of cellular machinery reorganization,** following stress exposure as they were not overrepresented in terminal neurological disorders[424]. With repeated rounds of signal encoding and decoding via the synaptic-nuclei coupling, minimal differences in molecular synaptic compositions, for example, differences in endocytosis, could, eventually, lead to highly divergent epigenome landscapes, thereby altering behavior[401]. This highlights a mechanism for development of PTSD in some individuals. Indeed, ETS (Elk)/SRF signaling pathway, that acts as the downstream nuclear effector of GTPase signaling, was affected in the PTSD patients[198]. This enhances the suitability of the GTPases to be a potent therapeutic target to hijack disease trajectories during the tumultuous phase following stress exposure. Hypothetically, the time period of our sample collection point can indeed be a critical window period for altering the flow of information in the synaptic-nuclei coupling, via *Arf6* GTPase as therapeutic target, for effective rescue of the path to inefficient homeostatic levels.

6. Significance of tissue-specific stress response for drug applications.

Distinct regions of the brain consist of diverse cell types, each possessing unique molecular machineries[487], contributing to specific functional attributes of each region. Therefore, it is reasonable to anticipate distinct tissue responses in regulating stress susceptibility or resilience. Indeed, our observations in **Chapter 6**, align with the existing literature, where divergent tissue-specific molecular response to stress have been highlighted[183,442,488]. For example, within the same hippocampal tissue, the dorsal and ventral regions show characteristic difference in expression patterns in response to stress[488]. Thus, such tissue-level variations should be considered carefully, where cross-research results are compared.

On the other hand, the differences in regional level reactivity to stress suggest caution on the indiscriminate administration of drugs for global inhibition or enhancement of the activity of certain genes or processes, identified to be dysregulated only in a certain brain region. One way to reduce such a global effect is by using nanodrugs[453,489] that can be delivered to specific targets. Other strategies for regional manipulation include drug injections locally[490] or the use of optogenetics[491] or designer receptors activated only by designer drugs (DREADDs)[492,493]. This is also true for our case of *Arf6* as the drug target. We posit that local drug/viral manipulations for the vHipp, within a specific temporal window, could provide better results than global targeting.

7. Concluding remarks

7.1. Major findings of the thesis and their implications in stress research

During the interim of the thesis, we have highlighted the importance of investigating mechanisms behind resilience and susceptibility. Indeed, studies using bulk tissues have provided undeniable insights into certain mechanisms, underlying the development of stress disorders. However, bulk tissues often possess multiple cell types with their own distinct molecular signatures, often masking signals from engram population. Subsequently, this reduces the confidence with which a pathway can be claimed to be pathogenic using bulk studies, as different cell types bear different biological cascades. As such, studies using only target cell populations, for a particular study design, have increased[494–496]. On the other hand, the contemporary use of a single omics level provides only a snapshot of the molecular environment, following stress exposure. However, from a snapshot, it is often difficult to dissect the disease trajectory, i.e., distinguishing the causative factors from the reactive factors. In fact, with one set of omics data, more often than not, we fail to identify the causative factors, which are more valuable for therapeutic purposes. Thus, with an attempt to bridge the research gaps created by the use of bulk tissues and single omics, appropriate study designs employing engram nuclei and multiomics were introduced. The resulting outcomes have led to the advancement in multiple facets of technique employment and mechanism mining. A summary is listed below. The work on the thesis -

1. Determined for the first time the usability of the TAM-inducible Arc-GFP mouse line for chronic social defeat (CSD) paradigm. This would bear positive consequences on researchers, who aim at employing engram studies in stress-research.
2. Contributed to the increasing findings on the off-target effects of TAM administered to facilitate Cre recombination, i.e., impacts on SI and other behavioral tests.
3. Presented optimal engram nuclei extraction protocols suitable for microvolumes of tissues.
4. Delivered strategies to process the less accessible RRBS-seq and miR-seq for low-input nuclei.
5. Employed a cutting-edge multiomics network approach to generate a higher resolution picture of the changing cellular environment following stress exposure. This led to the identification of the skewed GTPase signaling dynamics in the divergent phenotypes, for the first time. The study also suggested a plausible mechanism for biological embedding of experience via the GTPase-ETS nuclear

targets, thereby reshaping the genomic action potential of the epigenome for future environmental demands.

6. Contributed to additional data supporting the growing literature on the non-traditional relationship between methylome and transcriptome, along with a phase lag between the epigenomic and transcriptomic waves. In the scenario of resilience-susceptibility research, it is indeed the first report to identify a reversal of phenotype-specificity for certain BPs (biological processes), when transitioning to a different omics level, at a particular time point. I posit that this could plausibly be due to the phase lags between the distinct omics layers. More explicitly, the observations suggest the existence of a continuously changing cellular environment following stress exposure with time or phase lags between the different omics levels. I hypothesize that this tumultuous phase can be meticulously exploited as critical window periods for drug targeting to effectively alter disease trajectories, for example, targeting *Arf6* mRNA.
7. Facilitated the contribution of high-resolution data identifying distinct tissue stress responses for susceptibility and resilience in the vHipp-PFC methylome for the first time.
8. Contributed a repository of small RNA data that highlighted for the first time the involvement of piRs and other nuclear RNAs in the susceptibility-resilience divergence.

Thus, in conclusion, the thesis has contributed major findings that can form the cornerstone to further advance scientific work in the field of multiomics-engram studies. Multiomics combined with engram nuclei, allowed for a better view of the morphing cellular environment as well as tracing of important gene family members critical for the manifestation of a certain phenotype, following stress exposure. For example, overrepresentation of GTPase and actin-related genes, transcending different omics levels, increases the significance of the associated synaptic and chromatin remodelling, following stress exposure[497]. In addition to this, the integrated approach allowed for the proposition of a mechanism that partially explains the maintenance of long-term effects of stress by GTPase signaling through its control of nuclear targets as well as endocytosis. Additionally, I **highlight the plausible exploitation of the phase lag between the epigenome and transcriptome waves as window periods for localised drug delivery, to rescue disease trajectories**. Last but not the least, the identification of alterations in multiple small RNAs, apart from miRs, signify their crucial role in the phenotype divergence following stress, for

the first time. I advocate that the access to the small RNAs, as a result of this thesis, should be fully exploited to understand more intricate crosstalks between the different layers. For example, piRNAs, that form the topmost altered small RNAs, are important for regulating neuronal functions, including synaptic plasticity, learning and memory and local translation at the dendritic regions in the brain[436–438]. Meanwhile, piRNAs can also drive DNA methylation, at the germ cells[498,499]. As such, one can hypothesize that the alterations in piRs observed in our data in the brain could also be reflected in the germ cells. Therefore, an in-depth analysis of crosstalks with small RNAs within a tissue region as well as cross-tissue regions would deliver more mechanistic and holistic insights in stress research as small RNAs are also the machineries for transgenerational inheritance of stress effects[500,501].

V. Considerations and drawbacks

1. Limitations in the epigenetics study

Though the work on this thesis have contributed to the existing stress research and increased the existing knowledge substantially, I acknowledge the existence of certain open-ended questions and drawbacks. While I report that multiple sites for transcription and synaptic genes are differentially methylated in the resilient and susceptible phenotypes, I do not claim that all the modifications attribute to functional relevance at the timepoint of the experiment. The functionality of all DNA methylation modifications is still a debatable question, but it may prime the cell or gene to respond in an altered pathway to future cues [29,205,426,475]. Due to the limited time for a thesis, the postulation that the methylome alterations will manifest as gene expression alterations at a future timepoint could not be validated. The interpretations were largely drawn from the available scientific literature. Indeed, a longitudinal study, as conducted by Marco and colleagues[213] would provide a stronger claim to the existence of priming.

On the other hand, it is unclear whether the divergent molecular outcomes from the stressed phenotypes were a result of a pre-existing epigenetic difference revealed by the stress exposure, or whether the divergence is a direct consequence of the stress exposure, that by a chance of repository proteins present in the synapse at the time of the insult, snowballed into such divergence. Apart from this, since we focussed mostly on the genic differential methylation in this study, it is highly likely that an exhaustive analysis inclusive of the intergenic methylation in a 3D genomic context and chromatin accessibility as well as histone methylation/acetylation dynamics could further increase the resolution and interpretation of the findings. Moreover, our study is limited in that we cannot distinguish between methylation and hydroxymethylation[502], a byproduct of iterative oxidation catalysis by TET enzymes, which possess distinct physiological roles as well as relationships with the transcriptome. For example, hydroxymethylation at the promoter regions is known to promote gene expression as opposed to the more accepted function of gene repression by promoter methylation (see review by [503]). Perhaps differentiating the hydroxymethylation from methylation and inclusion of chromatin accessibility assays in future studies, could add a possible piece to the jigsaw puzzle of the observed non-coordination between methylation and gene expression in the few genes that overlapped in our data. Last but not the least, bisulfite treatment of DNA for RRBS-seq is a harsh technique and leads to loss of some DNA. Therefore, for rare samples, more recent techniques[504] that use a reportedly less harsh

technique should be explored. Regarding the queer trend of only upregulation in Res_c and downregulation in Sus_c in the miRs, we could not perform follow-up studies to ascertain if it was because of technical deficits or a previously unknown biological phenomenon that we detected by chance in our study. Therefore, replicative studies should be conducted in the future to investigate the origin of the observation.

2. Plausible limitations for cross-data comparisons

2.1. Use of Arc promoter and TAM-inducible mouse lines

The thesis has undoubtedly introduced proper controls for several loopholes that are usually prevalent in complex study designs, and hence advanced the understanding of the mechanisms behind susceptibility and resilience. However, it is possible that the findings are biased towards cells that express *Arc*. Indeed, there might be other neurons and other cell types, which express alternative IEGs, upon receipt of a stimulus. Consequently, they have been left out from the engram trace. Therefore, performing similar experiments using TG lines with other IEG promoters might give a more complete picture of all evoked engrams, which was not possible within the scope of a PhD thesis.

On the other hand, while we ascertained that the HPA stress response of TAM-injected mice remained similar to that of the non-injected or oil-injected mice and inferred no discernible influence of a one-time TAM injection on DNA methylation[462], we did not include experiments with oil-injected groups in the molecular studies, for a proper validation. Although the focus of the thesis was on comparing the TAM-injected stressed populations with the non-stressed controls, the inclusion of comparisons for oil-injected groups would, invariably, enhance the claims from the molecular results, as derived solely from the introduction of the stress procedure. Therefore, for future studies, this control should be introduced not only at the behavior level but also at the molecular level for a more substantial validation.

2.2. Use of CSD models

Though multiple studies using the CSD paradigm, have contributed immensely to the field of stress research, cross-comparisons between studies are often complicated by the employment of varied stressor intensities and duration. For example, in a study by Bondar and colleagues[482], they showed that gene expression patterns after 10 days of CSD exposure were very different from that obtained after 30 days of CSD exposure. On the other hand, a recent study using both the dorsal and ventral hippocampus identified different patterns of

gene expression following the application of different types of acute stressors[488]. Thus, such non-generalisability of results complicates the search for optimal targets. Apart from the variant protocols, CSD studies are largely conducted in male mice and studies on female mice are hugely underrepresented. Females and males have been shown to possess different stress response patterns[47,197]. In this aspect, our study also recognizes the caveat of non-inclusion of female mice. Indeed, a branch study using the female Arc-GFP mice had been conducted by [423] using chronic social instability models. However, it only dealt with the neurogenesis pathway, and hence the spectrum of multiomics approach is not available. Apart from this, the results using chronic instability models could be very different from the CSD models. Therefore, it would be interesting to validate our findings in females using a stable form of social defeat[505] applicable to females.

VI. Perspectives and future scope

Although the existence of differential methylation states in the resilience and susceptible phenotypes is clear, it is unknown whether these were pre-existing primed epigenetic states leading to the development of the resilience and susceptibility behavioral states during the social defeat or an effect of the environmental insult. However, the vast number of modulations in the GTPase and actin related genes in the multiomics data indicate major synaptic and chromatin remodelling, consistent with the literature on effects of stress[497]. Indeed, with the decrease in cost for omics sequencing, multiomics approaches will be a norm in the future. Such an increase can be exploited with more robust bioinformatic tools incorporating the concept of the 3D genome, to enhance the in-depth study of the complicated interactions between different epigenetic levels. On the other hand, as the crosstalks between the non-coding RNAs as well as epigenetic marks are less known, we believe that an in-depth analysis of crosstalks with small RNAs would deliver more mechanistic and holistic insights in stress research as small RNAs are also the machineries for transgenerational inheritance of stress effects. More importantly, the use of new approaches demands a serious 'conceptual shift' in the research community[199], to allow for incorporation of novel ideas. With meticulous integration of such approaches, a new era in therapeutic discoveries could emerge. Indeed, with the limited tools, the phase lag between transcriptome and epigenome is already visible. This phase lag is an interesting avenue for mRNA related therapies[506,507] to be exploited, before the transient alterations are stabilized in the epigenome code for achieving a new homeostatic equilibrium. The identification of *Arf6* as a plausible therapeutic was indeed boosted by the knowledge of the phase lag between the transcriptome and the epigenome. I believe that the phase lags accompanied by the continually changing molecular environments, following stress exposure, suggest the existence of distinct window periods for different drug targets. In fact, one can speculate that one of the reasons for the non-translatability of therapeutic targets (from animal studies to humans) could be due to the non-consideration of critical window periods for a particular drug target. Apart from this, because of tissue differences in stress response, the generalization of a therapeutic determined in a study using a specific brain region and the global application of the therapeutic can be a stumbling block in application of effective drugs, even within the critical window period. Thus, I advocate that adoption of new techniques for **targeted drug delivery** within **critical window periods** would be crucial in rescuing disease trajectories, effectively (see **Figure 28a**). In this regard, the developing field

of nanomedicine with spatiotemporal control of drug release [452,453,489] could immensely boost the benefits of the therapeutic interventions. Indeed, such approaches to improve resilience could rescue the declining global mental health, which is, unfortunately, increasing following COVID-19[9,11]. On another note, as TAM used for treating cancer improves stress effects, Arf6 GTPase, which is also a new therapeutic target in cancer studies, carries a huge potential in rescuing susceptible phenotypes. However, while searching for drugs to modulate epigenetic mechanisms, one should not forget to consider the genetic predisposition of an individual[508]. In this regard, personalized medicine with distinct drug targets, derived from instant multiomics results, for different individuals at different phases post-stress exposure, would prove to be a formidable therapeutic intervention strategy in the future[236] (see **Figure 28b**).

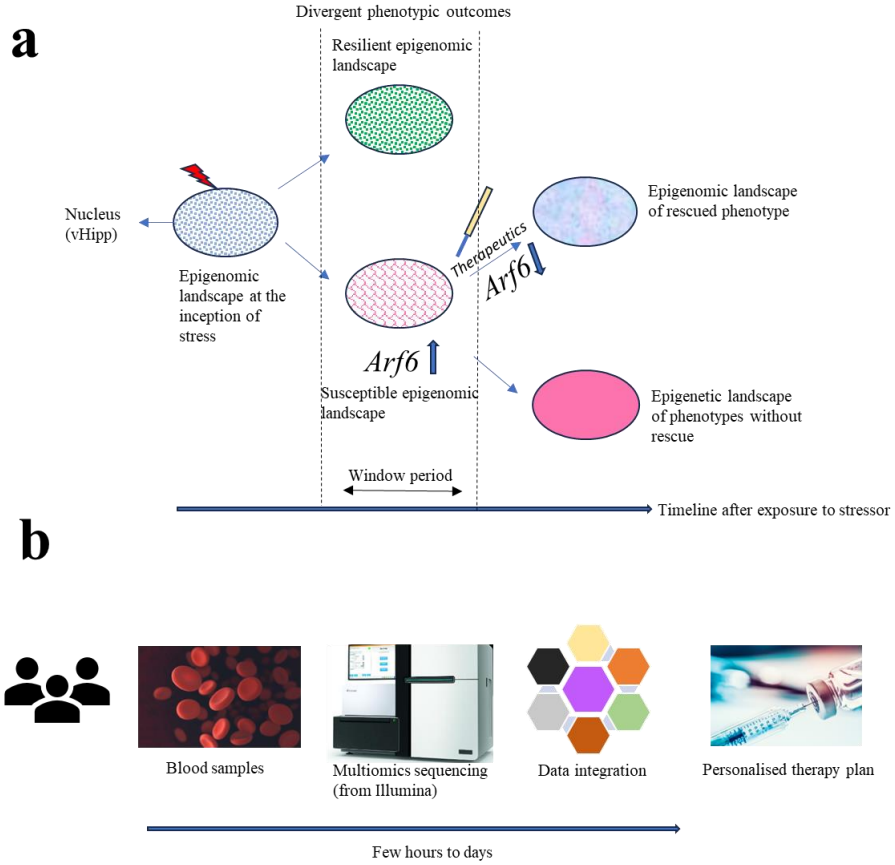

Figure 28: Proposed model for phenotype rescue.

a. Targeting the upregulated mRNA (*Arf6*) spatiotemporally within a window period to rescue susceptible phenotypes**. b.** Hypothetical futuristic scenario, depicting the increase in diagnostics capacity via multiomics integration. The incoming AI technology and better bioinformatic tools could facilitate a quick determination of the most plausible therapeutic targets to initiate a personalized therapy protocol.

VII. Supplementary

1. Supplementary Figures

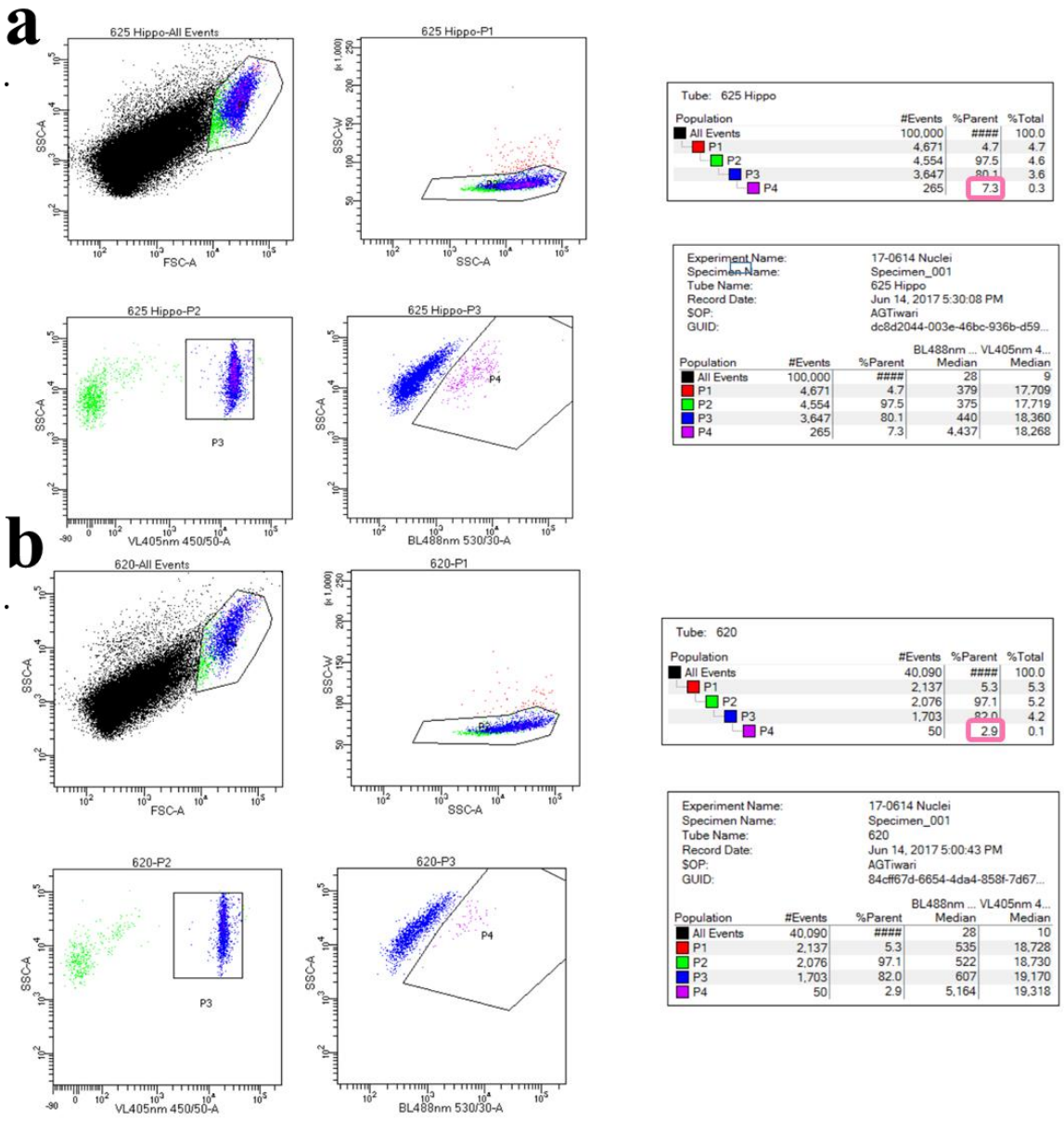

Supplementary Figure 1: Flow cytometry of nuclei collected from mice with different time points of TAM injection before stimulus presentation.

a. Detected GFP% (red box) following TAM injection 5 hours before stimuli presentation **b.** detected GFP% (red box) following TAM injection 24 hours before stimuli presentation. (NB: Flow cytometry was performed by the IMB core facility.)

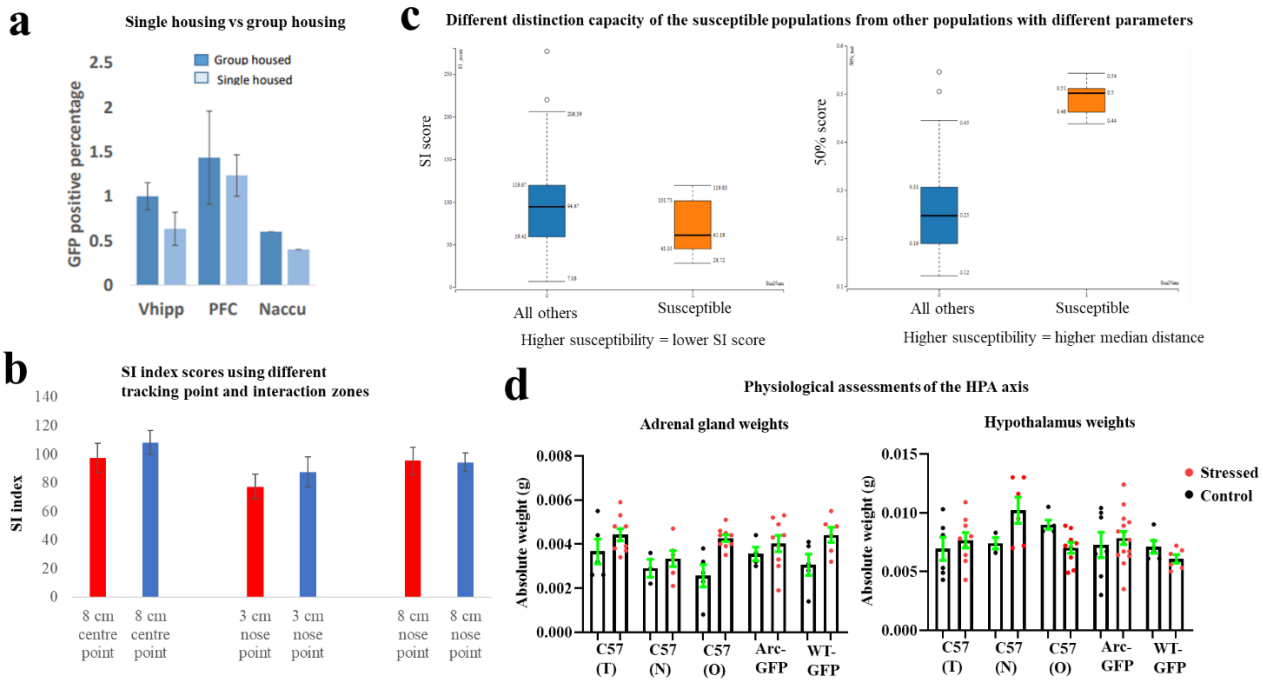

Supplementary Figure 2: Preliminary results to identify the usability of the TAM-inducible Arc-GFP mouse line.

a. GFP expression in single-housed and group-housed mice. **b.** No differences in the stress-control relationship with different tracking points and interaction zone radii in the SI test (red - stressed group, blue – control group). Error bars represent ± S.E.M. **c.** Observation of stark differences in the behavior of the susceptible mice using a different parameter (right panel) compared to that of SI (left panel) (NB: Figure c created by Nicolas Ruffini). **d.** Physiological assessments of the HPA axis components. **Abbreviations**: T - tamoxifen-injected, N – non-injected, O – oil-injected

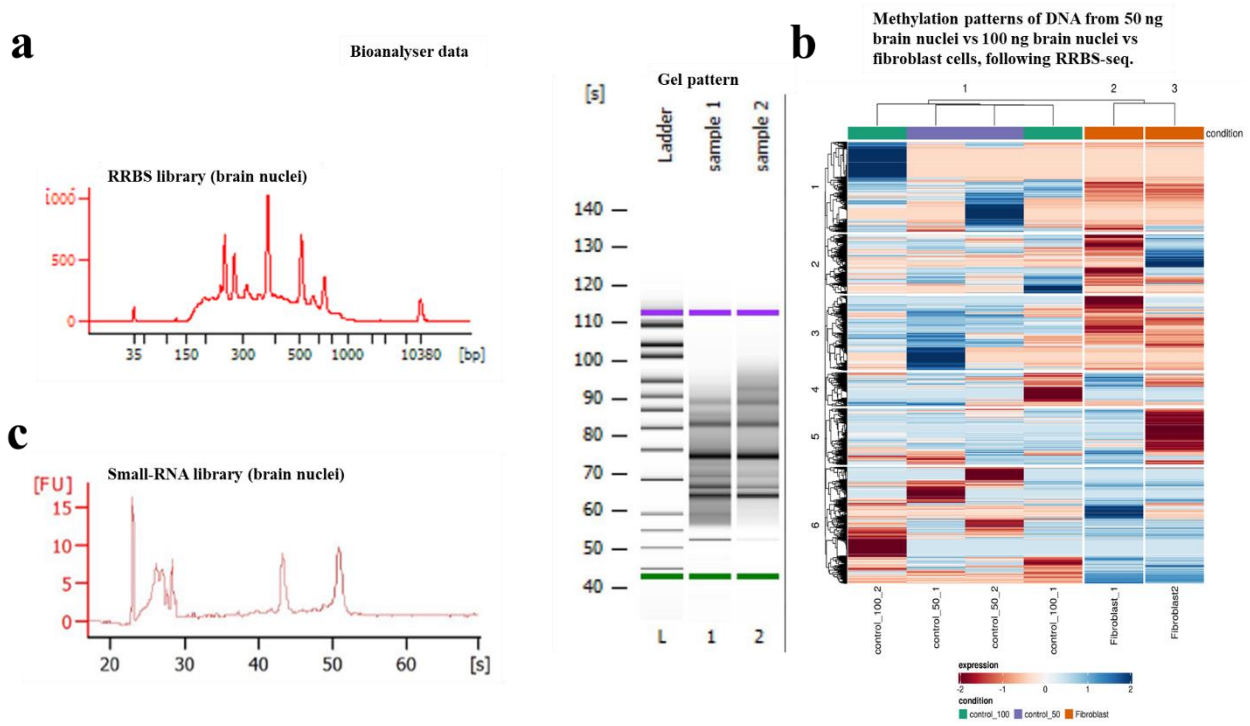

Supplementary Figure 3: Bioanalyzer patterns of RRBS libraries and small-RNA libraries from mouse samples.

a. Bioanalyzer patterns along with the gel image (right) of the fragmented DNA generated from the RRBS library preparation (Diagenode) using DNA from mouse brain nuclei samples. **b.** Heatmap shows a higher semblance of methylation patterns between RRBS libraries prepared from the starting amounts of 50 ng and 100 ng brain nuclei, compared to that generated from skin fibroblasts -100 ng (DNA from different tissue type compared to varying amounts of DNA from brain nuclei). **c.** Bioanalyzer pattern of the small RNA library prepared from total RNA extracted from mouse brain nuclei samples (NB: Heatmap for Figure b was generated by Dewi Hartwich.).

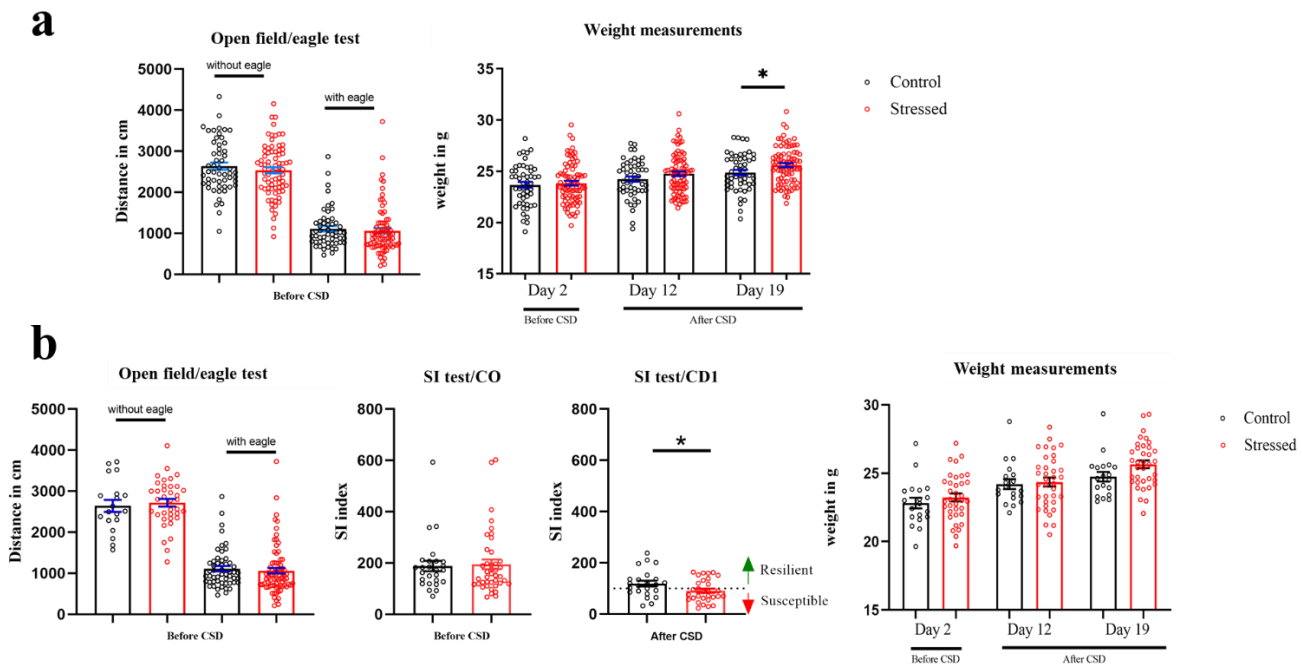

Supplementary Figure 4: Results from the behavior experiments of Arc-GFP and WT-GFP mice.

a. Equivalent distribution of Arc-GFP mice to control and stressed group using OF/E test (left). Significant weight gain ($p<0.05$) in the stressed group on Day 19 of the experiments (right). **b.** Results from the OF/E, SI/CO, SI/CD1 and weight measurements from the WT-GFP, showing behavioral trends of stress-control comparisons. The trends are similar to that of the Arc-GFP mice.

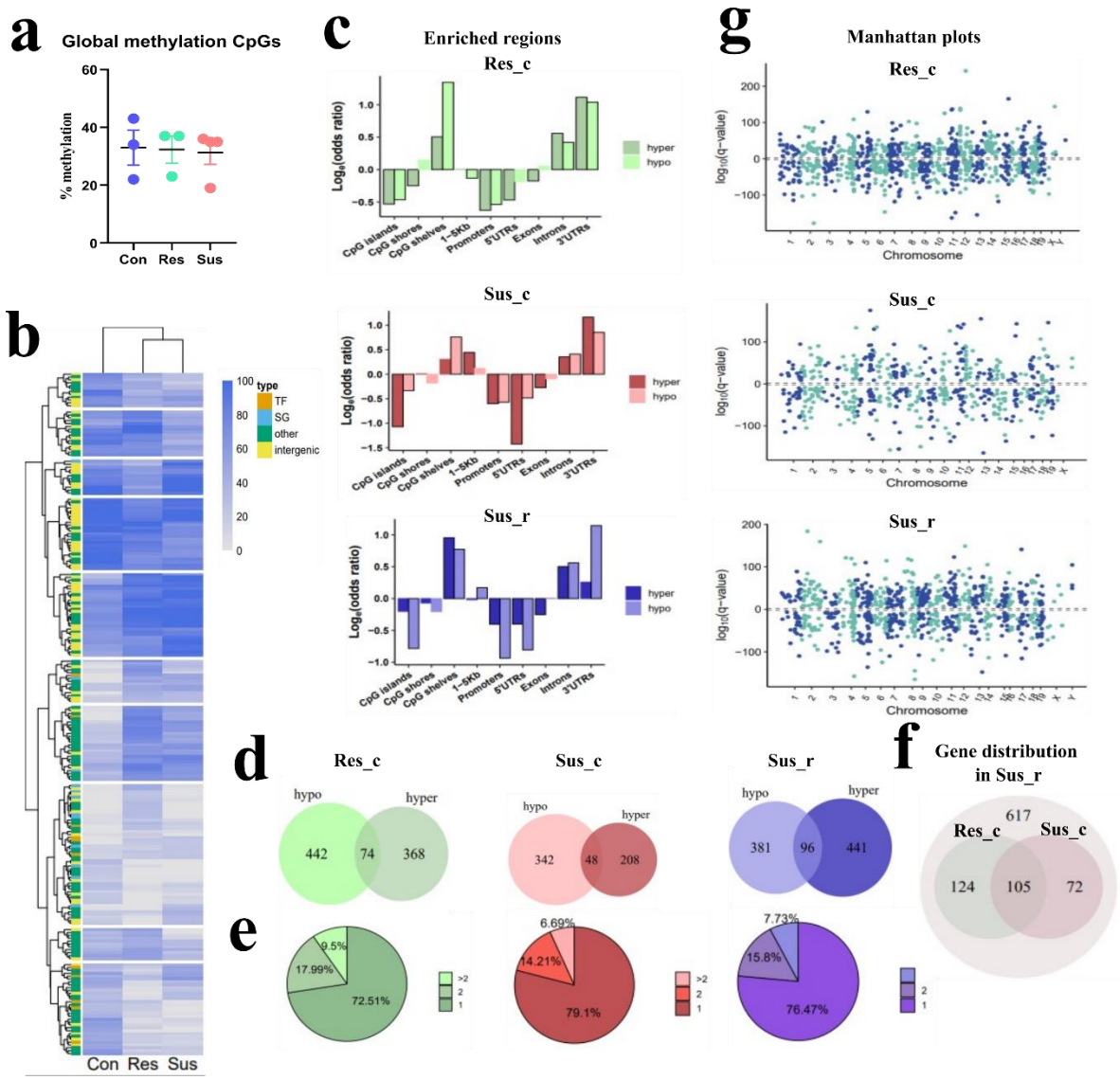

Supplementary Figure 5: Base resolution methylation landscape of differentially methylated cytosines from RRBS-seq.

a. Global methylation percentage of control, resilient and susceptible populations (n = 3, 3 and 4, respectively). **b.** Heatmap depicting methylation percentage of all differentially methylated cytosines (dmCs) detected in all three phenotypes, segregated into intergenic regions and genic regions (further classified by their known functions as transcription factors, synaptic genes and **o**ther genes). Cytosines with similar methylation levels were grouped together using hierarchical clustering. **c.** Log odds ratio depicting enrichment of the dmCs in CpG shelves, introns and 3'UTRs. Black frames around the bars indicate statistically significant log odds ratios ($p<0.05$). **d.** Venn diagrams depicting the number of genes (dmGs) that contain hypomethylated or hypermethylated cytosines (CpGs) in the respective comparisons of resilient to control (Res_c), susceptible to control (Sus_c) and susceptible to resilient (Sus_r) **e.** Pie chart showing the fraction of genes classified by the criterion of harbouring only 1 dmC, 2 dmCs or more **f.** Venn diagram showing the genes specific to Res_c (green) or Sus_c (red) in the direct comparison of the two stressed phenotypes **g.** Manhattan plot of the dmCs along their chromosomal positions. Q values indicate significance of the difference in methylation, with the sign corresponding to the direction of change (gain or loss of methylation). (NB: Figure b-g were plotted by Hristo Todorov)

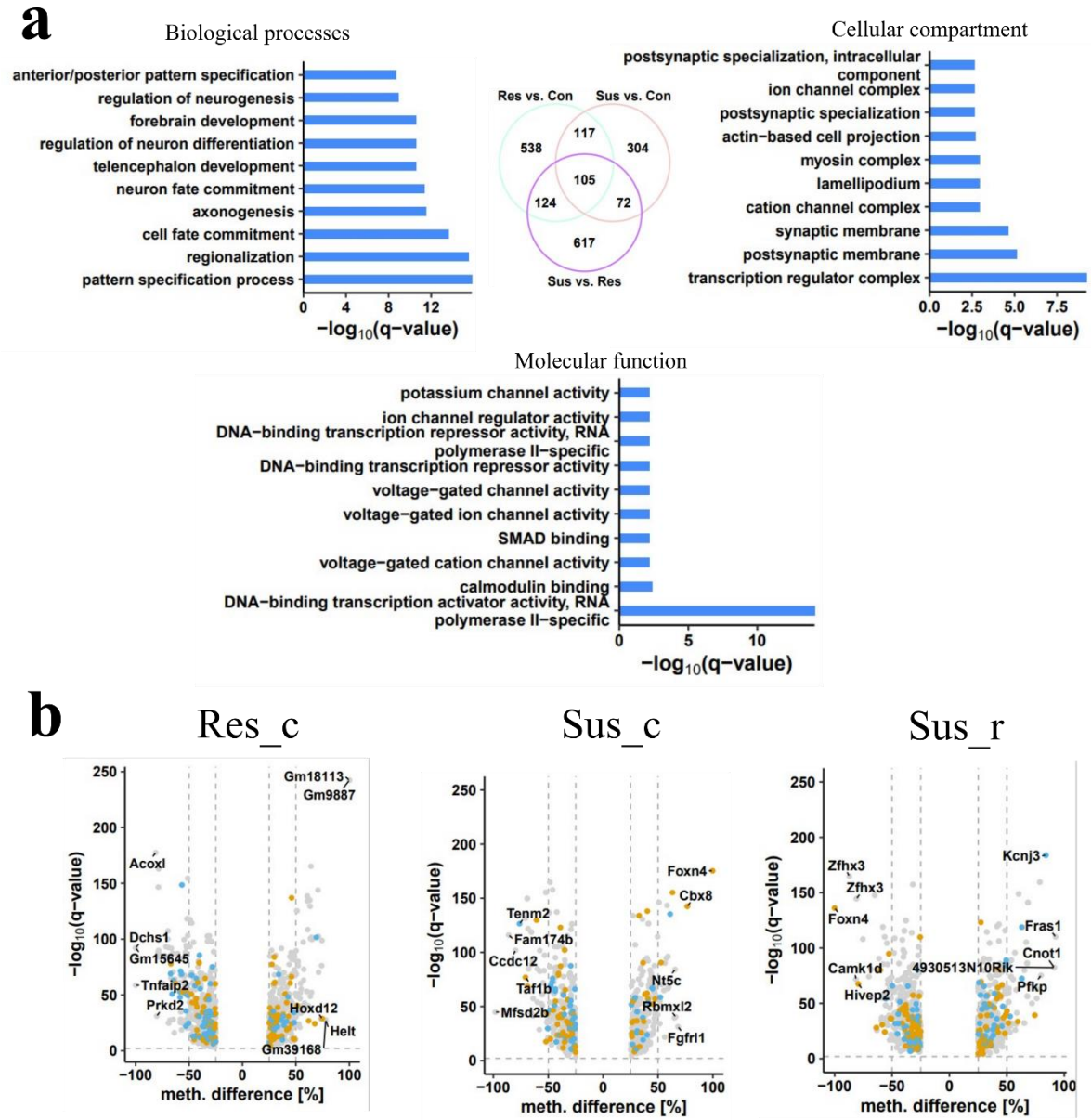

Supplementary Figure 6: Functional assignment of the genes harbouring differentially methylated cytosines (dmGs).

a. Venn diagram of the collective stress response dmGs (combined from all pairwise comparisons) and the top 10 GO terms for dmGs. **b.** Volcano plots of the dmGs depicting the distribution of TFs (orange) and synaptic genes (blue) in the population of dmGs for Res_c, Sus_c and Sus_r. (NB: Figure plots by Dewi Hartwich and Hristo Todorov).

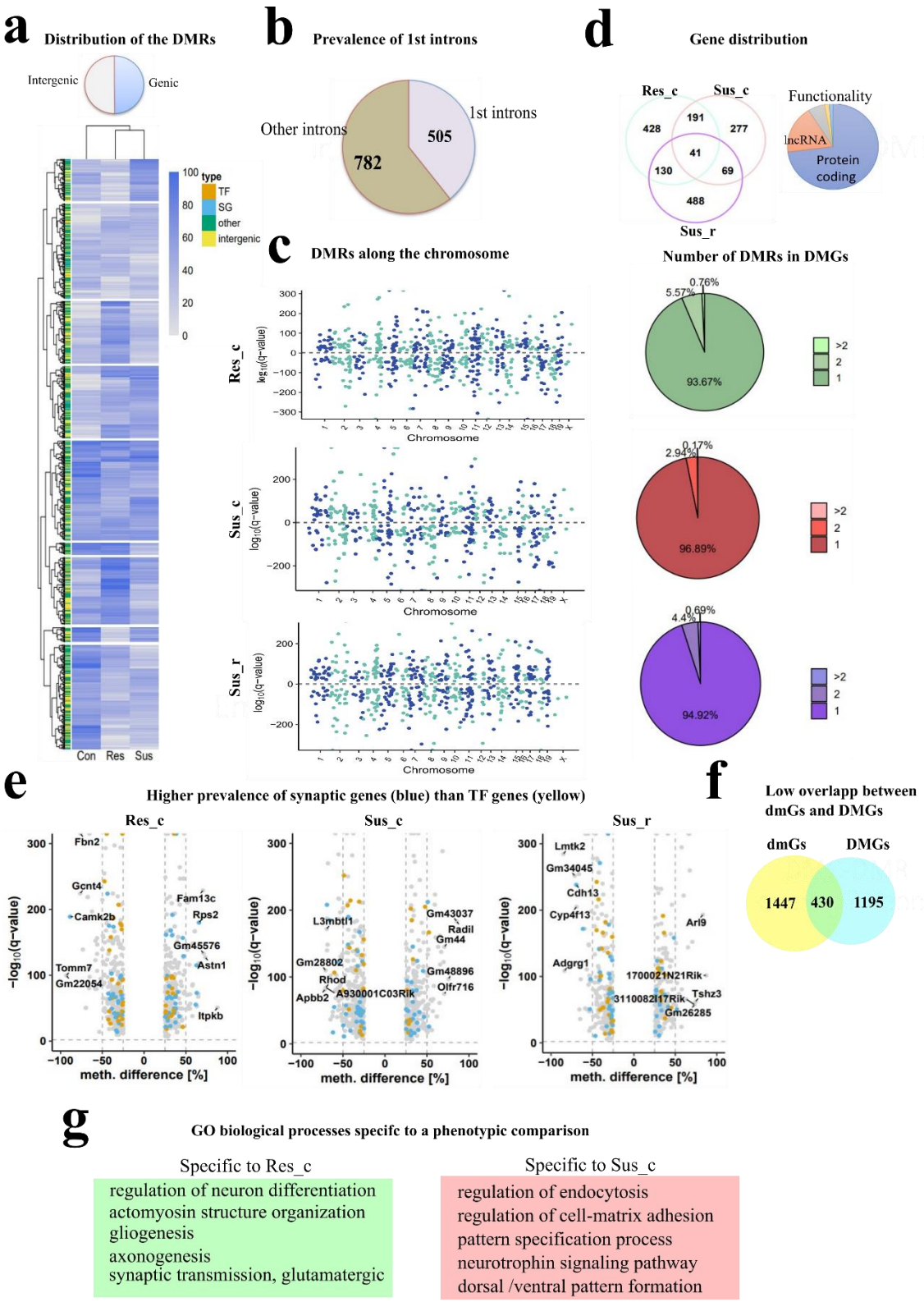

Supplementary Figure 7: Regional methylation landscape of differentially methylated regions and biological processes following stress exposure.

a. Heatmap of absolute methylation percentage of differentially methylated regions detected in all three phenotypes segregated into intergenic regions and genic regions. **b.** Most intronic DMRs are located in the 1st introns. **c.** Manhattan plots of the DMRs over the chromosomes. q values indicate significance of the difference in methylation, with the sign corresponding to the direction of change (gain

or loss of methylation). **d.** Venn diagram depicting the number of genes overlapping between the different phenotypic comparisons of Res_c, Sus_c and Sus_r, with most genes belonging to protein coding genes. Pie charts identify the fraction of DMGs harbouring 1 or more DMRs in the respective comparisons of Res_c (green), Sus_c (red) and Sus_r (purple) **e.** Volcano plots of the DMRs showing the distribution of synaptic genes (blue) and transcription factors (orange) **f.** Venn diagram showing the overlap between the dmGs and DMGs. **g.** GO BPs specifically enriched in the particular phenotypic comparisons ($q<0.05$). (NB: Figures c and e, heatmap of Figure a and Venn diagram and Number of DMRs pie charts of Figure e were plotted by Dewi Hartwich and Hristo Todorov)

Supplementary Figure 8: Multiomics analyses.

a. Absolute methylation levels and read counts of selected genes common to both DMGs and DEGs. **b.** Top represented Pfam and SMART protein domains in the network of methylome (DMGs) and transcriptome (DEGs), combined from all phenotypic comparisons. Graphs were plotted in GraphPad Prism and sizes were adjusted in Inkscape. **c.** Top 10 hub genes of Sus_r DMGs. Top 10 hub genes of Sus_r DEGs. Colour code from red to yellow denotes ranks of the hubs in ascending order, where connectivity decreases as rank increases. **d.** Top 10 hub genes of RES_C, SUS_C and SUS_R of the DMGs and DEGs combined as per their specific comparison groups. Though Src (denoted by blue star) appears in both RES_C and SUS_C, the connectivities are different in the two phenotypic comparisons. **e.** GO terms of BPs specific to either Res_c or Sus_c at a particular omics level. Black star indicates peculiar examples of BP reversing phenotype-specificity when transitioning to a different omics level (DMGs and DEGs), while cyan star indicates a particular example of a BP where phenotype-specificity is retained in both omics levels.

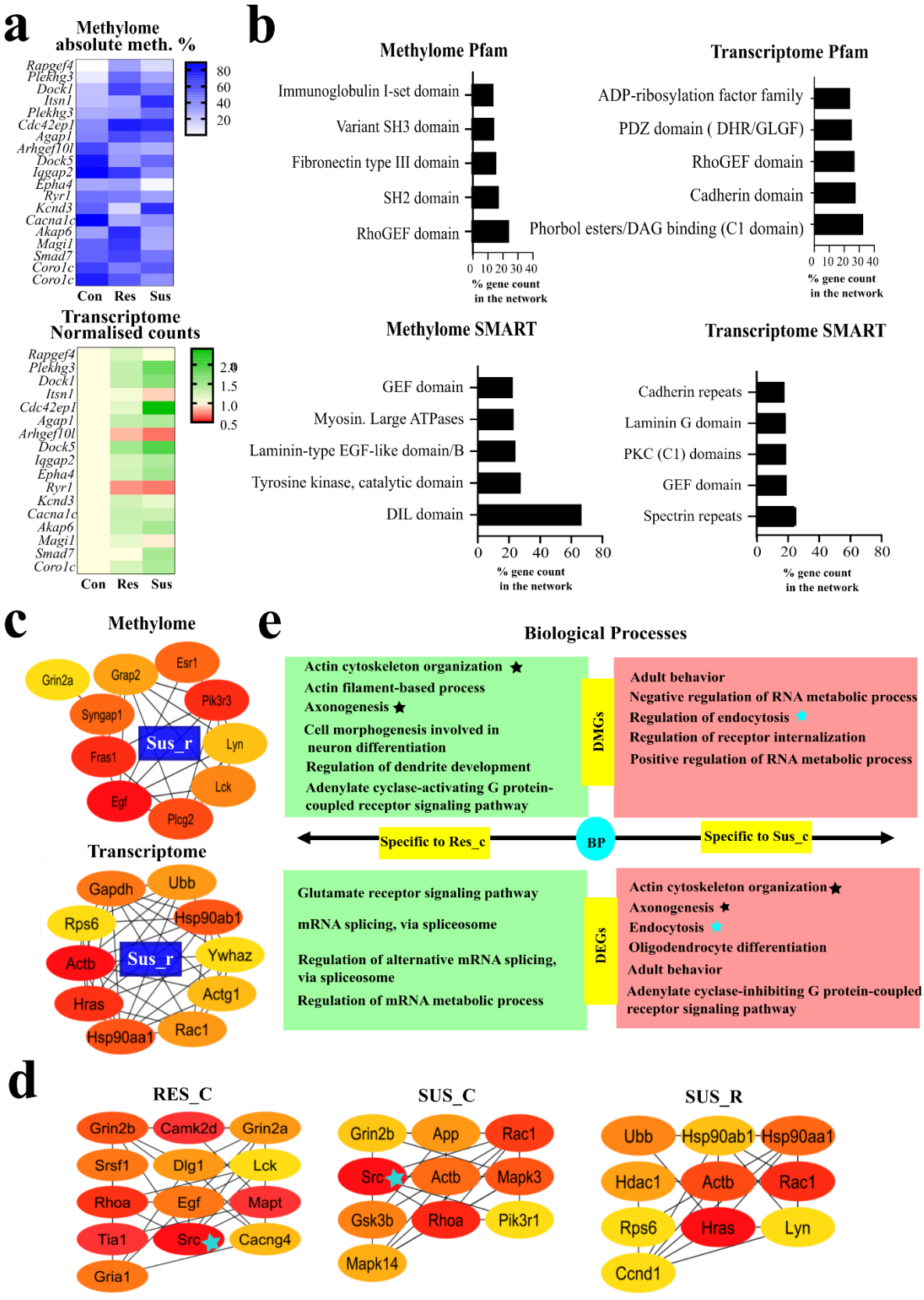
a
Methylome
absolute meth. %
Rapgef4
Plekhg3
Dock1
Itsn1
Plekhg3
Cdc42ep1
Agap1
Arhgef10l
Dock5
Iqgap2
Epha4
Ryr1
Kcnd3
Cacna1c
Akap6
Magi1
Smad7
Coro1c
Coro1c
80
60
40
20
Con Res Sus
Transcriptome
Normalised counts
2.0
1.5
1.0
0.5
Con Res Sus
b
Methylome Pfam
Immunoglobulin I-set domain
Variant SH3 domain
Fibronectin type III domain
SH2 domain
RhoGEF domain
0 10 20 30 40
% gene count
in the network
Transcriptome Pfam
ADP-ribosylation factor family
PDZ domain (DHR/GLGF)
RhoGEF domain
Cadherin domain
Phorbol esters/DAG binding (C1 domain)
0 10 20 30 40
% gene count
in the network
Methylome SMART
GEF domain
Myosin. Large ATPases
Laminin-type EGF-like domain/B
Tyrosine kinase, catalytic domain
DIL domain
0 20 40 60 80
% gene count
in the network
Transcriptome SMART
Cadherin repeats
Laminin G domain
PKC (C1) domains
GEF domain
Spectrin repeats
0 20 40 60 80
% gene count
in the network
c
Methylome
Grin2a
Grap2
Esr1
Pik3r3
Syngap1
Sus_r
Lyn
Fras1
Lck
Egf
Plcg2
Transcriptome
Gapdh
Ubb
Rps6
Hsp90ab1
Actb
Sus_r
Ywhaz
Hras
Actg1
Hsp90aa1
Rac1
e
Biological Processes
Actin cytoskeleton organization
Actin filament-based process
Axonogenesis
Cell morphogenesis involved in neuron differentiation
Regulation of dendrite development
Adenylate cyclase-activating G protein-coupled receptor signaling pathway
DMGs
Adult behavior
Negative regulation of RNA metabolic process
Regulation of endocytosis
Regulation of receptor internalization
Positive regulation of RNA metabolic process
Specific to Res_c
BP
Specific to Sus_c
Glutamate receptor signaling pathway
mRNA splicing, via spliceosome
Regulation of alternative mRNA splicing, via spliceosome
Regulation of mRNA metabolic process
DEGs
Actin cytoskeleton organization
Axonogenesis
Endocytosis
Oligodendrocyte differentiation
Adult behavior
Adenylate cyclase-inhibiting G protein-coupled receptor signaling pathway
d
RES_C
Grin2b
Camk2d
Grin2a
Srsf1
Dlg1
Lck
Rhoa
Egf
Mapt
Tia1
Src
Cacng4
Gria1
SUS_C
Grin2b
App
Rac1
Src
Actb
Mapk3
Gsk3b
Rhoa
Pik3r1
Mapk14
SUS_R
Ubb
Hsp90ab1
Hsp90aa1
Hdac1
Actb
Rac1
Rps6
Hras
Lyn
Ccnd1

2. Supplementary Tables

Supplementary Table 1: List of selected GO BPs significantly enriched in multiomics SUS_C but not in multiomics RES_C (STRING).

Wnt signaling pathway	Postsynaptic cytoskeleton organization
Vesicle-mediated transport in synapse	**Postsynaptic actin cytoskeleton organization**
Vesicle localization	Postsynapse organization
Synaptic vesicle recycling	Positive regulation of Wnt signaling pathway
Synaptic vesicle cycle	Positive regulation of small GTPase mediated signal transduction
Supramolecular fiber organization	
Regulation of Wnt signaling pathway	Phosphatidylinositol-mediated signaling
Regulation of vesicle-mediated transport	Pattern specification process
Regulation of transferase activity	Oligodendrocyte differentiation
Regulation of synaptic vesicle exocytosis	**Oligodendrocyte development**
Regulation of synapse assembly	**Myelination**
Regulation of supramolecular fiber organization	**Myelin assembly**
Regulation of stress fiber assembly	Microtubule-based process
Regulation of presynapse organization	Inositol lipid-mediated signaling
Regulation of presynapse assembly	Gliogenesis
Regulation of potassium ion transport	Establishment of vesicle localization
Regulation of postsynaptic neurotransmitter receptor activity	Enzyme-linked receptor protein signaling pathway
	Endocytosis
Regulation of microtubule-based process	Cytoskeleton-dependent intracellular transport
Regulation of microtubule cytoskeleton organization	Cytoskeleton organization
Regulation of GTPase activity	Cell-cell junction organization
Regulation of exocytosis	Cell-cell junction assembly
Regulation of endocytosis	Calcium ion transport
Regulation of amyloid precursor protein catabolic process	Calcium ion homeostasis
	Adult locomotory behavior
Regulation of actomyosin structure organization	Adult behavior
Regulation of actin polymerization or depolymerization	Adherens junction organization
	Activation of protein kinase activity
Regulation of actin filament-based process	Activation of GTPase activity
Regulation of actin filament organization	**Actin nucleation**
Regulation of actin cytoskeleton organization	**Actin filament organization**
Regulated exocytosis	

Supplementary Table 2: List of GO BPs significantly enriched in multiomics RES_C but not in multiomics SUS_C (STRING).

Synaptic transmission, glutamatergic
Rho protein signal transduction
Regulation of smooth muscle cell migration
Regulation of modification of synaptic structure
Regulation of modification of postsynaptic structure
Protein localization to extracellular region
Nephron tubule morphogenesis
Nephron morphogenesis
mRNA processing
Chordate embryonic development
Adenylate cyclase-**activating** G protein-coupled receptor signaling pathway

Supplementary Table 3: Local network clusters of multiomics SUS_C from STRING.

#term ID	term description	observed gene count	background gene count	strength	false discovery rate
CL:8197	Mixed, incl. Intrinsic component of synaptic membrane, and Neurexins and neuroligins	49	188	0.52	8.17E-08
CL:6604	Axon guidance, and Catenin complex	42	150	0.56	1.75E-07
CL:8665	Mixed, incl. Oligodendrocyte development, and Negative regulation of neuron projection regeneration	18	33	0.85	1.19E-05
CL:8200	Mixed, incl. Ionotropic glutamate receptor complex, and GABA-A receptor complex	29	105	0.55	9.46E-05
CL:8201	Ionotropic glutamate receptor complex, and GABA-A receptor complex	25	80	0.6	9.46E-05
CL:8199	Mixed, incl. Ionotropic glutamate receptor complex, and Gamma-aminobutyric acid A receptor/Glycine receptor alpha	30	115	0.53	0.00011
CL:6605	Axon guidance, and SDK interactions	27	97	0.55	0.00013
CL:8198	Mixed, incl. Ionotropic glutamate receptor complex, and Gamma-aminobutyric acid A receptor/Glycine receptor alpha	32	132	0.49	0.00013
CL:8667	Mixed, incl. Structural constituent of myelin sheath, and DNA-binding protein inhibitor	12	20	0.89	0.00061
CL:6606	Axon guidance, and Chimaerin, RhoGAP domain	24	91	0.53	0.00097

CL:5993	RHO GTPase cycle, and Actin nucleation	33	167	0.4	0.0031
CL:8202	Ionotropic glutamate receptor complex, and Neurexins and neuroligins	18	59	0.59	0.0031
CL:8461	Mixed, incl. Synaptic membrane adhesion, and Cell-cell adhesion mediator activity	17	56	0.59	0.005
CL:29993	Mostly uncharacterized, incl. Domain of unknown function DUF4939, and Paraneoplastic antigen Ma	23	111	0.43	0.0288
CL:6798	Mixed, incl. Catenin complex, and Nephrin family interactions	15	53	0.56	0.0288
CL:5994	Mixed, incl. RHO GTPases Activate WASPs and WAVEs, and RHOB GTPase cycle	26	136	0.39	0.0307
CL:6774	Mixed, incl. Chimaerin, RhoGAP domain, and TIAM1, CC-Ex domain	6	7	1.04	0.0447

Supplementary Table 4: Local network cluster of multiomics RES_C from STRING.

#term ID	term description	observed gene count	background gene count	strength	false discovery rate
CL:38951	Cadherin C-terminal cytoplasmic tail, catenin-binding region	9	10	1.35	5.69E-05
CL:38948	Cadherin C-terminal cytoplasmic tail, catenin-binding region, and Tropomyosin	10	19	1.12	0.00017
CL:8197	Mixed, incl. Intrinsic component of synaptic membrane, and Neurexins and neuroligins	26	188	0.54	0.00038
CL:6604	Axon guidance, and Catenin complex	22	150	0.56	0.001
CL:16175	RNA recognition motif domain, and CRD-mediated mRNA stability complex	12	58	0.71	0.0109
CL:8201	Ionotropic glutamate receptor complex, and GABA-A receptor complex	14	80	0.64	0.0109
CL:38953	Cadherin C-terminal cytoplasmic tail, catenin-binding region	5	5	1.4	0.011
CL:16171	RNA recognition motif domain, and U2-type post-mRNA release spliceosomal complex	13	79	0.61	0.0272
CL:16178	Mixed, incl. Negative regulation of mRNA splicing, via spliceosome, and Zinc finger, CHHC-type	9	38	0.77	0.0318
CL:8202	Ionotropic glutamate receptor complex, and Neurexins and neuroligins	11	59	0.67	0.0318

Supplementary Table 5: List of selected significantly enriched BPs from Enrichr.

In multiomics RES_C but not in multiomics SUS_C	In multiomics SUS_C but not in multiomics RES_C
Vasculogenesis	Regulation of synapse structure or activity
Substrate adhesion-dependent cell spreading	Regulation of synapse organization
Regulation of vesicle-mediated transport	Regulation of small GTPase mediated signal transduction
Regulation of protein-containing complex assembly	Regulation of signaling
Regulation of protein metabolic process	Regulation of RNA metabolic process
Regulation of peptidyl-tyrosine phosphorylation	Regulation of Rho protein signal transduction
Regulation of ERK1 and ERK2 cascade	Regulation of Ras protein signal transduction
Regulation of actin filament-based process	Regulation of postsynaptic membrane potential
Regulation of actin filament organization	Regulation of postsynapse organization
Positive regulation of organelle assembly	Regulation of neuron projection development
Positive regulation of neurogenesis	Regulation of neuron differentiation
Positive regulation of MAPK cascade	Regulation of neurogenesis
Positive regulation of kinase activity	Regulation of modification of postsynaptic actin cytoskeleton
Positive regulation of hydrolase activity	Regulation of intracellular signal transduction
Positive regulation of ERK1 and ERK2 cascade	Ras protein signal transduction
Positive regulation of epithelial cell migration	Protein localization to extracellular region
Positive regulation of endopeptidase activity	Positive regulation of neuron projection development
Peptidyl-tyrosine phosphorylation	Positive regulation of excitatory postsynaptic potential
Peptidyl-serine phosphorylation	Neuron projection development
Homeostatic process	mRNA processing
Endothelium development	Ionotropic glutamate receptor signaling pathway
Endothelial cell migration	Homophilic cell adhesion via plasma membrane adhesion molecules
Cell-matrix adhesion	Head development
Calcium-mediated signaling	**Exocytosis**
Axon guidance	Cell-cell signaling
Adult walking behavior	**Cell-cell adhesion** via plasma-membrane adhesion molecules
Actin filament-based process	Cell-cell adhesion
	Cell morphogenesis involved in neuron differentiation
	cAMP-mediated signaling

	Adenylate cyclase-modulating G protein-coupled receptor signaling pathway

Supplementary Table 6: List of selected significantly enriched BPs in SUS_R (Enrichr).

Vesicle-mediated transport in synapse	Positive regulation of actin filament polymerization
Synaptic vesicle cycle	Peptidyl-tyrosine phosphorylation
Synapse organization	Peptidyl-amino acid modification
Synapse assembly	Oligodendrocyte differentiation
Supramolecular fiber organization	Oligodendrocyte development
Small GTPase mediated signal transduction	**Neurogenesis**
Regulation of vesicle-mediated transport	**Negative regulation of ERK1 and ERK2 cascade**
Regulation of synaptic vesicle exocytosis	**Myelination**
Regulation of synaptic vesicle cycle	miRNA mediated inhibition of translation
Regulation of synaptic plasticity	Microtubule cytoskeleton organization
Regulation of synapse structure or activity	Ionotropic glutamate receptor signaling pathway
Regulation of synapse maturation	Homophilic cell adhesion via plasma membrane
Regulation of supramolecular fiber organization	adhesion molecules
Regulation of stress fiber assembly	Glutamate receptor signaling pathway
Regulation of exocytosis	Gliogenesis
Regulation of endocytosis	Generation of neurons
Regulation of dendritic spine development	**Exocytosis**
Regulation of cytoskeleton organization	Exocytic process
Regulation of actin polymerization or	Ephrin receptor signaling pathway
depolymerization	Enzyme linked receptor protein signaling pathway
Regulation of actin filament-based process	**Endocytosis**
Regulation of actin cytoskeleton organization	Dendrite development
Regulated exocytosis	Cytoskeleton organization
Postsynaptic actin cytoskeleton organization	Cell-cell adhesion via plasma-membrane adhesion
Postsynapse organization	molecules
Positive regulation of Wnt signaling pathway	Cell-cell adhesion
Positive regulation of stress fiber assembly	Cell adhesion
Positive regulation of GTPase activity	Calcium-ion regulated exocytosis
Positive regulation of gliogenesis	Axonogenesis
Positive regulation of endocytosis	Axon guidance
Positive regulation of cytoskeleton organization	Adenylate cyclase-inhibiting G protein-coupled
Positive regulation of axonogenesis	glutamate receptor signaling pathway
	Actin filament-based process
	Actin filament organization
	Actin cytoskeleton organization

Supplementary Table 7: Synaptic gene network comparison with literature.

Synaptic genes, newly discovered as relevant to stress, in our data	GTPases, Rho GAPS and GEFs, common with literature	RhoGEFs/GAPs and GTPases, identified as novel in the comparison.	Comments from add-on PubMed search for screening the 'mention' of the acclaimed novel RhoGEFs/GAPs and GTPases.
TFR2	TRIO	RAB6B	*Rab6b*, already in depression studies
TENT2	TIAM1	RAB5A	*Rab5,* not yet in stress research, though in AD
TENM1	RHOB	OPHN1	*Ophn1,* in recent literature
TDRD1	RHOA	ARHGEF15	*Arhgef15,* not yet in stress research
TANC2	RHEB	ARF6	***Arf6,*** in synaptic long-term depression research but not yet in stress-depression studies
SLITRK3	RAP1B		
SLITRK2	RALA		
SLC6A5	RAC1		
SLC1A6	RAB8B		
SHISA9	RAB8A		
RTN3	RAB6B		
RPS26	RAB5A		
RPS2	RAB3C		
RPLP1	RAB3A		
RPL36A	RAB33B		
ROR2	RAB2A		
ROGDI	RAB1B		
RAPH1	RAB11B		
RAB6B	RAB10		
RAB5A	PLEKHG5		
PPFIA4	OPHN1		
PPFIA1	KALRN		
PLS3	ITSN1		
PLPPR4	HRAS		
PCDH15	FARP1		
OPHN1	DOCK1		
NTNG2	ARL8B		
NECTIN3	ARHGEF2		
MAGI3	ARHGEF15		
LAMP1	ARHGAP39		
KPNA1	ARHGAP22		
KLHL17	ARF6		

HNRNPK	ARF1		
GPC4			
GLRA2			
GABRE			
FXYD6			
FRRS1L			
FRMPD4			
FILIP1			
FBXO2			
DLG3			
DGKI			
DCC			
CYTH2			
CHRNB3			
CDKL5			
CAMKV			
CACNA1B			
ARHGEF15			
ARF6			
APPL1			
ADGRB3			
ACTR2			
ABHD17C			

NB: The gene lists in the above are not in their usual nomenclature as we used STRING protein-protein interaction platform to put them in the context of a network.

Supplementary Table 8: GO CCs of tissue comparisons for susceptible phenotypes.

Index	Name	P-value	Adjusted p-value	Odds Ratio	Combined score
1	Cytoskeleton (GO:0005856)	0.01195	0.9101	1.73	7.67
2	Actin-Based Cell Projection (GO:0098858)	0.01289	0.9101	3.3	14.35
3	Adherens Junction (GO:0005912)	0.02289	0.9101	2.42	9.13
4	Catenin Complex (GO:0016342)	0.02586	0.9101	5.12	18.73
5	Clathrin Vesicle Coat (GO:0030125)	0.02991	0.9101	8.53	29.93
6	Filopodium (GO:0030175)	0.04915	0.9101	3.05	9.2
7	Clathrin Coat (GO:0030118)	0.05121	0.9101	6.09	18.1
8	Clathrin-Coated Vesicle Membrane (GO:0030665)	0.0566	0.9101	2.52	7.22
9	AMPA Glutamate Receptor Complex (GO:0032281)	0.06978	0.9101	5.01	13.35
10	Heterotrimeric G-protein Complex (GO:0005834)	0.1046	0.9101	3.87	8.75

Supplementary Table 9: Biotypes of the small RNAs involved in stress research.

	vHipp Res_c		vHipp Sus_c		vHipp Sus_r	
biotype	**upregulated**	**downregulated**	**upregulated**	**downregulated**	**upregulated**	**downregulated**
miRNA					3	
misc_RNA	1			1		1
mmu_piR	3	3		8	1	12
mmu-let						10
mmu-miR	23			19		137
Mt_rRNA						
Mt_tRNA						
rRNA				2		3
scaRNA		1				1
scRNA						
snoRNA		2	2		40	1
snRNA			1		11	4

3. Supplementary Data

Supplementary data for the dmCs (dmGs) and DMRs (DMGs) are available at the link

Thesis supplementary data

VIII. Bibliography

1. Halbreich, U. Stress-related physical and mental disorders: a new paradigm. *BJPsych Adv* **27**, 145–152 (2021).

2. De Kloet, E. R., Joëls, M. & Holsboer, F. Stress and the brain: From adaptation to disease. *Nature Reviews Neuroscience* vol. 6 463–475 Preprint at https://doi.org/10.1038/nrn1683 (2005).

3. Rigó, M., Dragano, N., Wahrendorf, M., Siegrist, J. & Lunau, T. Work stress on rise? Comparative analysis of trends in work stressors using the European working conditions survey. *Int Arch Occup Environ Health* **94**, 459–474 (2021).

4. Global, regional, and national burden of 12 mental disorders in 204 countries and territories, 1990–2019: a systematic analysis for the Global Burden of Disease Study 2019. *Lancet Psychiatry* **9**, 137–150 (2022).

5. WHO. WHO report 2019. *https://www.who.int/news-room/fact-sheets/detail/mental-disorders* (2019).

6. Khan, A. R., Geiger, L., Wiborg, O. & Czéh, B. Stress-Induced Morphological, Cellular and Molecular Changes in the Brain-Lessons Learned from the Chronic Mild Stress Model of Depression. *Cells* vol. 9 Preprint at https://doi.org/10.3390/cells9041026 (2020).

7. Kindred, R. & Bates, G. W. The Influence of the COVID-19 Pandemic on Social Anxiety: A Systematic Review. *International Journal of Environmental Research and Public Health* vol. 20 Preprint at https://doi.org/10.3390/ijerph20032362 (2023).

8. Salari, N. *et al.* Prevalence of stress, anxiety, depression among the general population during the COVID-19 pandemic: A systematic review and meta-analysis. *Globalization and Health* vol. 16 Preprint at https://doi.org/10.1186/s12992-020-00589-w (2020).

9. Murata, S. *et al.* The psychiatric sequelae of the COVID-19 pandemic in adolescents, adults, and health care workers. *Depress Anxiety* **38**, 233–246 (2021).

10. Tang, S., Xiang, M., Cheung, T. & Xiang, Y. T. Mental health and its correlates among children and adolescents during COVID-19 school closure: The importance of parent-child discussion. *J Affect Disord* **279**, 353–360 (2021).

11. Ferrando, S. J. *et al.* Anxiety and posttraumatic stress in post-acute sequelae of COVID-19: prevalence, characteristics, comorbidity, and clinical correlates. *Front Psychiatry* **14**, (2023).

12. Bhatnagar, S. Rethinking stress resilience. *Trends in Neurosciences* vol. 44 936–945 Preprint at https://doi.org/10.1016/j.tins.2021.09.005 (2021).

13. Rice, V. & Liu, B. Personal resilience and coping with implications for work. Part I: A review. *Work* vol. 54 325–333 Preprint at https://doi.org/10.3233/WOR-162300 (2016).

14. Agorastos, A. & Chrousos, G. P. The neuroendocrinology of stress: the stress-related continuum of chronic disease development. *Molecular Psychiatry* vol. 27 502–513 Preprint at https://doi.org/10.1038/s41380-021-01224-9 (2022).

15. Wood, S. K. & Bhatnagar, S. Resilience to the effects of social stress: Evidence from clinical and preclinical studies on the role of coping strategies. *Neurobiology of Stress* vol. 1 164–173 Preprint at https://doi.org/10.1016/j.ynstr.2014.11.002 (2015).

16. Basile, F. *et al.* Omics insights into animal resilience and stress factors. *Animals* vol. 11 1–24 Preprint at https://doi.org/10.3390/ani11010047 (2021).

17. Barak, Y., Barson, D., Davie, G., Glue, P. & Paleacu, D. Internalize at your peril: internalizing disorders as risk factors for dementia—cohort study. *Geroscience* **43**, 253–261 (2021).

18. Wallensten, J. *et al.* Stress, depression, and risk of dementia – a cohort study in the total population between 18 and 65 years old in Region Stockholm. *Alzheimers Res Ther* **15**, (2023).

19. Sieurin, J. *et al.* Occupational stress and risk for Parkinson's disease: A nationwide cohort study. *Movement Disorders* **33**, 1456–1464 (2018).

20. Speyer, L. G., Brown, R. H., Ribeaud, D., Eisner, M. & Murray, A. L. The role of moment-to-moment dynamics of perceived stress and negative affect in co-occurring ADHD and internalising symptoms. *J Autism Dev Disord* **53**, 1213–1223 (2023).

21. de Vaan, G. *et al.* Associations Between Cortisol Stress Levels and Autism Symptoms in People With Sensory and Intellectual Disabilities. *Front Educ (Lausanne)* **5**, (2020).

22. Yaribeygi, H., Panahi, Y., Sahraei, H., Johnston, T. P. & Sahebkar, A. The impact of stress on body function: A review. *EXCLI Journal* vol. 16 1057–1072 Preprint at https://doi.org/10.17179/excli2017-480 (2017).

23. Russell, G. & Lightman, S. The human stress response. *Nat Rev Endocrinol* **15**, 525–534 (2019).

24. Mcewen, B. S., Mirsky, A. E. & Hatch, M. M. Physiology and Neurobiology of Stress and Adaptation: Central Role of the Brain. (2007) doi:10.1152/physrev.00041.2006.-The.

25. Li, L. *et al.* Stress Accelerates Defensive Responses to Looming in Mice and Involves a Locus Coeruleus-Superior Colliculus Projection. *Current Biology* **28**, 859-871.e5 (2018).

26. Kirby, E. D. *et al.* Acute stress enhances adult rat hippocampal neurogenesis and activation of newborn neurons via secreted astrocytic FGF2. *Elife* **2013**, (2013).

27. Surget, A. & Belzung, C. Adult hippocampal neurogenesis shapes adaptation and improves stress response: a mechanistic and integrative perspective. *Molecular Psychiatry* vol. 27 403–421 Preprint at https://doi.org/10.1038/s41380-021-01136-8 (2022).

28. Okamoto, M. *et al.* High-intensity Intermittent Training Enhances Spatial Memory and Hippocampal Neurogenesis Associated with BDNF Signaling in Rats. *Cerebral Cortex* **31**, 4386–4397 (2021).

29. Stankiewicz, A. M., Swiergiel, A. H. & Lisowski, P. Epigenetics of stress adaptations in the brain. *Brain Research Bulletin* vol. 98 76–92 Preprint at https://doi.org/10.1016/j.brainresbull.2013.07.003 (2013).

30. Sukhareva, E. V. The role of the corticotropin-releasing hormone and its receptors in the regulation of stress response. *Vavilovskii Zhurnal Genetiki i Selektsii* vol. 25 216–223 Preprint at https://doi.org/10.18699/VJ21.025 (2021).

31. Deussing, J. M. & Chen, A. A. The Corticotropin-Releasing Factor Family: Physiology of the Stress Response. *Physiol Rev* **98**, 2225–2286 (2018).

32. Herman, J. P. *et al.* Regulation of the hypothalamic-pituitary- adrenocortical stress response. *Compr Physiol* **6**, 603–621 (2016).

33. Tasker, J. G., Di, S. & Malcher-Lopes, R. Minireview: Rapid glucocorticoid signaling via membrane-associated receptors. *Endocrinology* vol. 147 5549–5556 Preprint at https://doi.org/10.1210/en.2006-0981 (2006).

34. Tsigos, C. & Chrousos, G. P. Hypothalamic–pituitary–adrenal axis, neuroendocrine factors and stress. *J Psychosom Res* **53**, 865–871 (2002).

35. Gjerstad, J. K., Lightman, S. L. & Spiga, F. Role of glucocorticoid negative feedback in the regulation of HPA axis pulsatility. *Stress* vol. 21 403–416 Preprint at https://doi.org/10.1080/10253890.2018.1470238 (2018).

36. Taborsky, B. *et al.* An evolutionary perspective on stress responses, damage and repair. *Horm Behav* **142**, (2022).

37. Nesse, R. M. & Young, E. A. *Evolutionary Origins and Functions of the Stress Response*. (2000).

38. Picard, K., St-Pierre, M. K., Vecchiarelli, H. A., Bordeleau, M. & Tremblay, M. È. Neuroendocrine, neuroinflammatory and pathological outcomes of chronic stress: A story of microglial remodeling. *Neurochem Int* **145**, (2021).

39. Song, H. *et al.* Perceived stress level and risk of cancer incidence in a Japanese population: The Japan Public Health Center (JPHC)-based Prospective Study. *Sci Rep* **7**, (2017).

40. Sapolsky, R. M. Glucocorticoids, the evolution of the stress-response, and the primate predicament. *Neurobiology of Stress* vol. 14 Preprint at https://doi.org/10.1016/j.ynstr.2021.100320 (2021).

41. Folkman, S. & Lazarus, R. S. *An Analysis of Coping in a Middle-Aged Community Sample*. *Source: Journal of Health and Social Behavior* vol. 21 (1980).

42. Gonzalez, M. J. & Miranda-Massari, J. R. Diet and stress. *Psychiatric Clinics of North America* vol. 37 579–589 Preprint at https://doi.org/10.1016/j.psc.2014.08.004 (2014).

43. Marinov, T. *et al.* Influence of Yoga Practices on Stress Coping Strategies. *An International Peer-reviewed Journal* **39**, (2017).

44. Tellhed, U., Daukantaitė, D., Maddux, R. E., Svensson, T. & Melander, O. Yogic Breathing and Mindfulness as Stress Coping Mediate Positive Health Outcomes of Yoga. *Mindfulness (N Y)* **10**, 2703–2715 (2019).

45. Herrman, H. *et al.* What is Resilience? *The Canadian Journal of Psychiatry* **56**, 258–265 (2011).

46. Bracha, H. S. *Freeze, Flight, Fight, Fright, Faint: Adaptationist Perspectives on the Acute Stress Response Spectrum*. vol. 9 (2004).

47. Sanacora, G., Yan, Z. & Popoli, M. The stressed synapse 2.0: pathophysiological mechanisms in stress-related neuropsychiatric disorders. *Nat Rev Neurosci* **23**, 86–103 (2022).

48. Mateos-Aparicio, P. & Rodríguez-Moreno, A. The impact of studying brain plasticity. *Frontiers in Cellular Neuroscience* vol. 13 Preprint at https://doi.org/10.3389/fncel.2019.00066 (2019).

49. Francis, J. T. & Song, W. Neuroplasticity of the sensorimotor cortex during learning. *Neural Plast* **2011**, (2011).

50. Citri, A. & Malenka, R. C. Synaptic plasticity: Multiple forms, functions, and mechanisms. *Neuropsychopharmacology* vol. 33 18–41 Preprint at https://doi.org/10.1038/sj.npp.1301559 (2008).

51. Brown, R. E., Bligh, T. W. B. & Garden, J. F. The Hebb Synapse Before Hebb: Theories of Synaptic Function in Learning and Memory Before Hebb (1949), With a Discussion of the Long-Lost Synaptic Theory of William McDougall. *Frontiers in Behavioral Neuroscience* vol. 15 Preprint at https://doi.org/10.3389/fnbeh.2021.732195 (2021).

52. Bechtel, W. Minding the gap: discovering the phenomenon of chemical transmission in the nervous system. *Hist Philos Life Sci* **45**, (2023).

53. Monteggia, L. M., Scarnati, M. S., Kataria, R., Biswas, M. & Paradiso, K. G. Active presynaptic ribosomes in the mammalian brain, and altered transmitter release after protein synthesis inhibition. (2018) doi:10.7554/eLife.36697.001.

54. Rosenberg, T. *et al.* The roles of protein expression in synaptic plasticity and memory consolidation. *Frontiers in Molecular Neuroscience* vol. 7 Preprint at https://doi.org/10.3389/fnmol.2014.00086 (2014).

55. He, R. *et al.* New Insights Into Interactions of Presynaptic Calcium Channel Subtypes and SNARE Proteins in Neurotransmitter Release. *Front Mol Neurosci* **11**, (2018).

56. Kaeser, P. S. & Regehr, W. G. The readily releasable pool of synaptic vesicles. *Current Opinion in Neurobiology* vol. 43 63–70 Preprint at https://doi.org/10.1016/j.conb.2016.12.012 (2017).

57. Powell, C. M. Gene targeting of presynaptic proteins in synaptic plasticity and memory: Across the great divide. *Neurobiology of Learning and Memory* vol. 85 2–15 Preprint at https://doi.org/10.1016/j.nlm.2005.08.014 (2006).

58. Yuan, Y., Huo, H. & Fang, T. Effects of Metabolic Energy on Synaptic Transmission and Dendritic Integration in Pyramidal Neurons. *Front Comput Neurosci* **12**, (2018).

59. Li, S., Xiong, G.-J., Huang, N. & Sheng, Z.-H. The cross-talk of energy sensing and mitochondrial anchoring sustains synaptic efficacy by maintaining presynaptic metabolism. *Nat Metab* **2**, 1077–1095 (2020).

60. Kennedy, M. B. Signal-Processing Machines at the Postsynaptic Density. *Science (1979)* **290**, 750–754 (2000).

61. Koopmans, F. *et al.* SynGO: An Evidence-Based, Expert-Curated Knowledge Base for the Synapse. *Neuron* **103**, 217-234.e4 (2019).

62. McEwen, B. S. & Gianaros, P. J. Stress- and allostasis-induced brain plasticity. *Annu Rev Med* **62**, 431–445 (2011).

63. Radley, J. J. *et al.* Repeated stress induces dendritic spine loss in the rat medial prefrontal cortex. *Cerebral Cortex* **16**, 313–320 (2006).

64. Krishnan, V. *et al.* Molecular Adaptations Underlying Susceptibility and Resistance to Social Defeat in Brain Reward Regions. *Cell* **131**, 391–404 (2007).

65. Madur, L. *et al.* Stress deficits in reward behaviour are associated with and replicated by dysregulated amygdala-nucleus accumbens pathway function in mice. *Commun Biol* **6**, (2023).

66. Pearson-Leary, J. *et al.* Inflammation and vascular remodeling in the ventral hippocampus contributes to vulnerability to stress. *Transl Psychiatry* **7**, e1160 (2017).

67. Roddy, D. *et al.* Amygdala substructure volumes in Major Depressive Disorder. *Neuroimage Clin* **31**, (2021).

68. Reuveni, E., Getselter, D., Oron, O. & Elliott, E. Differential contribution of cis and trans gene transcription regulatory mechanisms in amygdala and prefrontal cortex and modulation by social stress. *Sci Rep* **8**, 1–10 (2018).

69. Sarowar, T. & Grabrucker, A. M. Rho GTPases in the Amygdala-A Switch for Fears? *Cells* vol. 9 Preprint at https://doi.org/10.3390/cells9091972 (2020).

70. Schumacher, A., Vlassov, E. & Ito, R. The ventral hippocampus, but not the dorsal hippocampus is critical for learned approach-avoidance decision making. *Hippocampus* **26**, 530–542 (2016).

71. Kenworthy, C. A. *et al.* Social defeat induces changes in histone acetylation and expression of histone modifying enzymes in the ventral hippocampus, prefrontal cortex, and dorsal raphe nucleus. *Neuroscience* **264**, 88–98 (2014).

72. Luczynski, P., Moquin, L. & Gratton, A. Chronic stress alters the dendritic morphology of callosal neurons and the acute glutamate stress response in the rat medial prefrontal cortex. *Stress* **18**, 654–667 (2015).

73. Yang, L. *et al.* Toward Antifragility: Social Defeat Stress Enhances Learning and Memory in Young Mice Via Hippocampal Synaptosome Associated Protein 25. *Psychol Sci* **34**, 616–632 (2023).

74. Phillips, M. L., Robinson, H. A. & Pozzo-Miller, L. Ventral hippocampal projections to the medial prefrontal cortex regulate social memory. doi:10.7554/eLife.44182.001.

75. Khan, R., Kulasiri, D. & Samarasinghe, S. Functional repertoire of protein kinases and phosphatases in synaptic plasticity and associated neurological disorders. *Neural Regeneration Research* vol. 16 1150–1157 Preprint at https://doi.org/10.4103/1673-5374.300331 (2021).

76. Carlezon, W. A. & Thomas, M. J. Biological substrates of reward and aversion: A nucleus accumbens activity hypothesis. *Neuropharmacology* vol. 56 122–132 Preprint at https://doi.org/10.1016/j.neuropharm.2008.06.075 (2009).

77. Frodl, T. & O'Keane, V. How does the brain deal with cumulative stress? A review with focus on developmental stress, HPA axis function and hippocampal structure in humans. *Neurobiol Dis* **52**, 24–37 (2013).

78. Çalışkan, G. & Stork, O. Hippocampal network oscillations at the interplay between innate anxiety and learned fear. *Psychopharmacology (Berl)* **236**, 321–338 (2019).

79. MacQueen, G. & Frodl, T. The hippocampus in major depression: Evidence for the convergence of the bench and bedside in psychiatric research. *Mol Psychiatry* **16**, 252–264 (2011).

80. Czéh, B. & Lucassen, P. J. What causes the hippocampal volume decrease in depression? Are neurogenesis, glial changes and apoptosis implicated? *European Archives of Psychiatry and Clinical Neuroscience* vol. 257 250–260 Preprint at https://doi.org/10.1007/s00406-007-0728-0 (2007).

81. Schoenfeld, T. J. & Gould, E. Stress, stress hormones, and adult neurogenesis. *Experimental Neurology* vol. 233 12–21 Preprint at https://doi.org/10.1016/j.expneurol.2011.01.008 (2012).

82. Yoshida, K. *et al.* Chronic social defeat stress impairs goal-directed behavior through dysregulation of ventral hippocampal activity in male mice. *Neuropsychopharmacology* **46**, 1606–1616 (2021).

83. Carrion, V. G., Weems, C. F., Richert, K., Hoffman, B. C. & Reiss, A. L. Decreased prefrontal cortical volume associated with increased bedtime cortisol in traumatized youth. *Biol Psychiatry* **68**, 491–493 (2010).

84. Haris, E. M., Bryant, R. A., Williamson, T. & Korgaonkar, M. S. Functional connectivity of amygdala subnuclei in PTSD: a narrative review. *Molecular Psychiatry* Preprint at https://doi.org/10.1038/s41380-023-02291-w (2023).

85. Lo Martire, V., Caruso, D., Palagini, L., Zoccoli, G. & Bastianini, S. Stress & sleep: A relationship lasting a lifetime. *Neurosci Biobehav Rev* **117**, 65–77 (2020).

86. Han, K. S., Kim, L. & Shim, I. Stress and Sleep Disorder. *Exp Neurobiol* **21**, 141–150 (2012).

87. Gellner, A. K. *et al.* Stress vulnerability shapes disruption of motor cortical neuroplasticity. *Transl Psychiatry* **12**, (2022).

88. Krüger, M. & Lux, V. Failure of motor function—A Developmental Embodiment Research perspective on the systemic effects of stress. *Front Hum Neurosci* **17**, (2023).

89. Gyles, T. M., Nestler, E. J. & Parise, E. M. Advancing preclinical chronic stress models to promote therapeutic discovery for human stress disorders. *Neuropsychopharmacology* (2023) doi:10.1038/s41386-023-01625-0.

90. Romanova, E. V. & Sweedler, J. V. Animal Model Systems in Neuroscience. *ACS Chemical Neuroscience* vol. 9 1869–1870 Preprint at https://doi.org/10.1021/acschemneuro.8b00380 (2018).

91. Atrooz, F., Alkadhi, K. A. & Salim, S. Understanding stress: Insights from rodent models. *Current Research in Neurobiology* **2**, 100013 (2021).

92. Söderlund, J. & Lindskog, M. Relevance of rodent models of depression in clinical practice: Can we overcome the obstacles in translational neuropsychiatry? *International Journal of Neuropsychopharmacology* vol. 21 668–676 Preprint at https://doi.org/10.1093/ijnp/pyy037 (2018).

93. Flati, T. *et al.* (No Title). doi:10.1038/s41597-020-00772-z.

94. Planchez, B., Surget, A. & Belzung, · Catherine. Animal models of major depression: drawbacks and challenges. *J Neural Transm* **126**, 1383–1408 (2084).

95. Mo, C., Renoir, T. & Hannan, A. J. Stress and glucocorticoids as experience-dependent modulators of huntington's disease. in *Stress: Physiology, Biochemistry, and Pathology Handbook of Stress Series, Volume 3* 243–278 (Elsevier, 2019). doi:10.1016/B978-0-12-813146-6.00020-5.

96. Golden, S. A., Covington, H. E., Berton, O. & Russo, S. J. A standardized protocol for repeated social defeat stress in mice. *Nat Protoc* **6**, 1183–1191 (2011).

97. Hollis, F. & Kabbaj, M. Social defeat as an animal model for depression. *ILAR J* **55**, 221–232 (2014).

98. Krishnan, V. & Nestler, E. J. Animal models of depression: Molecular perspectives. *Curr Top Behav Neurosci* **7**, 121–147 (2011).

99. Koolhaas, J. M. *et al.* The resident-intruder paradigm: a standardized test for aggression, violence and social stress. *J Vis Exp* (2013) doi:10.3791/4367.

100. Sgoifo, A. *et al. Social Stress, Autonomic Neural Activation, and Cardiac Activity in Rats*. www.elsevier.com/locate/neubiorev.

101. Wood, S. K. Cardiac autonomic imbalance by social stress in rodents: Understanding putative biomarkers. *Front Psychol* **5**, (2014).

102. Bhatnagar, S., Vining, C., Iyer, V. & Kinni, V. Changes in hypothalamic-pituitary-adrenal function, body temperature, body weight and food intake with repeated social stress exposure in rats. *J Neuroendocrinol* **18**, 13–24 (2006).

103. Wood, S. K., Walker, H. E., Valentino, R. J. & Bhatnagar, S. Individual differences in reactivity to social stress predict susceptibility and resilience to a depressive phenotype: Role of corticotropin-releasing factor. *Endocrinology* **151**, 1795–1805 (2010).

104. Sgoifo, A. *et al. Social Stress, Autonomic Neural Activation, and Cardiac Activity in Rats*. www.elsevier.com/locate/neubiorev.

105. Yang, W., Chen, X., Li, S. & Li, X. J. Genetically modified large animal models for investigating neurodegenerative diseases. *Cell and Bioscience* vol. 11 Preprint at https://doi.org/10.1186/s13578-021-00729-8 (2021).

106. Chaible, L. M., Kinoshita, D., Finzi Corat, M. A. & Zaidan Dagli, M. L. Chapter 27 - Genetically Modified Animal Models. in *Animal Models for the Study of Human Disease (Second*

Edition) (ed. Conn, P. M.) 703–726 (Academic Press, 2017). doi:https://doi.org/10.1016/B978-0-12-809468-6.00027-9.

107. Ortega-De San Luis, C. & Ryan, T. J. Understanding the physical basis of memory: Molecular mechanisms of the engram. *Journal of Biological Chemistry* vol. 298 Preprint at https://doi.org/10.1016/j.jbc.2022.101866 (2022).

108. Minatohara, K., Akiyoshi, M. & Okuno, H. Role of immediate-early genes in synaptic plasticity and neuronal ensembles underlying the memory trace. *Front Mol Neurosci* **8**, (2016).

109. Nambu, M. F., Lin, Y. J., Reuschenbach, J. & Tanaka, K. Z. What does engram encode?: Heterogeneous memory engrams for different aspects of experience. *Current Opinion in Neurobiology* vol. 75 Preprint at https://doi.org/10.1016/j.conb.2022.102568 (2022).

110. Rao-Ruiz, P., Visser, E., Mitrić, M., Smit, A. B. & van den Oever, M. C. A Synaptic Framework for the Persistence of Memory Engrams. *Frontiers in Synaptic Neuroscience* vol. 13 Preprint at https://doi.org/10.3389/fnsyn.2021.661476 (2021).

111. Albo, Z. & Gräff, J. Engram Excitement. *Neuron* **101**, 198–200 (2019).

112. Zhang, T. R. *et al.* Negative memory engrams in the hippocampus enhance the susceptibility to chronic social defeat stress. *Journal of Neuroscience* **39**, 7576–7590 (2019).

113. Tian, X. & Zhou, B. Strategies for site-specific recombination with high efficiency and precise spatiotemporal resolution. *Journal of Biological Chemistry* vol. 296 Preprint at https://doi.org/10.1016/j.jbc.2021.100509 (2021).

114. Hürkey, S. *et al.* Gap junctions desynchronize a neural circuit to stabilize insect flight. *Nature* **618**, 118–125 (2023).

115. Halpern, M. E. *et al. Review Gal4=UAS Transgenic Tools and Their Application to Zebrafish*.

116. Amaral, I. M., Scheffauer, L., Langeder, A. B., Hofer, A. & El Rawas, R. Rewarding social interaction in rats increases camkii in the nucleus accumbens. *Biomedicines* **9**, (2021).

117. Dai, B. *et al.* Responses and functions of dopamine in nucleus accumbens core during social behaviors. *Cell Rep* **40**, (2022).

118. Tseng, Y. T. *et al.* Systematic evaluation of a predator stress model of depression in mice using a hierarchical 3D-motion learning framework. *Transl Psychiatry* **13**, (2023).

119. Komada, M., Takao, K. & Miyakawa, T. Elevated plus maze for mice. *Journal of Visualized Experiments* (2008) doi:10.3791/1088.

120. Crawley, J. & Goodwin, F. K. Preliminary report of a simple animal behavior model for the anxiolytic effects of benzodiazepines. *Pharmacol Biochem Behav* **13**, 167–170 (1980).

121. Kraeuter, A. K., Guest, P. C. & Sarnyai, Z. The Y-Maze for Assessment of Spatial Working and Reference Memory in Mice. in *Methods in Molecular Biology* vol. 1916 105–111 (Humana Press Inc., 2019).

122. Liu, M. Y. *et al.* Sucrose preference test for measurement of stress-induced anhedonia in mice. *Nat Protoc* **13**, 1686–1698 (2018).

123. porsolt1977.

124. Wirkner, J., Ventura-Bort, C., Schwabe, L., Hamm, A. O. & Weymar, M. Chronic stress and emotion: Differential effects on attentional processing and recognition memory. *Psychoneuroendocrinology* **107**, 93–97 (2019).

125. McEwen, B. S. Neurobiological and Systemic Effects of Chronic Stress. *Chronic Stress* vol. 1 Preprint at https://doi.org/10.1177/2470547017692328 (2017).

126. Alves-dos-Santos, L., Resende, L. de S. & Chiavegatto, S. Susceptibility and resilience to chronic social defeat stress in adolescent male mice: No correlation between social avoidance and sucrose preference. *Neurobiol Stress* **12**, (2020).

127. Milic, M., Schmitt, U., Lutz, B. & Müller, M. B. Individual baseline behavioral traits predict the resilience phenotype after chronic social defeat. *Neurobiol Stress* **14**, (2021).

128. Davidson, J. R., Stein, D. J., Shalev, A. Y. & Yehuda, R. *Posttraumatic Stress Disorder: Acquisition, Recognition, Course, and Treatment*. *The Journal of Neuropsychiatry and Clinical Neurosciences* vol. 16 (2004).

129. Hemdahl, A.-L., Caligiuri, G., Hansson, G. K. & Thorén, P. *Electrocardiographic Characterization of Stress-Induced Myocardial Infarction in Atherosclerotic Mice*.

130. Henderson, F., Vialou, V., El Mestikawy, S. & Fabre, V. Effects of social defeat stress on sleep in mice. *Front Behav Neurosci* **11**, (2017).

131. Deichmann, U. Epigenetics: The origins and evolution of a fashionable topic. *Dev Biol* **416**, 249–254 (2016).

132. Waddington, C. H. The epigenotype. 1942. *Int J Epidemiol* **41**, 10–13 (2012).

133. Berger, S. L., Kouzarides, T., Shiekhattar, R. & Shilatifard, A. An operational definition of epigenetics. *Genes Dev* **23**, 781–783 (2009).

134. Fitz-James, M. H. & Cavalli, G. Molecular mechanisms of transgenerational epigenetic inheritance. *Nat Rev Genet* **23**, 325–341 (2022).

135. Moosavi, A. & Ardekani, A. M. Role of epigenetics in biology and human diseases. *Iranian Biomedical Journal* vol. 20 246–258 Preprint at https://doi.org/10.22045/ibj.2016.01 (2016).

136. Dick, A. & Chen, A. The role of TET proteins in stress-induced neuroepigenetic and behavioural adaptations. *Neurobiology of Stress* vol. 15 Preprint at https://doi.org/10.1016/j.ynstr.2021.100352 (2021).

137. Aristizabal, M. J. *et al.* Biological embedding of experience: A primer on epigenetics. *Proceedings of the National Academy of Sciences of the United States of America* vol. 117 23261–23269 Preprint at https://doi.org/10.1073/pnas.1820838116 (2020).

138. Katrinli, S. *et al.* DNA methylation GrimAge acceleration in US military veterans with PTSD. *Neuropsychopharmacology* **48**, 773–780 (2023).

139. Katrinli, S. *et al.* PTSD is associated with increased DNA methylation across regions of HLA-DPB1 and SPATC1L. *Brain Behav Immun* **91**, 429–436 (2021).

140. Yang, R. *et al.* A DNA methylation clock associated with age-related illnesses and mortality is accelerated in men with combat PTSD. *Mol Psychiatry* **26**, 4999–5009 (2021).

141. Feng, S. *et al.* Conservation and divergence of methylation patterning in plants and animals. *Proc Natl Acad Sci U S A* **107**, 8689–8694 (2010).

142. Clemens, A. W. & Gabel, H. W. Emerging Insights into the Distinctive Neuronal Methylome. *Trends in Genetics* vol. 36 816–832 Preprint at https://doi.org/10.1016/j.tig.2020.07.009 (2020).

143. Shipony, Z. *et al.* Dynamic and static maintenance of epigenetic memory in pluripotent and somatic cells. *Nature* **513**, 115–119 (2014).

144. Kim, M. & Costello, J. DNA methylation: An epigenetic mark of cellular memory. *Experimental and Molecular Medicine* vol. 49 Preprint at https://doi.org/10.1038/emm.2017.10 (2017).

145. Mattei, A. L., Bailly, N. & Meissner, A. DNA methylation: a historical perspective. *Trends in Genetics* vol. 38 676–707 Preprint at https://doi.org/10.1016/j.tig.2022.03.010 (2022).

146. Gräff, J. & Mansuy, I. M. Epigenetic codes in cognition and behaviour. *Behavioural Brain Research* vol. 192 70–87 Preprint at https://doi.org/10.1016/j.bbr.2008.01.021 (2008).

147. Moore, L. D., Le, T. & Fan, G. DNA methylation and its basic function. *Neuropsychopharmacology* vol. 38 23–38 Preprint at https://doi.org/10.1038/npp.2012.112 (2013).

148. Parry, A., Rulands, S. & Reik, W. Active turnover of DNA methylation during cell fate decisions. *Nature Reviews Genetics* vol. 22 59–66 Preprint at https://doi.org/10.1038/s41576-020-00287-8 (2021).

149. Jambhekar, A., Dhall, A. & Shi, Y. Roles and regulation of histone methylation in animal development. *Nature Reviews Molecular Cell Biology* vol. 20 625–641 Preprint at https://doi.org/10.1038/s41580-019-0151-1 (2019).

150. Arzumanian, V. A., Dolgalev, G. V., Kurbatov, I. Y., Kiseleva, O. I. & Poverennaya, E. V. Epitranscriptome: Review of Top 25 Most-Studied RNA Modifications. *International Journal of Molecular Sciences* vol. 23 Preprint at https://doi.org/10.3390/ijms232213851 (2022).

151. Kurdyukov, S. & Bullock, M. DNA methylation analysis: Choosing the right method. *Biology* vol. 5 Preprint at https://doi.org/10.3390/biology5010003 (2016).

152. Tost, J. & Gut, I. G. DNA methylation analysis by pyrosequencing. *Nat Protoc* **2**, 2265–2275 (2007).

153. Staunstrup, N. H. *et al.* Genome-wide DNA methylation profiling with MeDIP-seq using archived dried blood spots. *Clin Epigenetics* **8**, (2016).

154. Aberg, K. A., Chan, R. F. & van den Oord, E. J. C. G. MBD-seq - realities of a misunderstood method for high-quality methylome-wide association studies. *Epigenetics* **15**, 431–438 (2020).

155. Olova, N. *et al.* Comparison of whole-genome bisulfite sequencing library preparation strategies identifies sources of biases affecting DNA methylation data. *Genome Biol* **19**, (2018).

156. Perzel Mandell, K. A. *et al.* Genome-wide sequencing-based identification of methylation quantitative trait loci and their role in schizophrenia risk. *Nat Commun* **12**, (2021).

157. Veillard, A. C., Datlinger, P., Laczik, M., Squazzo, S. & Bock, C. Diagenode® Premium RRBS technology: cost-effective DNA methylation mapping with superior coverage. *Nat Methods* **13**, i–ii (2016).

158. Meissner, A. *et al.* Reduced representation bisulfite sequencing for comparative high-resolution DNA methylation analysis. *Nucleic Acids Res* **33**, 5868–5877 (2005).

159. Wiechmann, T. *et al.* Identification of dynamic glucocorticoid-induced methylation changes at the FKBP5 locus. *Clin Epigenetics* **11**, (2019).

160. Mourtzi, N., Sertedaki, A. & Charmandari, E. Glucocorticoid signaling and epigenetic alterations in stress-related disorders. *International Journal of Molecular Sciences* vol. 22 Preprint at https://doi.org/10.3390/ijms22115964 (2021).

161. Ryan, J. *et al.* Investigating the epigenetic profile of the inflammatory gene IL-6 in late-life depression. *BMC Psychiatry* **17**, (2017).

162. Janusek, L. W., Tell, D., Gaylord-Harden, N. & Mathews, H. L. Relationship of childhood adversity and neighborhood violence to a proinflammatory phenotype in emerging adult African American men: An epigenetic link. *Brain Behav Immun* **60**, 126–135 (2017).

163. Roberts, S. *et al.* DNA methylation of FKBP5 and response to exposure-based psychological therapy. *American Journal of Medical Genetics, Part B: Neuropsychiatric Genetics* **180**, 150–158 (2019).

164. Cheng, Z., Su, J., Zhang, K., Jiang, H. & Li, B. Epigenetic Mechanism of Early Life Stress-Induced Depression: Focus on the Neurotransmitter Systems. *Frontiers in Cell and Developmental Biology* vol. 10 Preprint at https://doi.org/10.3389/fcell.2022.929732 (2022).

165. Lin, T. *et al.* The impact and mechanism of methylated metabotropic glutamate receptors 1 and 5 in the hippocampus on depression-like behavior in prenatal stress offspring rats. *J Clin Med* **7**, (2018).

166. Fachim, H. A. *et al.* Early-life stress effects on BDNF DNA methylation in first-episode psychosis and in rats reared in isolation. *Prog Neuropsychopharmacol Biol Psychiatry* **108**, (2021).

167. Levenson, J. M. *et al.* Evidence that DNA (cytosine-5) methyltransferase regulates synaptic plasticity in the hippocampus. *Journal of Biological Chemistry* **281**, 15763–15773 (2006).

168. Heijmans, B. T. *et al. Persistent Epigenetic Differences Associated with Prenatal Exposure to Famine in Humans*. https://www.pnas.org (2008).

169. Efstathopoulos, P. *et al.* NR3C1 hypermethylation in depressed and bullied adolescents. *Transl Psychiatry* **8**, (2018).

170. Cicchetti, D. & Handley, E. D. Methylation of the glucocorticoid receptor gene, nuclear receptor subfamily 3, group C, member 1 (NR3C1), in maltreated and nonmaltreated children: Associations with behavioral undercontrol, emotional lability/negativity, and externalizing and internalizing symptoms. *Dev Psychopathol* **29**, 1795–1806 (2017).

171. Schier, A. C. & Taatjes, D. J. Structure and mechanism of the RNA polymerase II transcription machinery. (2020) doi:10.1101/gad.335679.

172. Aranda-Abreu, G. E., Hernández Aguilar, M. E., Durán, F. R., Mestizo Gutiérrez, S. L. & Denes, J. M. Tau alternative splicing in alzheimer's disease. in *Alternative Splicing and Disease* 39–50 (Nova Science Publishers, Inc., 2016). doi:10.13188/2376-922x.1000010.

173. O'Brien, J., Hayder, H., Zayed, Y. & Peng, C. Overview of microRNA biogenesis, mechanisms of actions, and circulation. *Frontiers in Endocrinology* vol. 9 Preprint at https://doi.org/10.3389/fendo.2018.00402 (2018).

174. Huntzinger, E. & Izaurralde, E. Gene silencing by microRNAs: Contributions of translational repression and mRNA decay. *Nature Reviews Genetics* vol. 12 99–110 Preprint at https://doi.org/10.1038/nrg2936 (2011).

175. Liang, H., Zhang, J., Zen, K., Zhang, C. Y. & Chen, X. Nuclear microRNAs and their unconventional role in regulating non-coding RNAs. *Protein and Cell* vol. 4 325–330 Preprint at https://doi.org/10.1007/s13238-013-3001-5 (2013).

176. Roberts, T. C. The MicroRNA biology of the Mammalian nucleus. *Mol Ther Nucleic Acids* (2014) doi:10.1038/mtna.2014.40.

177. Xiao, M. *et al.* MicroRNAs activate gene transcription epigenetically as an enhancer trigger. *RNA Biol* **14**, 1326–1334 (2017).

178. Tan, H. *et al.* Pan-cancer analysis on microRNA-associated gene activation. *EBioMedicine* **43**, 82–97 (2019).

179. Felger, J. C. & Lotrich, F. E. Inflammatory cytokines in depression: Neurobiological mechanisms and therapeutic implications. *Neuroscience* vol. 246 199–229 Preprint at https://doi.org/10.1016/j.neuroscience.2013.04.060 (2013).

180. Sakai, Y. *et al.* Gene-environment interactions mediate stress susceptibility and resilience through the CaMKIIβ/TARPγ-8/AMPAR pathway. *iScience* **24**, (2021).

181. Dwivedi, Y. *Neuropsychiatric Disease and Treatment Brain-Derived Neurotrophic Factor: Role in Depression and Suicide*. *Neuropsychiatric Disease and Treatment* vol. 5 www.dovepress.com (2009).

182. Hu, X. *et al.* Reduction of BDNF Levels and Biphasic Changes in Glutamate Release in the Prefrontal Cortex Correlate with Susceptibility to Chronic Stress-Induced Anhedonia. *eNeuro* **10**, (2023).

183. Bagot, R. C. C. *et al.* Circuit-wide Transcriptional Profiling Reveals Brain Region-Specific Gene Networks Regulating Depression Susceptibility. *Neuron* (2016) doi:10.1016/j.neuron.2016.04.015.

184. Ortega, M. A. *et al.* Micrornas as critical biomarkers of major depressive disorder: A comprehensive perspective. *Biomedicines* vol. 9 Preprint at https://doi.org/10.3390/biomedicines9111659 (2021).

185. Dwivedi, Y. Emerging role of microRNAs in major depressive disorder: Diagnosis and therapeutic implications. *Dialogues Clin Neurosci* **16**, 43–61 (2014).

186. Wang, J. *et al.* MiR-137 targets the inhibition of TCF4 to reverse the progression of osteoarthritis through the AMPK/NF-κB signaling pathway. *Biosci Rep* **40**, (2020).

187. Smalheiser, N. R. *et al.* MicroRNA expression is down-regulated and reorganized in prefrontal cortex of depressed suicide subjects. *PLoS One* **7**, (2012).

188. Żurawek, D. & Turecki, G. The mirnome of depression. *International Journal of Molecular Sciences* vol. 22 Preprint at https://doi.org/10.3390/ijms222111312 (2021).

189. Xu, J. *et al.* Short- and long-term alterations of FKBP5-GR and specific microRNAs in the prefrontal cortex and hippocampus of male rats induced by adolescent stress contribute to depression susceptibility. *Psychoneuroendocrinology* **101**, 204–215 (2019).

190. Issler, O. *et al.* MicroRNA 135 is essential for chronic stress resiliency, antidepressant efficacy, and intact serotonergic activity. *Neuron* **83**, 344–360 (2014).

191. Żurawek, D. & Turecki, G. The mirnome of depression. *International Journal of Molecular Sciences* vol. 22 Preprint at https://doi.org/10.3390/ijms222111312 (2021).

192. Zhang, Y. *et al.* Dopamine receptor D2 and associated microRNAs are involved in stress susceptibility and resistance to escitalopram treatment. *International Journal of Neuropsychopharmacology* **18**, 1–10 (2015).

193. Zhang, Z., Zhang, J., Diao, L. & Han, L. Small non-coding RNAs in human cancer: function, clinical utility, and characterization. *Oncogene* vol. 40 1570–1577 Preprint at https://doi.org/10.1038/s41388-020-01630-3 (2021).

194. Watson, C. N., Belli, A. & Di Pietro, V. Small non-coding RNAs: New class of biomarkers and potential therapeutic targets in neurodegenerative disease. *Frontiers in Genetics* vol. 10 Preprint at https://doi.org/10.3389/fgene.2019.00364 (2019).

195. Gururajan, A. Stress The impact of chronic stress on the PFC transcriptome: a bioinformatic meta-analysis of publicly available RNA-sequencing datasets The impact of chronic stress on the PFC transcriptome: a bioinformatic meta-analysis of publicly available RNA-sequencing datasets. (2022) doi:10.1080/10253890.2022.2111211.

196. Piantadosi, S. C. *et al.* Transcriptome alterations are enriched for synapse-associated genes in the striatum of subjects with obsessive-compulsive disorder. *Transl Psychiatry* **11**, (2021).

197. Peña, C. J. *et al.* Early life stress alters transcriptomic patterning across reward circuitry in male and female mice. *Nat Commun* **10**, (2019).

198. Rutten, B. P. F. *et al.* Longitudinal analyses of the DNA methylome in deployed military servicemen identify susceptibility loci for post-traumatic stress disorder. *Mol Psychiatry* **23**, 1145–1156 (2018).

199. Hasin, Y., Seldin, M. & Lusis, A. Multi-omics approaches to disease. *Genome Biology* vol. 18 Preprint at https://doi.org/10.1186/s13059-017-1215-1 (2017).

200. Grau, J., Schmidt, F. & Schulz, M. H. Widespread effects of DNA methylation and intra-motif dependencies revealed by novel transcription factor binding models. doi:10.1101/2020.10.21.348193.

201. Lin, Q. X. X. *et al.* Methmotif: An integrative cell specific database of transcription factor binding motifs coupled with DNA methylation profiles. *Nucleic Acids Res* **47**, D145–D154 (2019).

202. Yin, Y. *et al.* Impact of cytosine methylation on DNA binding specificities of human transcription factors. *Science (1979)* **356**, (2017).

203. Martin-Trujillo, A. *et al.* Rare genetic variation at transcription factor binding sites modulates local DNA methylation profiles. *PLoS Genet* **16**, (2020).

204. Medvedeva, Y. A. *et al.* Effects of cytosine methylation on transcription factor binding sites. *BMC Genomics* **15**, (2014).

205. Guo, J. U. *et al.* Neuronal activity modifies the DNA methylation landscape in the adult brain. *nature neurOSCIenCe VOLUME* **14**, (2011).

206. Zhang, T. Y. *et al.* Environmental enrichment increases transcriptional and epigenetic differentiation between mouse dorsal and ventral dentate gyrus. *Nat Commun* **9**, (2018).

207. Yap, E. L. & Greenberg, M. E. Activity-Regulated Transcription: Bridging the Gap between Neural Activity and Behavior. *Neuron* vol. 100 330–348 Preprint at https://doi.org/10.1016/j.neuron.2018.10.013 (2018).

208. Matamales, M. Neuronal activity-regulated gene transcription: How are distant synaptic signals conveyed to the nucleus? *F1000Research* vol. 1 Preprint at https://doi.org/10.12688/f1000research.1-69.v1 (2012).

209. Provençal, N. *et al.* Glucocorticoid exposure during hippocampal neurogenesis primes future stress response by inducing changes in DNA methylation. *Proc Natl Acad Sci U S A* **117**, 23280–23285 (2020).

210. Vasudevan, S. & Steitz, J. A. AU-Rich-Element-Mediated Upregulation of Translation by FXR1 and Argonaute 2. *Cell* **128**, 1105–1118 (2007).

211. Place, R. F., Li, L.-C., Pookot, D., Noonan, E. J. & Dahiya, R. *MicroRNA-373 Induces Expression of Genes with Complementary Promoter Sequences*. www.pnas.org/cgi/content/full/ (2008).

212. Takahashi, H. *et al.* Dynamics of time-lagged gene-to-metabolite networks of Escherichia coli elucidated by integrative omics approach. *OMICS* **15**, 15–23 (2011).

213. Marco, A. *et al.* Mapping the epigenomic and transcriptomic interplay during memory formation and recall in the hippocampal engram ensemble. *Nat Neurosci* **23**, 1606–1617 (2020).

214. Knyazev, G. G., Bocharov, A. V, Savostyanov, A. N. & Proshina, E. A. Effects of Stress and Genetic Predisposition on Symptoms of Psychopathology. *Neurosci Behav Physiol* **53**, 70–80 (2023).

215. Arnau-Soler, A. *et al.* Genome-wide interaction study of a proxy for stress-sensitivity and its prediction of major depressive disorder. *PLoS One* **13**, (2018).

216. Wang, R., Hartman, C. A. & Snieder, H. Stress-related exposures amplify the effects of genetic susceptibility on depression and anxiety. *Transl Psychiatry* **13**, (2023).

217. Schübeler, D. Function and information content of DNA methylation. *Nature* vol. 517 321–326 Preprint at https://doi.org/10.1038/nature14192 (2015).

218. Klengel, T. *et al.* Allele-specific FKBP5 DNA demethylation mediates gene-childhood trauma interactions. *Nat Neurosci* **16**, 33–41 (2013).

219. Kline, S. A. & Mega, M. S. Stress-Induced Neurodegeneration: The Potential for Coping as Neuroprotective Therapy. *American Journal of Alzheimer's Disease and other Dementias* vol. 35 Preprint at https://doi.org/10.1177/1533317520960873 (2020).

220. Kivimäki, M. & Kawachi, I. Work Stress as a Risk Factor for Cardiovascular Disease. *Current Cardiology Reports* vol. 17 Preprint at https://doi.org/10.1007/s11886-015-0630-8 (2015).

221. Yang, T. *et al.* Work stress and the risk of cancer: A meta-analysis of observational studies. *Int J Cancer* **144**, 2390–2400 (2019).

222. Bromis, K., Calem, M., Reinders, A. A. T. S., Williams, S. C. R. & Kempton, M. J. Meta-Analysis of 89 Structural MRI studies in posttraumatic stress disorder and comparison with major depressive disorder. *American Journal of Psychiatry* **175**, 989–998 (2018).

223. Katmah, R. *et al.* A review on mental stress assessment methods using eeg signals. *Sensors* vol. 21 Preprint at https://doi.org/10.3390/s21155043 (2021).

224. Ramaker, R. C. *et al.* Post-mortem molecular profiling of three psychiatric disorders. *Genome Med* **9**, (2017).

225. Rahman, M. F. & McGowan, P. O. Cell-type-specific epigenetic effects of early life stress on the brain. *Translational Psychiatry* vol. 12 Preprint at https://doi.org/10.1038/s41398-022-02076-9 (2022).

226. Mathys, H. *et al.* Single-cell transcriptomic analysis of Alzheimer's disease. *Nature* **570**, 332–337 (2019).

227. Doostparast Torshizi, A., Duan, J. & Wang, K. Cell-Type-Specific Proteogenomic Signal Diffusion for Integrating Multi-Omics Data Predicts Novel Schizophrenia Risk Genes. *Patterns* **1**, (2020).

228. Skene, N. G. *et al.* Genetic identification of brain cell types underlying schizophrenia. *Nat Genet* **50**, 825–833 (2018).

229. Velmeshev, D. *et al.* Single-cell genomics identifies cell type–specific molecular changes in autism. *Science (1979)* **364**, 685–689 (2019).

230. Finkelstein, A. B. *et al.* Social reactivation of fear engrams enhances memory recall. (2022) doi:10.1073/pnas.

231. Roy, D. S. *et al.* Brain-wide mapping reveals that engrams for a single memory are distributed across multiple brain regions. *Nat Commun* **13**, (2022).

232. Josselyn, S. A. & Tonegawa, S. Memory engrams: Recalling the past and imagining the future. *Science* vol. 367 Preprint at https://doi.org/10.1126/science.aaw4325 (2020).

233. Liu, X. *et al.* Optogenetic stimulation of a hippocampal engram activates fear memory recall. *Nature* (2012) doi:10.1038/nature11028.

234. Qin, H., Niu, T. & Zhao, J. Identifying multi-omics causers and causal pathways for complex traits. *Front Genet* **10**, (2019).

235. Mohammadi-Shemirani, P., Sood, T. & Paré, G. From 'Omics to Multi-omics Technologies: the Discovery of Novel Causal Mediators. *Current Atherosclerosis Reports* vol. 25 55–65 Preprint at https://doi.org/10.1007/s11883-022-01078-8 (2023).

236. Wang, R. S., Maron, B. A. & Loscalzo, J. Multiomics Network Medicine Approaches to Precision Medicine and Therapeutics in Cardiovascular Diseases. *Arterioscler Thromb Vasc Biol* **43**, 493–503 (2023).

237. von Ziegler, L. M. *et al.* Multiomic profiling of the acute stress response in the mouse hippocampus. *Nat Commun* **13**, (2022).

238. Subramanian, I., Verma, S., Kumar, S., Jere, A. & Anamika, K. Multi-omics Data Integration, Interpretation, and Its Application. *Bioinformatics and Biology Insights* vol. 14 Preprint at https://doi.org/10.1177/1177932219899051 (2020).

239. Misiewicz, Z. *et al.* Multi-omics analysis identifies mitochondrial pathways associated with anxiety-related behavior. *PLoS Genet* **15**, (2019).

240. Niu, L. *et al.* Defining NASH from a Multi-Omics Systems Biology Perspective. *J Clin Med* **10**, 4673 (2021).

241. Denny, C. A. *et al.* Hippocampal Memory Traces Are Differentially Modulated by Experience, Time, and Adult Neurogenesis. *Neuron* **83**, 189–201 (2014).

242. Guenthner, C. J., Miyamichi, K., Yang, H. H., Heller, H. C. & Luo, L. Permanent genetic access to transiently active neurons via TRAP: Targeted recombination in active populations. *Neuron* (2013) doi:10.1016/j.neuron.2013.03.025.

243. Mo, A. *et al.* Epigenomic Signatures of Neuronal Diversity in the Mammalian Brain. *Neuron* **86**, 1369–1384 (2015).

244. Vennin, C. *et al.* A Resilience Related Glial-Neurovascular Network Is Transcriptionally Activated after Chronic Social Defeat in Male Mice. *Cells* **11**, (2022).

245. Xu, P. *et al.* A Systematic Way to Infer the Regulation Relations of miRNAs on Target Genes and Critical miRNAs in Cancers. *Front Genet* **11**, (2020).

246. Gerber, S. *et al.* Characterization of transcriptional proles associated with stress-induced neuronal activation in Arc-GFP mice. (2023) doi:10.21203/rs.3.rs-3273083/v1.

247. Han, D. H., Park, P., Choi, D. Il, Bliss, T. V. P. & Kaang, B.-K. The essence of the engram: Cellular or synaptic? *Semin Cell Dev Biol* **125**, 122–135 (2022).

248. Ryan, T. J., Ortega-de San Luis, C., Pezzoli, M. & Sen, S. Engram cell connectivity: an evolving substrate for information storage. *Curr Opin Neurobiol* **67**, 215–225 (2021).

249. Jiang, Y. & Van Dongen, A. M. J. Selective increase of correlated activity in arc-positive neurons after chemically induced long-term potentiation in cultured hippocampal neurons. *eNeuro* **8**, (2021).

250. Ons, S., Martí, O. & Armario, A. Stress-induced activation of the immediate early gene Arc (activity-regulated cytoskeleton-associated protein) is restricted to telencephalic areas in the rat brain: Relationship to c-fos mRNA. *J Neurochem* (2004) doi:10.1111/j.1471-4159.2004.02396.x.

251. Guzowski, J. F., Setlow, B., Wagner, E. K. & Mcgaugh, J. L. *Experience-Dependent Gene Expression in the Rat Hippocampus after Spatial Learning: A Comparison of the Immediate-Early Genes Arc, c-Fos, and Zif268*. (2001).

252. Terleph, T. A. & Tremere, L. A. *The Use of Immediate Early Genes as Mapping Tools for Neuronal Activation: Concepts and Methods*.

253. Raju, K. S. R. *et al.* No effect on pharmacokinetics of tamoxifen and 4-hydroxytamoxifen by multiple doses of red clover capsule in rats. *Sci Rep* **5**, (2015).

254. Fernandez-Albert, J. *et al.* Immediate and deferred epigenomic signatures of in vivo neuronal activation in mouse hippocampus. *Nat Neurosci* **22**, 1718–1730 (2019).

255. Brinks, V., Van Der Mark, M., De Kloet, R. & Oitzl, M. Emotion and cognition in high and low stress sensitive mouse strains: a combined neuroendocrine and behavioral study in BALB/c and C57BL/6J mice. doi:10.3389/neuro.08/008.2007.

256. Mozhui, K. *et al.* Strain differences in stress responsivity are associated with divergent amygdala gene expression and glutamate-mediated neuronal excitability. *Journal of Neuroscience* **30**, 5357–5367 (2010).

257. Guilherme, M. D. S. *et al.* Resilience and the Gut Microbiome: Insights from Chronically Socially Stressed Wild-Type Mice. *Microorganisms* **10**, (2022).

258. Palacios, J., Yildiz, A., Young, A. H. & Taylor, M. J. Tamoxifen for bipolar disorder: Systematic review and meta-analysis. *Journal of Psychopharmacology* **33**, 177–184 (2019).

259. Choleris, E. *et al. An Estrogen-Dependent Four-Gene Micronet Regulating Social Recognition: A Study with Oxytocin and Estrogen Receptor-and-Knockout Mice*. *PNAS May* vol. 13 www.pnas.orgcgidoi10.1073pnas.0631699100 (2003).

260. Laredo, S. A., Villalon Landeros, R. & Trainor, B. C. Rapid effects of estrogens on behavior: Environmental modulation and molecular mechanisms. *Frontiers in Neuroendocrinology* vol. 35 447–458 Preprint at https://doi.org/10.1016/j.yfrne.2014.03.005 (2014).

261. Tang, A. C. *et al.* Effects of long-term estrogen replacement on social investigation and social memory in ovariectomized C57BL/6 mice. *Horm Behav* **47**, 350–357 (2005).

262. Li, X. *et al.* The effects of tamoxifen on mouse behavior. *Genes Brain Behav* **19**, (2020).

263. Mikedis, M. M. & Downs, K. M. Chapter One - Mouse Primordial Germ Cells: A Reappraisal. in *International Review of Cell and Molecular Biology* (ed. Jeon, K. W.) vol. 309 1–57 (Academic Press, 2014).

264. Galvano, E. *et al.* Behavioral and transcriptomic effects of the cancer treatment tamoxifen in mice. *Front Neurosci* **17**, (2023).

265. Özakman, S. *et al.* Effects of tamoxifen and glutamate and glutamine levels in brain regions in repeated sleep deprivation–induced mania model in mice. *Naunyn Schmiedebergs Arch Pharmacol* **394**, 619–629 (2021).

266. Blum, K. M. *et al.* Sex and Tamoxifen confound murine experimental studies in cardiovascular tissue engineering. *Sci Rep* **11**, (2021).

267. Novick, A. M., Scott, A. T., Neill Epperson, C. & Schneck, C. D. Neuropsychiatric effects of tamoxifen: Challenges and opportunities. *Frontiers in Neuroendocrinology* vol. 59 Preprint at https://doi.org/10.1016/j.yfrne.2020.100869 (2020).

268. Pandey, D., Banerjee, S., Basu, M. & Mishra, N. Memory enhancement by Tamoxifen on amyloidosis mouse model. *Horm Behav* **79**, 70–73 (2016).

269. Smith, B. M. *et al.* Oral and Injected Tamoxifen Alter Adult Hippocampal Neurogenesis in Female and Male Mice. *eNeuro* **9**, (2022).

270. Katholnig Karl and Poglitsch, M. and H. M. and W. T. Lysis Gradient Centrifugation: A Flexible Method for the Isolation of Nuclei from Primary Cells. in *The Nucleus* (ed. Hancock, R.) 15–23 (Springer New York, New York, NY, 2015). doi:10.1007/978-1-4939-1680-1_2.

271. Blobel, G. & Potter, V. R. Nuclei from Rat Liver: Isolation Method That Combines Purity with High Yield. *Science (1979)* **154**, 1662–1665 (1966).

272. Krishnaswami, S. R. *et al.* Using single nuclei for RNA-seq to capture the transcriptome of postmortem neurons. *Nat Protoc* **11**, 499–524 (2016).

273. Graham, J. M. Isolation of nuclei and nuclear membranes from animal tissues. *Current protocols in cell biology / editorial board, Juan S. Bonifacino ... [et al.]* vol. Chapter 3 Preprint at https://doi.org/10.1002/0471143030.cb0310s12 (2001).

274. OptiPrep. *OptiPrep™ The Ideal Density Gradient Medium for Purification of Subcellular Organelles*. https://www.axis-shield-density-gradient-media.com/S10.pdf.

275. Caille, N., Thoumine, O., Tardy, Y. & Meister, J.-J. *Contribution of the Nucleus to the Mechanical Properties of Endothelial Cells*. *Journal of Biomechanics* vol. 35 (2002).

276. thoumine1999.

277. Tan, S. J., Li, Q. & Lim, C. T. Manipulation and Isolation of Single Cells and Nuclei. *Methods Cell Biol* **98**, 79–96 (2010).

278. Chongtham MC, Todorov H, Wettschereck JE, Gerber S & Winter J. Isolation of nuclei and downstream processing of cell-type-specific nuclei from micro-dissected mouse brain regions – techniques and caveats. doi:10.1101/2020.11.18.374223.

279. Schindelin, J. *et al.* Fiji: An open-source platform for biological-image analysis. *Nature Methods* vol. 9 676–682 Preprint at https://doi.org/10.1038/nmeth.2019 (2012).

280. Lovtrup-Rein, H. & Mcewen, B. S. Isolation and fractionation of rat brain nuclei. *Journal of Cell Biology* **30**, 404–415 (1966).

281. Liao, P. C., Bergamini, C., Fato, R., Pon, L. A. & Pallotti, F. Isolation of mitochondria from cells and tissues. in *Methods in Cell Biology* vol. 155 3–31 (Academic Press Inc., 2020).

282. Wilczok, T. & Chorazy, K. Isolation of Liver Nuclei. *Nature* **188**, 516–517 (1960).

283. Graham, J. M. Rapid purification of nuclei from animal and plant tissues and cultured cells. *ScientificWorldJournal* **2**, 1551–1554 (2002).

284. Mita, A. *et al.* Antiproinflammatory effects of iodixanol (OptiPrep)-based density gradient purification on human islet preparations. *Cell Transplant* **19**, 1537–1546 (2010).

285. Cantin, R., Diou, J., Bélanger, D., Tremblay, A. M. & Gilbert, C. Discrimination between exosomes and HIV-1: Purification of both vesicles from cell-free supernatants. *J Immunol Methods* **338**, 21–30 (2008).

286. Van Veldhoven, P. P., Baumgart, E. & Mannaerts, G. P. *Iodixanol (Optiprep), an Improved Density Gradient Medium for the Iso-Osmotic Isolation of Rat Liver Peroxisomes*. *ANALYTICAL BIOCHEMISTRY* vol. 237 (1996).

287. Tauro, B. J. *et al.* Comparison of ultracentrifugation, density gradient separation, and immunoaffinity capture methods for isolating human colon cancer cell line LIM1863-derived exosomes. *Methods* **56**, 293–304 (2012).

288. Marion-Poll, L., Montalban, E., Munier, A., Hervé, D. & Girault, J. A. Fluorescence-activated sorting of fixed nuclei: A general method for studying nuclei from specific cell populations that preserves post-translational modifications. *European Journal of Neuroscience* **39**, 1234–1244 (2014).

289. Onódi, Z. *et al.* Isolation of high-purity extracellular vesicles by the combination of iodixanol density gradient ultracentrifugation and bind-elute chromatography from blood plasma. *Front Physiol* **9**, (2018).

290. Kovacovicova, K. & Vinciguerra, M. Isolation of senescent cells by iodixanol (OptiPrep) density gradient-based separation. *Cell Prolif* **52**, (2019).

291. Quasem, I., Luby, C. J., Mace, C. R. & Fuchs, S. M. Density separation of quiescent yeast using iodixanol. *Biotechniques* **63**, 169–173 (2017).

292. Erö, C., Gewaltig, M. O., Keller, D. & Markram, H. A cell atlas for the mouse brain. *Front Neuroinform* **12**, (2018).

293. Herculano-Houzel, S., Messeder, D. J., Fonseca-Azevedo, K. & Pantoja, N. A. When larger brains do not have more neurons: Increased numbers of cells are compensated by decreased average cell size across mouse individuals. *Front Neuroanat* **9**, (2015).

294. Herculano-Houzel, S., Mota, B. & Lent, R. Cellular scaling rules for rodent brains. *Proceedings of the National Academy of Sciences of he United States of America* **103**, 12138–12143 (2006).

295. Murakami, T. C. *et al.* A three-dimensional single-cell-resolution whole-brain atlas using CUBIC-X expansion microscopy and tissue clearing. *Nat Neurosci* **21**, 625–637 (2018).

296. Chen, P. B. *et al.* Mapping gene expression in excitatory neurons during hippocampal late-phase long-term potentiation. *Front Mol Neurosci* **10**, (2017).

297. Williams, R. W. *Mapping Genes That Modulate Mouse Brain Development: A Quantitative Genetic Approach*. http://nervenet.org.

298. Yu, P., Mckinney, E. C., Kandasamy, M. M., Albert, A. L. & Meagher, R. B. Characterization of brain cell nuclei with decondensed chromatin. *Dev Neurobiol* **75**, 738–756 (2015).

299. Sporn, M. B., Wanko, T. & Dingman, W. *THE ISOLATION OF CELL NUCLEI FROM RAT BRAIN*. *Journal of Cell Biology* vol. 15 109–120 (1962).

300. 10xGenomics. What are the best practices for working with nuclei samples for 3' single-cell gene expression? https://kb.10xgenomics.com/hc/en-us/articles/360050780051-What-are-the-best-practices-for-working-with-nuclei-samples-for-3-single-cell-gene-expression-.

301. Maitra, M. *et al.* Extraction of nuclei from archived postmortem tissues for single-nucleus sequencing applications. *Nature Protocols* vol. 16 2788–2801 Preprint at https://doi.org/10.1038/s41596-021-00514-4 (2021).

302. Livshits, M. A. *et al.* Vavilova str., Moscow, 119991, Russia. 2 Fededal Research and Clinical Center of Physical-Chemical Medicine, 1a, Malaya Pirogovskaya str. *Nature Publishing Group* **32**, (2015).

303. Liu, P. Y. *et al.* Cell refractive index for cell biology and disease diagnosis: Past, present and future. *Lab on a Chip* vol. 16 634–644 Preprint at https://doi.org/10.1039/c5lc01445j (2016).

304. Peterson, B. W., Sharma, P. K., van der Mei, H. C. & Busscher, H. J. Bacterial cell surface damage due to centrifugal compaction. *Appl Environ Microbiol* **78**, 120–125 (2012).

305. Yamashita, T., Takahashi, Y., Nishikawa, M. & Takakura, Y. Effect of exosome isolation methods on physicochemical properties of exosomes and clearance of exosomes from the blood circulation. *European Journal of Pharmaceutics and Biopharmaceutics* **98**, 1–8 (2016).

306. Duong, P., Chung, A., Bouchareychas, L. & Raffai, R. L. Cushioned-Density Gradient Ultracentrifugation (C-DGUC) improves the isolation efficiency of extracellular vesicles. *PLoS One* **14**, (2019).

307. Livshts, M. A. *et al.* Isolation of exosomes by differential centrifugation: Theoretical analysis of a commonly used protocol. *Sci Rep* **5**, (2015).

308. Linares, R., Tan, S., Gounou, C., Arraud, N. & Brisson, A. R. High-speed centrifugation induces aggregation of extracellular vesicles. *J Extracell Vesicles* **4**, (2015).

309. Huh, S., Fei, D., Ker, E., Su, H. & Kanade, T. *Apoptosis Detection for Adherent Cell Populations in Time-Lapse Phase-Contrast Microscopy Images*. *Medical image computing and computer-assisted intervention : MICCAI ... International Conference on Medical Image Computing and Computer-Assisted Intervention,* vol. 15 331–339 (2012).

310. Jeppesen, D. K. *et al.* Comparative analysis of discrete exosome fractions obtained by differential centrifugation. *J Extracell Vesicles* **3**, (2014).

311. Kurdzinski, M. E. *et al.* Dynamics of high viscosity contrast confluent microfluidic flows. *Sci Rep* **7**, (2017).

312. Dammer, E. B. *et al.* Neuron enriched nuclear proteome isolated from human brain. *J Proteome Res* **12**, 3193–3206 (2013).

313. Whytock, K. L. *et al.* Isolation of nuclei from frozen human subcutaneous adipose tissue for full-length single-nuclei transcriptional profiling. *STAR Protoc* **4**, (2023).

314. Nadelmann, E. R. *et al.* Isolation of Nuclei from Mammalian Cells and Tissues for Single-Nucleus Molecular Profiling. *Curr Protoc* **1**, (2021).

315. Nott, A., Schlachetzki, J. C. M., Fixsen, B. R. & Glass, C. K. Nuclei isolation of multiple brain cell types for omics interrogation. *Nat Protoc* **16**, 1629–1646 (2021).

316. Daniels, R. R. *et al.* A versatile nuclei extraction protocol for single nucleus sequencing in non-model species–Optimization in various Atlantic salmon tissues. *PLoS One* **18**, (2023).

317. Haenni, S. *et al.* Analysis of C. elegans intestinal gene expression and polyadenylation by fluorescence-activated nuclei sorting and 3'-end-seq. *Nucleic Acids Res* **40**, 6304–6318 (2012).

318. Moreno-Romero, J., Santos-González, J., Hennig, L. & Köhler, C. Applying the INTACT method to purify endosperm nuclei and to generate parental-specific epigenome profiles. *Nat Protoc* (2017) doi:10.1038/nprot.2016.167.

319. Wang, D. & Deal, R. B. Epigenome profiling of specific plant cell types using a streamlined INTACT protocol and ChIP-seq. in *Plant Functional Genomics: Methods and Protocols: Second Edition* (2015). doi:10.1007/978-1-4939-2444-8_1.

320. Deal, R. B. & Henikoff, S. *A Simple Method for Gene Expression and Chromatin Profiling of Individual Cell Types within a Tissue*. (2010).

321. Holt, L. M. & Olsen, M. L. Novel applications of magnetic cell sorting to analyze cell-type specific gene and protein expression in the central nervous system. *PLoS One* **11**, (2016).

322. Box, A. *et al.* Evaluating the Effects of Cell Sorting on Gene Expression. (2020) doi:10.7171/jbt.20203103004.

323. Llufrio, E. M., Wang, L., Naser, F. J. & Patti, G. J. Sorting cells alters their redox state and cellular metabolome. *Redox Biol* **16**, 381–387 (2018).

324. Binek, A. *et al. Flow Cytometry Has a Significant Impact on the Cellular Metabolome*. *J. Proteome Res., Just Accepted Manuscript • Publication Date* http://pubs.acs.org (2018).

325. Andrä, I. *et al.* An Evaluation of T-Cell Functionality After Flow Cytometry Sorting Revealed p38 MAPK Activation. *Cytometry Part A* **97**, 171–183 (2020).

326. Bohlen, C. J., Bennett, F. C. & Bennett, M. L. Isolation and Culture of Microglia. *Curr Protoc Immunol* **125**, (2019).

327. Handley, A., Schauer, T., Ladurner, A. G. & Margulies, C. E. Designing Cell-Type-Specific Genome-wide Experiments. *Molecular Cell* vol. 58 621–631 Preprint at https://doi.org/10.1016/j.molcel.2015.04.024 (2015).

328. Chitikova, Z. & Steiner, F. A. Cell type-specific epigenome profiling using affinity-purified nuclei. *Genesis* vol. 54 160–169 Preprint at https://doi.org/10.1002/dvg.22919 (2016).

329. Chongtham, M. C., Butto, T., Mungikar, K., Gerber, S. & Winter, J. Intact vs. Fans for cell-type-specific nuclei sorting: A comprehensive qualitative and quantitative comparison. *Int J Mol Sci* **22**, (2021).

330. Webster, M., Wikin, K. L. & Cohen-Fix, O. Sizing up the nucleus: Nuclear shape, size and nuclear-envelope assembly. *Journal of Cell Science* vol. 122 1477–1486 Preprint at https://doi.org/10.1242/jcs.037333 (2009).

331. Young, I. T., Verbeek, P. W. & Mayall, B. H. Characterization of chromatin distribution in cell nuclei. *Cytometry* **7**, 467–474 (1986).

332. Schreiner, S. M., Koo, P. K., Zhao, Y., Mochrie, S. G. J. & King, M. C. The tethering of chromatin to the nuclear envelope supports nuclear mechanics. *Nat Commun* **6**, (2015).

333. Stephens, A. D., Banigan, E. J., Adam, S. A., Goldman, R. D. & Marko, J. F. Chromatin and lamin a determine two different mechanical response regimes of the cell nucleus. *Mol Biol Cell* **28**, 1984–1996 (2017).

334. Dahl, K. N., Ribeiro, A. J. S. & Lammerding, J. Nuclear shape, mechanics, and mechanotransduction. *Circulation Research* vol. 102 1307–1318 Preprint at https://doi.org/10.1161/CIRCRESAHA.108.173989 (2008).

335. Lima, A. F. *et al.* Osmotic modulation of chromatin impacts on efficiency and kinetics of cell fate modulation. *Sci Rep* **8**, (2018).

336. Shu, Y. & Xu, T. Chronic Social Defeat Stress Modulates Dendritic Spines Structural Plasticity in Adult Mouse Frontal Association Cortex. *Neural Plast* **2017**, (2017).

337. Colyn, L., Venzala, E., Marco, S., Perez-Otaño, I. & Tordera, R. M. Chronic social defeat stress induces sustained synaptic structural changes in the prefrontal cortex and amygdala. *Behavioural Brain Research* **373**, 112079 (2019).

338. Okamura, H. *et al.* Long-Term Effects of Repeated Social Defeat Stress on Brain Activity during Social Interaction in BALB/c Mice. *eNeuro* **9**, (2022).

339. Han, Q. Q. *et al.* Differential GR expression and translocation in the hippocampus mediates susceptibility vs. resilience to chronic social defeat stress. *Front Neurosci* **11**, (2017).

340. Hammels, C. *et al.* Differential susceptibility to chronic social defeat stress relates to the number of Dnmt3a-immunoreactive neurons in the hippocampal dentate gyrus. *Psychoneuroendocrinology* **51**, 547–556 (2015).

341. Bonnefil, V. *et al.* Region-specific myelin differences define behavioral consequences of chronic social defeat stress in mice. (2019) doi:10.7554/eLife.40855.001.

342. Rowson, S. A. *et al.* Chronic adolescent stress sex-specifically alters the hippocampal transcriptome in adulthood. (2019) doi:10.1038/s41386-019-0321-z.

343. Girgenti, M. J., Pothula, S. & Newton, S. S. Stress and Its Impact on the Transcriptome. *Biological Psychiatry* vol. 90 102–108 Preprint at https://doi.org/10.1016/j.biopsych.2020.12.011 (2021).

344. van Marle, H. PTSD as a memory disorder. *Eur J Psychotraumatol* **6**, (2015).

345. Nelson, C. A. Hazards to Early Development: The Biological Embedding of Early Life Adversity. *Neuron* vol. 96 262–266 Preprint at https://doi.org/10.1016/j.neuron.2017.09.027 (2017).

346. Li, M. *et al.* Effect of Early Life Stress on the Epigenetic Profiles in Depression. *Frontiers in Cell and Developmental Biology* vol. 8 Preprint at https://doi.org/10.3389/fcell.2020.00867 (2020).

347. Rodgers, A. B., Morgan, C. P., Leu, N. A. & Bale, T. L. Transgenerational epigenetic programming via sperm microRNA recapitulates effects of paternal stress. *Proc Natl Acad Sci U S A* **112**, 13699–13704 (2015).

348. Zheng, Y. *et al.* Multi-omics data integration using ratio-based quantitative profiling with Quartet reference materials. *Nat Biotechnol* (2023) doi:10.1038/s41587-023-01934-1.

349. Wu, L., Zhu, J., Liu, D., Sun, Y. & Wu, C. An integrative multiomics analysis identifies putative causal genes for COVID-19 severity. *Genetics in Medicine* **23**, 2076–2086 (2021).

350. Scott, K. A., Melhorn, S. J. & Sakai, R. R. Effects of Chronic Social Stress on Obesity. *Curr Obes Rep* **1**, 16–25 (2012).

351. Krueger, F. & Andrews, S. R. Bismark: A flexible aligner and methylation caller for Bisulfite-Seq applications. *Bioinformatics* **27**, 1571–1572 (2011).

352. Akalin, A. *et al.* MethylKit: a comprehensive R package for the analysis of genome-wide DNA methylation profiles. *Genome Biol* **13**, (2012).

353. Cavalcante, R. G. & Sartor, M. A. Annotatr: Genomic regions in context. *Bioinformatics* **33**, 2381–2383 (2017).

354. Xie, Z. *et al.* Gene Set Knowledge Discovery with Enrichr. *Curr Protoc* **1**, (2021).

355. Chen, E. Y. *et al. Enrichr: Interactive and Collaborative HTML5 Gene List Enrichment Analysis Tool*. http://amp.pharm.mssm.edu/Enrichr. (2013).

356. Kuleshov, M. V. *et al.* Enrichr: a comprehensive gene set enrichment analysis web server 2016 update. *Nucleic Acids Res* **44**, W90–W97 (2016).

357. Rozowsky, J. *et al.* exceRpt: A Comprehensive Analytic Platform for Extracellular RNA Profiling. *Cell Syst* **8**, 352-357.e3 (2019).

358. Love, M. I., Huber, W. & Anders, S. Moderated estimation of fold change and dispersion for RNA-seq data with DESeq2. *Genome Biol* **15**, (2014).

359. Robinson, M. D., McCarthy, D. J. & Smyth, G. K. edgeR: A Bioconductor package for differential expression analysis of digital gene expression data. *Bioinformatics* **26**, 139–140 (2009).

360. Yu, G., Wang, L. G., Han, Y. & He, Q. Y. ClusterProfiler: An R package for comparing biological themes among gene clusters. *OMICS* **16**, 284–287 (2012).

361. Gao, T. & Qian, J. EnhancerAtlas 2.0: An updated resource with enhancer annotation in 586 tissue/cell types across nine species. *Nucleic Acids Res* **48**, D58–D64 (2020).

362. Zocher, S., Overall, R. W., Lesche, M., Dahl, A. & Kempermann, G. Environmental enrichment preserves a young DNA methylation landscape in the aged mouse hippocampus. *Nat Commun* **12**, (2021).

363. Li, Y. E. *et al.* An atlas of gene regulatory elements in adult mouse cerebrum. *Nature* **598**, 129–136 (2021).

364. Heinz, S. *et al.* Simple Combinations of Lineage-Determining Transcription Factors Prime cis-Regulatory Elements Required for Macrophage and B Cell Identities. *Mol Cell* **38**, 576–589 (2010).

365. Szklarczyk, D. *et al.* The STRING database in 2021: Customizable protein-protein networks, and functional characterization of user-uploaded gene/measurement sets. *Nucleic Acids Res* **49**, D605–D612 (2021).

366. Szklarczyk, D. *et al.* STRING v11: Protein-protein association networks with increased coverage, supporting functional discovery in genome-wide experimental datasets. *Nucleic Acids Res* **47**, D607–D613 (2019).

367. Szklarczyk, D. *et al.* The STRING database in 2023: protein-protein association networks and functional enrichment analyses for any sequenced genome of interest. *Nucleic Acids Res* **51**, D638–D646 (2023).

368. Chin, C. H. *et al.* cytoHubba: Identifying hub objects and sub-networks from complex interactome. *BMC Syst Biol* **8**, (2014).

369. Shannon, P. *et al.* Cytoscape: A software Environment for integrated models of biomolecular interaction networks. *Genome Res* **13**, 2498–2504 (2003).

370. Lutz, P. E. *et al.* Non-CG methylation and multiple histone profiles associate child abuse with immune and small GTPase dysregulation. *Nat Commun* **12**, (2021).

371. Wei, J. *et al.* DNA Methyltransferase 3A Is Involved in the Sustained Effects of Chronic Stress on Synaptic Functions and Behaviors. *Cerebral Cortex* **31**, 1998–2012 (2021).

372. Halder, R. *et al.* DNA methylation changes in plasticity genes accompany the formation and maintenance of memory. *Nat Neurosci* **19**, 102–110 (2015).

373. Michels, K. B. *et al.* Recommendations for the design and analysis of epigenome-wide association studies. *Nature Methods* vol. 10 949–955 Preprint at https://doi.org/10.1038/nmeth.2632 (2013).

374. Xie, Z. *et al.* Gene Set Knowledge Discovery with Enrichr. *Curr Protoc* **1**, (2021).

375. Wei, G. H. *et al.* Genome-wide analysis of ETS-family DNA-binding in vitro and in vivo. *EMBO Journal* **29**, 2147–2160 (2010).

376. Costello, P. *et al.* Ternary Complex Factors SAP-1 and Elk-1, but Not Net, Are Functionally Equivalent in Thymocyte Development. *The Journal of Immunology* **185**, 1082–1092 (2010).

377. Hollenhorst, P. C. RAS/ERK pathway transcriptional regulation through ETS/AP-1 binding sites. *Small GTPases* **3**, 154–158 (2012).

378. Flavell, S. W. & Greenberg, M. E. Signaling mechanisms linking neuronal activity to gene expression and plasticity of the nervous system. *Annual Review of Neuroscience* vol. 31 563–590 Preprint at https://doi.org/10.1146/annurev.neuro.31.060407.125631 (2008).

379. Qin, Y. *et al.* State-dependent Ras signaling and AMPA receptor trafficking. *Genes Dev* **19**, 2000–2015 (2005).

380. Pavlowsky, A., Chelly, J. & Billuart, P. Emerging major synaptic signaling pathways involved in intellectual disability. *Molecular Psychiatry* vol. 17 682–693 Preprint at https://doi.org/10.1038/mp.2011.139 (2012).

381. Chen, Q. Y. *et al.* Presynaptic long-term potentiation requires extracellular signal-regulated kinases in the anterior cingulate cortex. *Molecular Pain* vol. 16 Preprint at https://doi.org/10.1177/1744806920917245 (2020).

382. Emmert-Streib, F., Dehmer, M. & Haibe-Kains, B. Gene regulatory networks and their applications: Understanding biological and medical problems in terms of networks. *Frontiers in Cell and Developmental Biology* vol. 2 Preprint at https://doi.org/10.3389/fcell.2014.00038 (2014).

383. He, X. & Zhang, J. Why do hubs tend to be essential in protein networks? *PLoS Genet* **2**, 0826–0834 (2006).

384. Mistry, J. *et al.* Pfam: The protein families database in 2021. *Nucleic Acids Res* **49**, D412–D419 (2021).

385. Letunic, I. & Bork, P. 20 years of the SMART protein domain annotation resource. *Nucleic Acids Res* **46**, D493–D496 (2018).

386. Musazzi, L., Mingardi, J., Ieraci, A., Barbon, A. & Popoli, M. Stress, microRNAs, and stress-related psychiatric disorders: an overview. *Mol Psychiatry* (2023) doi:10.1038/s41380-023-02139-3.

387. Hu, Z. & Li, Z. miRNAs in synapse development and synaptic plasticity. *Current Opinion in Neurobiology* vol. 45 24–31 Preprint at https://doi.org/10.1016/j.conb.2017.02.014 (2017).

388. Rouillard, A. D. *et al.* The harmonizome: a collection of processed datasets gathered to serve and mine knowledge about genes and proteins. *Database (Oxford)* **2016**, (2016).

389. Fan, T., Hu, Y., Xin, J., Zhao, M. & Wang, J. Analyzing the genes and pathways related to major depressive disorder via a systems biology approach. *Brain Behav* **10**, (2020).

390. Scarpa, J. R. *et al.* Shared Transcriptional Signatures in Major Depressive Disorder and Mouse Chronic Stress Models. *Biol Psychiatry* **88**, 159–168 (2020).

391. Gammie, S. C. Creation of a gene expression portrait of depression and its application for identifying potential treatments. *Sci Rep* **11**, (2021).

392. Wang, M., Gallo, N. B., Tai, Y., Li, B. & Van Aelst, L. Oligophrenin-1 moderates behavioral responses to stress by regulating parvalbumin interneuron activity in the medial prefrontal cortex. *Neuron* **109**, 1636-1656.e8 (2021).

393. Acker, T. Van, Tavernier, J. & Peelman, F. The small GTPase Arf6: An overview of its mechanisms of action and of its role in host- pathogen interactions and innate immunity. *Int J Mol Sci* **20**, (2019).

394. Sabe, H. KRAS, MYC, and ARF6: inseparable relationships cooperatively promote cancer malignancy and immune evasion. *Cell Communication and Signaling* vol. 21 Preprint at https://doi.org/10.1186/s12964-023-01130-3 (2023).

395. Marcetteau, J., Matusek, T., Luton, F. & Thérond, P. P. Arf6 is necessary for high level Wingless signalling during Drosophila 1 wing development Running title: Arf6 requirement in Wingless signaling. doi:10.1101/2021.04.14.439835.

396. Franssen, E. H. P. *et al.* Exclusion of integrins from CNS axons is regulated by Arf6 activation and the AIS. *Journal of Neuroscience* **35**, 8359–8375 (2015).

397. Tagliatti, E., Fadda, M., Falace, A., Benfenati, F. & Fassio, A. Arf6 regulates the cycling and the readily releasable pool of synaptic vesicles at hippocampal synapse. (2016) doi:10.7554/eLife.10116.001.

398. Herzine, A. *et al.* Perinatal exposure to glufosinate ammonium herbicide impairs neurogenesis and neuroblast migration through cytoskeleton destabilization. *Front Cell Neurosci* **10**, (2016).

399. Sun, D., Guo, Y., Tang, P., Li, H. & Chen, L. Arf6 as a therapeutic target: Structure, mechanism, and inhibitors. *Acta Pharm Sin B* (2023) doi:https://doi.org/10.1016/j.apsb.2023.06.008.

400. Gyurkó, M. D., Csermely, P., Soti, C. & Steták, A. Distinct roles of the RasGAP family proteins in C. elegans associative learning and memory. *Sci Rep* **5**, (2015).

401. Campbell, R. R. & Wood, M. A. How the epigenome integrates information and reshapes the synapse. *Nature Reviews Neuroscience* vol. 20 133–147 Preprint at https://doi.org/10.1038/s41583-019-0121-9 (2019).

402. Foy, A. M. H., Hudock, R. L., Shanley, R. & Pierpont, E. I. Social behavior in RASopathies and idiopathic autism. *J Neurodev Disord* **14**, (2022).

403. Geoffray, M. M. *et al.* Autism Spectrum Disorder Symptom Profile Across the RASopathies. *Front Psychiatry* **11**, (2021).

404. Singh, G. *et al.* Altered genome-wide hippocampal gene expression profiles following early life lead exposure and their potential for reversal by environmental enrichment. *Sci Rep* **12**, (2022).

405. Tao, T., Sun, J. & Zhu, M.-S. *Tao T, Sun J, Zhu MS. The Triple Functional Domain Protein Trio with Multiple Functions in the Nervous The Triple Functional Domain Protein Trio with Multiple Functions in the Nervous System*. *J Neurol Neuromed* vol. 5 www.jneurology.comNeuromedicine (2020).

406. Eagle, A. L., Gajewski, P. A. & Robison, A. J. Role of hippocampal activity-induced transcription in memory consolidation. *Rev Neurosci* **27**, 559–573 (2016).

407. Liston, C. ELK-1: A molecular substrate of depression. *Sci Transl Med* **10**, eaau0468 (2018).

408. Slack, C. *et al.* The Ras-Erk-ETS-Signaling Pathway Is a Drug Target for Longevity. *Cell* **162**, 72–83 (2015).

409. Gutièrrez-Mecinas, M. *et al.* Long-lasting behavioral responses to stress involve a direct interaction of glucocorticoid receptors with ERK1/2-MSK1-Elk-1 signaling. *Proc Natl Acad Sci U S A* **108**, 13806–13811 (2011).

410. Wozniak, M. A. *et al.* Adhesion regulates MAP kinase/ternary complex factor exchange to control a proliferative transcriptional switch. *Current Biology* **22**, 2017–2026 (2012).

411. Esnault, C. *et al.* Rho-actin signaling to the MRTF coactivators dominates the immediate transcriptional response to serum in fibroblasts. *Genes Dev* **28**, 943–958 (2014).

412. Gallo, F. T., Katche, C., Morici, J. F., Medina, J. H. & Weisstaub, N. V. Immediate early genes, memory and psychiatric disorders: Focus on c-Fos, Egr1 and Arc. *Frontiers in Behavioral Neuroscience* vol. 12 Preprint at https://doi.org/10.3389/fnbeh.2018.00079 (2018).

413. Rajakylä, E. K. & Vartiainen, M. K. Rho, nuclear actin, and actin-binding proteins in the regulation of transcription and gene expression. *Small GTPases* vol. 5 Preprint at https://doi.org/10.4161/sgtp.27539 (2014).

414. Xie, X. & Percipalle, P. An actin-based nucleoskeleton involved in gene regulation and genome organization. *Biochem Biophys Res Commun* **506**, 378–386 (2018).

415. Percipalle, P. & Vartiainen, M. Cytoskeletal proteins in the cell nucleus: A special nuclear actin perspective. *Molecular Biology of the Cell* vol. 30 1781–1785 Preprint at https://doi.org/10.1091/mbc.E18-10-0645 (2019).

416. Dubash, A. D. *et al.* The small GTPase RhoA localizes to the nucleus and is activated by Net1 and DNA damage signals. *PLoS One* **6**, (2011).

417. Apazoglou, K. *et al.* Antidepressive effects of targeting ELK-1 signal transduction. *Nat Med* **24**, 591–597 (2018).

418. Cho, C. H. Commentary: Antidepressive effects of targeting ELK-1 signal transduction. *Front Mol Neurosci* **11**, (2018).

419. Rueda, D., Navarro, B., Martínez-Serrano, A., Guzmán, M. & Galve-Roperh, I. The endocannabinoid anandamide inhibits neuronal progenitor cell differentiation through attenuation of the Rap1/B-Raf/ERK pathway. *Journal of Biological Chemistry* **277**, 46645–46650 (2002).

420. Liu, W. *et al.* Physical exercise promotes proliferation and differentiation of endogenous neural stem cells via ERK in rats with cerebral infarction. *Mol Med Rep* **18**, 1455–1464 (2018).

421. Chongtham, M. C. *et al.* Transcriptome Response and Spatial Pattern of Gene Expression in the Primate Subventricular Zone Neurogenic Niche After Cerebral Ischemia. *Front Cell Dev Biol* **8**, (2020).

422. Sawada, N., Kim, H.-H., Moskowitz, M. A. & Liao, J. K. *Rac1* Is a Critical Mediator of Endothelium-Derived Neurotrophic Activity. *Sci Signal* **2**, ra10–ra10 (2009).

423. dos Santos Guilherme, M. *et al.* Selective targeting of chronic social stress-induced activated neurons identifies neurogenesis-related genes to be associated with resilience in female mice. *Psychoneuroendocrinology* **139**, 105700 (2022).

424. Ruffini, N., Klingenberg, S., Schweiger, S. & Gerber, S. Common Factors in Neurodegeneration: A Meta-Study Revealing Shared Patterns on a Multi-Omics Scale. *Cells* **9**, (2020).

425. Li, X., Wei, W., Ratnu, V. S. & Bredy, T. W. On the potential role of active DNA demethylation in establishing epigenetic states associated with neural plasticity and memory. *Neurobiol Learn Mem* **105**, 125–132 (2013).

426. Oliveira, A. M. M. DNA methylation: a permissive mark in memory formation and maintenance. doi:10.1101/lm.042739.

427. Baker-Andresen, D., Ratnu, V. S. & Bredy, T. W. Dynamic DNA methylation: A prime candidate for genomic metaplasticity and behavioral adaptation. *Trends in Neurosciences* vol. 36 3–13 Preprint at https://doi.org/10.1016/j.tins.2012.09.003 (2013).

428. Chastain, L. G. *et al.* Early life alcohol exposure primes hypothalamic microglia to later-life hypersensitivity to immune stress: possible epigenetic mechanism. *Neuropsychopharmacology* **44**, 1579–1588 (2019).

429. Ghosh, M. *et al. C E L L B I O L O G Y CD13 Tethers the IQGAP1-ARF6-EFA6 Complex to the Plasma Membrane to Promote ARF6 Activation, β1 Integrin Recycling, and Cell Migration*. *Sci. Signal* vol. 12 https://www.science.org (2019).

430. Gillingham, A. K. & Munro, S. The small G proteins of the Arf family and their regulators. *Annual Review of Cell and Developmental Biology* vol. 23 579–611 Preprint at https://doi.org/10.1146/annurev.cellbio.23.090506.123209 (2007).

431. Donaldson, J. G. & Jackson, C. L. ARF family G proteins and their regulators: Roles in membrane transport, development and disease. *Nature Reviews Molecular Cell Biology* vol. 12 362–375 Preprint at https://doi.org/10.1038/nrm3117 (2011).

432. Wang, M., Gallo, N. B., Tai, Y., Li, B. & Van Aelst, L. Oligophrenin-1 moderates behavioral responses to stress by regulating parvalbumin interneuron activity in the medial prefrontal cortex. *Neuron* **109**, 1636-1656.e8 (2021).

433. Shoubridge, C., Walikonis, R. S., Gécz, J. & Harvey, R. J. Subtle functional defects in the Arf-specific guanine nucleotide exchange factor IQSEC2 cause non-syndromic X-linked intellectual disability. *Small GTPases* **1**, 98–103 (2010).

434. Knizhnik, A. V. *et al.* Arf6 promotes cell proliferation via the PLD-mTORC1 and p38MAPK pathways. *J Cell Biochem* **113**, 360–371 (2012).

435. Luo, Y. F. *et al.* mTORC1 Signaling Pathway Mediates Chronic Stress-Induced Synapse Loss in the Hippocampus. *Front Pharmacol* **12**, (2021).

436. Zuo, L., Wang, Z., Tan, Y., Chen, X. & Luo, X. *PiRNAs and Their Functions in the Brain*.

437. Kim, K. W. PIWI proteins and piRNAs in the nervous system. *Molecules and Cells* vol. 42 828–835 Preprint at https://doi.org/10.14348/molcells.2019.0241 (2019).

438. Sato, K., Takayama, K. I. & Inoue, S. Role of piRNA biogenesis and its neuronal function in the development of neurodegenerative diseases. *Frontiers in Aging Neuroscience* vol. 15 Preprint at https://doi.org/10.3389/fnagi.2023.1157818 (2023).

439. Dauth, S. *et al.* Neurons derived from different brain regions are inherently different in vitro: a novel multiregional brain-on-a-chip. *J Neurophysiol* **117**, 1320–1341 (2017).

440. Zurawek, D. *et al.* Time-dependent miR-16 serum fluctuations together with reciprocal changes in the expression level of miR-16 in mesocortical circuit contribute to stress resilient phenotype in chronic mild stress – An animal model of depression. *European Neuropsychopharmacology* **26**, 23–36 (2016).

441. Zurawek, D. *et al.* Reciprocal MicroRNA Expression in Mesocortical Circuit and Its Interplay with Serotonin Transporter Define Resilient Rats in the Chronic Mild Stress. *Mol Neurobiol* **54**, 5741–5751 (2017).

442. Pascual Cuadrado, D. *et al.* Long-term molecular differences between resilient and susceptible mice after a single traumatic exposure. *Br J Pharmacol* **179**, 4161–4180 (2022).

443. Roth, T. L., Zoladz, P. R., Sweatt, J. D. & Diamond, D. M. Epigenetic modification of hippocampal Bdnf DNA in adult rats in an animal model of post-traumatic stress disorder. *J Psychiatr Res* **45**, 919–926 (2011).

444. Yi, X. *et al.* Genetic and functional analysis reveals TENM4 contributes to schizophrenia. *iScience* **24**, (2021).

445. Chen, W. W. *et al.* Increased Axin expression enhances adult hippocampal neurogenesis and exerts an antidepressant effect. *Sci Rep* **9**, (2019).

446. Wang, X. *et al.* The C. elegans homolog of human panic-disorder risk gene TMEM132D orchestrates neuronal morphogenesis through the WAVE-regulatory complex. *Mol Brain* **14**, (2021).

447. Yamada, M. *et al.* Cux2 activity defines a subpopulation of perinatal neurogenic progenitors in the hippocampus. *Hippocampus* **25**, 253–267 (2015).

448. Li, Y. (Jamie), Kresock, E., Kuplicki, R., Savitz, J. & McKinney, B. A. Differential expression of MDGA1 in major depressive disorder. *Brain Behav Immun Health* **26**, (2022).

449. Rizzardi #1, L. F. *et al.* Neuronal brain region-specific DNA methylation and chromatin accessibility are associated with neuropsychiatric trait heritability HHS Public Access. doi:10.5281/zenodo.1469577.

450. Ladd-Acosta, C. *et al.* DNA methylation signatures within the human brain. *Am J Hum Genet* **81**, 1304–1315 (2007).

451. Zhou, J. *et al.* Tissue-specific DNA methylation is conserved across human, mouse, and rat, and driven by primary sequence conservation. *BMC Genomics* **18**, (2017).

452. Zuzarte, M., Vitorino, C., Salgueiro, L. & Girão, H. Plant Nanovesicles for Essential Oil Delivery. *Pharmaceutics* vol. 14 Preprint at https://doi.org/10.3390/pharmaceutics14122581 (2022).

453. Patra, J. K. *et al.* Nano based drug delivery systems: Recent developments and future prospects. *Journal of Nanobiotechnology* vol. 16 Preprint at https://doi.org/10.1186/s12951-018-0392-8 (2018).

454. Cameron, H. A. & Schoenfeld, T. J. Behavioral and structural adaptations to stress. *Frontiers in Neuroendocrinology* vol. 49 106–113 Preprint at https://doi.org/10.1016/j.yfrne.2018.02.002 (2018).

455. Davis, M. T., Holmes, S. E., Pietrzak, R. H. & Esterlis, I. Neurobiology of Chronic Stress-Related Psychiatric Disorders: Evidence from Molecular Imaging Studies. *Chronic Stress* vol. 1 Preprint at https://doi.org/10.1177/2470547017710916 (2017).

456. Tandon, R. COVID-19 and mental health: Preserving humanity, maintaining sanity, and promoting health. *Asian Journal of Psychiatry* vol. 51 Preprint at https://doi.org/10.1016/j.ajp.2020.102256 (2020).

457. Kathirvel, N. Post COVID-19 pandemic mental health challenges. *Asian Journal of Psychiatry* vol. 53 Preprint at https://doi.org/10.1016/j.ajp.2020.102430 (2020).

458. Galea, S., Merchant, R. M. & Lurie, N. The Mental Health Consequences of COVID-19 and Physical Distancing: The Need for Prevention and Early Intervention. *JAMA Internal Medicine* vol. 180 817–818 Preprint at https://doi.org/10.1001/jamainternmed.2020.1562 (2020).

459. Zhong, Z. A. *et al.* Optimizing tamoxifen-inducible Cre/loxp system to reduce tamoxifen effect on bone turnover in long bones of young mice. *Bone* **81**, 614–619 (2015).

460. Quirke, V. M. Tamoxifen from failed contraceptive pill to best-selling breast cancer medicine: A case-study in pharmaceutical innovation. *Front Pharmacol* **8**, (2017).

461. Zhang, Z. *et al.* Estrogen receptor alpha in the brain mediates tamoxifen-induced changes in physiology in mice. *Elife* **10**, (2021).

462. Chucair-Elliott, A. J. *et al.* Tamoxifen induction of Cre recombinase does not cause long-lasting or sexually divergent responses in the CNS epigenome or transcriptome: implications for the design of aging studies. *Geroscience* **41**, 691–708 (2019).

463. Wu, H., Kirita, Y., Donnelly, E. L. & Humphreys, B. D. Advantages of single-nucleus over single-cell RNA sequencing of adult kidney: Rare cell types and novel cell states revealed in fibrosis. *Journal of the American Society of Nephrology* **30**, 23–32 (2019).

464. Grindberg, R. V. *et al.* RNA-sequencing from single nuclei. *Proc Natl Acad Sci U S A* **110**, 19802–19807 (2013).

465. Bakken, T. E. *et al.* Single-nucleus and single-cell transcriptomes compared in matched cortical cell types. *PLoS One* **13**, (2018).

466. Biology, C. *et al.* Epigenomic landscapes of retinal rods and cones. (2016) doi:10.7554/eLife.11613.001.

467. McGuire, M. H. *et al.* Pan-cancer genomic analysis links 3'UTR DNA methylation with increased gene expression in T cells. *EBioMedicine* **43**, 127–137 (2019).

468. Jones, P. A. Functions of DNA methylation: islands, start sites, gene bodies and beyond. *Nat Rev Genet* **13**, 484–492 (2012).

469. Shayevitch, R., Askayo, D., Keydar, I. & Ast, G. The importance of DNA methylation of exons on alternative splicing. (2018) doi:10.1261/rna.

470. Shukla, S. *et al.* CTCF-promoted RNA polymerase II pausing links DNA methylation to splicing. *Nature* **479**, 74–79 (2011).

471. Li, D., McIntosh, C. S., Mastaglia, F. L., Wilton, S. D. & Aung-Htut, M. T. Neurodegenerative diseases: a hotbed for splicing defects and the potential therapies. *Translational Neurodegeneration* vol. 10 Preprint at https://doi.org/10.1186/s40035-021-00240-7 (2021).

472. Nikom, D. & Zheng, S. Alternative splicing in neurodegenerative disease and the promise of RNA therapies. *Nat Rev Neurosci* **24**, 457–473 (2023).

473. Clayton, D. F. *et al.* The role of the genome in experience-dependent plasticity: Extending the analogy of the genomic action potential. *Proceedings of the National Academy of Sciences of the United States of America* vol. 117 23252–23260 Preprint at https://doi.org/10.1073/pnas.1820837116 (2020).

474. Gräff, J. & Tsai, L. H. Histone acetylation: Molecular mnemonics on the chromatin. *Nature Reviews Neuroscience* vol. 14 97–111 Preprint at https://doi.org/10.1038/nrn3427 (2013).

475. Bacon, E. R. & Brinton, R. D. Epigenetics of the developing and aging brain: Mechanisms that regulate onset and outcomes of brain reorganization. *Neuroscience and Biobehavioral Reviews* vol. 125 503–516 Preprint at https://doi.org/10.1016/j.neubiorev.2021.02.040 (2021).

476. O'neil, S. D. *et al.* Action potential-coupled rho gtpase signaling drives presynaptic plasticity. *Elife* **10**, (2021).

477. Zhang, H., Ben Zablah, Y., Zhang, H. & Jia, Z. Rho Signaling in Synaptic Plasticity, Memory, and Brain Disorders. *Frontiers in Cell and Developmental Biology* vol. 9 Preprint at https://doi.org/10.3389/fcell.2021.729076 (2021).

478. Bai, Y., Xiang, X., Liang, C. & Shi, L. Regulating Rac in the nervous system: Molecular function and disease implication of Rac GEFs and GAPs. *BioMed Research International* vol. 2015 Preprint at https://doi.org/10.1155/2015/632450 (2015).

479. Phuyal, S. & Farhan, H. Multifaceted Rho GTPase Signaling at the Endomembranes. *Front Cell Dev Biol* **7**, (2019).

480. Senese, N. B., Rasenick, M. M. & Traynor, J. R. The role of G-proteins and G-protein regulating proteins in depressive disorders. *Frontiers in Pharmacology* vol. 9 Preprint at https://doi.org/10.3389/fphar.2018.01289 (2018).

481. Droppelmann, C. A. *et al.* The emerging role of guanine nucleotide exchange factors in ALS and other neurodegenerative diseases. *Frontiers in Cellular Neuroscience* vol. 8 Preprint at https://doi.org/10.3389/fncel.2014.00282 (2014).

482. Bondar, N. *et al.* Molecular Adaptations to Social Defeat Stress and Induced Depression in Mice. *Mol Neurobiol* **55**, 3394–3407 (2018).

483. Plotnik, J. P., Budka, J. A., Ferris, M. W. & Hollenhorst, P. C. ETS1 is a genome-wide effector of RAS/ERK signaling in epithelial cells. *Nucleic Acids Res* **42**, 11928–11940 (2014).

484. Sheu, S. H. *et al.* A serotonergic axon-cilium synapse drives nuclear signaling to alter chromatin accessibility. *Cell* **185**, 3390-3407.e18 (2022).

485. Iacono, G., Massoni-Badosa, R. & Heyn, H. Single-cell transcriptomics unveils gene regulatory network plasticity. *Genome Biol* **20**, (2019).

486. Li, C. Y., Cai, J. H., Tsai, J. J. P. & Wang, C. C. N. Identification of Hub Genes Associated With Development of Head and Neck Squamous Cell Carcinoma by Integrated Bioinformatics Analysis. *Front Oncol* **10**, (2020).

487. Lake, B. B. *et al.* Neuronal subtypes and diversity revealed by single-nucleus RNA sequencing of the human brain. *Science (1979)* **352**, 1586–1590 (2016).

488. Floriou-Servou, A. *et al.* Distinct Proteomic, Transcriptomic, and Epigenetic Stress Responses in Dorsal and Ventral Hippocampus. *Biol Psychiatry* **84**, 531–541 (2018).

489. Zorkina, Y. *et al.* Nano Carrier Drug Delivery Systems for the Treatment of Neuropsychiatric Disorders: Advantages and Limitations. *Molecules* vol. 25 Preprint at https://doi.org/10.3390/MOLECULES25225294 (2020).

490. Xu, C., Peng, B. & Liu, S. Using intra-brain drug infusion to investigate neural mechanisms underlying reward-seeking behavior in mice. *STAR Protoc* **3**, (2022).

491. Mazzitelli, M., Yakhnitsa, V., Neugebauer, B. & Neugebauer, V. Optogenetic manipulations of CeA-CRF neurons modulate pain- and anxiety-like behaviors in neuropathic pain and control rats. *Neuropharmacology* **210**, (2022).

492. Horii-Hayashi, N. & Nishi, M. Protocol for behavioral tests using chemogenetically manipulated mice. *STAR Protoc* **2**, (2021).

493. Campbell, E. J. & Marchant, N. J. The use of chemogenetics in behavioural neuroscience: receptor variants, targeting approaches and caveats. *British Journal of Pharmacology* vol. 175 994–1003 Preprint at https://doi.org/10.1111/bph.14146 (2018).

494. Meng, G., Tang, W., Huang, E., Li, Z. & Feng, H. A comprehensive assessment of cell type-specific differential expression methods in bulk data. *Briefings in Bioinformatics* vol. 24 Preprint at https://doi.org/10.1093/bib/bbac516 (2023).

495. Rahmani, E. *et al.* Cell-type-specific resolution epigenetics without the need for cell sorting or single-cell biology. *Nat Commun* **10**, (2019).

496. Qi, L. & Teschendorff, A. E. Cell-type heterogeneity: Why we should adjust for it in epigenome and biomarker studies. *Clin Epigenetics* **14**, (2022).

497. Christoffel, D. J., Golden, S. A. & Russo, S. J. Structural and synaptic plasticity in stress-related disorders. *Rev Neurosci* **22**, 535–549 (2011).

498. Watanabe, T., Cui, X., Yuan, Z., Qi, H. & Lin, H. MIWI 2 targets RNAs transcribed from pi RNA -dependent regions to drive DNA methylation in mouse prospermatogonia . *EMBO J* **37**, (2018).

499. Aravin, A. A. *et al.* A piRNA Pathway Primed by Individual Transposons Is Linked to De Novo DNA Methylation in Mice. *Mol Cell* **31**, 785–799 (2008).

500. Houri-Zeevi, L., Teichman, G., Gingold, H. & Rechavi, O. Stress resets ancestral heritable small RNA responses. *Elife* **10**, (2021).

501. Cecere, G. Small RNAs in epigenetic inheritance: from mechanisms to trait transmission. *FEBS Letters* vol. 595 2953–2977 Preprint at https://doi.org/10.1002/1873-3468.14210 (2021).

502. Huang, Y. *et al.* The behaviour of 5-hydroxymethylcytosine in bisulfite sequencing. *PLoS One* **5**, (2010).

503. Johnson, N. D. & Conneely, K. N. The role of DNA methylation and hydroxymethylation in immunosenescence. *Ageing Res Rev* **51**, 11–23 (2019).

504. Vaisvila, R. *et al.* Enzymatic methyl sequencing detects DNA methylation at single-base resolution from picograms of DNA. *Genome Res* **31**, 1280–1289 (2021).

505. Iñiguez, S. D. *et al.* Vicarious Social Defeat Stress Induces Depression-Related Outcomes in Female Mice. *Biol Psychiatry* **83**, 9–17 (2018).

506. Anthony, K. RNA-based therapeutics for neurological diseases. *RNA Biology* vol. 19 176–190 Preprint at https://doi.org/10.1080/15476286.2021.2021650 (2022).

507. Damase, T. R. *et al.* The Limitless Future of RNA Therapeutics. *Frontiers in Bioengineering and Biotechnology* vol. 9 Preprint at https://doi.org/10.3389/fbioe.2021.628137 (2021).

508. Gregory, S. G. Genetic predisposition of behavioral response. *Proceedings of the National Academy of Sciences of the United States of America* vol. 111 1672–1673 Preprint at https://doi.org/10.1073/pnas.1323421111 (2014).

NB: Personal communications with ChatGPT for paraphrasing suggestions/synonyms will be available on request till the date of PhD defense.

IX. Appendices

1. List of Abbreviations

NB: As the multiomics sequencing generates a huge number of gene lists, genes that are mentioned only once and are not mentioned to be of specific relevance are not abbreviated.

4

4-hydroxytamoxifen
4-OHT, 34

A

Activity-regulated cytoskeleton-associated gene
Arc, 12
ADP-ribosylation factor 6
Arf6, 113
adrenocorticotropic hormones
ACTH, 4
Alzheimer's dementia
AD, 3
analysis of variance
ANOVA, 51
attention deficit hyperactivity disorder
ADHD, 3

B

biological processes
BP, 100
brain derived neurotrophic factor
BDNF, 19

C

cellular compartments
CC, 100
chronic social defeat
CSD, 10
corticosterone
CORT, 4
corticotrophin releasing hormone
CRH, 4
counts per million
CPM, 96
Cut-like homeobox2
Cux2, 126

D

differentially expressed genes
DEGs, 107
differentially methylated cytosines
dmCs, 99
differentially methylated regions
DMRs, 100
dithiothreitol
dTT, 63
DMRs overlapping with regulatory regions
rrDMRs, 104
DNA methyl transferases
DNMTs, 17

E

E26 Transformation Specific
ETS, 104
electrocardiography
ECG, 14
electroencephalography
EEG, 14
elevated plus maze
EPM, 13
enzyme-linked immunosorbent assay
ELISA, 41
ETS-like 1
Elk1, 105
ETS-like 4
Elk4, 104
extracellular matrix
ECM, 101
extracellular signal-regulated kinase
ERK, 105

F

FKBP Prolyl Isomerase 5
FKBP5, 18
fluorescence activated nuclei sorting
FANS, 43
Forced swim
FS, 13
Fos proto-oncogene, AP-1 transcription factor subunit
cFos, 12

G

Gene ontology
GO, 100
genes containing dmCs
dmGs, 99
genes containing the DMRs

DMGs, 100
genes, containing DMRs overlapping with enhancer regions
eDMGs, 104
genetically modified
GM, 12
glucocorticoid receptors
GRs, 18
glucocorticoids
GCs, 4
GTPase activating proteins
GAPs, 113
guanine nucleotide exchange factors
GEFs, 101

H

heterogenous nuclear ribonucleoprotein particles
hnrnps, 108
home cage
HC, 44
homogenization buffer
HB, 62
hypergeometric optimization of Motif EnRichment
HOMER, 104
hypothalamic-pituitary-adrenal axis
HPA, 4

I

immediate early genes
IEGs, 12
insulin growth factor 2
IGF2, 19
Interleukin-6
IL-6, 18
Isolation of Nuclei Tagged in specific Cell Types
INTACT, 79

L

light-dark preference
LDP, 13

M

major depressive disorders
MDD, 1
MAM Domain Containing Glycosylphosphatidylinositol Anchor 1
Mdga1, 126
metabotropic glutamate receptors
mGluR, 18
methylated cytosines
mCs, 19
methyl-DNA immunoprecipitation sequencing
MeDIP_seq, 17
molecular functions
MF, 100
multiomics resilient compared to control
RES_C, 109
multiomics susceptible compared to control
SUS_C, 109
multiomics susceptible compared to resilient
SUS_R, 109
mutant
M, 30

N

Next generation sequencing
NGS, 94
non-coding RNAs
ncRNAs, 19
non-injected
N, 56
nuclear receptor subfamily 3 group C member 1
NR3C1, 19
nucleus accumbens
Naccu, 4

O

Oligophrenin 1
Ophn1, 113
Open field and eagle exploration test
OF/E, 38

P

paraformaldehyde
PFA, 66
paraventricular nucleus
PVN, 4
phosphate-buffered saline
PBS, 65
Piwi interacting RNAs
piRNAs, 20
polyethylenimine
PEI, 66
Polyvinylchloride
PVC, 70
post-traumatic disorder
PTSD, 15
pre-frontal cortex
PFC, 4
primary miR transcript
pri-miR, 19

R

reduced representation bisulfite sequencing
RRBS-seq, 17
resilient
Res, 99
resilient compared to control
Res_c, 99
resilient compared to either control or susceptible
Res_c_s, 107

S

serine/arginine rich splicing factors
srsfs, 108
serum response factor
SRF, 117
sfGFP negative
sfGFP-, 75
SI test with conspecifics
SI/CO, 96
small nuclear RNAs
snRNAs, 20
small nucleolar RNAs
snoRNAs, 20
social interaction
SI, 13
Soluble N-ethylmaleimide-sensitive factor activating protein receptors
SNAREs, 7
solute carrier family 6, member 4
SLC6A4, 19
sucrose preference
SP, 13
super folder GFP positive
sfGFP+, 27
superfolder GFP
sfGFP, 26
susceptible
Sus, 99
susceptible compared to control
Sus_c, 99
susceptible compared to either control or resilient
Sus_c_r, 107
susceptible compared to resilient
Sus_r, 99
synaptic genes
SGs, 100

T

TAM-injected (T)
T, 56
Tamoxifen
TAM, 25
ten-eleven translocation enzymes
TETs, 17
transcription factors
TFs, 21
transgenic
TG, 30

U

untranslated regions
UTRs, 99

V

vehicle-injected
O, 56
ventral hippocampus
vHipp, 8

W

whole genome bisulfite sequencing
WGBS_seq, 17
wild type allele
WT, 30
World Health Organisation
WHO, 1

2. List of Figures

Figure 1: Stress response following stress exposure to chronic social stressors 5
Figure 2: Chronic social defeat (CSD) stress paradigm and measures of stress effects. 11
Figure 3: Simplified representation of the cellular omics machineries to be accessed within the framework of the thesis. 16
Figure 4: Blueprint of the project design. 28
Figure 5: Optimization of experimental strategy for acquiring maximum stimulus-induced GFP accumulated engram using TG constructs. 33
Figure 6. Stimulus-specific engram tracing with GFP accumulation. 44
Figure 7: The differential impacts of the chronic social defeat paradigm on the Arc-GFP mice with and without TAM injection. 45
Figure 8:. Scheme of the behavioral battery tests and physiological assays along the longitudinal timeline. 48
Figure 9: Arc-GFP mice exhibited stress effects in the new scheme with the use of a more aggressive stressor. 50
Figure 10: Genotype differences in behavior patterns of non-stressed controls as observed in multiple assays. 53
Figure 11: Similarities in the stress response despite genotypic differences in the TAM-injected groups. 55

Figure 12: Implications of TAM injections. 58
Figure 13: Regions for tissue dissections. 62
Figure 14: Nuclei isolation procedure and data quantification. 70
Figure 15: Comparison of ultracentrifugation with (w) and without (w/o) the 40% cushion layer. 72
Figure 16: Strategies for optimizing nuclei processing duration. 74
Figure 17: Effects of different buffers on nuclei detection and nuclei degradation. 76
Figure 18: FANS vs INTACT: Procedural differences and purity estimation. 83
Figure 19: Morphological comparisons between FANS-and INTACT-nuclei. 86
Figure 20: Experimental design for the engram-multiomics approach. 98
Figure 21: Divergent regional methylation landscape of the differentially activated engram nuclei from the resilient and susceptible phenotypes post CSD stress. 102
Figure 22: Assessing plausible regulatory functions of the DMRs. 106
Figure 23: Multiomics network approach identifies phenotype-specific divergence in important biological processes. 109
Figure 24: miRs show convergence with the results from the methylome and the RNA transcriptome. 111
Figure 25: Overview of the multiomics modifications and determination of novel therapeutic targets. 115
Figure 26: Enriched GO BPs in the phenotypic comparisons of PFC following stress exposure. 122
Figure 27: Between tissue comparisons of vHipp and PFC for each phenotype. 125
Figure 28: Proposed model for phenotype rescue. 148

3. List of Supplementary Figures

Supplementary Figure 1: Flow cytometry of nuclei collected from mice with different time points of TAM injection before stimulus presentation. 149
Supplementary Figure 2: Preliminary results to identify the usability of the TAM-inducible Arc-GFP mouse line. 150
Supplementary Figure 3: Bioanalyzer patterns of RRBS libraries and small-RNA libraries from mouse samples. 151
Supplementary Figure 4: Results from the behavior experiments of Arc-GFP and WT-GFP mice. 152
Supplementary Figure 5: Base resolution methylation landscape of differentially methylated cytosines from RRBS-seq. 153
Supplementary Figure 6: Functional assignment of the genes harbouring differentially methylated cytosines (dmGs). 154
Supplementary Figure 7: Regional methylation landscape of differentially methylated regions and biological processes following stress exposure. 155
Supplementary Figure 8: Multiomics analyses. 156

4. List of Tables

Table 1: INTACT vs FANS comparison of yield and purity 87
Table 2: Top 20 significantly enriched (q<0.05) BPs of combined DMGs, ranked according to the detected number of genes involved in the process. 123
Table 3: Top enriched GO MFs from Enrichr of PFC and vHipp comparisons for the resilient phenotype. 127
Table 4: Top enriched GO MFs from Enrichr for between tissue susceptible group comparisons. 128

5. List of Supplementary Tables

Supplementary Table 1: List of selected GO BPs significantly enriched in multiomics SUS_C but not in multiomics RES_C (STRING). 158
Supplementary Table 2: List of GO BPs significantly enriched in multiomics RES_C but not in multiomics SUS_C (STRING) 159
Supplementary Table 3: Local network clusters of multiomics SUS_C from STRING. 159
Supplementary Table 4: Local network cluster of multiomics RES_C from STRING. 160
Supplementary Table 5: List of selected significantly enriched BPs from Enrichr. 161
Supplementary Table 6: List of selected significantly enriched BPs in SUS_R (Enrichr). 162
Supplementary Table 7: Synaptic gene network comparison with literature. 163
Supplementary Table 8: GO CCs of tissue comparisons for susceptible phenotypes. 165
Supplementary Table 9: Biotypes of the small RNAs involved in stress research. 165

6. Contributions to other projects during the interim of the thesis

Tissue clearing to uncover new regions in the brain differentially activated in the susceptible and resilient phenotypes.

To visualize the different brain activation patterns in the susceptible and resilient animals, I initiated a collaboration with Margaryta Tevosian (Post-doc, Lutz lab) to perform tissue clearing on the Arc-GFP mouse line after CSD stress. The organization and experimentation for the behavior part was conducted by me. Anaesthesia, perfusion and CUBIC (tissue clearing) experiments were performed by Margaryta Tevosian. The imaging of the cleared tissues as well as analyzes are still in progress.

Molecular underpinnings behind stress susceptibility and resilience in female stressed populations

As increasing amount of research show sex-dependent effects of stress exposure, we also wanted to determine the molecular changes behind chronic stress in females using the activated nuclei from Arc-GFP mice. The study was performed in collaboration with Endres lab. I performed breeding planning, genotyping and nuclei isolation for this project. Apart from this, I participated in editing the manuscript published as 'Selective targeting of chronic social stress-induced activated neurons identifies neurogenesis-related genes to be associated with resilience in female mice'. In brief, we identified Artemin, to be upregulated in resilient compared to susceptible populations.

Changes in the gut after chronic stress effects

The gut-brain axis has gained a particular interest in the neuroscience field. A number of gut symptoms have been identified as associated with stress. On the contrary, a change in the gut microbiome can affect reactivity to stressors. In the study, resulting in the publication

'Resilience and the Gut Microbiome: Insights from Chronically Socially Stressed Wild-Type Mice', Endres group examined the GFP expression in the Arc-GFP male mice that underwent the aggressive CSD experiments compared to control groups (experiments from **Chapter 2**).

Python App to predict resilience or susceptibility apart from the ratio results of SI index.
During the SI test, different animals revealed different behavioral patterns, which might not be well reflected in the SI index. Therefore, I proposed the idea to find another mode to assess stress effects apart from the SI index. The proposition led to the collaboration with Nicolas Ruffini (Gerber lab), where we worked closely on the datasets from **Chapter 2** and **Chapter 5**, to identify different elements in the body language of the animal that could help in the classification of stress-susceptible or stress-resilient groups, apart from the SI. To access these different features and identify whether there is a marked difference to able to distinguish susceptible populations from resilient groups, Nicolas used the SI tracks and converted them to machine readable format. The bioinformatics programming and identification of different parameters were contributions from Nicolas Ruffini, while I gave relevant inputs pertaining to the behavior of the animals and the feasibility/usability of the identified parameter. The collaborative efforts resulted in the development of the App ResiliPy.

7. Other co-curricular work or achievements during the interim of the thesis

Supervision experience

- Bachelor's student (Gerber group) – full supervision
- Master's student (Winter group) - partial supervision
- Bachelor's student for ResiliPy (Gerber group) – partial supervision
- Internship student (Gerber group) – partial supervision

Other activities that do not fall under academic training.

- ❖ Founded the Sci Comm Channel 'Stresspunsch' to turn my extensive knowledge on stress susceptibility and resilience, into action to help the general populace to adopt pro-active resilience strategies. The Channel received the competitive IBRO 'Global Engagement Seed Grant' for 2023 and has organised four different workshops to educate the youth, both online and offline.
- ❖ FENS digital image selection for contributing captivating microscopy photography.

- ❖ Winner of Negotiate Up – group negotiation competitions organised by MIT and Standford university.
- ❖ Participated in the ADA lovelace mentorship program, where I learnt a lot from my mentors.
- ❖ Having learnt the influence of mentors on my attitude towards career, communications and general conduct, I participated in the FEA mentorship program and mentored 15 students for 4 months to guide them towards their career goals, while providing networking opportunities.

8. Declaration of online publications as co-authors for scientific work during the PhD, peer-reviewed and non-peer reviewed.

Chongtham MC, Todorov H, Wettschereck JE, Gerber S & Winter J. Isolation of nuclei and downstream processing of cell-type-specific nuclei from micro-dissected mouse brain regions – techniques and caveats. *BioRxiv.* doi:10.1101/2020.11.18.374223. – **Chapter 3.**

Chongtham MC, Butto T, Mungikar K, Gerber S, & Winter J. Intact vs. Fans for cell-type-specific nuclei sorting: A comprehensive qualitative and quantitative comparison. *Int J Mol Sci* **22**, (2021). doi: 10.3390/ijms22105335 – **Chapter 4.**

Guilherme M, Tsoutsouli T, Chongtham MC, Winter J, Gerber S, Müller M, Endres K. Selective targeting of chronic social stress-induced activated neurons identifies neurogenesis-related genes to be associated with resilience in female mice. *Psychoneuroendocrinology* **139** (2022). doi: 10.1016/j.psyneuen.2022.105700.- Contributions to other projects -2

Gerber, S. et al. Characterization of transcriptional proles associated with stress-induced neuronal activation in Arc-GFP mice. (2023) doi:10.21203/rs.3.rs-3273083/v1. –Parts of **Chapter 5**, under review in Molecular Psychiatry.

9. Breakdown of the timeline for the thesis

Timeline	Work distribution	Funded by	In thesis
2017-2018	Choice of mouse line Mouse line expansion Genotyping CSD behavior trials and optimization Nuclei isolation protocol development FANS vs INTACT data procurement	CRC 1193	Chapters 1-4
2018-2019	Mouse line expansion CSD behavior optimization and application FANS vs INTACT data analysis	CRC 1193	
2019-2020	CSD behavior application for nuclei collection Low-input RRBS – seq protocol development Nuclei isolation manuscript compilation FANS-INTACT manuscript compilation	CRC 1193	
2020-2021	RRBS -seq protocol optimization & application miR-seq protocol optimization & application Research on omics analytical tools FANS-INTACT paper publication Multiomics manuscript initiation	CRC 1193	Chapters 5-6
2022 & 2023	Multiomics data analysis Multiomics data integration & interpretation Public science communications on stress resilience Gain of academic writing skills from communications with ChatGPT Thesis compilation and submission Multiomics manuscript compilation and submission	Stresspunsch Sci Comm (self-funded)	

10. Curriculum vitae

Stress can either be a source of destruction or creativity.

Change your perception and see the transformation.

-Monika Chanu Chongtham

Founder (Stresspunsch)